Direct Inversion for the Heston Model

Jiaqi Shen

Submitted for the degree of
Doctor of Philosophy

Heriot-Watt University

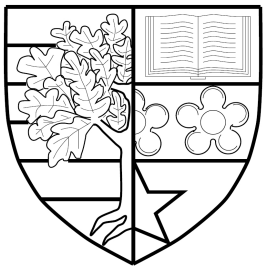

Department of Actuarial Mathematics and Statistics,
School of Mathematical and Computer Sciences.

March, 2020

Abstract

The Heston stochastic volatility model is commonly used in financial mathematics. While closed form solutions for pricing vanilla European options are available, this is not the case for other exotic options, especially for path dependent ones, where Monte Carlo methods are often applied. In this thesis, we develop an accurate and efficient simulation method for the Heston model, which is then employed in the pricing of options that are computationally challenging.

We consider the problem of sampling the asset price based on its exact distribution. One key step is to sample from the time integrated variance process conditional on its endpoints. We construct a new series expansion for this integral in terms of infinite weighted sums of exponential and gamma random variables through measure transformation and decompositions of squared Bessel bridges. This representation has exponentially decaying truncation errors, which allows efficient simulations of the Heston model.

We develop direct inversion algorithms combined with series truncations, leading to an almost exact simulation for the model. The direct inversion is based on approximating the inverse distribution functions by Chebyshev polynomials. We derive asymptotic expansions for the corresponding distribution functions to evaluate the Chebyshev coefficients. We also design feasible strategies such that those coefficients are independent of any model parameters, whence the resulting Chebyshev polynomials can be used under any market conditions. Efficiency of our method is confirmed by numerical comparisons with existing methods.

Acknowledgements

I would like to express my deepest appreciation to my supervisors Dr. Anke Wiese and Dr. Simon J.A. Malham for their continuous support, enthusiastic encouragement, patient guidance and constructive suggestions during the past four years. Without them, the development of this project would not have been possible.

I would also like to acknowledge the James Watt Scholarship and the School of Mathematical and Computer Sciences in Heriot-Watt University for the funding I received, which has provided me with such a great opportunity to work on this research. My sincere thanks goes to the helpful academics and staff members of the school. It has always been my pleasure and privilege to meet and work with them.

I am particularly grateful to all my peer colleagues, Sabrina, Chunxiao, Francesco, Zhaoxun, Spery, Fandi, Andres, Oytun, Jie, Chaofan and Aidana for making the tough PhD journey fun and enjoyable.

Finally, my special thanks are extended to my family for always believing in me, respecting my decisions and encouraging me to follow my dreams. My appreciation also goes to my future husband, who has never appeared in my life so far so that I could concentrate on my research and complete what I started.

Research Thesis Submission

Please note this form should be bound into the submitted thesis.

Name*:*			
School:			
Version: *(i.e. First, Resubmission, Final)*		Degree Sought:	

Declaration

In accordance with the appropriate regulations I hereby submit my thesis and I declare that:

1. The thesis embodies the results of my own work and has been composed by myself
2. Where appropriate, I have made acknowledgement of the work of others
3. The thesis is the correct version for submission and is the same version as any electronic versions submitted*.
4. My thesis for the award referred to, deposited in the Heriot-Watt University Library, should be made available for loan or photocopying and be available via the Institutional Repository, subject to such conditions as the Librarian may require
5. I understand that as a student of the University I am required to abide by the Regulations of the University and to conform to its discipline.
6. I confirm that the thesis has been verified against plagiarism via an approved plagiarism detection application e.g. Turnitin.

ONLY for submissions including published works

Please note you are only required to complete the Inclusion of Published Works Form (page 2) if your thesis contains published works)

7. Where the thesis contains published outputs under Regulation 6 (9.1.2) or Regulation 43 (9) these are accompanied by a critical review which accurately describes my contribution to the research and, for multi-author outputs, a signed declaration indicating the contribution of each author (complete)
8. Inclusion of published outputs under Regulation 6 (9.1.2) or Regulation 43 (9) shall not constitute plagiarism.

* *Please note that it is the responsibility of the candidate to ensure that the correct version of the thesis is submitted.*

Signature of Candidate*:*		Date:	

Submission

Submitted By *(name in capitals):*	
Signature of Individual Submitting:	
Date Submitted:	

For Completion in the Student Service Centre (SSC)

Limited Access	Requested	Yes		No		Approved	Yes		No	
*E-thesis Submitted (**mandatory for final theses)***										
Received in the SSC by *(name in capitals):*						Date:				

Inclusion of Published Works

Please note you are only required to complete the Inclusion of Published Works Form if your thesis contains published works under Regulation 6 (9.1.2)

Declaration

This thesis contains one or more multi-author published works. In accordance with Regulation 6 (9.1.2) I hereby declare that the contributions of each author to these publications is as follows:

Citation details	
Author 1	
Author 2	
Signature:	
Date:	

Citation details	
Author 1	
Author 2	
Signature:	
Date:	

Citation details	
Author 1	
Author 2	
Signature:	
Date:	

Please included additional citations as required.

Contents

List of Figures

List of Tables

List of Algorithms

Chapter 1

Introduction

Stochastic volatility models involving a pair of stochastic differential equations, with the diffusion term of the first one governed by the evolution of the second equation, are immensely popular in the pricing of derivatives. These models are often used to capture the dynamics of a financial variable such as stock price or interest rate, coupled with the underlying volatility of its instantaneous returns treated as a random process. By relaxing the restrictions on constant volatility of the well-known Black-Scholes model to allow uncertainty, we are now able to explain the long-term features of the implied volatility surface in a self-consistent way.

Among all the existing stochastic volatility models, e.g. SABR model, GARCH model and 3/2 model, the Heston model (Heston [38]) plays an important role and is used widely. Under the Heston settings, the volatility process is modelled as a mean-reverting process. This assumes that the volatility has a tendency to move towards its average over the time. If the current volatility is above the average level, then the volatility is expected to show a falling trend. If the current volatility is below the average level, then the volatility tends to develop upwards. In other words, with mean reversion it is less likely for the volatility to diverge or attain zero eventually. This is a typical characteristic that can be observed in the financial markets.

On top of that, the Heston model introduces a correlation between the returns and the volatility, meaning that the changes in the price level of the assets will impact on the volatility. This assumption is in accordance with the behaviour reflected in

the markets as well. For instance, volatility is usually anticipated to increase when decreasing in the asset price occurs, which is known as the leverage effect.

The Heston model thus provides a more realistic framework to describe the movements of the asset price and the correlated volatility by taking into account many of the aspects that are observed in the financial markets. What makes the Heston model even more attractive is the existence of closed form solutions for prices of plain vanilla European options. This property is particularly useful when calibrating the model.

Despite its tractability for certain options, the Heston model does not always yield analytical forms for other exotic options, especially for path-dependent options. Hence, alternative techniques are required for pricing purposes under the Heston model, among which Monte Carlo simulation is one of the most important and widely applicable schemes. The aim of this thesis is to develop an accurate and efficient numerical simulation method for the Heston model with applications in pricing challenging options when combined with the Monte Carlo approach.

1.1 The Heston stochastic volatility model

In this section, we give a brief review of the Heston stochastic volatility model and some of its properties.

The Heston model is expressed in the following form of a two-dimensional system:

$$\frac{dS_t}{S_t} = \mu\, dt + \sqrt{V_t}\left(\rho\, dW_t^1 + \sqrt{1-\rho^2}\, dW_t^2\right), \tag{1.1}$$

$$dV_t = \kappa\left(\theta - V_t\right)\, dt + \sigma\sqrt{V_t}\, dW_t^1, \tag{1.2}$$

where the component S characterises the dynamics of the stock price while the component V specifies the variances of its returns and W^1 and W^2 are two independent standard Brownian motions. The model parameters include the rate of return of the stock μ, the speed of mean reversion of the variance κ, the long-term average variance θ, the volatility of the variance σ and the instantaneous correlation be-

tween the return and the volatility ρ. Here, κ, θ, σ and typically also μ are positive constants with $\rho \in [-1, 1]$.

To complete the understanding of the motivation for the work carried out below, we first quote some analytical properties with regard to the Heston model. We start from the variance process governed by (1.2). First, the variance process follows a mean-reverting square-root Cox-Ingersoll-Ross (CIR) process (Cox, Ingersoll and Ross [18]). By the Yamada condition (Yamada and Watanabe [69]), we can verify that there is a unique strong solution for this equation, yet the explicit form of which is not available. However, we are able to find its transition probability analytically, which is given as a scaled noncentral chi-squared distribution. With the degrees of freedom for this process defined to be $\delta := 4\kappa\theta/\sigma^2$, we have the following proposition which can be found in Cox, Ingersoll and Ross [18] or Andersen [6].

Proposition 1.1.1

Conditional on the initial value $V_0 > 0$, V_t has a scaled noncentral chi-squared distribution

$$V_t = \frac{\sigma^2 \left(1 - \exp\left(-\kappa t\right)\right)}{4\kappa} \chi^2_\delta \left(\frac{4\kappa \exp\left(-\kappa t\right)}{\sigma^2 \left(1 - \exp\left(-\kappa t\right)\right)} V_0 \right) \tag{1.3}$$

for $t > 0$, where $\chi^2_\delta(\lambda)$ denotes a noncentral chi-squared random variable with degrees of freedom δ and noncentrality parameter λ.

This tells us that V_t is distributed as a constant $\sigma^2 \left(1 - \exp\left(-\kappa t\right)\right) / \left(4\kappa\right)$ multiplied by a noncentral chi-squared distribution with degrees of freedom δ and noncentrality parameter

$$\lambda := \frac{4\kappa \exp\left(-\kappa t\right)}{\sigma^2 \left(1 - \exp\left(-\kappa t\right)\right)} V_0$$

given V_0. The above law provides a way to exactly simulating the variance process from time 0 to t, see Scott [62], Glasserman [31], Broadie and Kaya [15] and Malham and Wiese [51] for details.

Second, the variance process is non-negative. In particular, the classical Feller boundary classification criteria leads to the proposition stated below on the bound-

ary behaviour; see Feller [27] and Karlin and Taylor [46].

Proposition 1.1.2

The variance process V_t has the following properties:

- *the zero boundary is attainable and strongly reflecting if $\delta < 2$;*
- *the zero boundary is unattainable if $\delta \geq 2$.*

Importantly, when the process hits zero, it will move away from it immediately to the positive domain. This phenomenon is referred to as strongly reflecting, meaning that the time spent by the process at the origin is zero, see Revuz and Yor [60].

Now we turn to the stock price process satisfying (1.1). By employing Itô's formula, the exact solution of (1.1) can be written as

$$S_t = S_0 \exp\left(\mu t - \frac{1}{2}\int_0^t V_s\, ds + \rho \int_0^t \sqrt{V_s}\, dW_s^1 + \sqrt{1-\rho^2}\int_0^t \sqrt{V_s}\, dW_s^2\right). \quad (1.4)$$

Integrating equation (1.2) which defines the variance process, we obtain

$$V_t - V_0 = \int_0^t \kappa\left(\theta - V_s\right)\, ds + \sigma \int_0^t \sqrt{V_s}\, dW_s^1.$$

This gives an alternative form for the integral of the square root of the variance process $\sqrt{V}$ with respect to the Brownian motion W^1 as

$$\int_0^t \sqrt{V_s}\, dW_s^1 = \frac{1}{\sigma}\left(V_t - V_0 - \int_0^t \kappa\left(\theta - V_s\right)\, ds\right) = \frac{V_t - V_0 - \kappa\theta t}{\sigma} + \frac{\kappa}{\sigma}\int_0^t V_s\, ds,$$

which depends on the values of V_0 and V_t and the time integrated variance $\int_0^t V_s\, ds$. Taking logarithms and substituting the previous results, (1.4) becomes

$$\log\frac{S_t}{S_0} = \mu t + \frac{\rho}{\sigma}\left(V_t - V_0 - \kappa\theta t\right) + \left(\frac{\rho\kappa}{\sigma} - \frac{1}{2}\right)\int_0^t V_s\, ds + \sqrt{1-\rho^2}\int_0^t \sqrt{V_s}\, dW_s^2.$$

Since the process V is independent of the Brownian motion W^2, the Itô integral $\int_0^t \sqrt{V_s}\, dW_s^2$ is normally distributed conditional on the trajectory generated by V. Then, the next proposition regarding the conditional distribution of the log return follows; see Broadie and Kaya [15], Andersen [6] or Glassermand and Kim [32].

Proposition 1.1.3

Assume V_0 is given. Then conditional on the variance process V_t at time t and its time integral $\int_0^t V_s\,ds$, the distribution of $\log(S_t/S_0)$ *is normal, i.e.*

$$\log\frac{S_t}{S_0} \sim \mathrm{N}\left(\mu t + \frac{\rho}{\sigma}\left(V_t - V_0 - \kappa\theta t\right) + \left(\frac{\rho\kappa}{\sigma} - \frac{1}{2}\right)\int_0^t V_s\,ds, \left(1-\rho^2\right)\int_0^t V_s\,ds\right). \tag{1.5}$$

Hence, an exact simulation for the stock price S_t given the initial conditions S_0 and V_0 is now reduced to sampling a conditional normal random variable given in (1.5) provided there is a way to sampling from the joint distribution $\left(V_t, \int_0^t V_s\,ds\right)$. As V_t can be simulated using the transition law in (1.3), it is clear that the main challenge becomes to design a tractable method for sampling from the conditional distribution of the time integral of the variance process V_s over the interval $[0,t]$ given its values at the endpoints V_0 and V_t, i.e.

$$\left(\int_0^t V_s\,ds \middle| V_0, V_t\right).$$

Once we have a mechanism for drawing samples for the stock price S_t, the Monte Carlo estimator $\hat{C}$ for a European call option price can be evaluated by taking the sample average of the simulated discounted payoff at maturity, i.e.

$$\hat{C} = \exp(-rT)\frac{1}{M}\sum_{i=1}^{M}\left(S_T^i - K\right)^+,$$

where M is the sample size, T is the maturity time, K is the strike price, r is the interest rate and S_T^i are independent samples for the terminal stock price for $i = 1, 2, \ldots, M$.

For pricing path-dependent options such as Asian options, the payoff functions will be depending on a series of simulated stock prices S_t at certain times. For example, we have the following price estimator $\hat{A}$ for an Asian call option with

discrete arithmetic average for the period $[0, T]$:

$$\hat{A} = \exp(-rT)\frac{1}{M}\sum_{i=1}^{M}\left(\frac{1}{N}\sum_{j=1}^{N} S_{t_j}^i - K\right)^+,$$

where the underlying asset price is monitored at the times $t_j = jT/N$ for $j = 1, 2, \ldots, N$ and $\mathbf{S}^i = \left(S_{t_1}^i, S_{t_2}^i, \ldots, S_{t_N}^i\right)$ are independent observations for the asset path for $i = 1, 2, \ldots, M$. Similarly, the Monte Carlo estimator $\hat{B}$ for the price of a digital double no touch barrier option with lower barrier level L and and upper barrier level U is given by

$$\hat{B} = \exp(-rT)\frac{1}{M}\sum_{i=1}^{M}\left(\prod_{j=1}^{N}\mathbf{1}_{\left\{L<S_{t_j}^i<U\right\}}\right),$$

where $\mathbf{1}_{\{L<S<U\}}$ is the indicator function. Such an option pays either zero or one unit of currency depending on whether the asset price has touched one of the barriers.

We end this section with the following analytical results for the price of a standard vanilla option under the Heston model. This result is based on Fourier inversion of the corresponding characteristic functions; see Heston [38], Lipton [49], Carr and Madan [16] and Kahl and Jäckel [45].

Proposition 1.1.4

The price of a European call option with maturity time T, strike price K and interest rate r is

$$C = \exp(-rT)\left(S_0 - \frac{K}{2\pi}\int_{-\infty}^{\infty}\frac{\exp\left(\left(\frac{1}{2} - \mathrm{i}k\right)\log\frac{S_0}{K} + \alpha(k) - \left(\frac{1}{4} + k^2\right)\beta(k)V_0\right)}{k^2 + \frac{1}{4}}\,dk\right),$$

where

$$\alpha(k) = -\frac{\kappa\theta}{\sigma^2}\left(\Psi_+(k)T + 2\log\frac{\Psi_-(k) + \Psi_+(k)\exp(-\zeta(k)T)}{2\zeta(k)}\right),$$

$$\beta(k) = -\frac{1 - \exp(-\zeta(k)T)}{\Psi_-(k) + \Psi_+(k)\exp(-\zeta(k)T)},$$

$$\Psi_\pm(k) = \zeta(k) \mp (\mathrm{i}k\rho\sigma + \hat{\kappa}),$$

$$\zeta(k) = \sqrt{k^2\sigma^2(1-\rho^2) + 2\mathrm{i}k\sigma\rho\hat{\kappa} + \hat{\kappa}^2 + \frac{\sigma^2}{4}},$$

$$\hat{\kappa} = \kappa - \frac{\rho\sigma}{2}.$$

The above proposition is useful for comparing different methods as the closed form solution for the European option price can serve as a benchmark. When evaluating this formula, numerical integration technique such as fast Fourier transform is a convenient way.

1.2 Literature review

Driven by the aim to investigate new numerical scheme for simulating the Heston model and pricing derivatives, we review a number of standard methods that exist in the literature in this section.

First of all, as mentioned earlier, explicit expressions for the prices of standard vanilla options are available under the Heston setting. These often take the form of Fourier transform methods expressed in terms of the corresponding characteristic functions, see Heston [38], Lipton [49], Carr and Madan [16] and Kahl and Jäckel [45].

Second, Monte Carlo simulation still serves as a popular way to handling exotic options, especially to pricing path-dependent options, where closed form solutions are unknown in general. Typically, continuous stochastic processes are approximated by paths simulated on discrete time grids. Often the Euler-Maruyama scheme is considered, which converges weakly with convergence rate one under certain regularity conditions; see Section 14.5 in Kloeden and Platen [47], or other standard higher-order discretization approaches such as the Milstein [54] and Itô-Taylor schemes introduced in Chapter 14 and 15 in Kloeden and Platen [47]; see Section 6.2 in Glasserman [31] as well. However, these conditions do not hold in the Heston model, which will be discussed in detail below.

Discretization schemes such as those have several drawbacks for the Heston model. The first issue is that the probability of the discretised variance process

becoming negative is nonzero, which will bring considerable biases to the simulation estimators. Correction techniques such as absorption and reflection are designed to overcome this problem, see Gatheral [28], Bossy and Diop [12] and Higham and Mao [39]. Lord, Koekkoek and Van Dijk [50] unify a large number of traditional correction techniques and design a new scheme, the full truncation method, which seems to perform well in many situations. Taking advantage of the qualitative properties of the true distributions, Andersen [6] proposes two new time-discretization algorithms based on moment-matching strategies, namely the truncated Gaussian scheme and the quadratic-exponential scheme. These positivity-preserving schemes are reported to have substantial improvements in efficiency and robustness over other existing methods; see Andersen [6], Lord, Koekkoek and Van Dijk [50] and Haastrecht and Pelsser [66].

The second issue is related to convergence, which requires the drift and diffusion coefficients to be globally Lipschitz, see Kloeden and Platen [47]. However, the square root functions embedded in the Heston model are not Lipschitz around zero. Thus, convergence of these discretization schemes is difficult to establish; see Glasserman [31] and Andersen [6]. Recently, Altmayer and Neuenkirch [5] have studied the weak convergence rate for a numerical scheme under the Heston model, which consists of an Euler scheme and a drift-implicit Milstein scheme (Kahl, Günther and Rossberg [44]) for the log-asset price and the volatility, respectively. With mild assumptions for the payoff functions, the scheme reaches weak order one in the case of unattainable boundaries when the Feller ratio is greater than two. Neuenkirch and Szpruch [56] consider the one-dimensional CIR process restricted to the regime where the zero boundary is not accessible and show strong convergence with order one for the backward (or drift-implicit) Euler-Maruyama scheme of Alfonsi [3] applied to the SDE with constant diffusion coefficient after Lamperti transformation. Cozma and Reisinger [21] prove that the full truncation scheme in Lord, Koekkoek and Van Dijk [50] for the CIR process converges strongly with order $1/2$ in L^p. This result is established under the assumptions on the model parameters such that the boundary point is unattainable and the Feller ratio is above three. More general cases with accessible boundaries are discussed in Hutzenthaler, Jentzen and Noll [41], where they derive a positive strong convergence rate for the drift-implicit Euler

approximation (Alfonsi [3]) when the Feller ratio is bigger than 1/2. Hefter and Herzwurm [36] propose a truncated Milstein scheme, which achieves strong convergence at a polynomial rate for the full parameter range. Hefter and Jentzen [37] show that the time stepping methods for the CIR process based on equidistant evaluations of the underlying Brownian motions, such as the implicit or explicit Milstein or Euler scheme, may have an arbitrarily slow convergence rate in the strong sense. In fact, the strong convergence order for each such method is at most $\delta/2$, where δ is the degrees of freedom for the CIR process. See Alfonsi [4], Chassagneux, Jacquier and Mihaylov [17], Bossy and Olivero [13], Cozma, Mariapragassam and Reisinger [19] for more discussions on the convergence of the discretised univariate variance process.

Apart from discretization schemes, there are also (almost) exact simulation methods based on the exact conditional distributions of the stock price and variance processes stated in Proposition 1.1.1 and Proposition 1.1.3, respectively. Broadie and Kaya [15] take this approach to generate sample variance and stock price. They apply an acceptance-rejection method to the noncentral chi-square sampling for the variance process. Malham and Wiese [51] propose an exact and robust acceptance-rejection method and a high-accuracy direct inversion method for the simulation of the generalised Gaussian distribution, which are then applied to the noncentral chi-squared sampling. Haastrecht and Pelsser [66] focus on the efficient approximation of the variance. They explore the features of the distribution for the variance process and suggest a cache for its inverse distribution functions, leading to an almost exact simulation scheme.

To realise the stock price, the key task of Broadie and Kaya [15] is to sample from the time integrated variance conditional at the endpoints, i.e. $\left(\int_0^t V_s\, ds \middle| V_0, V_t\right)$. They build on the results (2.m) and (6.d) in Pitman and Yor [57] to derive the explicit form for the corresponding characteristic function. Fourier inversion techniques in conjunction with the trapezoidal rule are applied to numerically evaluate the probability distribution function. This is followed by inverse transform sampling to simulate the value of the above integral. Their numerical results imply that the proposed method has a faster convergence rate compared to the Euler scheme with bias-free simulation.

Because of the dependence on V_0 and V_t , Broadie and Kaya [15] compute the characteristic function for each step and path in the Monte Carlo simulation. At the expense of a small bias, Smith [64] presents an approximation to the characteristic function, which makes it possible to precalculate and store the values of the characteristic function for all the points required in advance. Glasserman and Kim [32] provide another sampling method for the time integrated conditional variance, which relies on an explicit representation as infinite sums and mixtures of gamma random variables. When combined with the exact simulation method suggested by Broadie and Kaya [15], their method is highly effective in terms of both accuracy and computational speed for pricing non-path-dependent options across a full range of model parameter values.

Other approximation methods such as the Fokker-Planck or Kolmogorov forward equation method are also available. This method is based on a partial differential equation describing the time evolution of the joint probability density function of the log return and the variance with initial and boundary conditions, which is often solved in the form of Fourier and inverse Laplace transforms (Drăgulescu and Yakovenko [23] and Fang and Oosterlee [26]) or by alternating direction implicit time discretization schemes (Haentjens and In 't Hout [35], Wyns and Du Toit [67] and Wyns and In 't Hout [68]) and the finite element method with a backward differential formula (Cozma, Mariapragassam and Reisinger [20]).

Motivated by the decomposition of squared Bessel bridges in Pitman and Yor [57] and Glasserman and Kim [32], we focus on developing a new series expansion for the above integral in this thesis. After applying a measure transformation, we represent this quantity by a linear combination of double infinite weighted sums of particular independent random variables and establish a relationship between the probability density functions for the distributions of the conditional integral under the new and original probability measures. For practical implementation of those series, direct inversion algorithms are used combined with an acceptance-rejection method for tracing back to the original measure. The inverse distribution functions are approximated by Chebyshev polynomials of a uniform error of order 10^{-12}. To predetermine and cache the coefficients of the polynomials outside the Monte Carlo simulation loop, we develop an asymptotic expansion up to all orders for the relevant

distribution function through the steepest descent method.

1.3 Outline

This thesis is structured as follows.

Serving as a preparation work, Chapter 2 contains a comprehensive discussion on the relevant concepts, properties and theorems that will be revisited in subsequent chapters.

In Chapter 3, we present the new series representation for the time integrated conditional variance. We transform the CIR variance process to a special case, i.e. a squared Bessel process through change of measure, whence the integral can be decomposed using its properties under the new probability measure. A relation between the distributions of the integral with respect to these two measures is also established there.

Chapter 4 addresses the simulation processes for the conditional integral and the Heston model. Specifically, we apply direct inversion and acceptance-rejection methods to realise the theorems developed in Chapter 3. To improve the computational speed, these algorithms are constructed to allow for caching purposes.

In Chapter 5, we provide the framework for completing the main step in direct inversion, i.e. approximations of the inverse distribution functions. In fact, starting with the characteristic functions, we detail the derivation of the asymptotic series expansion for the distribution function. Based upon that, we approximate the inverse functions by Chebyshev polynomials with coefficients computed and tabulated using the limiting behaviour of the distribution functions.

In Chapter 6, we carry out empirical studies by sampling the conditional integral using four typical sets of model parameters for the Heston model. We also apply the new method to pricing some challenging European call options and two path-dependent derivatives, one Asian call option and one double no touch barrier option. The results are compared with that of Glasserman and Kim [32] for the consideration of both accuracy and efficiency. To further examine the performance of the new

method, we also benchmark it against Lord, Koekkoek and Van Dijk's [50] full truncation scheme, which is a standard time stepping simulation method.

Conclusions are drawn in Chapter 7.

Chapter 2

Preliminaries

In this chapter, we set up a collection of notations, definitions and lemmas that will be fundamental to our analysis throughout the thesis. Specifically, we introduce the concepts and properties related to asymptotic series, squared Bessel bridge and Chebyshev polynomial approximation.

2.1 Asymptotic expansion

In Chapter 5, we are concerned with the study of the limiting behaviour of certain functions when their arguments approach some fixed values, such as zero and infinity. This motivates the following introduction of the so-called order relations; see Bleistein and Handelsman [11, Chapter 1.2] and Ablowitz and Fokas [1, Chapter 6.1].

Definition 2.1.1

Suppose that $f(z)$ and $g(z)$ are two functions of z defined on some domain D of the complex plane $\mathbb{C}$ with its closure $\bar{D}$ containing z_0. Then we write

$$f(z) = \mathrm{O}(g(z)), \quad as \quad z \to z_0$$

if there exist constants $K, \delta > 0$ such that

$$|f(z)| \leq K|g(z)|, \quad for \quad z \in D \cap \{z : 0 < |z - z_0| < \delta\}.$$

The preceding definition implies that $|f(z)/g(z)|$ is bounded in a neighbourhood of z_0 except z_0, where $g(z)$ is nonzero. Similarly, we have the following when the point z_0 is at infinity.

Definition 2.1.2
Suppose that $f(z)$ and $g(z)$ are two functions of z defined on an unbounded domain D of the complex plane $\mathbb{C}$. Then we write

$$f(z) = \mathrm{O}(g(z)), \quad as \quad z \to \infty$$

if there exists a constant $K > 0$ such that

$$|f(z)| \leq K|g(z)|, \quad for \quad z \in D \cap \{z : |z| > K\}.$$

The above statements claim that $f(z)$ is bounded by a fixed multiple of $|g(z)|$. This can be extended to the case when $f(z)$ is bounded by any multiple of $|g(z)|$ for $z \in D$ that is close enough to z_0, leading to the following definitions.

Definition 2.1.3
Suppose that $f(z)$ and $g(z)$ are two functions of z defined on some domain D of the complex plane $\mathbb{C}$ with its closure $\bar{D}$ containing z_0. Then we write

$$f(z) = \mathrm{o}(g(z)), \quad as \quad z \to z_0$$

if for any $\epsilon > 0$, there exists a constant $\delta > 0$ such that

$$|f(z)| \leq \epsilon|g(z)|, \quad for \quad z \in D \cap \{z : 0 < |z - z_0| < \delta\}.$$

This equivalently means that the limit of $f(z)/g(z)$ is zero as z approaches z_0 provided $g(z)$ is nonzero in a neighbourhood of z_0 except z_0. Notice that an alternative notation for $f(z) = \mathrm{o}(g(z))$ as $z \to z_0$ is

$$f(z) \ll g(z), \quad \text{as} \quad z \to z_0.$$

Similar order relation near infinity is defined as follows.

Definition 2.1.4

Suppose that $f(z)$ and $g(z)$ are two functions of z defined on an unbounded domain D of the complex plane $\mathbb{C}$. Then we write

$$f(z) = \mathrm{o}(g(z)), \quad as \quad z \to \infty$$

if for any $\epsilon > 0$, there exists a constant $M > 0$ such that

$$|f(z)| \leq \epsilon |g(z)|, \quad for \quad z \in D \cap \{z : |z| > M\}.$$

We are now ready to introduce another relative behaviour of two functions given below.

Definition 2.1.5

Suppose that $f(z)$ and $g(z)$ are two functions of z defined on some domain D of the complex plane $\mathbb{C}$. If

$$f(z) = g(z) + \mathrm{o}(g(z)), \quad as \quad z \to z_0,$$

then we write

$$f(z) \sim g(z), \quad as \quad z \to z_0.$$

Equivalently, this definition indicates that $f(z)/g(z)$ tends to one as $z \to z_0$ provided $g(z)$ does not vanish at nearby points of z_0.

The above order relations allow us to introduce the general structures of asymptotic sequences and expansions given in Definition 2.1.6 and Definition 2.1.7 respectively, which can be found in Bender and Orszag [8, Chapter 3.5] and Miller [53, Chapter 1.3] as well.

Definition 2.1.6

Let $\{\phi_n(z)\}_{n=0}^{\infty}$ be a sequence of functions defined on some domain D of the complex plane $\mathbb{C}$. Then $\{\phi_n(z)\}_{n=0}^{\infty}$ is said to be an asymptotic sequence as $z \to z_0$ in D if

for all $n \geq 0$,

$$\phi_{n+1}(z) = \mathrm{o}(\phi_n(z)), \quad as \quad z \to z_0.$$

Definition 2.1.7

Let $\{\phi_n(z)\}_{n=0}^{\infty}$ *be an asymptotic sequence of functions as* $z \to z_0$ *in* D *and* $\{a_n\}_{n=0}^{\infty}$ *be a sequence of complex constants. We say that the infinite series*

$$\sum_{n=0}^{\infty} a_n \phi_n(z)$$

is an asymptotic expansion (or asymptotic approximation) of $f(z)$ *as* $z \to z_0$, *denoted by*

$$f(z) \sim \sum_{n=0}^{\infty} a_n \phi_n(z), \quad as \quad z \to z_0,$$

if for each N,

$$f(z) - \sum_{n=0}^{N} a_n \phi_n(z) = \mathrm{o}(\phi_N(z)), \quad as \quad z \to z_0.$$

Hence, an asymptotic expansion is not necessarily convergent. It only requires that the remainder

$$R_N(z) \coloneqq f(z) - \sum_{n=0}^{N} a_n \phi_n(z)$$

decays faster than the last retained term $\phi_N(z)$ as $z \to z_0$ for fixed N, but needs not go to zero as $N \to \infty$ for fixed z. In particular, the partial sum $\sum_{n=0}^{N} a_n \phi_n(z)$ gives a good approximation to $f(z)$ if z is sufficiently close to z_0, however, the accuracy of which will not always increase as N increases.

2.2 Squared Bessel bridge

Since much of our work is based upon the squared Bessel process and bridge, we outline a brief discussion on the related definitions and properties in this section. For preparation, we start with the definition stated below for the Bessel random variable; see Yuan and Kalbfleisch [70, Section 1].

Definition 2.2.1

A discrete random variable X is said to be a Bessel random variable with parameters $\nu > -1$ and $z > 0$ if, for $n = 0, 1, 2, \ldots$, the probability mass function of X is given by

$$\mathbb{P}(X = n) = \frac{1}{I_v(z)\, n!\Gamma(n + \nu + 1)} \left(\frac{z}{2}\right)^{2n+\nu},$$

where $\Gamma(\alpha)$ is the gamma function and $I_\nu(z)$ is the modified Bessel function of the first kind given by

$$I_\nu(z) = \left(\frac{z}{2}\right)^{\nu} \sum_{k=0}^{\infty} \frac{1}{k!\Gamma(k + \nu + 1)} \left(\frac{z}{2}\right)^{2k}$$

for $z > 0$ and $\nu > -1$.

We are now ready to define the squared Bessel process and bridge.

Definition 2.2.2

For any real $\delta \geq 0$ and $x \geq 0$, a process A is called a δ-dimensional squared Bessel process starting at x if it is the unique strong solution of the stochastic differential equation

$$dA_t = \delta\, dt + 2\sqrt{A_t}\, dW_t$$

with $A_0 = x$ and a standard Brownian motion W.

A description of the preceding definition can be found in for example Pitman and Yor [57, Section 1] or Revuz and Yor [60, Chapter XI Definition (1.1)]. Note that the squared Bessel process is a reduced case of the squared Ornstein-Uhlenbeck

(OU) process defined below; see Pitman and Yor [57, Section 1] and Göing-Jaeschke and Yor [33, Section 2].

Definition 2.2.3

For any $\delta, x \geq 0$ and $a \in \mathbb{R}$, a process A is called a δ-dimensional squared Ornstein-Uhlenbeck (OU) process starting at x with parameter a if it is the unique strong solution of the stochastic differential equation

$$dA_t = (\delta + 2aA_t)\, dt + 2\sqrt{A_t}\, dW_t$$

with $A_0 = x$ and a standard Brownian motion W.

Clearly, with $a = 0$ the squared OU process becomes a squared Bessel process. In fact, Pitman and Yor [57] have suggested two methods for reducing the family of squared OU processes to the case of squared Bessel process, namely transformation of space-time (Theorem (6.1)) and change of law (Theorem (6.3)). We will make use of the second approach in this thesis with formula presented in the next lemma.

Lemma 2.2.4

Suppose that under the probability measure $\mathbb{Q}$, A is a δ-dimensional squared OU process with parameter a, i.e.

$$dA_t = (\delta + 2aA_t)\, dt + 2\sqrt{A_t}\, dW_t^{\mathbb{Q}},$$

where $W^{\mathbb{Q}}$ is a standard Brownian motion under $\mathbb{Q}$. Under the probability measure $\mathbb{P}$, A is a δ-dimensional squared Bessel process, i.e.

$$dA_t = \delta\, dt + 2\sqrt{A_t}\, dW_t^{\mathbb{P}},$$

where $W^{\mathbb{P}}$ is a standard Brownian motion under $\mathbb{P}$. Then, we have

$$\frac{d\mathbb{Q}}{d\mathbb{P}} = \exp\left(\frac{a}{2}\left(A_t - A_0 - \delta t\right) - \frac{a^2}{2}\int_0^t A_s\, ds\right).$$

Let us consider the conditional law of the squared Bessel process A, which leads to the definition for the squared Bessel bridge.

Definition 2.2.5

Suppose that A is a δ-dimensional squared Bessel process starting at x. For $\delta, x, y \geq 0$, a δ-dimensional squared Bessel bridge from x to y over the time interval $[0,1]$, denoted by $A^{\delta,1}_{x,y} = \left\{A^{\delta,1}_{x,y}(s)\right\}_{0\leq s\leq 1}$, is the stochastic process A_s for $0 \leq s \leq 1$ conditioned on $A_1 = y$, i.e.

$$(A_s, 0 \leq s \leq 1 | A_0 = x, A_1 = y).$$

A more rigorous definition is made by Pitman and Yor [57, Section 5], who treat the conditional distribution as a probability defined on the space $\mathrm{C}([0,1];[0,\infty))$ with weak continuity in y wherever possible. Similarly, the definition can be generalised to that of a squared OU bridge.

Definition 2.2.6

Suppose that A is a δ-dimensional squared OU process starting at x with parameter a. For $\delta, x, y \geq 0$, a δ-dimensional squared OU bridge from x to y over the time interval $[0,1]$, denoted by ${}^{a}A^{\delta,1}_{x,y} = \left\{{}^{a}A^{\delta,1}_{x,y}(s)\right\}_{0\leq s\leq 1}$, is the stochastic process A_s for $0 \leq s \leq 1$ conditioned on $A_1 = y$, i.e.

$$(A_s, 0 \leq s \leq 1 | A_0 = x, A_1 = y).$$

We are interested in the integration form of a squared Bessel bridge, i.e.

$$\int_0^1 A^{\delta,1}_{x,y}(s)\, ds.$$

The lemma below summarises its Laplace transform. Detailed proof is derived in Revuz and Yor [60, Chapter XI Corollary (3.3)] and for a more general case in Pitman and Yor [57, formula (2.m)].

Lemma 2.2.7

For any $b \geq 0$, the Laplace transform of $\int_0^1 A_{x,y}^{\delta,1}(s)\, ds$ is given by

$$\mathbb{E}\left[\exp\left(-b\int_0^1 A_{x,y}^{\delta,1}(s)\, ds\right)\right] = \frac{\sqrt{2b}}{\sinh\sqrt{2b}}\exp\left(\frac{x+y}{2}\left(1-\sqrt{2b}\coth\sqrt{2b}\right)\right)\frac{I_\nu\left(\frac{\sqrt{2bz}}{\sinh\sqrt{2b}}\right)}{I_\nu\left(\sqrt{z}\right)}, \tag{2.1}$$

where $\nu = \delta/2 - 1$ and $z = xy$. In particular, we have

$$\mathbb{E}\left[\exp\left(-b\int_0^1 A_{x,0}^{\delta,1}(s)\, ds\right)\right] = \left(\frac{\sqrt{2b}}{\sinh\sqrt{2b}}\right)^{\delta/2}\exp\left(\frac{x}{2}\left(1-\sqrt{2b}\coth\sqrt{2b}\right)\right). \tag{2.2}$$

The above Laplace transforms are expressed in a product of several terms, which suggest there may exist an interesting decomposition for the squared Bessel bridge. Indeed, Pitman and Yor [57] have found such a decomposition; see Theorem 5.8. Inspired by Glasserman and Kim [32, Proof of Theorem 2.2], we apply an additivity property (Shiga and Watanabe [63, Theorem 1.2]) and time reversal (Pitman and Yor [57, Section (5.2)]) to the squared Bessel bridges, leading to the following alternative form for the decomposition.

Lemma 2.2.8

A δ-dimensional squared Bessel bridge $A_{x,y}^{\delta,1}$ for $\delta, x, y \geq 0$ admits the following decomposition

$$A_{x,y}^{\delta,1} \overset{d}{=} A_{x+y,0}^{0,1} + A_{0,0}^{\delta,1} + \sum_{j=1}^{\eta}\left(A_{0,0}^{4,1}\right)_j,$$

where the processes $\left(A_{0,0}^{4,1}\right)_j$ are independent copies of $A_{0,0}^{4,1}$ for any $1 \leq j \leq \eta$, $A_{x+y,0}^{0,1}$, $A_{0,0}^{\delta,1}$ and $A_{0,0}^{4,1}$ are independent, η is an independent Bessel random variable with parameters ν and $\sqrt{z}$.

Next, we introduce two families of random variables S^h and C^h with infinitely divisible distributions, which arise frequently in the study of Bessel processes. Their Laplace transforms, associated with the hyperbolic functions sinh and cosh, will be repeatedly revisited in later discussions. Assume that $\Gamma_{h,n}$ are independent gamma

random variables with shape parameter $h > 0$ and rate parameter 1 for $n \geq 1$. Let S^h and C^h be random variables such that

$$S^h := \frac{2}{\pi^2} \sum_{n=1}^{\infty} \frac{\Gamma_{h,n}}{n^2},$$

$$C^h := \frac{2}{\pi^2} \sum_{n=1}^{\infty} \frac{\Gamma_{h,n}}{\left(n - \frac{1}{2}\right)^2}.$$

Then, their Laplace transforms are reported in the lemma as follows.

Lemma 2.2.9

For any $b \geq 0$, the random variables S^h and C^h have the Laplace transforms

$$\mathbb{E}\left[\exp\left(-bS^h\right)\right] = \left(\frac{\sqrt{2b}}{\sinh\sqrt{2b}}\right)^h,$$

$$\mathbb{E}\left[\exp\left(-bC^h\right)\right] = \left(\frac{1}{\cosh\sqrt{2b}}\right)^h.$$

Except for the Laplace transforms, Biane, Pitman and Yor [9, Section 3] have presented a number of other characterisations concerning the probability laws of S^h and C^h, including their Lévy densities, probability densities, reciprocal relations, moments and Mellin transforms with special emphasis on the cases $h = 1$ and $h = 2$; see Pitman and Yor [58] as well.

The last lemma of this section specifies the relationship between the Laplace transforms for the integral of the squared Bessel bridge and squared OU bridge. This result is adopted in both Broadie and Kaya [15, Proof of formula (13)] and Glasserman and Kim [32, Proof of Lemma 2.4] following from the law of changing the squared Bessel bridge to the squared OU bridge in Pitman and Yor [57, formula (6.d)], which is also a direct consequence of Lemma 2.2.4.

Lemma 2.2.10

For any $b \geq 0$, we have

$$\mathbb{E}^Q\left[\exp\left(-b\int_0^1 {}^a A_{x,y}^{\delta,1}(s)\, ds\right)\right] = \frac{\mathbb{E}^P\left[\exp\left(-\left(b + \frac{a^2}{2}\right)\int_0^1 A_{x,y}^{\delta,1}(s)\, ds\right)\right]}{\mathbb{E}^P\left[\exp\left(-\frac{a^2}{2}\int_0^1 A_{x,y}^{\delta,1}(s)\, ds\right)\right]},$$

where ${}^{a}A^{\delta,1}_{x,y}$ *and* $A^{\delta,1}_{x,y}$ *are a* δ*-dimensional squared OU bridge with parameter* a *under the probability measure* $\mathbb{Q}$ *and a* δ*-dimensional squared Bessel bridge under the probability measure* $\mathbb{P}$*, respectively.*

2.3 Chebyshev polynomial approximation

The simulation of the time integrated conditional variance is based on direct inversion sampling, where the complicated inverse distribution functions are approximated by some simpler functions, such as polynomials. Chebyshev polynomial approximation is a powerful technique in evaluating smooth functions as it is nearly optimal in terms of smallest maximum deviation from the original function. We give a overview of the relevant definitions and lemmas in this section. The definition for Chebyshev polynomials is given as follows; see Press *et al.* [59, Chapter 5.8].

Definition 2.3.1
For $n = 0, 1, 2, \ldots$*, the Chebyshev polynomial of degree* n*, denoted by* $T_n(x)$*, is defined on the interval* $x \in [-1, 1]$ *as*

$$T_n(x) = \cos(n \arccos x).$$

For a detailed summary of their properties and proofs, see for instance Gil, Segura and Temme [30, Chapter 3.3] and Arfken and Weber [7, Chapter 13.3]. Here, we quote propositions of their zeros and orthogonality relation, which are important for evaluation of the approximations.

Proposition 2.3.2
The polynomial $T_n(x)$ *has* n *zeros* x_k *for* $k = 0, 1, \ldots, n-1$ *in the interval* $[-1, 1]$ *given by*

$$x_k = \cos\left(\frac{\pi\left(k + \frac{1}{2}\right)}{n}\right).$$

Proposition 2.3.3

The Chebyshev polynomials satisfy the orthogonality relation

$$\sum_{k=0}^{n-1} T_i(x_k)\, T_j(x_k) = \begin{cases} 0, & i \neq j, \\ \frac{n}{2}, & i = j \neq 0, \\ n, & i = j = 0, \end{cases}$$

for $i, j < n$, where x_k, $k = 0, 1, \ldots, n-1$, are the n zeros of $T_n(x)$.

Using the properties above, we can now construct the Chebyshev polynomial approximation.

Definition 2.3.4

For arbitrary function $f(x)$ defined in the interval $[-1, 1]$, a degree N Chebyshev polynomial approximation $f^N(x)$ takes the form

$$f(x) \approx f^N(x) \coloneqq c_0 T_0(x) + c_1 T_1(x) + \cdots + c_N T_N(x) - \frac{1}{2} c_0, \tag{2.3}$$

where the $N+1$ coefficients c_j, $j = 0, 1, \ldots, N$, can be computed by

$$c_j = \frac{2}{N+1} \sum_{k=0}^{N} f(x_k)\, T_j(x_k)$$

with x_k denoting the $N+1$ zeros of $T_{N+1}(x)$ for $k = 0, 1, \ldots, N$.

It should be mentioned that the previous approximation is restricted to functions with domain $[-1, 1]$. However, it is certain that this approximation can be extended to allow the range of functions $f(x)$ being considered to be the interval with arbitrary lower and upper limits a and b, respectively, as long as appropriate scaling factors are applied. Specifically, by introducing the new variable y with

$$y \coloneqq \frac{x - \frac{1}{2}(b+a)}{\frac{1}{2}(b-a)},$$

the function $f(x)$ becomes

$$f(x) = f\left(\frac{b-a}{2}y + \frac{b+a}{2}\right) \coloneqq g(y)$$

with $y \in [-1, 1]$. Then, we approximate the function $g(y)$ by a Chebyshev polynomial in y.

Suppose that we have now computed the Chebyshev coefficients c_j, $j = 0, 1, \ldots, N$. To implement the Chebyshev polynomial approximation (2.3), it is better to employ Clenshaw's recurrence method without the need to compute every Chebyshev polynomials $T_j(x)$ for $j = 0, 1, \ldots, N$ explicitly. This approach turns out to be an efficient way to determine a sum involving known coefficients multiplied by functions which obey some recurrence relations, see Press *et al.* [59, Chapter 5.8 formula (5.8.11)].

Lemma 2.3.5

Clenshaw's recurrence formula to evaluate the the Chebyshev polynomial approximation $f^N(x)$ of degree N is

$$\begin{aligned} d_{N+2} &\equiv d_{N+1} \equiv 0, \\ d_j &= 2xd_{j+1} - d_{j+2} + c_j, \qquad j = N, N-1, \ldots, 1 \\ f^N(x) &\equiv d_0 = xd_1 - d_2 + \frac{1}{2}c_0 \end{aligned}$$

with Chebyshev coefficients c_j, $j = 0, 1, \ldots, N$ computed in advance.

Chapter 3

Time integrated conditional variance

In this chapter, we propose a new method for the realisation of the conditional integral of the variance process V_s over the time interval $[0, t]$ given its levels at the endpoints, i.e.

$$\left(\int_0^t V_s \, ds \middle| V_0, V_t \right).$$

We first transform the variance process V to a squared Bessel process by rescaling of time and change of measure. Then, the time integrated conditional variance can be expressed in the form of an integration of a squared Bessel bridge under the new probability measure, which, hence, can be decomposed into the sum of some independent random variables by the decomposition of Pitman and Yor [57] and Glasserman and Kim [32] on the squared Bessel bridge. For each element in the decomposition, we identify an alternative representation in terms of infinite series with the same distribution through Laplace transforms. To trace back to the original measure, we establish a connection between the probability density functions for the distribution of the integral with respect to the original and new measures. This will provide a basis for sampling our target, i.e. the conditional integral of the variance process, under the original measure.

3.1 Time and measure transformations

This section gives the details for the preparation work carried out before deriving the main results.

Recall that the variance process V follows

$$dV_t = \kappa\left(\theta - V_t\right)\, dt + \sigma\sqrt{V_t}\, dW_t^1.$$

To transform the above CIR process to a squared Bessel process, we proceed following the two steps outlined below.

First, define a new process $\tilde{A}$ by time-rescaling

$$\tilde{A}_t = V_{\frac{4t}{\sigma^2}}.$$

Then, $\tilde{A}$ satisfies the following stochastic differential equations

$$\begin{aligned} d\tilde{A}_t &= dV_{\frac{4t}{\sigma^2}} \\ &= \kappa\left(\theta - V_{\frac{4t}{\sigma^2}}\right)\, d\left(\frac{4t}{\sigma^2}\right) + \sigma\sqrt{V_{\frac{4t}{\sigma^2}}}\, dW^1_{\frac{4t}{\sigma^2}} \\ &= \frac{4}{\sigma^2}\kappa\left(\theta - \tilde{A}_t\right)\, dt + 2\sqrt{\tilde{A}_t}\left(\frac{\sigma}{2}\, dW^1_{\frac{4t}{\sigma^2}}\right) \\ &= \left(\delta - 2q\tilde{A}_t\right)\, dt + 2\sqrt{\tilde{A}_t}\, d\tilde{W}_t^1, \end{aligned}$$

where $\delta \coloneqq 4\kappa\theta/\sigma^2$, $q \coloneqq 2\kappa/\sigma^2$ and $\tilde{W}_t^1 \coloneqq \sigma W^1_{4t/\sigma^2}/2$ becomes a standard Brownian motion. Now, $\tilde{A}$ is a squared OU process with parameter $-q$. To further reduce the rescaled variance $\tilde{A}$ to a squared Bessel process, we apply a measure transformation. Suppose that the original model is established under the probability measure $\mathbb{Q}$, meaning that our target is to simulate from the distribution of the random variable

$$\left(\int_0^t V_s\, ds \middle| V_0 = v_0, V_t = v_t\right) = \left(\frac{4}{\sigma^2}\int_0^\tau \tilde{A}_s\, ds \middle| \tilde{A}_0 = a_0, \tilde{A}_\tau = a_\tau\right)$$

under $\mathbb{Q}$ with $\tau = \sigma^2 t/4$, $a_0 = v_0$ and $a_\tau = v_t$.

Second, we introduce a new probability measure $\mathbb{P}$ such that

$$\frac{d\mathbb{P}}{d\mathbb{Q}} = \exp\left(q\int_0^\tau \sqrt{\tilde{A}_s}\, d\tilde{W}_s^1 - \frac{q^2}{2}\int_0^\tau \tilde{A}_s\, ds\right). \tag{3.1}$$

According to the change of law formula presented in Lemma 2.2.4, the rescaled process $\tilde{A}$ becomes a δ-dimensional squared Bessel process under $\mathbb{P}$ with dynamics

$$d\tilde{A}_t = \delta\, dt + 2\sqrt{\tilde{A}_t}\, dW_t^P, \tag{3.2}$$

where by Glasserman and Kim [32], W^P is a standard Brownian motion under $\mathbb{P}$ satisfying $W_t^P = \tilde{W}_t^1 - \int_0^t q\sqrt{\tilde{A}_s}\, ds$.

Hence with these replacements, our objective is to sample from the time integral of a squared Bessel process $\tilde{A}$ given its values at the endpoints under the new probability measure $\mathbb{P}$ and to find out how the distributions for the conditional integral under the original and new measures are related to each other. For convenience, we denote the conditional integral by I, i.e.

$$I = \left(\int_0^\tau \tilde{A}_s\, ds \middle| \tilde{A}_0 = a_0, \tilde{A}_\tau = a_\tau\right).$$

3.2 Series expansion of time integrated squared Bessel bridges

Working on the probability measure $\mathbb{P}$, we put forward a new representation for the distribution of the time integrated conditional variance I and provide an explicit analysis in this section. Indeed, the new representation, based on decomposing the squared Bessel bridge, is formed as double infinite weighted sums of certain independent random variables. We state the main theorem below followed by its proof.

Theorem 3.2.1

Under the new probability measure $\mathbb{P}$, the conditional integral of the rescaled variance process $\tilde{A}$ is equivalent in distribution to the sum of three infinite series of random

variables

$$I = \left(\int_0^\tau \tilde{A}_s \, ds \middle| \tilde{A}_0 = a_0, \tilde{A}_\tau = a_\tau \right) \stackrel{d}{=} X_1 + X_2 + \sum_{j=1}^{\eta} Z_j,$$

where X_1, X_2, η, Z_1, Z_2, ... *are mutually independent, and* η *is a Bessel random variable with parameters* $\nu = \delta/2 - 1$ *and* $z = \sqrt{a_0 a_\tau}/\tau$, *i.e.* $\eta \sim Bessel(\nu, z)$. *Moreover,* X_1, X_2, Z_1, Z_2, ... *admit the following representations:*

(*a*) *We have*

$$X_1 \stackrel{d}{=} \sum_{n=0}^{\infty} \frac{\tau^2}{4^n} \sum_{k=1}^{P_n} S_{n,k},$$

where for $n = 0, 1, \ldots$, *the* P_n *are independent Poisson random variables with mean* $(a_0 + a_\tau) 2^{n-1}/\tau$ *and for* $k = 1, 2, \ldots, P_n$, *the* $S_{n,k}$ *are independent copies of the random variable* $S \coloneqq (2/\pi^2) \sum_{l=1}^{\infty} \epsilon_l / l^2$ *and* $\epsilon_l \sim Exp(1)$ *are independent exponential random variables for* $l = 1, 2, \ldots$;

(*b*) *Further we have*

$$X_2 \stackrel{d}{=} \sum_{n=1}^{\infty} \frac{\tau^2}{4^n} C_n^{\delta/2},$$

where for $n = 1, 2, \ldots$, *the* $C_n^{\delta/2}$ *are independent copies of the random variable* $C^{\delta/2} \coloneqq (2/\pi^2) \sum_{l=1}^{\infty} \Gamma_{\delta/2,l} / (l - 1/2)^2$ *and* $\Gamma_{\delta/2,l} \sim Gamma(\delta/2, 1)$ *are independent gamma random variables for* $l = 1, 2, \ldots$;

(*c*) *And also we have the* Z_j, $j = 1, 2, \ldots, \eta$, *which are independent copies of the random variable* Z *such that*

$$Z \stackrel{d}{=} \sum_{n=1}^{\infty} \frac{\tau^2}{4^n} C'_n,$$

where for $n = 1, 2, \ldots$, *the* C'_n *are independent copies of the random variable* $C^2 \coloneqq (2/\pi^2) \sum_{l=1}^{\infty} \Gamma_{2,l} / (l - 1/2)^2$ *and* $\Gamma_{2,l} \sim Gamma(2, 1)$ *are independent gamma random variables for* $l = 1, 2, \ldots$.

Proof. Instead of taking the integration from 0 to τ, we separate the time variable τ and fix the range to the unit interval $[0, 1]$ for easier computation. For a fixed $\tau > 0$

and $0 \leq s \leq 1$, set

$$A_s \coloneqq \frac{1}{\tau}\tilde{A}_{s\tau}.$$

Then, we find that

$$\left(\int_0^\tau \tilde{A}_s\, ds \middle| \tilde{A}_0 = a_0, \tilde{A}_\tau = a_\tau\right) = \left(\tau^2 \int_0^1 A_s\, ds \middle| A_0 = x, A_1 = y\right), \tag{3.3}$$

where $x = a_0/\tau$ and $y = a_\tau/\tau$. Further, using equation (3.2) which defines $\tilde{A}$, we can verify

$$\begin{aligned} dA_s &= \frac{1}{\tau}\, d\tilde{A}_{s\tau} \\ &= \frac{1}{\tau}\left(\delta\, d\,(s\tau) + 2\sqrt{\tilde{A}_{s\tau}}\, dW^P_{s\tau}\right) \\ &= \delta\, ds + 2\sqrt{A_s}\, dW_s, \end{aligned}$$

where $W_s \coloneqq W^P_{s\tau}/\sqrt{\tau}$ is a standard Brownian motion. We observe that $\{A_s\}_{0\leq s\leq 1}$ is a δ-dimensional squared Bessel process. Conditional on the end points, the process $(A_s, 0 \leq s \leq 1 | A_0 = x, A_1 = y)$ is then a squared Bessel bridge, denoted by $A^{\delta,1}_{x,y} = \left\{A^{\delta,1}_{x,y}(s)\right\}_{0\leq s\leq 1}$. As an immediate result, the right hand side of (3.3) has the same distribution as

$$\left(\tau^2 \int_0^1 A^{\delta,1}_{x,y}(s)\; ds\right). \tag{3.4}$$

Next, we construct the proof in three steps.

First, the integral (3.4) can be decomposed into the sum of three independent parts as follows:

$$\tau^2 \int_0^1 A^{\delta,1}_{x,y}(s)\; ds \overset{d}{=} X'_1 + X'_2 + \sum_{j=1}^{\eta} Z'_j,$$

where

$$X_1' = \tau^2 \int_0^1 A^{0,1}_{x+y,0}(s)\, ds,$$

$$X_2' = \tau^2 \int_0^1 A^{\delta,1}_{0,0}(s)\, ds,$$

$$Z_j' \stackrel{d}{=} Z' = \tau^2 \int_0^1 A^{4,1}_{0,0}(s)\, ds,$$

and η is an independent Bessel random variable with parameters $\nu = \delta/2 - 1$ and $\mu = \sqrt{xy} = \sqrt{a_0 a_\tau}/\tau$, i.e. $\eta \sim \text{Bessel}(\nu, \mu)$. Note that Z_j' are independent copies of Z' for $j = 1, 2, \ldots, \eta$. This is a direct result from Lemma 2.2.8 on the decomposition of the squared Bessel bridge, suggested by Pitman and Yor [57] and Glasserman and Kim [32].

Second, it follows from (2.2) in Lemma 2.2.7 that the Laplace transforms of X_1', X_2' and Z' for $b \geq 0$ are given by

$$\Phi_1'(b) = \exp\left(\frac{a_0 + a_\tau}{2\tau}\left(1 - \sqrt{2b}\tau \coth\left(\sqrt{2b}\tau\right)\right)\right), \tag{3.5}$$

$$\Phi_2'(b) = \left(\frac{\sqrt{2b}\,\tau}{\sinh\left(\sqrt{2b}\,\tau\right)}\right)^{\delta/2}, \tag{3.6}$$

$$\Phi_3'(b) = \left(\frac{\sqrt{2b}\,\tau}{\sinh\left(\sqrt{2b}\,\tau\right)}\right)^{2}. \tag{3.7}$$

Third, to confirm the random variables X_1', X_2' and Z' have the same distribution as the series expansions which define X_1, X_2 and Z respectively, it is sufficient to show that they have identical Laplace transforms. Before that, let us first rewrite Φ_i', $i = 1, 2, 3$ using some important identities regarding the hyperbolic functions coth and sinh; see Malham and Wiese [52]. Specifically, we observe

$$\coth z \equiv \coth\frac{z}{2} - \frac{1}{\sinh z},$$

$$\sinh z \equiv 2\sinh\frac{z}{2}\cosh\frac{z}{2}.$$

Iterating N times gives us

$$\coth z \equiv \coth \frac{z}{2^{N+1}} - \sum_{n=0}^{N} \frac{1}{\sinh \frac{z}{2^n}}, \tag{3.8}$$

$$\sinh z \equiv 2^N \sinh \frac{z}{2^N} \prod_{n=1}^{N} \cosh \frac{z}{2^n}. \tag{3.9}$$

Substituting (3.8) into the Laplace transform (3.5) of X_1' and setting $z \coloneqq \sqrt{2b}\tau$, we get that

$$\begin{aligned}
\Phi_1'(b) &= \exp\left(\frac{a_0 + a_\tau}{2\tau}\left(1 - z\coth z\right)\right) \\
&= \exp\left(\frac{a_0 + a_\tau}{2\tau}\left(1 - z\coth\frac{z}{2^N+1} + z\sum_{n=0}^{N}\frac{1}{\sinh\frac{z}{2^n}}\right)\right) \\
&= \exp\left(\frac{a_0 + a_\tau}{2\tau}\left(1 - z\coth\frac{z}{2^N+1}\right)\right)\exp\left(\frac{a_0 + a_\tau}{2\tau} z\sum_{n=0}^{N}\frac{1}{\sinh\frac{z}{2^n}}\right) \\
&= \prod_{n=0}^{N}\exp\left(\frac{a_0 + a_\tau}{2\tau}2^n\frac{\frac{z}{2^n}}{\sinh\frac{z}{2^n}}\right) I_N\left(z, \tau, a_0, a_\tau\right),
\end{aligned}$$

where

$$I_N\left(z, \tau, a_0, a_\tau\right) \coloneqq \exp\left(-\frac{a_0 + a_\tau}{2\tau}\left(z\coth\frac{z}{2^N+1} - 1\right)\right).$$

On the other hand, using $\sum_{n=0}^{N} 2^n = 2^{N+1} - 1$ leads to

$$\begin{aligned}
I_N\left(z, \tau, a_0, a_\tau\right) &= \exp\left(-\frac{a_0 + a_\tau}{2\tau}\left(z\coth\frac{z}{2^N+1} + \sum_{n=0}^{N}2^n - 2^{N+1}\right)\right) \\
&= \exp\left(-\frac{a_0 + a_\tau}{2\tau}\left(z\coth\frac{z}{2^{N+1}} - 2^{N+1}\right)\right)\exp\left(-\frac{a_0 + a_\tau}{2\tau}\sum_{n=0}^{N}2^n\right) \\
&= \prod_{n=0}^{N}\exp\left(-\frac{a_0 + a_\tau}{2\tau}2^n\right)\exp\left(\varepsilon_N^1\left(z, \tau, a_0, a_\tau\right)\right),
\end{aligned}$$

where

$$\varepsilon_N^1(z,\tau,a_0,a_\tau) \coloneqq -\frac{a_0+a_\tau}{2\tau}\left(z\coth\frac{z}{2^{N+1}}-2^{N+1}\right)\to 0, \quad \text{as} \quad N\to\infty.$$

Thus, for $z=\sqrt{2b}\,\tau$, Φ_1' can be expressed in the alternative form

$$\Phi_1'(b)=\prod_{n=0}^{\infty}\exp\left(\frac{a_0+a_\tau}{2\tau}\,2^n\left(\frac{\frac{\sqrt{2b}\,\tau}{2^n}}{\sinh\frac{\sqrt{2b}\,\tau}{2^n}}-1\right)\right).$$

Similarly, for Φ_2' after substitution and rearrangement, we have

$$\begin{aligned}\Phi_2'(b)&=\left(\frac{z}{\sinh z}\right)^{\delta/2}\\&=\left[z\left(2^N\sinh\frac{z}{2^N}\prod_{n=1}^{N}\cosh\frac{z}{2^n}\right)^{-1}\right]^{\delta/2}\\&=\prod_{n=1}^{N}\left(\cosh\frac{z}{2^n}\right)^{-\delta/2}\varepsilon_N^2(z,\delta),\end{aligned}$$

where

$$\varepsilon_N^2(z,\delta)\coloneqq\left(\frac{\frac{z}{2^N}}{\sinh\frac{z}{2^N}}\right)^{\delta/2}\to 1, \quad \text{as} \quad N\to\infty.$$

Therefore, plugging $z=\sqrt{2b}\,\tau$ into this expression yields

$$\Phi_2'(b)=\prod_{n=1}^{\infty}\left(\cosh\frac{\sqrt{2b}\,\tau}{2^n}\right)^{-\delta/2}.$$

In the context below, we derive the Laplace transforms of X_1 and X_2, denoted by Φ_1 and Φ_2 respectively. Notice that the infinite series defining X_1 and X_2 both converge almost surely since the respective sums of the corresponding variance $7\tau^3(a_0+a_\tau)\sum_{n=0}^{\infty}8^{-n}/90$ and $\delta\tau^4\sum_{n=1}^{\infty}16^{-n}/3$ are both finite. Then, for any $b\geq 0$, directly compute

$$\Phi_1(b)=\mathbb{E}\left[\exp\left(-bX_1\right)\right]$$

$$
\begin{aligned}
&= \mathbb{E}\left[\exp\left(-b\sum_{n=0}^{\infty}\frac{\tau^2}{4^n}\sum_{k=1}^{P_n}S_{n,k}\right)\right] \\
&= \prod_{n=0}^{\infty}\mathbb{E}\left[\exp\left(-b\frac{\tau^2}{4^n}\sum_{k=1}^{P_n}S_{n,k}\right)\right] \\
&= \prod_{n=0}^{\infty}\mathbb{E}\left[\prod_{k=1}^{P_n}\mathbb{E}\left(\exp\left(-b\frac{\tau^2}{4^n}S_{n,k}\right)\right)\right] \\
&= \prod_{n=0}^{\infty}\mathbb{E}\left[\left(\frac{\sqrt{\frac{2b\tau^2}{4^n}}}{\sinh\sqrt{\frac{2b\tau^2}{4^n}}}\right)^{P_n}\right] \\
&= \prod_{n=0}^{\infty}\exp\left[\frac{a_0+a_\tau}{2\tau}2^n\left(\frac{\frac{\sqrt{2b}\,\tau}{2^n}}{\sinh\frac{\sqrt{2b}\,\tau}{2^n}}-1\right)\right],
\end{aligned}
$$

where the third equality comes from the interchange of expectation and limit by the Bounded Convergence Theorem and the fifth equality holds due to the property of the random variable $S_{n,k}$ of an infinite divisible distribution in Lemma 2.2.9, with $h = 1$ here.

Following similar arguments, we now determine the Laplace transform Φ_2 for X_2. Indeed, from Lemma 2.2.9 that $\mathbb{E}\left[\exp\left(-bC_n^{\delta/2}\right)\right] = \left(\cosh\sqrt{2b}\right)^{-\delta/2}$ for any $n \geq 1$, we conclude that

$$
\begin{aligned}
\Phi_2(b) &= \mathbb{E}\left[\exp\left(-bX_2\right)\right] \\
&= \mathbb{E}\left[\exp\left(-b\sum_{n=1}^{\infty}\frac{\tau^2}{4^n}C_n^{\delta/2}\right)\right] \\
&= \prod_{n=1}^{\infty}\mathbb{E}\left[\exp\left(-b\frac{\tau^2}{4^n}C_n^{\delta/2}\right)\right] \\
&= \prod_{n=1}^{\infty}\left(\cosh\frac{\sqrt{2b}\,\tau}{2^n}\right)^{-\delta/2}.
\end{aligned}
$$

Hence, we can now deduce that $X_i' \overset{d}{=} X_i$ as $\Phi_i' = \Phi_i$ for $i = 1, 2$. In line with the steps explained above, $Z' \overset{d}{=} Z$ follows since this is a special case when $\delta = 4$,

completing the proof. □

We have represented the conditional time integral I by double infinite weighted sums and mixtures of simple independent random variables under the new probability measure $\mathbb{P}$. This serves as a theoretical basis for the exact simulation from the distribution of the random variable I under $\mathbb{P}$. However, our goal is set up under the probability measure $\mathbb{Q}$. We now focus on the task of generating a sample from the distribution of the conditional integral I under $\mathbb{Q}$ once we have generated a sample under $\mathbb{P}$ using the theorem introduced earlier. In particular, we explore the relationship between the probability density functions of the distributions of the integral under these two probability measures. We specify the details in the following section.

3.3 Probability density function of time integrated squared OU bridges

This section associates the distribution of the random variable I under measure $\mathbb{P}$ to its distribution under measure $\mathbb{Q}$. This is achieved by examining the connections between their respective Laplace transforms. In fact, the conditional integral I has the same distribution as the integral of a squared Bessel bridge and a squared OU bridge under $\mathbb{P}$ and $\mathbb{Q}$, respectively. A useful tool to work with these two bridges is Lemma 2.2.10.

Theorem 3.3.1

Suppose that f_P and f_Q are the probability density functions of I under the probability measures $\mathbb{P}$ and $\mathbb{Q}$, respectively. Then, we have

$$f_Q(x) = L(q, \nu, \tau, a_0, a_\tau) \exp\left(-\frac{q^2}{2}x\right) f_P(x),$$

where

$$L(q, \nu, \tau, a_0, a_\tau) = \frac{\sinh(q\tau)}{q\tau} \exp\left(\frac{a_0 + a_\tau}{2\tau}(q\tau \coth(q\tau) - 1)\right) \frac{I_\nu\left(\frac{\sqrt{a_0 a_\tau}}{\tau}\right)}{I_\nu\left(\frac{q\sqrt{a_0 a_\tau}}{\sinh(q\tau)}\right)},$$

and where $I_\nu(\cdot)$ denotes the modified Bessel function of the first kind.

Proof. We will make use of the shift property of the Laplace transform to justify the theorem. We first establish a relation between their respective Laplace transforms. For any $b \geq 0$, consider the Laplace transform $\mathcal{L}\{f_Q\}(b)$ of f_Q at b, which is the $\mathbb{Q}$-expectation of $\exp(-bI)$. Thus, we get

$$\begin{aligned}
\mathcal{L}\Big\{f_Q\Big\}(b) &= \mathbb{E}^{\mathbb{Q}}\left[\exp\left(-b\int_0^\tau \tilde{A}_s\,ds\right)\middle|\tilde{A}_0 = a_0, \tilde{A}_\tau = a_\tau\right] \\
&= \frac{\mathbb{E}^{\mathbb{P}}\left[\exp\left(-\left(b+\frac{q^2}{2}\right)\int_0^\tau \tilde{A}_s\,ds\right)\middle|\tilde{A}_0 = a_0, \tilde{A}_\tau = a_\tau\right]}{\mathbb{E}^{\mathbb{P}}\left[\exp\left(-\frac{q^2}{2}\int_0^\tau \tilde{A}_s\,ds\right)\middle|\tilde{A}_0 = a_0, \tilde{A}_\tau = a_\tau\right]} \\
&= \frac{\mathcal{L}\Big\{f_P\Big\}\left(b+\frac{q^2}{2}\right)}{\mathcal{L}\Big\{f_P\Big\}\left(\frac{q^2}{2}\right)} \\
&= \mathcal{L}\left\{\frac{f_P}{\mathcal{L}\Big\{f_P\Big\}\left(\frac{q^2}{2}\right)}\right\}\left(b+\frac{q^2}{2}\right).
\end{aligned}$$

The second equality is an immediate consequence of the change of law formula in Lemma 2.2.10.

Now by the application of the shift property, we can write

$$f_Q(x) = \frac{f_P(x)}{\mathcal{L}\Big\{f_P\Big\}\left(\frac{q^2}{2}\right)}\exp\left(-\frac{q^2}{2}x\right).$$

Using the formula (2.1) in Lemma 2.2.7 for the Laplace transform $\mathcal{L}\{f_P\}$ of f_P at $q^2/2$ given by

$$\begin{aligned}
\mathcal{L}\{f_P\}\left(\frac{q^2}{2}\right) &= \mathbb{E}^{\mathbb{P}}\left[\exp\left(-\frac{q^2}{2}\int_0^\tau \tilde{A}_s\,ds\right)\middle|\tilde{A}_0 = a_0, \tilde{A}_\tau = a_\tau\right] \\
&= \mathbb{E}^{\mathbb{P}}\left[\exp\left(-\frac{q^2}{2}\tau^2\int_0^1 A_s\,ds\right)\middle|A_0 = \frac{a_0}{\tau}, A_1 = \frac{a_\tau}{\tau}\right] \\
&= \frac{q\tau}{\sinh(q\tau)}\exp\left(\frac{a_0+a_\tau}{2\tau}\left(1-q\tau\coth(q\tau)\right)\right)\frac{\mathrm{I}_\nu\left(\frac{q\sqrt{a_0 a_\tau}}{\sinh(q\tau)}\right)}{\mathrm{I}_\nu\left(\frac{\sqrt{a_0 a_\tau}}{\tau}\right)}
\end{aligned}$$

and setting $L(q, \nu, \tau, a_0, a_\tau) \coloneqq \left(\mathcal{L}\left\{f_P\right\}(q^2/2)\right)^{-1}$ establish the stated result. □

The above theorem relates the density f_P, from which it is easy to obtain simulations by Theorem 3.2.1 to the density f_Q of our interested distribution. This means we can simulate the random variable I under measure $\mathbb{Q}$ provided an observation from its distribution under measure $\mathbb{P}$ is available. Practically, we apply the acceptance-rejection algorithm to generate samples from f_Q, which will be discussed in detail in Chapter 4.

So far, we have described the theories behind the simulation of the time integrated conditional variance. It is a matter of sampling infinite series, combined with the acceptance-rejection method. For the next stage, we will address some issues concerning the practical implementation of the theory. For example, as presented above, each individual term X_1, X_2 and Z contained in the series representation for I under $\mathbb{P}$ consists of a double infinite summation of some random variables. Furthermore, because of their dependence on the model parameters, it might be difficult to precompute those elements and tabulate them in advance, leaving the whole procedure rather time-consuming. We specify the strategies for how we put the theorems just derived into practice in the next chapter.

Chapter 4

Almost exact simulations

For the exact simulation of the Heston model, we closely follow the lead of Broadie and Kaya [15] and Glasserman and Kim [32] with one key difference for the conditional integral of the variance process. Given the initial values V_0 and S_0, the procedure breaks down into three steps as follows.

Algorithm 4.1 Exact simulation for S_t

1: Generate a sample for V_t from the scaled noncentral chi-squared distribution given in Proposition 1.1.1.

2: Generate a sample for $\int_0^t V_s \, ds$.

3: Generate a sample for $\log(S_t/S_0)$ from the normal distribution given in Proposition 1.1.3 and recover S_t from the normal sample.

In this chapter, we outline how to complete the second step by the decomposition theorem for the time integrated squared Bessel bridge and the theorem specifying its relationship with the time integrated squared OU bridge. In particular, we discuss the sampling techniques corresponding to each component for I, i.e. the random variables X_1, X_2 and Z defined by some infinite sums in Theorem 3.2.1. In addition, we give the details for the acceptance-rejection algorithm used to generate random values for variable I under probability measure $\mathbb{Q}$ once we have a sample for I under probability measure $\mathbb{P}$ according to Theorem 3.3.1.

In order to apply the decomposition theorem to sample the random variable I under the new probability measure $\mathbb{P}$, we need to determine a point at which the

infinite summation is terminated. We consider the truncation for the outer summation now, leaving the inner one to be discussed further in the following sections. Let us denote the truncation level by K and the resulting *remainder* random variables of X_1, X_2 and Z by R_1^K, R_2^K and R^K respectively, i.e.

$$R_1^K \coloneqq \sum_{n=K+1}^{\infty} \frac{\tau^2}{4^n} \sum_{k=1}^{P_n} S_{n,k},$$

$$R_2^K \coloneqq \sum_{n=K+1}^{\infty} \frac{\tau^2}{4^n} C_n^{\delta/2},$$

$$R^K \coloneqq \sum_{n=K+1}^{\infty} \frac{\tau^2}{4^n} C_n'.$$

We investigate the effect of truncation by summarising the means and variances of the remainder terms in the next lemma.

Lemma 4.0.1

Given the truncation level $K > 0$, we have

$$\mathbb{E}\left[R_1^K\right] = \frac{(a_0 + a_\tau)\,\tau}{6}\frac{1}{2^K}, \qquad \mathrm{Var}\left[R_1^K\right] = \frac{(a_0 + a_\tau)\,\tau^3}{90}\frac{1}{8^K},$$

$$\mathbb{E}\left[R_2^K\right] = \frac{\delta\tau^2}{6}\frac{1}{4^K}, \qquad \mathrm{Var}\left[R_2^K\right] = \frac{\delta\tau^4}{45}\frac{1}{16^K},$$

$$\mathbb{E}\left[R^K\right] = \frac{2\tau^2}{3}\frac{1}{4^K}, \qquad \mathrm{Var}\left[R^K\right] = \frac{4\tau^4}{45}\frac{1}{16^K}.$$

Proof. For the remainder R_1^K, as stated in Theorem 3.2.1, the $S_{n,k}$ are independent and identically distributed random variables and the P_n are independent Poisson random variables with mean $(a_0 + a_\tau)\,2^{n-1}/\tau$. Taking the expectation of R_1^K directly and interchanging expectation with summation by the Monotone Convergence Theorem, we have

$$\begin{aligned}\mathbb{E}\left[R_1^K\right] &= \sum_{n=K+1}^{\infty} \frac{\tau^2}{4^n}\mathbb{E}\left[\sum_{k=1}^{P_n} S_{n,k}\right] \\ &= \sum_{n=K+1}^{\infty} \frac{\tau^2}{4^n}\mathbb{E}\left[\mathbb{E}\left(\sum_{k=1}^{P_n} S_{n,k}\middle| P_n\right)\right]\end{aligned}$$

$$= \sum_{n=K+1}^{\infty} \frac{\tau^2}{4^n} \mathbb{E}\left[P_n \mathbb{E}\left(S_{n,k}\right)\right]$$

$$= \sum_{n=K+1}^{\infty} \frac{\tau^2}{4^n} \left(\frac{a_0 + a_\tau}{\tau} 2^{n-1}\right) \left(\frac{2}{\pi^2} \sum_{l=1}^{\infty} \frac{1}{l^2}\right)$$

$$= \frac{(a_0 + a_\tau)\,\tau}{6} \frac{1}{2^K},$$

where the last identity comes from the formulae for hyperharmonic series $\sum_{l=1}^{\infty} l^{-2} = \pi^2/6$ and partial geometric sum $\sum_{n=K+1}^{\infty} 2^{-(n+1)} = 2^{-(K+1)}$. Similarly, we can compute

$$\begin{aligned}
\mathrm{Var}\left[R_1^K\right] &= \sum_{n=K+1}^{\infty} \frac{\tau^4}{16^n} \mathrm{Var}\left[\sum_{k=1}^{P_n} S_{n,k}\right] \\
&= \sum_{n=K+1}^{\infty} \frac{\tau^4}{16^n} \left(\mathrm{Var}\left[\mathbb{E}\left(\sum_{k=1}^{P_n} S_{n,k} \middle| P_n\right)\right] + \mathbb{E}\left[\mathrm{Var}\left(\sum_{k=1}^{P_n} S_{n,k} \middle| P_n\right)\right]\right) \\
&= \sum_{n=K+1}^{\infty} \frac{\tau^4}{16^n} \left(\mathrm{Var}\left[P_n \mathbb{E}\left(S_{n,k}\right)\right] + \mathbb{E}\left[P_n \mathrm{Var}\left(S_{n,k}\right)\right]\right) \\
&= \sum_{n=K+1}^{\infty} \frac{\tau^4}{16^n} \left(\mathrm{Var}\left[P_n\right] \left(\mathbb{E}\left[S_{n,k}\right]\right)^2 + \mathbb{E}\left[P_n\right] \mathrm{Var}\left[S_{n,k}\right]\right) \\
&= \sum_{n=K+1}^{\infty} \frac{\tau^4}{16^n} \left(\frac{a_0 + a_\tau}{\tau} 2^{n-1}\right) \left(\left(\frac{2}{\pi^2} \sum_{l=1}^{\infty} \frac{1}{l^2}\right)^2 + \frac{4}{\pi^4} \sum_{l=1}^{\infty} \frac{1}{l^4}\right) \\
&= \frac{(a_0 + a_\tau)\,\tau^3}{90} \frac{1}{8^K},
\end{aligned}$$

where we use the formulae $\sum_{l=1}^{\infty} l^{-4} = \pi^4/90$ and $\sum_{n=K+1}^{\infty} 8^{-n} = 8^{-K}/7$.

For the remainder R_2^K, similar to the calculations for the moments of R_1^K, we find

$$\mathbb{E}\left[R_2^K\right] = \sum_{n=K+1}^{\infty} \frac{\tau^2}{4^n} \mathbb{E}\left[C_n^{\delta/2}\right]$$

$$= \sum_{n=K+1}^{\infty} \frac{\tau^2}{4^n} \left(\frac{2}{\pi^2} \sum_{l=1}^{\infty} \frac{\delta}{2} \frac{1}{\left(l - \frac{1}{2}\right)^2}\right)$$

$$= \frac{\delta\tau^2}{\pi^2}\left(\sum_{n=K+1}^{\infty}\frac{1}{4^n}\right)\left(4\sum_{l=1}^{\infty}\frac{1}{(2l-1)^2}\right)$$

$$= \frac{\delta\tau^2}{6}\frac{1}{4^K}.$$

Note that the last step is a direct result of $\sum_{l=1}^{\infty}(2l-1)^{-2} = \pi^2/8$ and $\sum_{n=K+1}^{\infty}4^{-n} = 4^{-K}/3$. Further we can proceed with the computation of the variance:

$$\begin{aligned}\mathrm{Var}\left[R_2^K\right] &= \sum_{n=K+1}^{\infty}\frac{\tau^4}{16^n}\mathrm{Var}\left[C_n^{\delta/2}\right]\\ &= \sum_{n=K+1}^{\infty}\frac{\tau^4}{16^n}\left(\frac{4}{\pi^4}\sum_{l=1}^{\infty}\frac{\delta}{2}\frac{1}{\left(l-\frac{1}{2}\right)^4}\right)\\ &= \frac{2\delta\tau^4}{\pi^4}\left(\sum_{n=K+1}^{\infty}\frac{1}{16^n}\right)\left(16\sum_{l=1}^{\infty}\frac{1}{(2l-1)^4}\right)\\ &= \frac{\delta\tau^4}{45}\frac{1}{16^K},\end{aligned}$$

in which we apply $\sum_{l=1}^{\infty}(2l-1)^{-4} = \pi^4/96$ and $\sum_{n=K+1}^{\infty}16^{-n} = 16^{-K}/15$.

Taking $\delta = 4$ we establish the results for R^K. □

The above lemma implies that the truncation errors decay exponentially. This is an appealing property of the new series as the truncation error will decrease so quickly that the Monte Carlo error will dominate the total error even for small truncation level K. Hence, including the terms at lower levels will be enough to produce an accurate approximation. This is supported by our numerical simulations in Chapter 6.

4.1 Direct inversion for weighted sums of exponential random variables

This section contains a description of the method for the practical realisation of the first component X_1 in the decomposition for I. Specifically, we sample X_1 by

truncating its series and approximating the tail sum by a moment-matching gamma random variable. To improve the efficiency, part of the series, namely the Poisson sum, is simulated by direct inversion method.

Recall that by dropping the remainder, we approximate X_1 by X_1^K where

$$X_1^K = \sum_{n=0}^{K} \frac{\tau^2}{4^n} \sum_{k=1}^{P_n} S_{n,k}.$$

Notice the that $S_{n,k}$ are independently and identically distributed as $S = (2/\pi^2) \sum_{l=1}^{\infty} \epsilon_l / l^2$. To reduce the truncation error further, we simulate the tail sum R_1^K as well. Glasserman and Kim [32] use the central limit theorem to show the validity of a normal approximation for the remainders. They also point out that a gamma approximation is feasible and better in the sense that its cumulant generating function is closer to that of the remainder random variable compared with that of a normal approximation. Therefore, inspired by this observation, the approximation to X_1 including tail simulation for a given truncation level K is

$$X_1 \approx X_1^K + \Gamma_1^K,$$

where Γ_1^K is a gamma random variable such that its first two moments are matched with those of the remainder R_1^K from Lemma 4.0.1.

We now detail our sampling procedure for X_1^K. The series which defines X_1^K suggests two potential problems. First, the random variables $S_{n,k} \stackrel{d}{=} S$ are represented by an infinite weighted sum of independent exponential random variables, which requires an efficient simulation method. Second, given a Poisson sample $P_n = P$ for a fixed level $n = 0, \ldots, K$, sampling the sum of P independent random variables S becomes increasingly computationally demanding when the sample P tends to be larger. Thus, an effective sampling scheme for the Poisson sum is fundamental to the simulation of X_1^K. We now incorporate these two tasks with each other and consider simulating the sum of P independent random variables S directly, denoted

by S^P, i.e.

$$S^P = \sum_{k=1}^{P} S_k,$$

where S_k are independent copies of S. By Lemma 2.2.9, S^P has the following Laplace transform:

$$\Phi_{S^P}(b) \coloneqq \mathbb{E}\left[\exp\left(-bS^P\right)\right] = \left(\frac{\sqrt{2b}}{\sinh\sqrt{2b}}\right)^P, \tag{4.1}$$

for $b \geq 0$.

Suggested by Malham and Wiese [52], we observe that any positive integer P can be expressed in the form

$$P = p_1 + 10p_{10} + 50p_{50} + 5000p_{5000} + 10^4 p_{10^4} + 10^5 p_{10^5} + 10^6 p_{10^6}.$$

Here p_{10^6} is the multiples of 10^6 present in the integer P, i.e. $p_{10^6} = \lfloor P/10^6 \rfloor$, p_{10^5} is the multiples of 10^5 present in the remainder of the division of P by 10^6, i.e. $p_{10^5} = \lfloor (P - 10^6 p_{10^6})/10^5 \rfloor$, and so forth. By the infinite divisibility, for any $P > 0$ the sum S^P admits

$$S^P \overset{d}{=} \sum_{k\in\mathbb{S}} \sum_{i=1}^{p_k} S_i^k,$$

where $\mathbb{S} = \{1, 10, 50, 5000, 10^4, 10^5, 10^6\}$ and for $i = 1, \ldots, p_k$, S_i^k are independent copies of S^k with $k \in \mathbb{S}$. Then, the above representation can be intended as a framework for an efficient sampling scheme for S^P for all $P > 0$ if we can realise S^k effectively for $k \in \mathbb{S}$. Indeed, we apply the direct inversion method to simulate S^k with their inverse distribution functions approximated by predetermined Chebyshev polynomials for each $k \in \mathbb{S}$. In general, the direct inversion algorithm for generating the samples of S^P for any $P > 0$ is described in Algorithm 4.2.

The advantage of this algorithm is that we only need to construct the Chebyshev polynomial approximations for the inverse distribution function of S^k for $k \in \mathbb{S}$. With this replacement, the complicated inverse distribution function becomes very

easy to compute at arbitrary points. Moreover, since S^k does not depend on any model parameters, the coefficients of the polynomials can be computed and tabulated in advance. As such, when a sample for X_1 is needed, we truncate the series representation to include the terms at $n \leq K$ with the tail approximated by a gamma distribution. For each $n = 0, \ldots, K$, we generate Poisson samples P_n and simulate the sums S^{P_n} by Algorithm 4.2, which requires evaluating some prescribed polynomials with coefficients drawn directly from the cached tables; see Appendix A.

Algorithm 4.2 Direct inversion for S^P

1: For each $k \in \mathbb{S}$, sample p_k independent random variables S_i^k, $i = 1, \ldots, p_k$ from the distribution of S^k using the inverse distribution functions based on the corresponding Chebyshev polynomial approximations.

2: Compute the accumulated sum, i.e. $\sum_k \sum_{i=1}^{p_k} S_i^k \sim S^P$.

To make the above process fast for implementation, we take advantage of the direct inversion to obtain Poisson samples $P_n = P$ when the mean μ is no bigger than 10. The inversion method for sampling discrete random variables is analogous to that for continuous random variables. The only difference is that the inverse of the cumulative distribution function is found by sequential search iterations for the discrete case. This is because the distribution function for the discrete random variable is no longer strictly monotonically increasing and continuous, whence its inverse is not unique. To solve this problem, we define the generalised inverse distribution function to be

$$F^{-1}(p) \coloneqq \inf\{x \in \mathbb{R} : F(x) \geq p\},$$

where F is a distribution function and p is a probability. Then the uniqueness of the inverse is preserved in its definition. Applied in Poisson sampling, the direct inversion is given in Algorithm 4.3. For larger means, Algorithm 4.4 for PTRD transformed rejection method suggested by Hörmann [40] will be applied.

To obtain the Chebyshev coefficients, it is crucial to determine the values of the distribution functions at several points efficiently and accurately. For large P,

we derive an asymptotic series expansion for the distribution function of S^P when $P \to \infty$ through the inverse Fourier transform of its characteristic function. While for small P, we utilise the explicit expression for the density function given by Biane and Yor [10], which involves the parabolic cylinder functions. To derive the representation for the distribution function, we use a routine consisting of the power series and asymptotic expansions for the parabolic cylinder functions to evaluate the density function followed by term-wise integration. We present the detailed analysis in Chapter 5.

Algorithm 4.3 Direct inversion for P ($\mu \leq 10$)

1: Generate a uniform sample U from $\mathrm{Unif}\,(0,1)$.

2: Set $k \coloneqq 0$, $p \coloneqq \exp(-\mu)$, $s \coloneqq 0$.

3: Update $s \coloneqq s + p$, $k \coloneqq k + 1$, $p \coloneqq p\mu/k$.

4: If $U \leq s$, return $k - 1$ as a sample for P.
Otherwise, go to the third step.

Algorithm 4.4 PTRD for P ($\mu > 10$)

1: Set $b \coloneqq 0.931 + 2.53\sqrt{\mu}$, $a \coloneqq -0.059 + 0.02483b$, $\alpha \coloneqq 1.1239 + 1.1328/(b - 3.4)$ and $v_r \coloneqq 0.9277 - 3.6224/(b - 2)$.

2: Generate a sample V from the uniform distribution $\mathrm{Unif}\,(0,1)$.

3: If $V \leq 0.86v_r$, set $U \coloneqq V/v_r - 0.43$ and return $\lfloor (2a/(0.5 - |U|) + b)\, U + \mu + 0.445 \rfloor$ as a sample for P.
If $V \geq v_r$, generate a uniform sample U from $\mathrm{Unif}\,(-0.5, 0.5)$.
If $0.86v_r < V < v_r$, set $U \coloneqq 0.5\mathrm{sign}\,(V/v_r - 0.93) - V/v_r + 0.93$ and update V by generating a uniform sample from $\mathrm{Unif}\,(0, v_r)$, where $\mathrm{sign}\,(x)$ denotes the signum function of a real number x.

4: Set $u_s \coloneqq 0.5 - |U|$. If $u_s < 0.013$ and $V > u_s$, go to the second step.

5: Set $k \coloneqq \lfloor (2a/u_s + b)\, U + \mu + 0.445 \rfloor$ and update $V \coloneqq \alpha V/(a/u_s^2 + b)$.
If $k \geq 10$ and $\log\left(V\sqrt{\mu}\right) \leq (k + 0.5)\log(\mu/k) - \mu - \log\sqrt{2\pi} + k - (1/12 - 1/(360k^2))/k$, return k as a sample for P.
If $0 \leq k \leq 9$ and $\log V \leq k\log\mu - \mu - \log(k!)$, return k as a sample for P.
Otherwise, return to the second step.

Remark 4.1

The set $\mathbb{S}$ is chosen for the consideration of convenience and efficiency. In particular, we choose this so that the distribution function for each S^k, $k \in \mathbb{S}$ can be computed with great accuracy at modest computational cost. We may improve the efficiency of sampling S^P by decomposing P more finely using more basis in $\mathbb{S}$, which, however, will increase the number of Chebyshev polynomial approximations we have to evaluate.

4.2 Direct inversion for weighted sums of gamma random variables

The truncation method established above for X_1 can be similarly employed here for X_2. However, the structure of the random variable X_2, along with its dependence on the model parameters, provides us with another possibility for sampling. In fact, the Laplace transform of X_2/τ^2 is identical to that for S^h. We can therefore extend the direct inversion of S^h for any $h \in \mathbb{N}$ outlined in Section 4.1 for the simulation of X_2.

Let us first introduce the notation $h \coloneqq \delta/2$, which is typically between zero and one. Hence, after separating the time parameter X_2 can be written in the form

$$X_2 = \sum_{n=1}^{\infty} \frac{\tau^2}{4^n} C_n^h = \tau^2 \sum_{n=1}^{\infty} \frac{1}{4^n} C_n^h = \tau^2 Y_2^h$$

with

$$Y_2^h := \sum_{n=1}^{\infty} \frac{C_n^h}{4^n}$$

depending only on the parameter h. We notice that the Laplace transform of Y_2^h

$$\Phi_{Y_2^h}(b) = \mathbb{E}\left[\exp\left(-bY_2^h\right)\right] = \left(\frac{\sqrt{2b}}{\sinh\sqrt{2b}}\right)^h, \quad \text{for} \quad b \geq 0$$

has the same expression as that of S^h given by (4.1) after replacing P by h. The

only difference is that the parameter h now is restricted to the interval $(0, 1)$ rather than positive integers. This suggests that Y_2^h is equivalent in distribution to S^h, i.e.

$$Y_2^h \stackrel{d}{=} S^h,$$

but the decomposition proposed in Section 4.1 for integer h and the resulting S^h is no longer reasonable. However, motivated by Malham and Wiese [51], we have the following alternative formula for $0 < h < 1$, which is given to the first three decimal places:

$$h = \frac{h_5}{5} + \frac{h_{10}}{10} + \frac{h_{20}}{20} + \frac{h_{50}}{50} + \frac{h_{100}}{100} + \frac{h_{200}}{200} + \frac{h_{500}}{500} + \frac{h_{1000}}{1000} + \frac{h_{2000}}{2000},$$

where $h_k \in \{0, 1, 2\}$ for $k \in \mathbb{H} = \{5, 10, 20, 50, 100, 200, 500, 1000, 2000\}$. Next, we give the direct inversion algorithm for generating Y_2^h for any $h \in (0, 1)$ given to the first three decimal places.

Algorithm 4.5 Direct inversion for Y_2^h

1: For each $k \in \mathbb{H}$, sample h_k independent random variables $Y_{2,i}^{1/k}$, $i = 1, \ldots, h_k$ from the distribution of $Y_2^{1/k}$ by inverse transform sampling based on the corresponding Chebyshev polynomial approximations.

2: Compute the accumulated sum, i.e. $\sum_k \sum_{i=1}^{h_k} Y_{2,i}^{1/k} \sim Y_2^h$.

Given Algorithm 4.5, for a general h the simulation of Y_2^h is reduced to simulating several particular random variables such as $Y_2^{1/5}$, $Y_2^{1/10}$, ... using their inverse distribution functions, which are approximated by the associated Chebyshev polynomials. We will apply the same approach for S^P with small integer P to design the Chebyshev polynomial approximations, which will be reported in the next chapter.

As Z is a special case of X_2 when $\delta = 4$, the strategy to generate samples of X_2 discussed earlier is fully applicable here. Indeed, we directly construct the Chebyshev polynomial approximations for the inverse distribution function $F_{Z'}^{-1}$ with $Z' \stackrel{d}{=} Z/\tau^2$ since Z' is independent of any model parameters.

Remark 4.2

Similar to the decomposition of P, we choose the set $\mathbb{H}$ in the consideration of

efficiency and convenience. The corresponding decomposition works for the case when h is rounded to three decimal digits only. But this decomposition can be generalised to $h \in (0,1)$ given to any decimal places in principle.

4.3 Direct inversion for Bessel random variables

To simulate the random variable I under the new probability measure $\mathbb{P}$, samples for the Bessel random variable $\eta \sim \text{Bessel}(\nu, z)$ with parameters

$$\nu = \frac{\delta}{2} - 1,$$

$$z = \frac{\sqrt{a_0 a_\tau}}{\tau},$$

as outlined in Theorem 3.2.1 are needed. While there are various exact ways to generate Bessel variates such as fast acceptance-rejection algorithms and conditional schemes (see Devroye [22] and Iliopoulos and Karlis [42]), Glasserman and Kim [32] apply the more stable inversion method based on the inverse of the cumulative distribution function; see the sequential search method in Iliopoulos and Karlis [42] as well. We briefly summarise this procedure in this section.

Algorithm 4.6 Direct inversion for η

1: Generate a uniform sample U from $\text{Unif}(0,1)$.

2: Set $k \coloneqq 0$, $p \coloneqq (z/2)^\nu / (\text{I}_\nu(z)\,\Gamma(\nu+1))$, $s_l \coloneqq 0$, $s_u \coloneqq 0$.

3: Update $k \coloneqq k+1$, $s_l \coloneqq s_u$, $s_u \coloneqq s_u + p$, $p \coloneqq z^2 p / (4k(k+\nu))$.

4: If $s_l < U \leq s_u$, return $k-1$ as a sample for η.

Otherwise, go to the third step.

Similar to the direct inversion of Poisson simulation, the Bessel distribution function is inverted at $u \in [0,1]$ by accumulating the probabilities until it exceeds u. The evaluation of the probability mass function and thus the distribution function is straightforward. Recall that the probability mass function, denoted by $p_n \coloneqq \mathbb{P}(\eta = n)$, for the Bessel random variable $\eta \sim \text{Bessel}(\nu, z)$ introduced in Definition 2.2.1 satisfies the following recursive relation (see Iliopoulos and Karlis [42] and

Glasserman and Kim [32]):

$$p_{n+1} = \frac{z^2}{4\,(n+1)\,(n+1+\nu)} p_n, \qquad n \geq 0,$$

$$p_0 = \frac{1}{\mathrm{I}_\nu\,(z)\,\Gamma\,(\nu+1)} \left(\frac{z}{2}\right)^\nu.$$

Taking advantage of these formulas, we perform the sequence of instructions given in Algorithm 4.6 to generate from the Bessel distribution.

Notice that the probability mass function for the Bessel random variable is concentrated around zero for parameters with values varying across a wide range. This property guarantees the efficiency of the above inversion method for the short-tailed distribution as it is not necessary to calculate the probabilities for a larger range of values for n. Numerical comparisons of the computing time with this approach across different parameter values are presented in Section 4.2 of Glasserman and Kim [32].

To sum up, we have described the steps to sample from the distribution of I under $\mathbb{P}$. The main process is to generate S^P random variables by direct inversion algorithms for some fixed values $P \in \mathbb{S}$, $P = 1/k$ with $k \in \mathbb{H}$ and $P = 2$. The question we now face becomes how can we develop accurate Chebyshev polynomial approximations to the inverse distribution function for S^P. We show this process step by step in Chapter 5.

4.4 Acceptance-rejection for time integrated squared OU bridges

After having samples from the distribution of I under measure $\mathbb{P}$, we now turn to the simulations for I under $\mathbb{Q}$. We apply the technique which makes use of a similar distribution other than the one of our interest, i.e. the acceptance-rejection sampling. Instead of sampling directly from the distribution of I under $\mathbb{Q}$, we accept those samples of I under $\mathbb{P}$ which fall inside the region of interest as samples for our target. The region of interest is indicated by the relationship between their

probability density functions given in Theorem 3.3.1. In general, we construct the following algorithm to generate samples for I under $\mathbb{Q}$.

Algorithm 4.7 Acceptance-rejection for I under $\mathbb{Q}$

1: Simulate a realisation Y of the random variable I under $\mathbb{P}$ using Theorem 3.2.1.

2: Obtain a sample U independently from the uniform distribution $\text{Unif}\,(0,1)$.

3: If $U \leq \exp\left(-q^2 Y/2\right)$, accept Y as a sample drawn from the distribution of I under $\mathbb{Q}$.

Otherwise, reject the value of Y and return to the first step.

On average, the probability p of accepting a proposed sample is

$$\begin{aligned}
p &= \mathbb{P}\left(U \leq \exp\left(-\frac{q^2 Y}{2}\right)\right) \\
&= \int_0^\infty \mathbb{P}\left(U \leq \exp\left(-\frac{q^2 Y}{2}\right) \middle| Y = y\right) f_P\left(y\right)\, dy \\
&= \int_0^\infty \mathbb{P}\left(U \leq \exp\left(-\frac{q^2 y}{2}\right)\right) f_P\left(y\right)\, dy \\
&= \int_0^\infty \exp\left(-\frac{q^2 y}{2}\right) f_P\left(y\right)\, dy \\
&= \int_0^\infty \frac{f_Q\left(y\right)}{L\left(q,\nu,\tau,a_0,a_\tau\right)}\, dy \\
&= \frac{1}{L\left(q,\nu,\tau,a_0,a_\tau\right)},
\end{aligned}$$

where $U \sim \text{Unif}\,(0,1)$ and independently Y follows the distribution of I under $\mathbb{P}$. Consequently, we require $L\left(q,\nu,\tau,a_0,a_\tau\right) \geq 1$ due to the fact that a probability only takes values between zero and one. In practice, we prefer a value of L closer to one as it implies higher acceptance probability on average, and thus fewer iteration steps needed.

To illustrate the efficiency of this method, we report its computational complexity for the test cases considered in this thesis. The complexity is measured by the expected number of iterations n performed to produce an accepted value, which is

the reciprocal of the probability of acceptance p on average, i.e.

$$n = \frac{1}{p} = L\left(q, \nu, \tau, a_0, a_\tau\right).$$

The sets of parameters are shown in Table 4.1. These four sets of European call options are taken from Glasserman and Kim [32] (see Andersen [6] and Duffie, Pan and Singleton [25] as well), which are found to be in the typical range of parameter values of the Heston model in practice. They describe Case 1 as being relevant to long-dated FX options, Case 2 as possible for long-dated interest rate options, Case 3 as related to equity options and Case 4 as corresponding to S&P 500 index options. Note that for Case 3 and Case 4, the risk-free interest rate r is assumed to be 0.05 and 0.0319 with reference to Haastrecht and Pelsser [66] and Broadie and Kaya [15], respectively.

Table 4.1: Parameters for European call options for the Heston model.

Parameters	**Case 1**	**Case 2**	**Case 3**	**Case 4**
κ	0.5	0.3	1	6.21
θ	0.04	0.04	0.09	0.019
σ	1	0.9	1	0.61
ρ	-0.9	-0.5	-0.3	-0.7
t	10	15	5	1
v_0	0.04	0.04	0.09	0.010201
S_0	100	100	100	100
r	0	0	0.05	0.0319
δ	0.08	0.059	0.36	1.268

Table 4.2 records the average number of iterative steps that are needed for all four cases. Since the simulated value of v_t differs for each path, we take three possible levels for it with a representative one being the middle and two extreme ones. As we can see from the table, the number of iterations required by Case 4 is larger than the double of that for the other three cases. However even for the less efficient

case, it turns out that the time needed to realise the Heston model using our new method is still less than that for Glasserman and Kim [32], which will be supported by numerical analysis in Chapter 6.

Table 4.2: Expected number of iterations required

Case 1				**Case 2**			
v_t	0.000004	0.04	4	v_t	0.000004	0.04	4
n	1.049	1.063	4.042	n	1.031	1.041	2.693
Case 3				**Case 4**			
v_t	0.000009	0.09	0.9	v_t	0.0025	0.010201	0.05
n	1.239	1.317	2.280	n	2.599	2.847	4.556

In this chapter, we have designed a series of algorithms for the simulation of the conditional time integrated variance process in the Heston model. The main ingredients are direct inversion and acceptance-rejection sampling. In particular, the direct inversion is based on approximating the inverse distribution functions by predetermined Chebyshev polynomials. Importantly, the underlying random variables are independent of any model parameters, which makes it possible to cache the Chebyshev coefficients before the Monte Carlo loop. Our discussion so far has not yet covered the construction of the approximations. In the next chapter, we address this issue.

Chapter 5

Chebyshev polynomial approximations

This chapter contains an introduction of the Chebyshev polynomial approximations for the inverse distribution functions of the random variable $S^P \stackrel{d}{=} Y_2^P$. As discussed in Chapter 4, we are concerned with two classes of fixed values for P, i.e. $P \in \mathbb{S} = \{1, 10, 50, 5000, 10^4, 10^5, 10^6\}$ and $P = 1/k$ with $k \in \mathbb{H} = \{5, 10, 20, 50, 100, 200, 500, 1000, 2000\}$. First, we derive the asymptotic expansions for the distribution function of S^P. Second, based on the asymptotic behaviour of the function we identify appropriate scaling factors to construct the approximated polynomials.

5.1 Asymptotic expansion for the distribution function of S^P for large P

In what follows, we present comprehensive details of analysis behind the development of the series representation for the distribution function of S^P in the large sum asymptotic limit. We start from its characteristic function to build the corresponding probability density function by inverse Fourier transform, followed by term-wise integration resulting in the asymptotic expansion for the distribution function in the limit $P \to +\infty$.

Recall that $S = (2/\pi^2)\sum_{l=1}^{\infty} \epsilon_l / l^2$ has the characteristic function

$$\varphi_S(\xi) \coloneqq \mathbb{E}\left[\exp(\mathrm{i}\xi S)\right] = \frac{\sqrt{-2\xi\mathrm{i}}}{\sinh\sqrt{-2\xi\mathrm{i}}}$$

for any $\xi \in \mathbb{R}$. By independence, we deduce that the characteristic function for the sum S^P is

$$\varphi_{S^P}(\xi) \coloneqq \mathbb{E}\left[\exp\left(\mathrm{i}\xi S^P\right)\right] = \left(\frac{\sqrt{-2\xi\mathrm{i}}}{\sinh\sqrt{-2\xi\mathrm{i}}}\right)^P.$$

Then taking the inverse Fourier transform of its characteristic function, the probability density function f_{S^P} of S^P can be expressed in the form

$$\begin{aligned}
f_{S^P}(x) &= \frac{1}{2\pi}\int_{-\infty}^{+\infty} \exp(-\mathrm{i}\xi x)\varphi_{S^P}(\xi)\, d\xi \\
&= \frac{1}{2\pi}\int_{-\infty}^{+\infty} \exp(-\mathrm{i}\xi x)\left(\frac{\sqrt{-2\xi\mathrm{i}}}{\sinh\sqrt{-2\xi\mathrm{i}}}\right)^P d\xi \\
&= \frac{1}{2\pi}\int_{+\infty}^{-\infty} \exp\left(\mathrm{i}\frac{1}{2}zx\right)\left(\frac{\sqrt{z\mathrm{i}}}{\sinh\sqrt{z\mathrm{i}}}\right)^P \left(-\frac{1}{2}\right) dz \\
&= \frac{1}{4\pi}\int_{-\infty}^{+\infty} \exp\left(\frac{1}{2}xz\mathrm{i}\right)\left(\frac{\sqrt{z\mathrm{i}}}{\sinh\sqrt{z\mathrm{i}}}\right)^P dz,
\end{aligned}$$

in which we make the change of variable $z = -2\xi$ for the third step. Note that the above integral converges absolutely.

Before moving on to the analysis, it is worth noticing that the expectation $\mathbb{E}\left[S^P\right] = P/3$ and variance $\mathrm{Var}\left[S^P\right] = 2P/45$ of S^P will diverge when $P \to \infty$. For easier calculation, we standardise the random variable S^P by

$$Z^P \coloneqq \frac{S^P - \frac{P}{3}}{\sqrt{\frac{2P}{45}}},$$

so that the new random variable Z^P has mean zero and variance one. As S^P is non-negative, the support for Z^P is $\left[-\sqrt{5P}/\sqrt{2}, +\infty\right)$. The classical theorem on

transforming the probability density functions yields

$$\begin{aligned} f_{Z^P}(x) &= \sqrt{\frac{2P}{45}} f_{S^P}\left(\frac{P}{3} + x\sqrt{\frac{2P}{45}}\right) \\ &= \sqrt{\frac{2P}{45}} \frac{1}{4\pi} \int_{-\infty}^{+\infty} \exp\left(\frac{1}{2}\left(\frac{P}{3} + x\sqrt{\frac{2P}{45}}\right) z\mathrm{i}\right) \left(\frac{\sqrt{z\mathrm{i}}}{\sinh\sqrt{z\mathrm{i}}}\right)^P dz \\ &= \frac{1}{4\pi}\sqrt{\frac{2P}{45}} \int_{-\infty}^{+\infty} \exp\left(\frac{1}{6}Pz\mathrm{i}\right) \exp\left(\sqrt{\frac{P}{90}}xz\mathrm{i}\right) \left(\frac{\sqrt{z\mathrm{i}}}{\sinh\sqrt{z\mathrm{i}}}\right)^P dz \end{aligned} \tag{5.1}$$

with f_{Z^P} denoting the probability density function of Z^P. To explore the asymptotic behaviour of this integral as $P \to +\infty$, we rewrite (5.1) by introducing $\beta \coloneqq x\sqrt{2/45}/\sqrt{P}$ as

$$f_{Z^P}(x) = \frac{1}{4\pi}\sqrt{\frac{2P}{45}} \int_{-\infty}^{+\infty} \exp\left(P\rho(z;\beta)\right) dz, \tag{5.2}$$

where $\rho(z;\beta)$ satisfies

$$\rho(z;\beta) = \log\left(\frac{\sqrt{z\mathrm{i}}}{\sinh\sqrt{z\mathrm{i}}}\right) + z\mathrm{i}\left(\frac{1}{6} + \frac{1}{2}\beta\right). \tag{5.3}$$

Here the integrand has a removable singularity at $z = 0$ and poles at $z = \pi^2 n^2 \mathrm{i}$ for all $n \in \mathbb{Z}^+$.

We apply the standard technique of the steepest descent method to develop the large P asymptotics of f_{Z^P}, where all the higher order terms are given in reciprocal powers of P; see Bender and Orszag [8], Bleistein and Handelsman [11] and Ablowitz and Fokas [1]. The expansion is then integrated term by term to generate the asymptotic approximation for the distribution function. We state the results in a series of lemmas and theorems.

Lemma 5.1.1

For fixed x such that $|x| \ll \sqrt{P}/\sqrt{2/45}$, i.e. $\beta \ll 1$, we have

$$f_{Z^P}(x) = \frac{1}{4\pi}\sqrt{\frac{2P}{45}} \int_{\mathcal{C}_r - \mathcal{C}_l} \exp\left(P\rho(z;\beta)\right) dz,$$

where $\mathcal{C}_r$ and $\mathcal{C}_l$ are the two steepest descent paths explicitly outlined in the proof.

Proof. We follow the general procedure of the steepest descent method and Cauchy's theorem summarised below to complete the deformation of the contour of integration for f_{Z^P}. We first identify the critical points including saddle points z_0 of $\rho(z;\beta)$ such that $\rho'(z_0;\beta) = 0$. Note that since $\rho(z;\beta)$ depends on the parameter β, the saddle point z_0 will also depend on β. Due to the fact that $\beta \ll 1$, we can establish a useful expression for z_0 as an asymptotic series in β. Afterwards, we obtain the steepest descent paths emanating from the saddle point z_0 by setting $\operatorname{Im}(\rho(z;\beta)) = \operatorname{Im}(\rho(z_0;\beta))$ and $\operatorname{Re}(\rho(z;\beta)) < \operatorname{Re}(\rho(z_0;\beta))$. Following this, we demonstrate that the original contour, i.e. the real line, can be deformed onto the steepest descent paths in the domain where the integrand is analytical. In this way, the rapid oscillations of the integrand can be removed when P is large, whence the asymptotic behaviour of the integral can be determined locally depending only on a small neighbourhood of the critical points.

Proceeding as indicated above, we are interested in the saddle point z_0 which solves $\rho'(z_0;\beta) = 0$. First, let

$$\varsigma(z) \coloneqq \frac{\sqrt{z\mathrm{i}}}{\sinh\sqrt{z\mathrm{i}}},$$

which gives

$$\rho(z;\beta) = \log(\varsigma(z)) + z\mathrm{i}\left(\frac{1}{6} + \frac{1}{2}\beta\right).$$

We observe that $\varsigma(z)$ and $\rho(z;\beta)$ are analytic when $\operatorname{Im}(z) < \pi^2$ after defining $\varsigma(0) \coloneqq 1$ and $\rho(0;\beta) \coloneqq 0$. Then for real z, we have

$$\begin{aligned}
|\varsigma(z)| &= \left|\mathbb{E}\left[\exp\left(-\frac{1}{2}\mathrm{i}zS\right)\right]\right| \\
&= \left|\int_{-\infty}^{+\infty} \exp\left(-\frac{1}{2}\mathrm{i}zx\right) f_S(x)\, dx\right| \\
&\leq \int_{-\infty}^{+\infty} \left|\exp\left(-\frac{1}{2}\mathrm{i}zx\right)\right| f_S(x)\, dx
\end{aligned}$$

$$= \int_{-\infty}^{+\infty} f_S(x)\, dx$$

$$= 1,$$

where f_S is the probability density function of the random variable S. Hence, we see

$$\mathrm{Re}\left(\rho\left(z;\beta\right)\right) = \mathrm{Re}\left(\log\left(\varsigma\left(z\right)\right)\right) = \log\left|\varsigma\left(z\right)\right| \leq \log(1) = 0$$

for all $z \in \mathbb{R}$ with equality when $z = 0$. This suggests that all points on the real axis are in the valley of ρ with respect to those saddle points z_0 such that $\mathrm{Re}\left(\rho\left(z_0;\beta\right)\right) > 0$. These saddle points are inadmissible since they are not able to contribute to the asymptotic expansion of the integral f_{Z^P}. In fact, the integrand along the real axis is exponentially smaller than any such contribution. Further, the real axis, except the origin, lies in the valley of ρ with respect to the origin.

Following the above arguments, Bleistein and Handelsman [11, Chapter 7.6, p. 300] suggest that we should seek a saddle point near $z = 0$, which will be the dominant one. To obtain an explicit form for the saddle point, we take advantage of the series expansions of $\rho\left(z;\beta\right)$ and its differentiation $\rho'\left(z;\beta\right)$. Let us first consider the series expansion of $\rho\left(z;\beta\right)$ about $z = 0$, which is of the form

$$\rho\left(z;\beta\right) = \frac{1}{2}\beta \mathrm{i} z + \sum_{k=2}^{\infty} \hat{r}_k z^k, \tag{5.4}$$

where $\hat{r}_2 = -1/180$, $\hat{r}_3 = \mathrm{i}/2835$ and so forth. Although we can compute the coefficients $\hat{r}_k$ analytically through Taylor expansion of $\rho\left(z;\beta\right)$ up to any order, we compute them using Maple in practice. Hence, its differentiation can be written as

$$\rho'\left(z;\beta\right) = \frac{1}{2}\beta \mathrm{i} + \sum_{k=2}^{\infty} k\hat{r}_k z^{k-1}.$$

Note that the above two series converge pointwise in the domain where $|z| < \pi^2$.

Then, the saddle point z_0 is the solution to

$$\rho'(z_0;\beta)=0.$$

It seems that a precise form for this saddle point is not obtainable. However, we can get a good approximation by making use of the smallness of β. For $\beta \ll 1$, i.e. $|x| \ll \sqrt{P}/\sqrt{2/45}$, we solve the above equation by iteration. In fact, after two iterations, we have the subsequent approximate form for the desired saddle point

$$z_0 = 45\mathrm{i}\beta - \frac{1350}{7}\mathrm{i}\beta^2 + \mathrm{O}\left(\beta^3\right).$$

In this sense by successive iterations, we can approximate the saddle point z_0 by an asymptotic expansion in β to any order, i.e.

$$z_0 \sim \beta \sum_{k=0}^{\infty} \hat{\xi}_k \beta^k, \tag{5.5}$$

in which $\hat{\xi}_0 = 45\mathrm{i}$, $\hat{\xi}_1 = -1350\mathrm{i}/7$ and so on. Again, all these coefficients $\hat{\xi}_k$ are calculated via Maple in practice. Notice that the saddle point z_0 is near the origin and along the imaginary axis. In order to deform the original contour, i.e. the real axis, into the steepest descent path passing through the saddle point in the domain of analyticity of $\rho(z;\beta)$, we need to show that the saddle point z_0 will not hit its singularity, i.e. $\mathrm{Im}(z_0) < \pi^2$. Indeed, we know that z_0 satisfies

$$\rho'(z_0;\beta) = \frac{\varsigma'(z_0)}{\varsigma(z_0)} + \mathrm{i}\left(\frac{1}{6}+\frac{1}{2}\beta\right) = 0.$$

Equivalently, there is

$$\mathrm{Im}\left(\frac{\varsigma'(\mathrm{Im}(z_0)\,\mathrm{i})}{\varsigma(\mathrm{Im}(z_0)\,\mathrm{i})}\right) + \left(\frac{1}{6}+\frac{1}{2}\beta\right) = 0.$$

If we introduce the function $\varkappa(z) \coloneqq \mathrm{Im}(\varsigma'(z\mathrm{i})/\varsigma(z\mathrm{i}))$, then by algebra we see $\varkappa(z)$ is a monotonically decreasing function for real $z < \pi^2$ and $\varkappa(z) \to -\infty$ as $z \uparrow \pi^2$. Adding a positive constant to $\varkappa(z)$ moves its graph upwards, whence the intersection with the real axis is shifted to the right. Due to the limiting behaviour as $z \uparrow \pi^2$, the zero of $\varkappa(z) + (1/6 + \beta/2)$ that we are interested in is always below π^2, yielding

$\mathrm{Im}\,(z_0) < \pi^2$.

Now, we can expand $\rho\,(z;\beta)$ as a Taylor series close to the saddle point z_0

$$\rho\,(z;\beta) = \rho\,(z_0;\beta) + \frac{1}{2!}\rho''\,(z_0;\beta)\,(z-z_0)^2 + (z-z_0)^3 \sum_{k\geq 0} \frac{\rho^{(k+3)}\,(z_0;\beta)}{(k+3)!}\,(z-z_0)^k\,, \tag{5.6}$$

which is convergent in a neighbourhood of z_0. For preparations, we must evaluate $\rho^{(k)}\,(z;\beta)$ for $k \geq 2$ at $z = z_0$. Differentiating (5.4) leads to

$$\rho^{(n)}\,(z;\beta) = \sum_{k=n}^{\infty} k\,(k-1)\cdots(k-n+1)\,\hat{r}_k z^{k-n} = \sum_{k=n}^{\infty} \hat{\varphi}_{k,n} z^{k-n}$$

for $n \geq 2$, where $\hat{\varphi}_{k,n} \coloneqq k\,(k-1)\cdots(k-n+1)\,\hat{r}_k$ for $k \geq n$. The above series converges in the same domain as (5.4). By substituting the asymptotic approximation (5.5) regarding the saddle point z_0 into the equation above and noting that

$$z_0^j \sim \beta^j \sum_{l=0}^{\infty} \hat{\upsilon}_{l,j}\beta^l \tag{5.7}$$

for $j \geq 0$, where

$$\hat{\upsilon}_{0,j} = \hat{\xi}_0^j,$$

$$\hat{\upsilon}_{l,j} = \frac{1}{l\hat{\xi}_0} \sum_{k=1}^{l} (kj - l + k)\,\hat{\xi}_k \hat{\upsilon}_{l-k,j}, \quad \text{for} \quad l \geq 1,$$

we can get that for $n \geq 2$,

$$\rho^{(n)}\,(z_0;\beta) \sim \sum_{l=0}^{\infty} \hat{\phi}_{l,n}\beta^l \tag{5.8}$$

with $\beta \ll 1$, where $\hat{\phi}_{l,n} = \sum_{k=0}^{l} \hat{\varphi}_{n+l-k,n}\hat{\upsilon}_{k,l-k}$ for $l \geq 0$.

With the completion of the foregoing, we are now ready to determine the paths of steepest descent through z_0 given by

$$\mathrm{Im}\,(\rho\,(z;\beta)) - \mathrm{Im}\,(\rho\,(z_0;\beta)) = \mathrm{Im}\,(\rho\,(z;\beta) - \rho\,(z_0;\beta)) = 0.$$

When expanding $\rho(z;\beta)$ in the Taylor series (5.6) near the saddle point z_0, we consider the leading order and set

$$\operatorname{Im}(\rho(z;\beta)-\rho(z_0;\beta))=\operatorname{Im}\left(\frac{1}{2!}\rho''(z_0;\beta)(z-z_0)^2+\mathrm{O}\left((z-z_0)^3\right)\right)=0. \quad (5.9)$$

On the other hand, from (5.8) we have

$$\rho''(z_0;\beta)\sim\hat{\phi}_{0,2}+\mathrm{O}(\beta)=\hat{\varphi}_{2,2}\hat{v}_{0,0}+\mathrm{O}(\beta)=2\hat{r}_2+\mathrm{O}(\beta)=-\frac{1}{90}+\mathrm{O}(\beta). \quad (5.10)$$

Indeed using the properties of the functions $\varsigma(z)$ and $\rho(z;\beta)$, we can show $\rho''(z_0;\beta)<0$. If we set $z\coloneqq u+\mathrm{i}v$ for $u,v\in\mathbb{R}$, then (5.9) implies that the paths of steepest descent and ascent from z_0 lie along the curves

$$2u(v-\operatorname{Im}(z_0))+\mathrm{O}\left(|z-z_0|^3\right)=0$$

since z_0 is purely imaginary. These two steepest paths, close enough to the saddle point z_0, that is when $|z-z_0|$ is small, are the two straight lines

$$u=0, \quad (5.11)$$

$$v=\operatorname{Im}(z_0). \quad (5.12)$$

To distinguish between the ascent and descent paths, we consider $\operatorname{Re}(\rho(z;\beta))$ along the two lines near $z=z_0$. Along (5.11) by application of (5.6) and (5.10), we have

$$\begin{aligned}
\operatorname{Re}(\rho(z;\beta)) &= \operatorname{Re}\left(\rho(z_0;\beta)+\frac{1}{2!}\rho''(z_0;\beta)(z-z_0)^2+\mathrm{O}\left((z-z_0)^3\right)\right)\\
&= \operatorname{Re}(\rho(z_0;\beta))+\frac{1}{2!}\rho''(z_0;\beta)\operatorname{Re}\left((z-z_0)^2\right)+\mathrm{O}\left(|z-z_0|^3\right)\\
&= \operatorname{Re}(\rho(z_0;\beta))+\frac{1}{2!}\rho''(z_0;\beta)\left(u^2-(v-\operatorname{Im}(z_0))^2\right)+\mathrm{O}\left(|z-z_0|^3\right)\\
&= \operatorname{Re}(\rho(z_0;\beta))-\frac{1}{2!}\rho''(z_0;\beta)(v-\operatorname{Im}(z_0))^2+\mathrm{O}\left(|z-z_0|^3\right)\\
&\geq \operatorname{Re}(\rho(z_0;\beta)),
\end{aligned}$$

when z is near z_0. Along (5.12) we proceed very much in the same way as above to write

$$\begin{aligned}\mathrm{Re}\left(\rho\left(z;\beta\right)\right) &= \mathrm{Re}\left(\rho\left(z_0;\beta\right)\right) + \frac{1}{2!}\rho''\left(z_0;\beta\right)\left(u^2 - \left(v - \mathrm{Im}\left(z_0\right)\right)^2\right) + \mathrm{O}\left(\left|z - z_0\right|^3\right) \\ &= \mathrm{Re}\left(\rho\left(z_0;\beta\right)\right) + \frac{1}{2!}\rho''\left(z_0;\beta\right)u^2 + \mathrm{O}\left(\left|z - z_0\right|^3\right) \\ &\leq \mathrm{Re}\left(\rho\left(z_0;\beta\right)\right)\end{aligned}$$

for z close enough to z_0. Thus, the path of steepest descents from z_0 is $v = \mathrm{Im}\left(z_0\right)$, parallel to the real axis.

We now show that the original contour of the integration (5.2) can be deformed onto the steepest descent paths through the saddle point z_0, denoted by $\mathcal{C}_l$ for $u < 0$ and $\mathcal{C}_r$ for $u > 0$, both pointing a direction away from z_0. As z_0 is in the domain of analyticity of $\rho\left(z;\beta\right)$, Cauchy's theorem tells us that

$$\begin{aligned}&\int_{-R}^{R}\exp\left(P\rho\left(z;\beta\right)\right)dz + \int_{R+\mathrm{Im}(z_0)\mathrm{i}}^{-R+\mathrm{Im}(z_0)\mathrm{i}}\exp\left(P\rho\left(z;\beta\right)\right)dz \\ =& -\int_{R}^{R+\mathrm{Im}(z_0)\mathrm{i}}\exp\left(P\rho\left(z;\beta\right)\right)dz - \int_{-R+\mathrm{Im}(z_0)\mathrm{i}}^{-R}\exp\left(P\rho\left(z;\beta\right)\right)dz\end{aligned}$$

for some $R > 0$. Further, we have

$$\begin{aligned}&\left|\int_{R}^{R+\mathrm{Im}(z_0)\mathrm{i}}\exp\left(P\rho\left(z;\beta\right)\right)dz\right| \\ \leq& \int_{0}^{\mathrm{Im}(z_0)}\left|\exp\left(P\rho\left(R + y\mathrm{i};\beta\right)\right)\right|\,dy \\ =& \int_{0}^{\mathrm{Im}(z_0)}\exp\left(P\mathrm{Re}\left(\rho\left(R + y\mathrm{i};\beta\right)\right)\right)dy.\end{aligned}$$

In the limit $R \to +\infty$, the above integral tends to zero because $z = R + y\mathrm{i}$ lies in the valley of ρ and $\mathrm{Re}\left(\rho\left(z;\beta\right)\right)$ tends to negative infinity as z descends away from

the saddle point. Similarly, we have

$$\left|\int_{-R+\mathrm{Im}(z_0)\mathrm{i}}^{-R} \exp\left(P\rho\left(z;\beta\right)\right)dz\right| \to 0, \quad \text{as} \quad R \to +\infty.$$

Then it follows that

$$\begin{aligned} f_{Z^P}\left(x\right) =& \frac{1}{4\pi}\sqrt{\frac{2P}{45}}\int_{-\infty}^{+\infty} \exp\left(P\rho\left(z;\beta\right)\right)dz \\ =& -\frac{1}{4\pi}\sqrt{\frac{2P}{45}}\int_{\mathrm{Im}(z_0)\mathrm{i}+\infty}^{\mathrm{Im}(z_0)\mathrm{i}-\infty} \exp\left(P\rho\left(z;\beta\right)\right)dz \\ =& \frac{1}{4\pi}\sqrt{\frac{2P}{45}}\int_{\mathcal{C}_r-\mathcal{C}_l} \exp\left(P\rho\left(z;\beta\right)\right)dz, \end{aligned} \tag{5.13}$$

completing the proof. □

Theorem 5.1.2

As $P \to +\infty$ with fixed x such that $|x| \ll \sqrt{P}/\sqrt{2/45}$, i.e. $\beta \ll 1$, we have

$$f_{Z^P}\left(x\right) \sim \frac{1}{4\pi}\sqrt{\frac{2}{45}}\exp\left(P\sum_{l=2}^{\infty}\hat{\rho}_l\beta^l\right)\sum_{j=0}^{\infty}\sum_{l=0}^{\infty}\sum_{n=0}^{\lfloor\frac{2}{3}j\rfloor}\hat{\alpha}_{n,l,j}\Gamma\left(j+\frac{1}{2}\right)\beta^l P^{n-j},$$

where $\hat{\rho}_l$ and $\hat{\alpha}_{n,l,j}$ are constants with explicit form given in the proof and $\Gamma\left(c\right)$ is the gamma function.

Proof. In Lemma 5.1.1, we have deformed the original contour of integration, i.e. the real axis, onto the steepest descent paths where $\mathrm{Im}\left(\rho\left(z;\beta\right)\right)$ is constant and $\mathrm{Re}\left(\rho\left(z;\beta\right)\right)$ reaches its maximum at the saddle point z_0. Hence, the main contributions to the asymptotic expansion of the integral comes from a small neighbourhood of z_0 for large P. We use Laplace's method to evaluate the integral (5.13). For some $\epsilon > 0$, we have the following asymptotic relation:

$$f_{Z^P}\left(x\right) \sim \frac{1}{4\pi}\sqrt{\frac{2P}{45}}\int_{\mathrm{Im}(z_0)\mathrm{i}-\epsilon}^{\mathrm{Im}(z_0)\mathrm{i}+\epsilon} \exp\left(P\rho\left(z;\beta\right)\right)dz, \quad \text{as} \quad P \to +\infty, \tag{5.14}$$

where by replacing the contour of integration $\mathcal{C}_r - \mathcal{C}_l$ with a narrow interval centred around z_0, only exponentially small errors are introduced for large P. Now, ϵ can be chosen so small that we can replace $\rho\left(z;\beta\right)$ by its Taylor expansion (5.6), which

converges on the interval $(\mathrm{Im}\,(z_0)\,\mathrm{i}-\epsilon, \mathrm{Im}\,(z_0)\,\mathrm{i}+\epsilon)$. Then, separating the quadratic term from all the higher-order terms of the series expansion (5.6) in $\exp\left(P\rho\left(z;\beta\right)\right)$ and setting

$$g\left(z;\beta\right) \coloneqq \exp\left(P\left(z-z_0\right)^3 \sum_{k\geq 0} \frac{\rho^{(k+3)}\left(z_0;\beta\right)}{(k+3)!}\left(z-z_0\right)^k\right), \tag{5.15}$$

the integral (5.14) becomes

$$f_{Z^P}\left(x\right) \sim \frac{1}{4\pi}\sqrt{\frac{2P}{45}}\exp\left(P\rho\left(z_0;\beta\right)\right)\int_{\mathrm{Im}(z_0)\mathrm{i}-\epsilon}^{\mathrm{Im}(z_0)\mathrm{i}+\epsilon} \exp\left(P\frac{1}{2!}\rho''\left(z_0;\beta\right)\left(z-z_0\right)^2\right) g\left(z;\beta\right)\,dz, \tag{5.16}$$

as $P\to+\infty$.

To find $\rho\left(z_0;\beta\right)$, we use (5.4), (5.5) and (5.7) to write

$$\begin{aligned}
\rho\left(z_0;\beta\right) &= \frac{1}{2}\beta\mathrm{i}z_0 + \sum_{k=2}^{\infty}\hat{r}_k z_0^k \\
&\sim \frac{1}{2}\beta\mathrm{i}\left(\beta\sum_{l=0}^{\infty}\hat{\xi}_l\beta^l\right) + \sum_{k=2}^{\infty}\hat{r}_k\left(\beta^k\sum_{l=0}^{\infty}\hat{\upsilon}_{l,k}\beta^l\right) \\
&\sim \frac{1}{2}\mathrm{i}\sum_{k=2}^{\infty}\hat{\xi}_{k-2}\beta^k + \sum_{k=2}^{\infty}\left(\sum_{m=2}^{k}\hat{r}_m\hat{\upsilon}_{k-m,m}\right)\beta^k \\
&\sim \sum_{k=2}^{\infty}\left(\frac{1}{2}\mathrm{i}\hat{\xi}_{k-2} + \sum_{m=2}^{k}\hat{r}_m\hat{\upsilon}_{k-m,m}\right)\beta^k \\
&\sim \sum_{k=2}^{\infty}\hat{\rho}_k\beta^k,
\end{aligned}$$

where for $k\geq 2$, $\hat{\rho}_k \coloneqq \mathrm{i}\hat{\xi}_{k-2}/2 + \sum_{m=2}^{k}\hat{r}_m\hat{\upsilon}_{k-m,m}$.

Since the series in the argument of the exponential function which defines $g\left(z;\beta\right)$ in (5.15) is convergent near z_0, we can write as $z\to z_0$,

$$g\left(z;\beta\right) = \exp\left(P\left(z-z_0\right)^3\sum_{k\geq 0}\hat{\sigma}_k\left(\beta\right)\left(z-z_0\right)^k\right)$$

$$\sim \sum_{n=0}^{\infty} \frac{1}{n!} P^n (z - z_0)^{3n} \left(\sum_{k \geq 0} \hat{\sigma}_k (\beta) (z - z_0)^k \right)^n, \tag{5.17}$$

where $\hat{\sigma}_k (\beta) \coloneqq \rho^{(k+3)} (z_0; \beta)/(k+3)!$ for $k \geq 0$. Further, the asymptotic approximation (5.8) for $\rho^{(k+3)} (z_0; \beta)$ gives us

$$\hat{\sigma}_k (\beta) \sim \sum_{l=0}^{\infty} \hat{\gamma}_{l,k} \beta^l$$

with $\hat{\gamma}_{l,k} \coloneqq \hat{\phi}_{l,k+3}/(k+3)!$ for $l, k \geq 0$ when β is small. As an immediate consequence of the properties for asymptotic series, we have for $n \geq 2$,

$$\left(\sum_{k \geq 0} \hat{\sigma}_k (\beta) (z - z_0)^k \right)^n \sim \sum_{k_1=0}^{\infty} \sum_{k_2=0}^{k_1} \cdots \sum_{k_n=0}^{k_{n-1}} \hat{\sigma}_{k_n} (\beta) \hat{\sigma}_{k_{n-1}-k_n} (\beta) \cdots \hat{\sigma}_{k_1-k_2} (\beta) (z - z_0)^{k_1},$$

as $z \to z_0$. In addition, we observe for $n \geq 2$ and $0 \leq k_n \leq k_{n-1} \leq \cdots \leq k_1$,

$$\begin{aligned}
&\hat{\sigma}_{k_n} (\beta) \hat{\sigma}_{k_{n-1}-k_n} (\beta) \cdots \hat{\sigma}_{k_1-k_2} (\beta) \\
&\sim \left(\sum_{l_1=0}^{\infty} \hat{\gamma}_{l_1,k_n} \beta^{l_1} \right) \left(\sum_{l_2=0}^{\infty} \hat{\gamma}_{l_2,k_{n-1}-k_n} \beta^{l_2} \right) \cdots \left(\sum_{l_n=0}^{\infty} \hat{\gamma}_{l_n,k_1-k_2} \beta^{l_n} \right) \\
&\sim \sum_{l_1=0}^{\infty} \sum_{l_2=0}^{l_1} \cdots \sum_{l_n=0}^{l_{n-1}} \hat{\gamma}_{l_n,k_n} \hat{\gamma}_{l_{n-1}-l_n,k_{n-1}-k_n} \cdots \hat{\gamma}_{l_1-l_2,k_1-k_2} \beta^{l_1} \\
&\sim \sum_{l_1=0}^{\infty} \hat{\mathcal{C}}_{l_1,k_1,k_2,\cdots,k_n} \beta^{l_1},
\end{aligned}$$

where $\hat{\mathcal{C}}_{l_1,k_1,k_2,\cdots,k_n} \coloneqq \sum_{l_2=0}^{l_1} \cdots \sum_{l_n=0}^{l_{n-1}} \hat{\gamma}_{l_n,k_n} \hat{\gamma}_{l_{n-1}-l_n,k_{n-1}-k_n} \cdots \hat{\gamma}_{l_1-l_2,k_1-k_2}$ for $l_1 \geq 0$. Generally, for $n \geq 0$ we see that

$$\left(\sum_{k \geq 0} \hat{\sigma}_k (\beta) (z - z_0)^k \right)^n \sim \sum_{k=0}^{\infty} \hat{\theta}_{k,n} (\beta) (z - z_0)^k, \quad \text{as} \quad z \to z_0.$$

Here $\hat{\theta}_{k,n}(\beta)$ are functions of β satisfying $\hat{\theta}_{k,n}(\beta) \sim \sum_{l=0}^{\infty} \hat{\mathcal{E}}_{l,k,n} \beta^l$ for $k \geq 0$ with the

constants $\hat{\mathcal{E}}_{l,k,n}$ as stated below: for $n = 0$,

$$\hat{\mathcal{E}}_{l,k,n} = \hat{\mathcal{E}}_{l,k,0} = \begin{cases} 1, & \text{for} \quad k = l = 0, \\ 0, & \text{otherwise}, \end{cases}$$

for $n = 1$,

$$\hat{\mathcal{E}}_{l,k,n} = \hat{\mathcal{E}}_{l,k,1} = \hat{\gamma}_{l,k}, \quad \text{for} \quad k, l \geq 0,$$

for $n = 2$,

$$\hat{\mathcal{E}}_{l,k,n} = \hat{\mathcal{E}}_{l,k,2} = \sum_{k_2=0}^{k} \hat{\mathcal{C}}_{l,k,k_2}, \quad \text{for} \quad k, l \geq 0,$$

for $n \geq 3$,

$$\hat{\mathcal{E}}_{l,k,n} = \sum_{k_2=0}^{k} \sum_{k_3=0}^{k_2} \cdots \sum_{k_n=0}^{k_{n-1}} \hat{\mathcal{C}}_{l,k,k_2,\cdots,k_n}, \quad \text{for} \quad k, l \geq 0.$$

Using these factors, we can rewrite $g(z;\beta)$ in (5.17) as

$$\begin{aligned} g(z;\beta) &\sim \sum_{n=0}^{\infty} \frac{1}{n!} P^n (z - z_0)^{3n} \left(\sum_{k=0}^{\infty} \hat{\theta}_{k,n}(\beta) (z - z_0)^k \right) \\ &\sim \sum_{n=0}^{\infty} \sum_{k=0}^{\infty} \frac{1}{n!} P^n \hat{\theta}_{k,n}(\beta) (z - z_0)^{3n+k} \\ &\sim \sum_{j=0}^{\infty} \sum_{3n+k=j} \frac{1}{n!} P^n \hat{\theta}_{k,n}(\beta) (z - z_0)^j \\ &\sim \sum_{j=0}^{\infty} \sum_{n=0}^{\lfloor \frac{j}{3} \rfloor} \frac{1}{n!} P^n \hat{\theta}_{j-3n,n}(\beta) (z - z_0)^j \\ &\sim \sum_{j=0}^{\infty} \hat{g}_j(\beta) (z - z_0)^j \end{aligned}$$

in the limit $z \to z_0$, where $\hat{g}_j(\beta) := \sum_{n=0}^{\lfloor j/3 \rfloor} P^n \hat{\theta}_{j-3n,n}(\beta)/n!$ for $j \geq 0$. Hence by

Definition 2.1.7, we have

$$g\left(z;\beta\right)-\sum_{j=0}^{J}\hat{g}_{j}\left(\beta\right)\left(z-z_{0}\right)^{j}=\mathrm{o}\left(\left(z-z_{0}\right)^{J}\right),\quad\text{as}\quad z\rightarrow z_{0}$$

for any $J\geq 0$. From this it follows from Definition 2.1.3 that for any $\epsilon^{*}>0$ there is an interval $|z-z_{0}|<L$ for some $L>0$, in which

$$\left|g\left(z;\beta\right)-\sum_{j=0}^{J}\hat{g}_{j}\left(\beta\right)\left(z-z_{0}\right)^{j}\right|\leq\epsilon^{*}\left|\left(z-z_{0}\right)^{J}\right|.$$

Therefore for any $0<\epsilon<L$, we have

$$\begin{aligned}
&\left|\int_{\mathrm{Im}(z_{0})\mathrm{i}-\epsilon}^{\mathrm{Im}(z_{0})\mathrm{i}}\exp\left(P\frac{1}{2}\rho''\left(z_{0};\beta\right)\left(z-z_{0}\right)^{2}\right)\left(g\left(z;\beta\right)-\sum_{j=0}^{J}\hat{g}_{j}\left(\beta\right)\left(z-z_{0}\right)^{j}\right)\,dz\right| \\
\leq&\int_{\mathrm{Im}(z_{0})\mathrm{i}-\epsilon}^{\mathrm{Im}(z_{0})\mathrm{i}}\exp\left(P\frac{1}{2}\rho''\left(z_{0};\beta\right)\left(z-z_{0}\right)^{2}\right)\left|g\left(z;\beta\right)-\sum_{j=0}^{J}\hat{g}_{j}\left(\beta\right)\left(z-z_{0}\right)^{j}\right|\,dz \\
\leq&\epsilon^{*}\int_{\mathrm{Im}(z_{0})\mathrm{i}-\epsilon}^{\mathrm{Im}(z_{0})\mathrm{i}}\exp\left(P\frac{1}{2}\rho''\left(z_{0};\beta\right)\left(z-z_{0}\right)^{2}\right)\left|\left(z-z_{0}\right)^{J}\right|\,dz \\
=&\epsilon^{*}\left(-1\right)^{J}\int_{\mathrm{Im}(z_{0})\mathrm{i}-\epsilon}^{\mathrm{Im}(z_{0})\mathrm{i}}\exp\left(P\frac{1}{2}\rho''\left(z_{0};\beta\right)\left(z-z_{0}\right)^{2}\right)\left(z-z_{0}\right)^{J}\,dz.
\end{aligned}$$

Then as $\epsilon\rightarrow 0^{+}$, we can write

$$\begin{aligned}
&\int_{\mathrm{Im}(z_{0})\mathrm{i}-\epsilon}^{\mathrm{Im}(z_{0})\mathrm{i}}\exp\left(P\frac{1}{2}\rho''\left(z_{0};\beta\right)\left(z-z_{0}\right)^{2}\right)g\left(z;\beta\right)\,dz \\
=&\sum_{j=0}^{J}\hat{g}_{j}\left(\beta\right)\int_{\mathrm{Im}(z_{0})\mathrm{i}-\epsilon}^{\mathrm{Im}(z_{0})\mathrm{i}}\exp\left(P\frac{1}{2}\rho''\left(z_{0};\beta\right)\left(z-z_{0}\right)^{2}\right)\left(z-z_{0}\right)^{j}\,dz \\
&+\mathrm{o}\left(\int_{\mathrm{Im}(z_{0})\mathrm{i}-\epsilon}^{\mathrm{Im}(z_{0})\mathrm{i}}\exp\left(P\frac{1}{2}\rho''\left(z_{0};\beta\right)\left(z-z_{0}\right)^{2}\right)\left(z-z_{0}\right)^{J}\,dz\right),
\end{aligned}$$

which gives

$$\int_{\mathrm{Im}(z_{0})\mathrm{i}-\epsilon}^{\mathrm{Im}(z_{0})\mathrm{i}}\exp\left(P\frac{1}{2}\rho''\left(z_{0};\beta\right)\left(z-z_{0}\right)^{2}\right)g\left(z;\beta\right)\,dz$$

$$\sim \sum_{j=0}^{\infty} \hat{g}_j(\beta) \int_{\mathrm{Im}(z_0)\mathrm{i}-\epsilon}^{\mathrm{Im}(z_0)\mathrm{i}} \exp\left(P\frac{1}{2}\rho''(z_0;\beta)(z-z_0)^2\right)(z-z_0)^j\,dz$$

for small ϵ. Now the above integrals can be evaluated by change of variables. For arbitrary $j \geq 0$, the substitution $z = \mathrm{Im}(z_0)\,\mathrm{i} + x$ yields

$$\int_{\mathrm{Im}(z_0)\mathrm{i}-\epsilon}^{\mathrm{Im}(z_0)\mathrm{i}} \exp\left(P\frac{1}{2}\rho''(z_0;\beta)(z-z_0)^2\right)(z-z_0)^j\,dz = \int_{-\epsilon}^{0} \exp\left(P\frac{1}{2}\rho''(z_0;\beta)\,x^2\right)x^j\,dx.$$

Let us introduce the new variable ζ by

$$\frac{1}{2}\rho''(z_0;\beta)\,x^2 = -\zeta.$$

This leads to

$$\begin{aligned}
&\int_{\mathrm{Im}(z_0)\mathrm{i}-\epsilon}^{\mathrm{Im}(z_0)\mathrm{i}} \exp\left(P\frac{1}{2}\rho''(z_0;\beta)(z-z_0)^2\right)(z-z_0)^j\,dz \\
=&\int_{-\frac{1}{2}\rho''(z_0;\beta)\epsilon^2}^{0} \exp(-P\zeta)\left(-\sqrt{\frac{-2\zeta}{\rho''(z_0;\beta)}}\right)^j\left(-\sqrt{\frac{-2}{\rho''(z_0;\beta)}}\frac{1}{2\sqrt{\zeta}}\right)d\zeta \\
=&\frac{1}{2}(-1)^j\left(\frac{-2}{\rho''(z_0;\beta)}\right)^{\frac{1}{2}(j+1)}\int_0^{-\frac{1}{2}\rho''(z_0;\beta)\epsilon^2}\zeta^{\frac{1}{2}(j-1)}\exp(-P\zeta)\,d\zeta.
\end{aligned}$$

Thus as $\epsilon \to 0^+$, we have

$$\begin{aligned}
&\int_{\mathrm{Im}(z_0)\mathrm{i}-\epsilon}^{\mathrm{Im}(z_0)\mathrm{i}} \exp\left(P\frac{1}{2}\rho''(z_0;\beta)(z-z_0)^2\right)g(z;\beta)\,dz \\
\sim&\sum_{j=0}^{\infty}\hat{g}_j(\beta)\frac{1}{2}(-1)^j\left(\frac{-2}{\rho''(z_0;\beta)}\right)^{\frac{1}{2}(j+1)}\int_0^{-\frac{1}{2}\rho''(z_0;\beta)\epsilon^2}\zeta^{\frac{1}{2}(j-1)}\exp(-P\zeta)\,d\zeta.
\end{aligned}$$

Similar arguments give us that

$$\begin{aligned}
&\int_{\mathrm{Im}(z_0)\mathrm{i}}^{\mathrm{Im}(z_0)\mathrm{i}+\epsilon} \exp\left(P\frac{1}{2}\rho''(z_0;\beta)(z-z_0)^2\right)g(z;\beta)\,dz \\
\sim&\sum_{j=0}^{\infty}\hat{g}_j(\beta)\frac{1}{2}\left(\frac{-2}{\rho''(z_0;\beta)}\right)^{\frac{1}{2}(j+1)}\int_0^{-\frac{1}{2}\rho''(z_0;\beta)\epsilon^2}\zeta^{\frac{1}{2}(j-1)}\exp(-P\zeta)\,d\zeta,
\end{aligned}$$

as $\epsilon \to 0^+$.

Hence, the integration in (5.16) can be expanded in an asymptotic series for small ϵ as follows:

$$\int_{\mathrm{Im}(z_0)\mathrm{i}-\epsilon}^{\mathrm{Im}(z_0)\mathrm{i}+\epsilon} \exp\left(P\frac{1}{2!}\rho''\left(z_0;\beta\right)\left(z-z_0\right)^2\right) g\left(z;\beta\right)\, dz$$

$$\sim \sum_{j=0}^{\infty} \frac{1}{2}\left(1+(-1)^j\right)\hat{g}_j\left(\beta\right)\left(\frac{-2}{\rho''\left(z_0;\beta\right)}\right)^{\frac{1}{2}(j+1)} \int_0^{-\frac{1}{2}\rho''(z_0;\beta)\epsilon^2} \zeta^{\frac{1}{2}(j-1)} \exp\left(-P\zeta\right) d\zeta,$$

where terms with odd j vanish. For large P, we can extend the integration region in each integral to infinity. With this replacement, we introduce only exponentially small errors for large P, whence we have as $P \to +\infty$,

$$\begin{aligned}
&\int_0^{-\frac{1}{2}\rho''(z_0;\beta)\epsilon^2} \zeta^{\frac{1}{2}(j-1)} \exp\left(-P\zeta\right) d\zeta \\
\sim &\int_0^{+\infty} \zeta^{\frac{1}{2}(j-1)} \exp\left(-P\zeta\right) d\zeta \\
= &P^{-\frac{1}{2}(j+1)}\Gamma\left(\frac{j}{2}+\frac{1}{2}\right)
\end{aligned}$$

for $j \geq 0$. Assembling the above results, we have the following asymptotic series for (5.16)

$$f_{Z^P}\left(x\right) \sim \frac{1}{4\pi}\sqrt{\frac{2P}{45}} \exp\left(P\sum_{l=2}^{\infty}\hat{\rho}_l\beta^l\right) \sum_{j=0}^{\infty}\hat{g}_{2j}\left(\beta\right)\left(\frac{-2}{\rho''\left(z_0;\beta\right)}\right)^{j+\frac{1}{2}} P^{-\left(j+\frac{1}{2}\right)}\Gamma\left(j+\frac{1}{2}\right) \tag{5.18}$$

in the limit $P \to +\infty$ for fixed x such that $|x| \ll \sqrt{P}/\sqrt{2/45}$.

Lastly, we wish to express the terms involving β, i.e. $\hat{g}_{2j}\left(\beta\right)\left(-2/\rho''\left(z_0;\beta\right)\right)^{j+1/2}$ as an asymptotic series in β. This can be achieved by collecting the coefficients from the product of their individual series. Assume that

$$\sqrt{\frac{-2}{\rho''\left(z_0;\beta\right)}} \sim \sum_{n=0}^{\infty}\hat{K}_n\beta^n \tag{5.19}$$

for some constants $\hat{K}_n$ for $n \geq 0$. Then taking the square on both sides yields

$$\frac{-2}{\rho''(z_0;\beta)} \sim \sum_{l=0}^{\infty} \sum_{k=0}^{l} \hat{K}_k \hat{K}_{l-k} \beta^l \sim \sum_{l=0}^{\infty} \hat{\mu}_l \beta^l,$$

where $\hat{\mu}_l \coloneqq \sum_{k=0}^{l} \hat{K}_k \hat{K}_{l-k}$ for $l \geq 0$. On the other hand, by performing simple arithmetical operations on the asymptotic series (5.8) with $n = 2$ for $\rho''(z_0;\beta)$, we see

$$\frac{-2}{\rho''(z_0;\beta)} \sim \sum_{l=0}^{\infty} \hat{\varpi}_l \beta^l,$$

where

$$\hat{\varpi}_0 = -\frac{2}{\hat{\phi}_{0,2}},$$

$$\hat{\varpi}_l = -\frac{1}{\hat{\phi}_{0,2}} \sum_{m=0}^{l-1} \hat{\varpi}_m \hat{\phi}_{l-m,2}, \quad \text{for} \quad l \geq 1.$$

Hence, by equating the coefficients following the uniqueness of asymptotic expansions (Bender and Orszag [8, Chapter 3.8, p. 125]), we find

$$\hat{\varpi}_l = \hat{\mu}_l = \sum_{k=0}^{l} \hat{K}_k \hat{K}_{l-k}, \quad \text{for} \quad l \geq 0,$$

providing the values for the constants $\hat{K}_k$ with $k \geq 0$.

Based on the previous analysis, we are now ready to derive the asymptotic approximation of $(-2/\rho''(z_0;\beta))^{j+1/2}$ for $\beta \ll 1$. Indeed, from (5.19) we have for $j \geq 0$,

$$\left(\frac{-2}{\rho''(z_0;\beta)}\right)^{j+\frac{1}{2}} \sim \left(\sum_{n=0}^{\infty} \hat{K}_n \beta^n\right)^{2j+1} \sim \sum_{n=0}^{\infty} \hat{\omega}_{n,j} \beta^n,$$

where for $j = 0$,

$$\hat{\omega}_{n,j} = \hat{\omega}_{n,0} = \hat{K}_n, \quad \text{for} \quad n \geq 0,$$

for $j \geq 1$,

$$\hat{\omega}_{n,j} = \sum_{n_2=0}^{n} \sum_{n_3=0}^{n_2} \cdots \sum_{n_{2j+1}=0}^{n_{2j}} \hat{K}_{n_{2j+1}} \hat{K}_{n_{2j}-n_{2j+1}} \cdots \hat{K}_{n_2-n_3} \hat{K}_{n-n_2}, \quad \text{for} \quad n \geq 0.$$

If we combine the series which is asymptotic to $\hat{g}_{2j}(\beta)$ with the explicit expansion given above, we obtain for $j \geq 0$,

$$\begin{aligned}
&\hat{g}_{2j}(\beta) \left(\frac{-2}{\rho''(z_0;\beta)} \right)^{j+\frac{1}{2}} \\
&\sim \left(\sum_{n=0}^{\lfloor \frac{2}{3}j \rfloor} \frac{1}{n!} P^n \sum_{l=0}^{\infty} \hat{\mathcal{E}}_{l,2j-3n,n} \beta^l \right) \left(\sum_{n=0}^{\infty} \hat{\omega}_{n,j} \beta^n \right) \\
&\sim \left(\sum_{l=0}^{\infty} \left(\sum_{n=0}^{\lfloor \frac{2}{3}j \rfloor} \frac{1}{n!} P^n \hat{\mathcal{E}}_{l,2j-3n,n} \right) \beta^l \right) \left(\sum_{k=0}^{\infty} \hat{\omega}_{k,j} \beta^k \right) \\
&\sim \sum_{l=0}^{\infty} \left(\sum_{k=0}^{l} \left(\sum_{n=0}^{\lfloor \frac{2}{3}j \rfloor} \frac{1}{n!} P^n \hat{\mathcal{E}}_{k,2j-3n,n} \right) \hat{\omega}_{l-k,j} \right) \beta^l \\
&\sim \sum_{l=0}^{\infty} \sum_{n=0}^{\lfloor \frac{2}{3}j \rfloor} \sum_{k=0}^{l} \frac{1}{n!} \hat{\omega}_{l-k,j} \hat{\mathcal{E}}_{k,2j-3n,n} P^n \beta^l \\
&\sim \sum_{l=0}^{\infty} \sum_{n=0}^{\lfloor \frac{2}{3}j \rfloor} \hat{\alpha}_{n,l,j} P^n \beta^l
\end{aligned}$$

with $\hat{\alpha}_{n,l,j} \coloneqq \sum_{k=0}^{l} \hat{\omega}_{l-k,j} \hat{\mathcal{E}}_{k,2j-3n,n}/n!$ for $0 \leq n \leq \lfloor 2j/3 \rfloor$ and $l \geq 0$. Then (5.18) becomes

$$f_{Z^P}(x) \sim \frac{1}{4\pi} \sqrt{\frac{2P}{45}} \exp\left(P \sum_{l=2}^{\infty} \hat{\rho}_l \beta^l \right) \sum_{j=0}^{\infty} \sum_{l=0}^{\infty} \sum_{n=0}^{\lfloor \frac{2}{3}j \rfloor} \hat{\alpha}_{n,l,j} P^n \beta^l P^{-\left(j+\frac{1}{2}\right)} \Gamma\left(j + \frac{1}{2}\right), \tag{5.20}$$

as $P \to +\infty$ with $\beta \ll 1$, which completes the proof. □

Having developed the large P asymptotic approximation for the probability density function f_{Z^P} with all the higher order terms given in reciprocal powers of P,

the next stage is to derive an asymptotic representation for the corresponding distribution function, which can be accomplished by taking the integration of (5.20). Before that, we first consider the integration on a finite interval (z_1, z_2), leading to an asymptotic expansion for the probability $\mathbb{P}\left(z_1 < Z^P \leq z_2\right)$. We then explain how this expression can be used to approximate the distribution function. The results are summarised in the next theorem.

Theorem 5.1.3

For $|z_1|$, $|z_2| \ll \sqrt{P}/\sqrt{2/45}$, the following asymptotic series expansion holds as $P \to +\infty$. For $z_1 < z_2 < 0$, we have

$$\int_{z_1}^{z_2} f_{Z^P}(x)\, dx \sim \frac{1}{4\pi}\sqrt{\frac{2}{45}} \sum_{j=0}^{\infty} P^{-\frac{j}{2}} \sum_{r=0}^{j} \sum_{n=0}^{r} \sum_{l=0}^{j-r} \hat{\eta}_{n,r} \hat{\lambda}_{l,j-r} (-1)^{r+l} \left(\sqrt{2}\right)^{2n+r+l-1} \cdot \left(\gamma\left(\frac{2n+r+l+1}{2}, \frac{(z_1)^2}{2}\right) - \gamma\left(\frac{2n+r+l+1}{2}, \frac{(z_2)^2}{2}\right)\right).$$

For $z_1 < 0 \leq z_2$, we have

$$\int_{z_1}^{z_2} f_{Z^P}(x)\, dx \sim \frac{1}{4\pi}\sqrt{\frac{2}{45}} \sum_{j=0}^{\infty} P^{-\frac{j}{2}} \sum_{r=0}^{j} \sum_{n=0}^{r} \sum_{l=0}^{j-r} \hat{\eta}_{n,r} \hat{\lambda}_{l,j-r} \left(\sqrt{2}\right)^{2n+r+l-1} \cdot \left((-1)^{r+l}\gamma\left(\frac{2n+r+l+1}{2}, \frac{(z_1)^2}{2}\right) + \gamma\left(\frac{2n+r+l+1}{2}, \frac{(z_2)^2}{2}\right)\right).$$

Here, $\hat{\eta}_{n,r}$ and $\hat{\lambda}_{l,j-r}$ are constants explicitly outlined in the proof and $\gamma(\alpha, \beta)$ is the lower incomplete gamma function.

Proof. Before integrating the density function, we first rewrite its asymptotic expansion in Theorem 5.1.2 in terms of the original variable x by using the identity $\beta = x\sqrt{2/45}/\sqrt{P}$. Accordingly in the limit $P \to +\infty$ with $|x| \ll \sqrt{P}/\sqrt{2/45}$, the probability density function admits

$$f_{Z^P}(x) \sim \frac{1}{4\pi}\sqrt{\frac{2}{45}} \exp\left(\sum_{l=2}^{\infty} \hat{\rho}_l \left(\frac{2}{45}\right)^{\frac{l}{2}} P^{1-\frac{l}{2}} x^l\right)$$

$$\cdot \sum_{j=0}^{\infty} \sum_{l=0}^{\infty} \sum_{n=0}^{\lfloor \frac{2}{3} j \rfloor} \hat{\alpha}_{n,l,j} \left(\frac{2}{45} \right)^{\frac{l}{2}} \Gamma \left(j + \frac{1}{2} \right) P^{n-\frac{l}{2}-j} x^l. \tag{5.21}$$

To justify that the integrated series is indeed asymptotic to the distribution function, we adjust the terms in (5.21) to form a more appropriate expression for easier computation.

Specifically, we separate the quadratic term $\hat{\rho}_2 (2/45) x^2$ from the argument $\sum_{l=2}^{\infty} \hat{\rho}_l (2/45)^{l/2} P^{1-l/2} x^l$ of the exponential function. As the integration is taken with respect to x, we expand the remaining term in an asymptotic approximation in P with all the coefficients given as polynomials of x. Note that

$$\hat{\rho}_2 = \frac{1}{2} \mathrm{i} \hat{\xi}_0 + \hat{r}_2 \left(\hat{\xi}_0 \right)^2 = -\frac{45}{4},$$

which gives

$$\exp \left(\sum_{l=2}^{\infty} \hat{\rho}_l \left(\frac{2}{45} \right)^{\frac{l}{2}} P^{1-\frac{l}{2}} x^l \right) \sim \exp \left(-\frac{1}{2} x^2 \right) \exp \left(\sum_{l=3}^{\infty} \hat{\rho}_l \left(\frac{2}{45} \right)^{\frac{l}{2}} P^{1-\frac{l}{2}} x^l \right), \tag{5.22}$$

as $P \to +\infty$, where

$$\begin{aligned}
&\exp \left(\sum_{l=3}^{\infty} \hat{\rho}_l \left(\frac{2}{45} \right)^{\frac{l}{2}} P^{1-\frac{l}{2}} x^l \right) \\
\sim &\sum_{n=0}^{\infty} \frac{1}{n!} \left(\sum_{l=3}^{\infty} \hat{\rho}_l \left(\frac{2}{45} \right)^{\frac{l}{2}} P^{1-\frac{l}{2}} x^l \right)^n \\
\sim &\sum_{n=0}^{\infty} \frac{1}{n!} \left(\sum_{l=0}^{\infty} \hat{\rho}_{l+3} \left(\frac{2}{45} \right)^{\frac{l+3}{2}} P^{1-\frac{l+3}{2}} x^{l+3} \right)^n \\
\sim &\sum_{n=0}^{\infty} \frac{1}{n!} \left(\frac{2}{45} \right)^{\frac{3n}{2}} P^{-\frac{n}{2}} x^{3n} \left(\sum_{k=0}^{\infty} \hat{\rho}_{k+3} \left(\frac{2}{45} \right)^{\frac{k}{2}} P^{-\frac{k}{2}} x^k \right)^n.
\end{aligned} \tag{5.23}$$

Analogous to the previous computations, the generalisation of multiplication of asymptotic expansions tells us for $n \geq 0$,

$$\left(\sum_{k=0}^{\infty} \hat{\rho}_{k+3} \left(\frac{2}{45} \right)^{\frac{k}{2}} P^{-\frac{k}{2}} x^k \right)^n \sim \sum_{k=0}^{\infty} \hat{\vartheta}_{k,n} \left(\frac{2}{45} \right)^{\frac{k}{2}} P^{-\frac{k}{2}} x^k, \tag{5.24}$$

where

$$\hat{\vartheta}_{0,n} = (\hat{\rho}_3)^n ,$$

$$\hat{\vartheta}_{k,n} = \frac{1}{k\hat{\rho}_3} \sum_{m=1}^{k} (mn - k + m)\, \hat{\rho}_{k+3} \hat{\vartheta}_{k-m,n}, \quad \text{for} \quad k \geq 1.$$

Using (5.22)−(5.24) amounts to

$$\begin{aligned}
&\exp\left(\sum_{l=2}^{\infty} \hat{\rho}_l \left(\frac{2}{45} \right)^{\frac{l}{2}} P^{1-\frac{l}{2}} x^l \right) \\
&\sim \exp\left(-\frac{1}{2}x^2 \right) \sum_{n=0}^{\infty} \frac{1}{n!} \left(\frac{2}{45} \right)^{\frac{3n}{2}} P^{-\frac{n}{2}} x^{3n} \sum_{k=0}^{\infty} \hat{\vartheta}_{k,n} \left(\frac{2}{45} \right)^{\frac{k}{2}} P^{-\frac{k}{2}} x^k \\
&\sim \exp\left(-\frac{1}{2}x^2 \right) \sum_{n=0}^{\infty} \sum_{k=0}^{\infty} \frac{1}{n!} \left(\frac{2}{45} \right)^{\frac{3n+k}{2}} \hat{\vartheta}_{k,n} P^{-\frac{n+k}{2}} x^{3n+k} \\
&\sim \exp\left(-\frac{1}{2}x^2 \right) \sum_{j=0}^{\infty} \left(\sum_{n=0}^{j} \frac{1}{n!} \left(\frac{2}{45} \right)^{\frac{2n+j}{2}} \hat{\vartheta}_{j-n,n} x^{2n+j} \right) P^{-\frac{j}{2}} \\
&\sim \exp\left(-\frac{1}{2}x^2 \right) \sum_{j=0}^{\infty} \hat{A}_j (x)\, P^{-\frac{j}{2}},
\end{aligned}$$

as $P \to +\infty$, where

$$\hat{A}_j (x) \coloneqq \sum_{n=0}^{j} \frac{1}{n!} \left(\frac{2}{45} \right)^{\frac{2n+j}{2}} \hat{\vartheta}_{j-n,n} x^{2n+j} = \sum_{n=0}^{j} \hat{\eta}_{n,j} x^{2n+j}, \quad \text{for} \quad j \geq 0$$

with $\hat{\eta}_{n,j} \coloneqq (2/45)^{n+j/2}\, \hat{\vartheta}_{j-n,n}/n!$ for $0 \leq n \leq j$. Further, we see that when $P \to +\infty$,

$$\begin{aligned}
&\sum_{j=0}^{\infty} \sum_{l=0}^{\infty} \sum_{n=0}^{\lfloor \frac{2}{3} j \rfloor} \hat{\alpha}_{n,l,j} \left(\frac{2}{45} \right)^{\frac{l}{2}} \Gamma\left(j + \frac{1}{2} \right) x^l P^{n-\frac{l}{2}-j} \\
&\sim \sum_{m=0}^{\infty} \sum_{l=0}^{\infty} \sum_{j=m}^{3m} \hat{\alpha}_{j-m,l,j} \left(\frac{2}{45} \right)^{\frac{l}{2}} \Gamma\left(j + \frac{1}{2} \right) x^l P^{-\left(m+\frac{l}{2}\right)}
\end{aligned}$$

$$\sim \sum_{\substack{r=0 \\ r \text{ even}}}^{\infty} \sum_{\substack{l=0 \\ l \text{ even}}}^{r} \sum_{j=\frac{r-l}{2}}^{\frac{3(r-l)}{2}} \hat{\alpha}_{j-\frac{r-l}{2},l,j} \left(\frac{2}{45}\right)^{\frac{l}{2}} \Gamma\left(j+\frac{1}{2}\right) x^l P^{-\frac{r}{2}}$$

$$+ \sum_{\substack{r=1 \\ r \text{ odd}}}^{\infty} \sum_{\substack{l=1 \\ l \text{ odd}}}^{r} \sum_{j=\frac{r-l}{2}}^{\frac{3(r-l)}{2}} \hat{\alpha}_{j-\frac{r-l}{2},l,j} \left(\frac{2}{45}\right)^{\frac{l}{2}} \Gamma\left(j+\frac{1}{2}\right) x^l P^{-\frac{r}{2}}$$

$$\sim \sum_{r=0}^{\infty} \hat{B}_r(x) P^{-\frac{r}{2}}$$

with

$$\hat{B}_r(x) \coloneqq \sum_{l=0}^{r} \hat{\lambda}_{l,r} x^l, \quad \text{for} \quad r \geq 0,$$

where for even r,

$$\hat{\lambda}_{l,r} \coloneqq \begin{cases} 0, & \text{for odd} \quad l, \\ \sum\limits_{j=\frac{r-l}{2}}^{\frac{3(r-l)}{2}} \hat{\alpha}_{j-\frac{r-l}{2},l,j} \left(\frac{2}{45}\right)^{\frac{l}{2}} \Gamma\left(j+\frac{1}{2}\right), & \text{for even} \quad l, \end{cases}$$

and for odd r,

$$\hat{\lambda}_{l,r} \coloneqq \begin{cases} 0, & \text{for even} \quad l, \\ \sum\limits_{j=\frac{r-l}{2}}^{\frac{3(r-l)}{2}} \hat{\alpha}_{j-\frac{r-l}{2},l,j} \left(\frac{2}{45}\right)^{\frac{l}{2}} \Gamma\left(j+\frac{1}{2}\right), & \text{for odd} \quad l. \end{cases}$$

Following the above discussion, (5.21) can be rearranged as

$$f_{Z^P}(x) \sim \frac{1}{4\pi}\sqrt{\frac{2}{45}} \exp\left(-\frac{1}{2}x^2\right) \left(\sum_{j=0}^{\infty} \hat{A}_j(x) P^{-\frac{j}{2}}\right) \left(\sum_{r=0}^{\infty} \hat{B}_r(x) P^{-\frac{r}{2}}\right)$$

$$\sim \frac{1}{4\pi}\sqrt{\frac{2}{45}} \exp\left(-\frac{1}{2}x^2\right) \sum_{j=0}^{\infty} \left(\sum_{r=0}^{j} \hat{A}_r(x) \hat{B}_{j-r}(x)\right) P^{-\frac{j}{2}}$$

$$\sim \frac{1}{4\pi}\sqrt{\frac{2}{45}} \exp\left(-\frac{1}{2}x^2\right) \sum_{j=0}^{\infty} \hat{\psi}_j(x) P^{-\frac{j}{2}},$$

where for $j \geq 0$,

$$\begin{aligned}\hat{\psi}_j(x) &:= \sum_{r=0}^{j} \hat{A}_r(x)\, \hat{B}_{j-r}(x) \\ &= \sum_{r=0}^{j} \left(\sum_{n=0}^{r} \hat{\eta}_{n,r} x^{2n+r} \right) \left(\sum_{l=0}^{j-r} \hat{\lambda}_{l,j-r} x^{l} \right) \\ &= \sum_{r=0}^{j} \sum_{n=0}^{r} \sum_{l=0}^{j-r} \hat{\eta}_{n,r} \hat{\lambda}_{l,j-r} x^{2n+r+l}.\end{aligned}$$

Then, by Definition 2.1.7 for asymptotic expansions, we have the order relation given below: for any $J \geq 0$,

$$f_{Z^P}(x) - \frac{1}{4\pi}\sqrt{\frac{2}{45}} \exp\left(-\frac{1}{2}x^2\right) \sum_{j=0}^{J} \hat{\psi}_j(x)\, P^{-\frac{j}{2}} = \mathrm{o}\left(P^{-\frac{J}{2}}\right),$$

as $P \to +\infty$ with $|x| \ll \sqrt{P}/\sqrt{2/45}$. Integrating on finite interval $(z_1, z_2]$ such that $|z_i| \ll \sqrt{P}/\sqrt{2/45}$ for $i = 1, 2$, we have

$$\int_{z_1}^{z_2} f_{Z^P}(x)\, dx = \frac{1}{4\pi}\sqrt{\frac{2}{45}} \sum_{j=0}^{J} P^{-\frac{j}{2}} \int_{z_1}^{z_2} \exp\left(-\frac{1}{2}x^2\right) \hat{\psi}_j(x)\, dx + \mathrm{o}\left(P^{-\frac{J}{2}}\right).$$

Next, we show the integrals on the right hand side are finite. In fact, for $0 \leq j \leq J$, we can write

$$\begin{aligned}&\left| \int_{z_1}^{z_2} \exp\left(-\frac{1}{2}x^2\right) \hat{\psi}_j(x)\, dx \right| \\ \leq &\int_{z_1}^{z_2} \exp\left(-\frac{1}{2}x^2\right) \left|\hat{\psi}_j(x)\right| dx \\ \leq &\sum_{r=0}^{j} \sum_{n=0}^{r} \sum_{l=0}^{j-r} \left|\hat{\eta}_{n,r} \hat{\lambda}_{l,j-r}\right| \int_{z_1}^{z_2} \exp\left(-\frac{1}{2}x^2\right) \left|x^{2n+r+l}\right| dx \\ < &+\infty.\end{aligned}$$

Notice that the constants $\hat{\eta}_{n,r}$ and $\hat{\lambda}_{l,j-r}$ are finite. Hence, we have the following

asymptotic expansion: when $P \to +\infty$,

$$\begin{aligned}
&\int_{z_1}^{z_2} f_{Z^P}(x)\, dx \\
\sim &\frac{1}{4\pi}\sqrt{\frac{2}{45}}\sum_{j=0}^{\infty} P^{-\frac{j}{2}} \int_{z_1}^{z_2} \exp\left(-\frac{1}{2}x^2\right)\hat{\psi}_j(x)\, dx \\
\sim &\frac{1}{4\pi}\sqrt{\frac{2}{45}}\sum_{j=0}^{\infty} P^{-\frac{j}{2}} \int_{z_1}^{z_2} \exp\left(-\frac{1}{2}x^2\right)\sum_{r=0}^{j}\sum_{n=0}^{r}\sum_{l=0}^{j-r}\hat{\eta}_{n,r}\hat{\lambda}_{l,j-r}x^{2n+r+l}\, dx \\
\sim &\frac{1}{4\pi}\sqrt{\frac{2}{45}}\sum_{j=0}^{\infty} P^{-\frac{j}{2}} \sum_{r=0}^{j}\sum_{n=0}^{r}\sum_{l=0}^{j-r}\hat{\eta}_{n,r}\hat{\lambda}_{l,j-r}\int_{z_1}^{z_2} \exp\left(-\frac{1}{2}x^2\right)x^{2n+r+l}\, dx. \qquad (5.25)
\end{aligned}$$

We apply the change of variable $v = x^2/2$ to compute the above integrals. For $z_1 < z_2 < 0$ and $q \geq 0$, we have

$$\begin{aligned}
&\int_{z_1}^{z_2} \exp\left(-\frac{1}{2}x^2\right)x^q\, dx \\
=&\int_{\frac{z_1^2}{2}}^{\frac{z_2^2}{2}} \exp(-v)\left(-\sqrt{2v}\right)^q\left(-\frac{1}{\sqrt{2v}}\right) dv \\
=&(-1)^q\left(\sqrt{2}\right)^{q-1}\int_{\frac{z_2^2}{2}}^{\frac{z_1^2}{2}} \exp(-v)v^{\frac{q+1}{2}-1}\, dv \\
=&(-1)^q\left(\sqrt{2}\right)^{q-1}\left(\gamma\left(\frac{q+1}{2},\frac{(z_1)^2}{2}\right)-\gamma\left(\frac{q+1}{2},\frac{(z_2)^2}{2}\right)\right).
\end{aligned}$$

For $z_1 < 0 \leq z_2$ and $q \geq 0$, we consider the integral on the two sub-intervals $[z_1, 0)$ and $[0, z_2]$ separately. By additivity, we get

$$\begin{aligned}
&\int_{z_1}^{z_2} \exp\left(-\frac{1}{2}x^2\right)x^q\, dx \\
=&\int_{\frac{z_1^2}{2}}^{0} \exp(-v)\left(-\sqrt{2v}\right)^q\left(-\frac{1}{\sqrt{2v}}\right) dv + \int_{0}^{\frac{z_2^2}{2}} \exp(-v)\left(\sqrt{2v}\right)^q\left(\frac{1}{\sqrt{2v}}\right) dv \\
=&(-1)^q\left(\sqrt{2}\right)^{q-1}\int_{0}^{\frac{z_1^2}{2}} \exp(-v)v^{\frac{q+1}{2}-1}\, dv + \left(\sqrt{2}\right)^{q-1}\int_{0}^{\frac{z_2^2}{2}} \exp(-v)v^{\frac{q+1}{2}-1}\, dv
\end{aligned}$$

$$= \left(\sqrt{2}\right)^{q-1} \left((-1)^q \, \gamma\left(\frac{q+1}{2}, \frac{(z_1)^2}{2}\right) + \gamma\left(\frac{q+1}{2}, \frac{(z_2)^2}{2}\right)\right).$$

Substituting the explicit form for the integrals back into (5.25) yields the stated representation, completing the proof. □

We have thus established a large P asymptotic series expansion for the probability that the random variable Z^P takes a value in $(z_1, z_2]$. Notice that this representation is valid only when $|z_i| \ll \sqrt{P}/\sqrt{2/45}$ for $i = 1, 2$. Next, we explain how the above theorem can be applied to approximate the distribution function in reality.

Recall that the restriction imposed on z_i for $i = 1, 2$ can be traced back to Lemma 5.1.1, where an asymptotic approximation for the saddle point is desired for $\beta \ll 1$. Hence, for each fixed P and β closer to zero, the truncated asymptotic expansion serves as an accurate estimate of the saddle point. More precisely, there is a region centred around zero with width $\tilde{\beta}$, throughout which the error of the estimate is below some threshold. The range of validity can be determined by numerical comparisons using Maple in practice. Following this, Theorem 5.1.3 can be applied to evaluate the probability $\mathbb{P}\left(z_1 < Z^P \leq z_2\right)$ as long as $|z_i| \leq \tilde{z}$ for $i = 1, 2$ with $\tilde{z} \coloneqq \tilde{\beta}\sqrt{P}/\sqrt{2/45}$.

Although we have put forward a restriction on Theorem 5.1.3, this result is still practically useful to compute the distribution function for large P with high accuracy because the integration of the density function f_{Z^P} outside the range of validity is negligible. Intuitively, the distribution of Z^P for large P is close to a standard normal distribution, approximately 99.7% of whose samples are within three standard deviation of its mean. In practice, the width $\tilde{z}$, and hence $\tilde{\beta}$, can be chosen sufficient large such that the integral of f_{Z^P} on the interval $(-\tilde{z}, \tilde{z}]$, evaluated by the asymptotic representation given in Theorem 5.1.3, is close enough to one. Due to the characteristics of normal distributions, often $\tilde{z}$ is not required to be too large, whence $\tilde{\beta}$ can still be near zero for large P.

Recall that the support for Z^P is $\left[-\sqrt{5P}/\sqrt{2}, +\infty\right)$. Suppose $\tilde{z}$ is chosen such

that

$$1 - \int_{-\tilde{z}}^{\tilde{z}} f_{Z^P}(x)\, dx = \int_{-\frac{\sqrt{5P}}{\sqrt{2}}}^{-\tilde{z}} f_{Z^P}(x)\, dx + \int_{\tilde{z}}^{+\infty} f_{Z^P}(x)\, dx = \epsilon.$$

Then, we have

$$F_{Z^P}(z) - \int_{-\tilde{z}}^{z} f_{Z^P}(x)\, dx = \int_{-\frac{\sqrt{5P}}{\sqrt{2}}}^{-\tilde{z}} f_{Z^P}(x)\, dx \leq \epsilon$$

for $z \in (-\tilde{z}, \tilde{z}]$. This means if $\epsilon \leq \epsilon_0$ for some predetermined threshold ϵ_0 for the error, then the integral of the density function along the interval $\left(-\sqrt{5P}/\sqrt{2}, -\tilde{z}\right]$ can be considered as insignificant to the distribution function. In other words, $\int_{-\tilde{z}}^{z} f_{Z^P}(x)\, dx$ can be used as an accurate approximation to the distribution function at z, the error of which is smaller than the threshold ϵ_0.

In summary, we have so far developed a tractable method to evaluate the distribution function $F_{Z^P}(z)$. This is approximated by integration of the corresponding density function on some restricted interval $(-\tilde{z}, z]$ with $\tilde{z}$ carefully chosen for each P. We derive an asymptotic expansion for the integral in reciprocal powers of P for all orders following the steepest descent method, which is essential for the computation of Chebyshev coefficients explained in Section 5.3. In practice, we compute enough terms for the representation to achieve the desirable accuracy in Maple for $P = 5000, 10^4, 10^5$ and 10^6, along with the root-finding for $F_{Z^P}^{-1}$ values at particular points required by Chebyshev polynomial approximations.

Remark 5.1

For all the cases considered here, we take $\tilde{z} = 20$ with the resulting $\tilde{\beta}$ being 0.0596, 0.0421, 0.0133 and 0.0042 for $P = 5000, 10^4, 10^5$ and 10^6, respectively.

5.2 Series expansion for the distribution function of S^P for small P

In this section, we turn to the specifics of the series expansion for the distribution function of S^P for small P. Similarly as the case for large P, we begin with the

probability density function and perform term by term integration to generate the required function. Indeed, we take advantage of the explicit expression for the probability density function suggested in Biane and Yor [10, formula (3x)].

Recall that S^P is characterised by the Laplace transform

$$\Phi_{S^P}(b) := \mathbb{E}\left[\exp\left(-bS^P\right)\right] = \left(\frac{\sqrt{2b}}{\sinh\sqrt{2b}}\right)^P,$$

for $b \geq 0$. Through application of the expansion (Biane and Yor [10, formula (3v)])

$$\left(\frac{b}{\sinh b}\right)^P = \frac{2^P b^P}{\Gamma(P)} \sum_{n=0}^{\infty} \frac{\Gamma(n+P)}{\Gamma(n+1)} \exp\left(-(2n+P)\, b\right)$$

and term-wise inversion employing Lévy's formula [48]

$$\int_0^\infty \exp(-\lambda t) \frac{a}{\sqrt{2\pi t^3}} \exp\left(-\frac{a^2}{2t}\right) dt = \exp\left(-a\sqrt{2\lambda}\right), \quad \text{for} \quad a \geq 0$$

to the above Laplace transform, Biane and Yor [10, formula (3x)] have developed an explicit formula for its probability density function f_{S^P}. Namely, for arbitrary $P > 0$, there exists the following infinite series for f_{S^P}:

$$f_{S^P}(y) = \frac{1}{\sqrt{2\pi}} \frac{2^P}{\Gamma(P)} y^{-\frac{1}{2}(P+2)} \sum_{n=0}^{\infty} \frac{\Gamma(n+P)}{\Gamma(n+1)} \exp\left(-\frac{(2n+P)^2}{4y}\right) D_{P+1}\left(\frac{2n+P}{\sqrt{y}}\right), \tag{5.26}$$

where $D_{P+1}(z)$ denotes the parabolic cylinder function with order $P+1$. For a review of its properties, see Chapter 19 in Abramowitz and Stegun [2]. To calculate these functions, we use different strategies according to the different ranges of the variable z. For small z, the power series is preferable while for large z an asymptotic expansion will be applied. Notice that the order $P+1$ is fixed to be small throughout this section. Next, we summarise these two methods.

First, the series expansion for the parabolic cylinder function can be written as

$$D_{P+1}(z) = D_{P+1}(0) \sum_{k=0}^{\infty} \hat{c}_{2k}(P) \frac{z^{2k}}{(2k)!} + D'_{P+1}(0) \sum_{k=0}^{\infty} \hat{c}_{2k+1}(P) \frac{z^{2k+1}}{(2k+1)!},$$

where the initial values are given by

$$D_{P+1}(0) = \frac{\sqrt{\pi}}{2^{-\frac{1}{2}(1+P)}\Gamma\left(-\frac{P}{2}\right)},$$

$$D'_{P+1}(0) = -\frac{\sqrt{\pi}}{2^{-\left(\frac{P}{2}+1\right)}\Gamma\left(-\frac{P+1}{2}\right)},$$

and the coefficients satisfy the recurrence relations given by

$$\hat{c}_{k+2}(P) = -\left(P+\frac{3}{2}\right)\hat{c}_k(P) + \frac{1}{4}k(k-1)\,\hat{c}_{k-2}(P), \quad \text{for} \quad k = 2,3,\ldots,$$

with $\hat{c}_0(P) = \hat{c}_1(P) = 1$; see Gil, Segura and Temme [29, formula (2), (14), (15), (16)] or Abramowitz and Stegun [2, formula (19.2.5), (19.2.6)]. We use Maple for their practical implementation. Hence if we denote the coefficients in front of z^k by $\hat{d}_k(P)$, then the power series for $D_{P+1}(z)$ is

$$D_{P+1}(z) = \sum_{k=0}^{\infty} \hat{d}_k(P)\, z^k. \tag{5.27}$$

Second, in the limit $z \to +\infty$, the parabolic cylinder function has the following asymptotic behaviour (Gil, Segura and Temme [29, formula (23), (24), (25)]):

$$D_{P+1}(z) \sim \exp\left(-\frac{1}{4}z^2\right) z^{P+1} \sum_{k=0}^{\infty} (-1)^k \frac{(-(P+1))_{2k}}{k!\,(2z^2)^k}, \tag{5.28}$$

where $(a)_k$ denotes the Pochhammer symbol such that $(a)_k = \Gamma(a+k)/\Gamma(a)$. For comparisons of different computational methods with the consideration of both accuracy and speed, see Temme [65] and Gil, Segura and Temme [29].

Finally, integrating the density function (5.26) for f_{S^P} term-wise after the computation of the parabolic cylinder functions using the routines described above yields the series representation for the distribution function F_{S^P} of S^P stated below.

Theorem 5.2.1

For any $0 \leq x < \infty$ and $P \in (0,1) \cup \mathbb{N}$, the distribution function $F_{S^P}(x)$ can be

written as the following convergent series

$$F_{S^P}(x) = \frac{1}{\sqrt{2\pi}} \frac{2^{P+1}}{\Gamma(P)} \sum_{n=0}^{\infty} \frac{\Gamma(n+P)}{\Gamma(n+1)} (2n+P)^{-P} G\left(\frac{2n+P}{\sqrt{x}}\right), \tag{5.29}$$

where the function $G(y)$ *for* $y > 0$ *is given by*

$$G(y) = \int_y^{+\infty} z^{P-1} \exp\left(-\frac{1}{4}z^2\right) D_{P+1}(z)\, dz. \tag{5.30}$$

Proof. The distribution function F_{S^P} is derived by term-wise integration of the series (5.26) for the probability density function f_{S^P}. First we show that $\sum_{n=0}^{\infty} \int_0^x |f_n(y)|\, dy < \infty$ for any finite $x \geq 0$, where

$$f_n(y) \coloneqq \frac{\Gamma(n+P)}{\Gamma(n+1)} \exp\left(-\frac{(2n+P)^2}{4y}\right) D_{P+1}\left(\frac{2n+P}{\sqrt{y}}\right) y^{-\frac{1}{2}(P+2)}.$$

For fixed $n \geq 0$, application of the variable transformation $z = (2n+P)/\sqrt{y}$ gives

$$\begin{aligned}
&\int_0^x |f_n(y)|\, dy \\
=&\frac{\Gamma(n+P)}{\Gamma(n+1)} \int_{+\infty}^{\frac{2n+P}{\sqrt{x}}} \exp\left(-\frac{1}{4}z^2\right) |D_{P+1}(z)| \left(\frac{z}{2n+P}\right)^{P+2} (2n+P)^2 \left(-2z^{-3}\right) dz \\
=&2\frac{\Gamma(n+P)}{\Gamma(n+1)} (2n+P)^{-P} \int_{\frac{2n+P}{\sqrt{x}}}^{+\infty} \exp\left(-\frac{1}{4}z^2\right) |D_{P+1}(z)|\, z^{P-1}\, dz.
\end{aligned}$$

Notice that the parabolic cylinder function $D_{P+1}(z)$ is square integrable on $[0, \infty)$ (Gradshteyn and Ryzhik [34, Chapter 7.711]), i.e.

$$\|D_{P+1}\|_2 \coloneqq \left(\int_0^{+\infty} |D_{P+1}(z)|^2\, dz\right)^{\frac{1}{2}} < \infty.$$

By Hölder's inequality, we have

$$\int_y^{+\infty} \exp\left(-\frac{1}{4}z^2\right) |D_{P+1}(z)|\, z^{P-1}\, dz \leq \left(\int_y^{+\infty} z^{2(P-1)} \exp\left(-\frac{1}{2}z^2\right) dz\right)^{\frac{1}{2}} \|D_{P+1}\|_2 \tag{5.31}$$

for $y \geq 0$. Next we consider the following two cases for P separately: $P \in (0,1)$ and

$P \in \mathbb{N}$.

For any $P \in (0,1)$, $z^{2(P-1)}$ is monotonically decreasing, which yields

$$\begin{aligned}
&\int_y^{+\infty} \exp\left(-\frac{1}{4}z^2\right) |D_{P+1}(z)|\, z^{P-1}\, dz \\
\leq & y^{P-1} \left(\int_y^{+\infty} \exp\left(-\frac{1}{2}z^2\right) dz\right)^{\frac{1}{2}} \|D_{P+1}\|_2 \\
= & y^{P-1} \left(\sqrt{2\pi}\frac{1}{\sqrt{2\pi}}\int_y^{+\infty} \exp\left(-\frac{1}{2}z^2\right) dz\right)^{\frac{1}{2}} \|D_{P+1}\|_2 \\
= & (2\pi)^{\frac{1}{4}} \|D_{P+1}\|_2\, y^{P-1} (1-\Phi(y))^{\frac{1}{2}}
\end{aligned}$$

for $y > 0$, where $\Phi(y)$ is the distribution function of a standard normal random variable. Then, it follows that the sequence $\int_0^x |f_n(y)|\, dy$ with $x < \infty$ is bounded by

$$\begin{aligned}
&\int_0^x |f_n(y)|\, dy \\
\leq & 2\frac{\Gamma(n+P)}{\Gamma(n+1)} (2n+P)^{-P} (2\pi)^{\frac{1}{4}} \|D_{P+1}\|_2 \left(\frac{2n+P}{\sqrt{x}}\right)^{P-1} \left(1-\Phi\left(\frac{2n+P}{\sqrt{x}}\right)\right)^{\frac{1}{2}} \\
= & 2(2\pi)^{\frac{1}{4}} \|D_{P+1}\|_2\, x^{\frac{1}{2}(1-P)} \frac{\Gamma(n+P)}{\Gamma(n+1)} \frac{1}{2n+P} \left(1-\Phi\left(\frac{2n+P}{\sqrt{x}}\right)\right)^{\frac{1}{2}}.
\end{aligned}$$

By the ratio test, we can deduce that the series $\sum_{n=0}^{\infty} b_n$ where

$$b_n := 2(2\pi)^{\frac{1}{4}} \|D_{P+1}\|_2\, x^{\frac{1}{2}(1-P)} \frac{\Gamma(n+P)}{\Gamma(n+1)} \frac{1}{2n+P} \left(1-\Phi\left(\frac{2n+P}{\sqrt{x}}\right)\right)^{\frac{1}{2}}$$

is convergent. In fact, we have

$$\left|\frac{b_{n+1}}{b_n}\right| = \frac{n+P}{n+1} \frac{2n+P}{2(n+1)+P} \left(\frac{1-\Phi\left(\frac{2(n+1)+P}{\sqrt{x}}\right)}{1-\Phi\left(\frac{2n+P}{\sqrt{x}}\right)}\right)^{\frac{1}{2}} \to 0, \quad \text{as} \quad n \to \infty.$$

The comparison test implies that the series $\sum_{n=0}^{\infty} \int_0^x |f_n(y)|\, dy$ is also convergent for any finite x.

For any $P \in \mathbb{N}$, the integral on the right hand side of (5.31) can be regarded as the moment of some transformation of a standard normal random variable Z, i.e.

$$\begin{aligned}
\int_y^{+\infty} z^{2(P-1)} \exp\left(-\frac{1}{2}z^2\right) dz &= \sqrt{2\pi}\frac{1}{\sqrt{2\pi}}\int_{-\infty}^{+\infty} z^{2(P-1)} \exp\left(-\frac{1}{2}z^2\right)\mathbf{1}_{\{z\geq y\}}\, dz \\
&= \sqrt{2\pi}\mathbb{E}\left[Z^{2(P-1)}\mathbf{1}_{\{Z\geq y\}}\right] \\
&\leq \sqrt{2\pi}\left(\mathbb{E}\left[Z^{4(P-1)}\right]\right)^{\frac{1}{2}}\left(\mathbb{E}\left[\left(\mathbf{1}_{\{Z\geq y\}}\right)^2\right]\right)^{\frac{1}{2}} \\
&= \sqrt{2\pi}\left(\mathbb{E}\left[Z^{4(P-1)}\right]\right)^{\frac{1}{2}}\left(\mathbb{P}\left(Z\geq y\right)\right)^{\frac{1}{2}} \\
&= \sqrt{2\pi}\left(\mathbb{E}\left[Z^{4(P-1)}\right]\right)^{\frac{1}{2}}\left(1-\Phi\left(y\right)\right)^{\frac{1}{2}}
\end{aligned}$$

for $y \geq 0$, where $\mathbf{1}_{\{z\geq y\}}$ is the indicator function and the inequality follows from Hölder's inequality. Hence, the above argument gives the bounds for $\int_0^x |f_n(y)|\, dy$ with $x < \infty$ as

$$\begin{aligned}
&\int_0^x |f_n(y)|\, dy \\
\leq& 2\frac{\Gamma(n+P)}{\Gamma(n+1)}(2n+P)^{-P}(2\pi)^{\frac{1}{4}}\left(\mathbb{E}\left[Z^{4(P-1)}\right]\right)^{\frac{1}{4}}\left(1-\Phi\left(\frac{2n+P}{\sqrt{x}}\right)\right)^{\frac{1}{4}}\|D_{P+1}\|_2 \\
=& 2(2\pi)^{\frac{1}{4}}\|D_{P+1}\|_2\left(\mathbb{E}\left[Z^{4(P-1)}\right]\right)^{\frac{1}{4}}\frac{\Gamma(n+P)}{\Gamma(n+1)}(2n+P)^{-P}\left(1-\Phi\left(\frac{2n+P}{\sqrt{x}}\right)\right)^{\frac{1}{4}}.
\end{aligned}$$

Similarly, with the notation

$$b_n \coloneqq 2(2\pi)^{\frac{1}{4}}\|D_{P+1}\|_2\left(\mathbb{E}\left[Z^{4(P-1)}\right]\right)^{\frac{1}{4}}\frac{\Gamma(n+P)}{\Gamma(n+1)}(2n+P)^{-P}\left(1-\Phi\left(\frac{2n+P}{\sqrt{x}}\right)\right)^{\frac{1}{4}},$$

the series $\sum_{n=0}^{\infty} b_n$ converges by the fact that

$$\left|\frac{b_{n+1}}{b_n}\right| = \frac{n+P}{n+1}\left(\frac{2n+P}{2(n+1)+P}\right)^P\left(\frac{1-\Phi\left(\frac{2(n+1)+P}{\sqrt{x}}\right)}{1-\Phi\left(\frac{2n+P}{\sqrt{x}}\right)}\right)^{\frac{1}{4}} \to 0, \quad \text{as} \quad n\to\infty,$$

suggesting the convergence of the series $\sum_{n=0}^{\infty}\int_0^x |f_n(y)|\, dy$ for finite x as well.

Thus, for fixed $0 \leq x < \infty$ and $P \in (0,1) \cup \mathbb{N}$, we have

$$\sum_{n=0}^{\infty} \int_0^x |f_n(y)| \, dy < \infty.$$

Then, applying a corollary of the Dominated Convergence Theorem (Rudin [61, Theorem 1.38]) yields

$$\sum_{n=0}^{\infty} \int_0^x f_n(y) \, dy = \int_0^x \sum_{n=0}^{\infty} f_n(y) \, dy,$$

where the integration and summation can be interchanged. This leads to the following convergent series expansion for the distribution function F_{S^P}: for any $x < \infty$,

$$\begin{aligned}
F_{S^P}(x) &= \int_0^x f_{S^P}(y) \, dy \\
&= \frac{1}{\sqrt{2\pi}} \frac{2^P}{\Gamma(P)} \int_0^x \sum_{n=0}^{\infty} f_n(y) \, dy \\
&= \frac{1}{\sqrt{2\pi}} \frac{2^P}{\Gamma(P)} \sum_{n=0}^{\infty} \int_0^x f_n(y) \, dy \\
&= \frac{1}{\sqrt{2\pi}} \frac{2^P}{\Gamma(P)} \sum_{n=0}^{\infty} \frac{\Gamma(n+P)}{\Gamma(n+1)} \int_0^x y^{-\frac{1}{2}(P+2)} \exp\left(-\frac{(2n+P)^2}{4y}\right) D_{P+1}\left(\frac{2n+P}{\sqrt{y}}\right) dy \\
&= \frac{1}{\sqrt{2\pi}} \frac{2^{P+1}}{\Gamma(P)} \sum_{n=0}^{\infty} \frac{\Gamma(n+P)}{\Gamma(n+1)} (2n+P)^{-P} G\left(\frac{2n+P}{\sqrt{x}}\right),
\end{aligned}$$

where the function $G(y)$ is defined in the statement of the theorem. □

Before computing the distribution function F_{S^P}, a clear strategy for the evaluation of the function G needs to be formulated. As G is given in the form of an integral, we first follow the methods mentioned earlier to calculate the parabolic cylinder functions D_{P+1} and hence its integrand. We may replace $D_{P+1}(z)$ by its convergent power series on the entire interval of integration to derive the corresponding series expansion for G. However, the power series converges too slowly to be of practical use for large z. Instead, we split the interval of integration $[y, +\infty)$ into two small elements, say $[y, y^*)$ and $[y^*, +\infty)$ for some sufficiently large $y^* \geq y$,

where we apply different representations for $D_{P+1}(z)$ depending on the value of z. This gives the following theorem.

Theorem 5.2.2

For any $y > 0$, we have

$$G(y) = G_1(y, y^*) + G_2(y^*)$$

for some $y^* \geq y$, where G_1 can be expressed as the convergent series

$$G_1(y, y^*) = \sum_{k=0}^{\infty} \hat{d}_k(P)\, 2^{P+k-1} \left(\Gamma\left(\frac{P+k}{2}, \frac{y^2}{4} \right) - \Gamma\left(\frac{P+k}{2}, \frac{(y^*)^2}{4} \right) \right) \tag{5.32}$$

and G_2 has the asymptotic approximation

$$G_2(y^*) \sim \sum_{k=0}^{\infty} (-1)^k \frac{(-(P+1))_{2k}}{k!} 2^{P-2k-\frac{1}{2}} \Gamma\left(P-k+\frac{1}{2}, \frac{(y^*)^2}{2} \right), \quad as \quad y^* \to +\infty. \tag{5.33}$$

Here, $\Gamma(\alpha, \beta)$ is the upper incomplete gamma function.

Proof. Considering the integral on sub-intervals $[y, y^*)$ and $[y^*, +\infty)$ for large $y^* \geq y$, we have

$$G(y) = G_1(y, y^*) + G_2(y^*),$$

where

$$G_1(y, y^*) := \int_y^{y^*} z^{P-1} \exp\left(-\frac{1}{4} z^2 \right) D_{P+1}(z)\, dz,$$

$$G_2(y^*) := \int_{y^*}^{+\infty} z^{P-1} \exp\left(-\frac{1}{4} z^2 \right) D_{P+1}(z)\, dz.$$

In this way, different techniques for approximating the respective integrand can be adopted on these intervals. Specifically, the asymptotic expansion (5.28) is a convenient way to compute $D_{P+1}(z)$ on $[y^*, +\infty)$ and hence G_2, otherwise the power series (5.27) will be useful on $[y, y^*)$ for G_1. Hence, we consider the integral on the

two sub-intervals case by case.

On $[y^*, +\infty)$, we can approximate the parabolic cylinder function $D_{p+1}(z)$ by its asymptotic series (5.28) on the entire interval under consideration. The series is then multiplied by $z^{P-1}\exp(-z^2/4)$ and integrated term by term to generate a series approximation for the integral G_2. To confirm that the resulting series is the correct asymptotic expansion for the integral with large y^*, we note that

$$z^{P-1}\exp\left(-\frac{1}{4}z^2\right)D_{P+1}(z) \sim z^{2P}\exp\left(-\frac{1}{2}z^2\right)\sum_{k=0}^{\infty}\hat{a}_k z^{-2k}, \quad \text{as} \quad z \to +\infty,$$

where $\hat{a}_k = (-1)^k 2^{-k}\left(-(P+1)\right)_{2k}/k!$ for $k \geq 0$. By Definition 2.1.7, we have for each K,

$$z^{P-1}\exp\left(-\frac{1}{4}z^2\right)D_{P+1}(z) - z^{2P}\exp\left(-\frac{1}{2}z^2\right)\sum_{k=0}^{K}\hat{a}_k z^{-2k} = \mathrm{o}\left(z^{2P}\exp\left(-\frac{1}{2}z^2\right)z^{-2K}\right),$$

as $z \to +\infty$, meaning that for any $\epsilon > 0$, there exists a $z_0 > 0$ such that for $z > z_0$,

$$\left|z^{P-1}\exp\left(-\frac{1}{4}z^2\right)D_{P+1}(z) - z^{2P}\exp\left(-\frac{1}{2}z^2\right)\sum_{k=0}^{K}\hat{a}_k z^{-2k}\right| \leq \epsilon\left|z^{2P}\exp\left(-\frac{1}{2}z^2\right)z^{-2K}\right|.$$

Then, properties of integration yield for any $y^* > z_0$,

$$\begin{aligned}
&\left|G_2(y^*) - \sum_{k=0}^{K}\hat{a}_k\int_{y^*}^{+\infty} y^{2P}\exp\left(-\frac{1}{2}y^2\right)y^{-2k}\,dy\right| \\
=&\left|\int_{y^*}^{+\infty}\left(y^{P-1}\exp\left(-\frac{1}{4}y^2\right)D_{P+1}(y) - y^{2P}\exp\left(-\frac{1}{2}y^2\right)\sum_{k=0}^{K}\hat{a}_k y^{-2k}\right)dy\right| \\
\leq&\int_{y^*}^{+\infty}\left|y^{P-1}\exp\left(-\frac{1}{4}y^2\right)D_{P+1}(y) - y^{2P}\exp\left(-\frac{1}{2}y^2\right)\sum_{k=0}^{K}\hat{a}_k y^{-2k}\right|dy \\
\leq&\epsilon\int_{y^*}^{+\infty}\left|y^{2P}\exp\left(-\frac{1}{2}y^2\right)y^{-2K}\right|dy \\
=&\epsilon\int_{y^*}^{+\infty} y^{2P}\exp\left(-\frac{1}{2}y^2\right)y^{-2K}\,dy.
\end{aligned}$$

Hence by Definition 2.1.4, we have the following asymptotic relation: as $y^* \to +\infty$,

$$G_2(y^*) - \sum_{k=0}^{K} \hat{a}_k \int_{y^*}^{+\infty} y^{2P} \exp\left(-\frac{1}{2}y^2\right) y^{-2k}\, dy = \mathrm{o}\left(\int_{y^*}^{+\infty} y^{2P} \exp\left(-\frac{1}{2}y^2\right) y^{-2K}\, dy\right),$$

which further gives the asymptotic expansion

$$G_2(y^*) \sim \sum_{k=0}^{\infty} \hat{a}_k \int_{y^*}^{+\infty} y^{2P} \exp\left(-\frac{1}{2}y^2\right) y^{-2k}\, dy, \quad \text{as} \quad y^* \to +\infty.$$

Introducing a new variable $\zeta = y^2/2$, we find that

$$\begin{aligned}
G_2(y^*) &\sim \sum_{k=0}^{\infty} \hat{a}_k \int_{y^*}^{+\infty} y^{2P-2k} \exp\left(-\frac{1}{2}y^2\right) dy \\
&= \sum_{k=0}^{\infty} \hat{a}_k \int_{\frac{(y^*)^2}{2}}^{+\infty} (2\zeta)^{P-k} \exp(-\zeta) \frac{\sqrt{2}}{2} \zeta^{-\frac{1}{2}}\, d\zeta \\
&= \sum_{k=0}^{\infty} \hat{a}_k 2^{P-k-\frac{1}{2}} \int_{\frac{(y^*)^2}{2}}^{+\infty} \zeta^{P-k-\frac{1}{2}} \exp(-\zeta)\, d\zeta \\
&= \sum_{k=0}^{\infty} \hat{a}_k 2^{P-k-\frac{1}{2}} \Gamma\left(P-k+\frac{1}{2}, \frac{(y^*)^2}{2}\right),
\end{aligned}$$

in the limit $y^* \to +\infty$. Replacing $\hat{a}_k$ by the explicit form given above generates the stated asymptotic expansion (5.33) for G_2.

On $[y, y^*)$, approximating the parabolic cylinder function $D_{P+1}(z)$ using the power series (5.27), we can write

$$\begin{aligned}
G_1(y, y^*) &= \int_{y}^{y^*} z^{P-1} \exp\left(-\frac{1}{4}z^2\right) \left(\sum_{k=0}^{\infty} \hat{d}_k(P)\, z^k\right) dz \\
&= \sum_{k=0}^{\infty} \hat{d}_k(P) \int_{y}^{y^*} z^{P+k-1} \exp\left(-\frac{1}{4}z^2\right) dz \\
&= \sum_{k=0}^{\infty} \hat{d}_k(P) \int_{\frac{y^2}{4}}^{\frac{(y^*)^2}{4}} \left(2\sqrt{\zeta}\right)^{P+k-1} \exp(-\zeta) \zeta^{-\frac{1}{2}}\, d\zeta
\end{aligned}$$

$$= \sum_{k=0}^{\infty} \hat{d}_k (P) 2^{P+k-1} \int_{\frac{y^2}{4}}^{\frac{(y^*)^2}{4}} \zeta^{\frac{P+k}{2}-1} \exp(-\zeta) d\zeta$$

$$= \sum_{k=0}^{\infty} \hat{d}_k (P) 2^{P+k-1} \left(\Gamma\left(\frac{P+k}{2}, \frac{y^2}{4}\right) - \Gamma\left(\frac{P+k}{2}, \frac{(y^*)^2}{4}\right) \right),$$

where the interchange of integration and summation in the second step follows from the fact that the power series is uniformly convergent over the interval of integration and a change of variable $\zeta = z^2/4$ is applied for the third step. Notice that the above series is convergent for any $0 < y \leq y^*$. □

The previous theorems provide an effective approach to calculating the distribution function F_{S^P} for small P across its support with high precision, as required by the construction of the Chebyshev polynomials in Section 5.4. In practice, we choose to use the asymptotic expansion for the parabolic cylinder function $D_{P+1}(z)$ whenever $z \geq \Delta(P + 3/2)$ for some positive $\Delta \gg 1$, suggested by Gil, Segura and Temme [29, Section 5]. Accordingly, we set

$$y^* = \max\left\{\Delta\left(P + \frac{3}{2}\right), y\right\}$$

when computing the function $G(y)$ for fixed $y \geq 0$. This means only asymptotic series is involved in the computation of $G(y) = G_2(y)$ for sufficiently large y such that $y \geq \Delta(P + 3/2)$. The constant Δ, which may vary depending on the value of P, can be determined by numerical trials of comparing the accuracy and efficiency of evaluating both the power series and asymptotic representations at particular points.

Notice that the series expansion (5.29) developed here is valid for any $P \in (0, 1)$, not only for integer P. This means that the expansion is also useful in evaluating the distribution functions for $Y_2^P \stackrel{d}{=} S^P$ with $P \in (0, 1)$ and $Z' \stackrel{d}{=} S^2$ defined in Section 4.2. As the case for large P, we compute the above series representation for F_{S^P} and perform the root-finding for $F_{S^P}^{-1}$ in Maple for $P = 1, 2, 10, 50$ and $P = 1/k$ with $k \in \mathbb{H}$.

5.3 Chebyshev polynomial approximation for the inverse distribution function of S^P for large P

As presented in Algorithm 4.2, for any positive integer P, the simulation of S^P is reduced to generating a series of random variables S^k for $k \in \mathbb{S}$ by direct inversion. This method takes a uniform sample $u \sim \text{Unif}(0,1)$ and returns the quantile function evaluated at u as a sample for the associated distribution, which requires computing the inverse of the distribution function. Although accurate approximations for the distribution function can be generated with great efficiency, it is often the case that the inverting process is computationally inefficient due to many factors such as poor initial guess and the lack of an analytical expression for the corresponding quantile function. Since a large number of samples is needed for the Monte Carlo simulation when the same number of inversions of the distribution function will be performed, we now look for a more tractable technique to complete this step.

Indeed, we employ approximations to the inverse distribution function for fixed P. More precisely in this section, we design Chebyshev polynomials to approximate the inverse distribution function $F^{-1}_{S^P}$ for large P, i.e. $P = 10, 50, 5000, 10^4, 10^5$ and 10^6, where the coefficients are computed based on the distribution function representations explained in Section 5.1 and Section 5.2. Despite the fact that the polynomial is just an approximation, we can still obtain highly accurate results by restricting the error, which is controlled by the degrees of the polynomials we construct. In practice, we require the uniform error to be far smaller than the Monte Carlo error, e.g. of order 10^{-12}.

Recall from Definition 2.3.4 that a degree n Chebyshev polynomial approximation

$$f^n(z) \coloneqq c_0 T_0(z) + c_1 T_1(z) + \cdots + c_n T_n(z) - \frac{1}{2} c_0$$

is defined on the interval $[-1, 1]$. Since polynomials often exhibit more rapid changes than the distribution functions, approximations by polynomials might not be able to fully capture the behaviour of the inverse function $F^{-1}_{S^P}(u)$ on its entire domain. Hence, identifying appropriate scaling schemes of the argument u is of great impor-

tance to allow the application of the Chebyshev polynomial approximation. The choices of the scales are mainly characterised by the behaviour of the function depending on the range of P. We briefly state the scaling and its rationale behind for large P below.

Instead of the sum S^P, we take the normalised random variable Z^P with zero mean and unit variance into consideration. For the approximation of the inverse distribution function $F^{-1}_{Z^P}$, we focus on the sub-interval $[F_{Z^P}(0), 1)$ of its support first, corresponding to the region where the random variable Z^P takes positive values. In the limit of large P, the distribution function of Z^P resembles that of a standard normal distribution. Thus, we generalise and apply the ideas underlying the Beasley-Springer-Moro direct inversion method for standard normal random variable; see Moro [55], Joy, Boyle and Tan [43] and Malham and Wiese [52].

The normal distribution function has three regions exhibiting different characteristic behaviours on the positive real line. Accordingly, we roughly split the interval $[F_{Z^P}(0), 1)$ into three regimes: the central $[F_{Z^P}(0), u_1]$, the middle $(u_1, u_2]$ and the tail $(u_2, 1 - 10^{-12}]$ regimes. In general, the central regime roughly represents the area where the decreasing density function has a increasing slope while the middle regime represents the area where the decreasing density function has a declining slope with the tail regime representing the region where the density function is flat taking values close to zero. We neglect the regimes from $1 - 10^{-12}$ to 1.

Remark 5.2

It should be pointed out here that the above rule is just for reference only. In reality, we can choose optimal values for the boundaries u_1 and u_2 by a small number of experiments in Maple to ensure that the resulting Chebyshev polynomial approximations have moderate degrees while retaining the accuracy for all three regimes. We may come across the circumstance that the approximations which achieves the desired accuracy have degrees of say 15 for both the central and middle regimes but a higher degree of say 50 for the tail regime for some given u_1 and u_2. Such a case should be avoided from the perspective of efficiency as higher degree is often together with higher computational cost. Hence, it is necessary to set the values u_1 and u_2 again through additional investigations so that the degrees of the approximation for

all regions are balanced with each other. If both of the degrees of the Chebyshev polynomials constructed for two neighbouring regions are at relative lower level, we may combine those two regimes to one and produce a unified approximation.

5.3.1 Central regime

In the central regime where $u \in [F_{Z^P}(0), u_1]$, we follow Malham and Wiese [52] to scale and shift the variable. Define

$$U \coloneqq \sqrt{2\pi}\left(u - F_{Z^P}(0)\right),$$

$$z \coloneqq k_1 U + k_2,$$

where the parameters k_1 and k_2 are chosen to make sure $z = -1$ when $u = F_{Z^P}(0)$ and $z = 1$ when $u = u_1$. Then, we approximate the inverse distribution function $F^{-1}_{Z^P}(u)$ by a degree n Chebyshev polynomial approximation applied to the scaled and shifted variable z as follows:

$$F^{-1}_{Z^P}(u) \approx U\left(c_0 T_0(z) + c_1 T_1(z) + \cdots + c_n T_n(z) - \frac{1}{2}c_0\right).$$

5.3.2 Middle and tail regimes

In the middle and tail regimes with $u \in (u_1, u_2]$ and $u \in (u_2, 1 - 10^{-12}]$, respectively, we approximate $F^{-1}_{Z^P}(u)$ by a degree n Chebyshev polynomial approximation of a scaled and shifted variable as follows:

$$F^{-1}_{Z^P}(u) \approx c_0 T_0(z) + c_1 T_1(z) + \cdots + c_n T_n(z) - \frac{1}{2}c_0,$$

where

$$U \coloneqq \log\left(-\log(1-u)\right),$$

$$z \coloneqq k_1 U + k_2,$$

with the parameters k_1 and k_2 suitably chosen such that $z = -1$ at the left endpoint and $z = 1$ at the right endpoint. The ansatz for U follows from inverting the asymptotic tail approximation for the distribution function of the standard normal, which is equivalent in distribution as Z^P when $P \to \infty$ by the central limit theorem; see Moro [55] and Malham and Wiese [52].

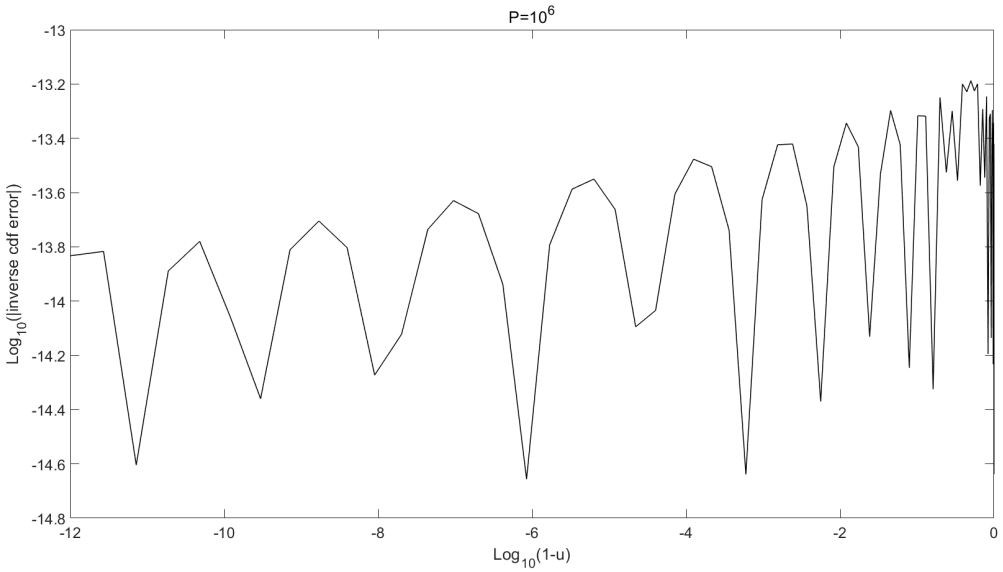

Figure 5.1: We plot the errors in the Chebyshev polynomial approximations to the inverse distribution function $F^{-1}_{Z^P}(u)$ with $P = 10^6$ across all regimes. Note that to highlight the tail we use a log-$\log_{10}$ scale with $1 - u$ on the abscissa.

The above serves as a general discussion for choosing the scaled variables and approximations in the region of $[F_{Z^P}(0), 1 - 10^{-12}]$ for large P. We apply this procedure to the cases $P = 10, 50, 5000, 10^4, 10^5$ and 10^6, the inverse distribution functions of which are roughly anti-symmetric. For the remaining half sub-interval of its support, we can apply similar results to the scaling and approximation following the arguments mentioned above. We list the values for the coefficients of the approximations in Appendix A, which are computed in the standard fashion (see Press *et al.* [59]) using Maple.

We end this section by showing the respective errors in the Chebyshev polynomial approximations to $F^{-1}_{Z^P}(u)$ with $u \in [10^{-12}, 1 - 10^{-12}]$ when $P = 10^6$ in Figure 5.1. To highlight the tail we plot the errors on a log-$\log_{10}$ scale with $1 - u$ on the abscissa. We split the interval $[10^{-12}, 1 - 10^{-12}]$ into two regimes: $[10^{-12}, 0.5001)$ and

$[0.5001, 1 - 10^{-12}]$, where both of the Chebyshev polynomials have degrees 16. The figure shows that across the two regions, the errors in the approximations generated by the coefficients quoted in Appendix A are of order 10^{-13}. Results for the other values of P, reported in Appendix B, share similar accuracy as those in Figure 5.1.

5.4 Chebyshev polynomial approximation for the inverse distribution function of S^P for small P

In the Chebyshev polynomial approximation for small P, the idea remains the same as that for large P introduced in Section 5.3. Notice that the random variable S^P takes positive values only. Since the distribution for S^P has a heavy right tail with small P, we break down the support of $F_{S^P}^{-1}$ into four regimes: the left $[10^{-12}, u_1]$, the central $(u_1, u_2]$, the middle $(u_2, u_3]$ and the right tail $(u_3, 1 - 10^{-12}]$ regimes. We neglect the regimes at a distance of 10^{-12} from its endpoints. In theory, these boundary points are determined in accordance with the behaviour of the distribution function, but again it is better to set them via empirical studies in practice.

The central limit theorem tells us the asymptotic distribution of the sum S^P when P is large. However, for small P we have to analyse the limiting behaviour of the distribution function F_{S^P} and its inverse $F_{S^P}^{-1}$ in order to help us find the proper scaled variables when we construct Chebyshev polynomial approximations. We build on the series representation for F_{S^P} given in Theorem 5.2.1 and Theorem 5.2.2 to derive the results below.

Corollary 5.4.1

For any $P \in (0, 1) \cup \mathbb{N}$, the distribution function F_{S^P} has the following asymptotic relation

$$F_{S^P}(x) \sim \frac{1}{\sqrt{\pi}} 2^{P+\frac{1}{2}} P^{P-1} x^{-P+\frac{1}{2}} \exp\left(-\frac{P^2}{2x}\right), \quad as \quad x \to 0^+. \tag{5.34}$$

Proof. Recall that we have

$$F_{S^P}(x) = \frac{1}{\sqrt{2\pi}} \frac{2^{P+1}}{\Gamma(P)} \sum_{n=0}^{\infty} \frac{\Gamma(n+P)}{\Gamma(n+1)} (2n+P)^{-P} G\left(\frac{2n+P}{\sqrt{x}}\right) \tag{5.35}$$

for any $0 \leq x < \infty$, where the function G has the asymptotic approximation

$$G(y) \sim \sum_{k=0}^{\infty} (-1)^k \frac{(-(P+1))_{2k}}{k!} 2^{P-2k-\frac{1}{2}} \Gamma\left(P-k+\frac{1}{2}, \frac{y^2}{2}\right), \quad \text{as} \quad y \to +\infty.$$

Then it follows from Definition 2.1.7 that

$$G(y) = 2^{P-\frac{1}{2}} \Gamma\left(P+\frac{1}{2}, \frac{y^2}{2}\right) + \mathrm{o}\left(\Gamma\left(P+\frac{1}{2}, \frac{y^2}{2}\right)\right), \quad \text{as} \quad y \to +\infty.$$

Further, by the asymptotic expansion for the incomplete gamma function (Abramowitz and Stegun [2, formula (6.5.32)])

$$\Gamma(s,z) \sim z^{s-1} \exp(-z) \sum_{k=0}^{\infty} \frac{\Gamma(s)}{\Gamma(s-k)} z^{-k}, \quad \text{as} \quad z \to +\infty, \tag{5.36}$$

we have

$$\Gamma\left(P+\frac{1}{2}, \frac{y^2}{2}\right) = \left(\frac{y^2}{2}\right)^{P-\frac{1}{2}} \exp\left(-\frac{y^2}{2}\right) + \mathrm{o}\left(y^{2P-1} \exp\left(-\frac{y^2}{2}\right)\right), \quad \text{as} \quad y \to +\infty.$$

The above analysis yields

$$G(y) = y^{2P-1} \exp\left(-\frac{y^2}{2}\right) + \mathrm{o}\left(y^{2P-1} \exp\left(-\frac{y^2}{2}\right)\right), \quad \text{as} \quad y \to +\infty.$$

Hence, we can write

$$\begin{aligned} G\left(\frac{2n+P}{\sqrt{x}}\right) = {} & (2n+P)^{2P-1} x^{\frac{1}{2}-P} \exp\left(-\frac{(2n+P)^2}{2x}\right) \\ & + \mathrm{o}\left((2n+P)^{2P-1} x^{\frac{1}{2}-P} \exp\left(-\frac{(2n+P)^2}{2x}\right)\right) \end{aligned}$$

in the limit $x \to 0^+$. The observation

$$(2n+P)^{2P-1} \frac{\exp\left(-\frac{(2n+P)^2}{2x}\right)}{\exp\left(-\frac{P^2}{2x}\right)} = (2n+P)^{2P-1} \exp\left(-\frac{4n^2+4nP}{2x}\right) \to 0, \quad \text{as} \quad x \to 0^+$$

for any $n \geq 1$ establishes

$$G\left(\frac{2n+P}{\sqrt{x}}\right) = \mathrm{o}\left(G\left(\frac{P}{\sqrt{x}}\right)\right), \quad \text{as} \quad x \to 0^+.$$

Therefore, (5.35) becomes

$$\begin{aligned} F_{S^P}(x) &= \frac{1}{\sqrt{2\pi}} \frac{2^{P+1}}{\Gamma(P)} \frac{\Gamma(P)}{\Gamma(1)} P^{-P} G\left(\frac{P}{\sqrt{x}}\right) + \mathrm{o}\left(G\left(\frac{P}{\sqrt{x}}\right)\right) \\ &= \frac{1}{\sqrt{2\pi}} 2^{P+1} P^{P-1} x^{\frac{1}{2}-P} \exp\left(-\frac{P^2}{2x}\right) + \mathrm{o}\left(x^{\frac{1}{2}-P} \exp\left(-\frac{P^2}{2x}\right)\right), \quad \text{as} \quad x \to 0^+. \end{aligned}$$

Using Definition 2.1.5 generates the stated result for F_{S^P}. □

The above expression describes the behaviour of the distribution function $F_{S^P}(y)$ as $y \to 0^+$. Now, our goal is to invert this relation to obtain the asymptotic approximation for the inverse distribution function $F_{S^P}^{-1}(u)$ as $u \to 0^+$. Let $u = F_{S^P}(y)$, then from (5.34) it is clear

$$\frac{u\sqrt{\pi}}{2^{P+\frac{1}{2}} P^{P-1}} \sim y^{-P+\frac{1}{2}} \exp\left(-\frac{P^2}{2y}\right), \quad \text{as} \quad y \to 0^+. \tag{5.37}$$

Introducing the new variable $v \coloneqq u\sqrt{\pi} / \left(2^{P+\frac{1}{2}} P^{P-1}\right)$ and taking logarithm on both sides, we can rewrite (5.37) as

$$\log v \sim \left(P - \frac{1}{2}\right) \log \frac{1}{y} - \frac{P^2}{2y}, \quad \text{as} \quad y \to 0^+.$$

After rearrangement, the above expression becomes

$$\frac{1}{y} \sim \frac{2}{P^2}\left(P - \frac{1}{2}\right) \log \frac{1}{y} - \frac{2}{P^2} \log v, \quad \text{as} \quad y \to 0^+.$$

We wish to write y in terms of v. Specifically, taking advantage of the asymptotic

inverse of these kinds of relationships we have

$$\frac{1}{y} \sim -\frac{2}{P^2}\log v + \frac{2}{P^2}\left(P-\frac{1}{2}\right)\log\left(-\frac{2}{P^2}\log v\right), \quad \text{as} \quad y \to 0^+.$$

In particular, as $y \to 0^+$, i.e. $u \to 0^+$, its leading order behaviour yields

$$\begin{aligned} y &\sim \left(\frac{2}{P^2}\left(P-\frac{1}{2}\right)\log\frac{2}{P^2} - \frac{2}{P^2}\log v\right)^{-1} \\ &= \left(\frac{2}{P^2}\left(P-\frac{1}{2}\right)\log\frac{2}{P^2} - \frac{2}{P^2}\log\left(\frac{u\sqrt{\pi}}{2^{P+\frac{1}{2}}P^{P-1}}\right)\right)^{-1}, \end{aligned}$$

where the last equation comes from the transformation $v = u\sqrt{\pi}/\left(2^{P+\frac{1}{2}}P^{P-1}\right)$.

As $u \to 1$, i.e. $y \to +\infty$, we adopt a gamma approximation for the tail. This is implied by empirical tests which show that the distribution is positively skewed with a longer right tail. Hence, by matching the mean and variance of S^P with those of a gamma random variable, the shape and rate parameters take the form $s = 5P/2$ and $r = 15/2$. Then, the distribution function F_{S^P} is approximated by the distribution function F_X of a gamma random variable X with parameters s and r given as follows:

$$F_X(y) = 1 - \frac{1}{\Gamma\left(\frac{5}{2}P\right)}\Gamma\left(\frac{5}{2}P, \frac{15}{2}y\right).$$

Again, making use of the asymptotic relationship given in (5.36) establishes as $y \to +\infty$,

$$F_X(y) \sim 1 - \frac{1}{\Gamma\left(\frac{5}{2}P\right)}\left(\frac{15}{2}y\right)^{\frac{5}{2}P-1}\exp\left(-\frac{15}{2}y\right) \tag{5.38}$$

Set $u = F_X(y)$. After rewriting (5.38), we obtain

$$(1-u)\,\Gamma\left(\frac{5}{2}P\right) \sim \left(\frac{15}{2}y\right)^{\frac{5}{2}P-1}\exp\left(-\frac{15}{2}y\right), \quad \text{as} \quad y \to +\infty.$$

To generate an asymptotic expression for y, we start by taking logarithm and defin-

ing the new variable $v \coloneqq (1-u)\,\Gamma(5P/2)$, which gives

$$\log v \sim \left(\frac{5}{2}P - 1\right)\log\left(\frac{15}{2}y\right) - \frac{15}{2}y, \quad \text{as} \quad y \to +\infty. \tag{5.39}$$

Rearranging (5.39) leads to

$$y \sim -\frac{2}{15}\log v + \frac{2}{15}\left(\frac{5}{2}P - 1\right)\log\left(\frac{15}{2}y\right), \quad \text{as} \quad y \to +\infty.$$

By a short calculation analogous to what is indicated earlier, we conclude

$$y \sim -\frac{2}{15}\log v + \frac{2}{15}\left(\frac{5}{2}P - 1\right)\log(-\log v), \quad \text{as} \quad y \to +\infty.$$

On substituting $v = (1-u)\,\Gamma(5P/2)$, as $y \to +\infty$, i.e. $u \to 1$, its leading order is of the form

$$y \sim -\frac{2}{15}\log\left((1-u)\,\Gamma\left(\frac{5}{2}P\right)\right).$$

The analysis above outlines the asymptotic approximation for $F_{S^P}^{-1}(u)$ as $u \to 0$ and $u \to 1$, providing us with the rationale in the choices of reasonable scaling variables for Chebyshev polynomial approximations for small P, i.e. $P = 1$. Accordingly, we report the routines for approximations of the inverse distribution function $F_{S^P}^{-1}(u)$ through Chebyshev polynomials for the four regimes identified in detail. Note again the parameters k_1 and k_2 given below restrict the ranges of the transformed variable z to the interval $[-1, 1]$.

5.4.1 Left regime

For the left regime where $u \in [10^{-12}, u_1]$, we approximate $F_{S^P}^{-1}(u)$ by a degree n Chebyshev polynomial approximation of a scaled and shifted variable as below:

$$F_{S^P}^{-1}(u) \approx c_0 T_0(z) + c_1 T_1(z) + \cdots + c_n T_n(z) - \frac{1}{2}c_0,$$

where

$$U \coloneqq \left(\frac{2}{P^2}\left(P-\frac{1}{2}\right)\log\frac{2}{P^2}-\frac{2}{P^2}\log\left(\frac{u\sqrt{\pi}}{2^{P+\frac{1}{2}}P^{P-1}}\right)\right)^{-1},$$

$$z \coloneqq k_1 U + k_2.$$

5.4.2 Central regime

For the central regime where $u \in (u_1, u_2]$, we apply a linear scaling for the variable u and a degree n Chebyshev polynomial approximation for $F_{S^P}^{-1}(u)$, i.e.

$$F_{S^P}^{-1}(u) \approx c_0 T_0(z) + c_1 T_1(z) + \cdots + c_n T_n(z) - \frac{1}{2}c_0,$$

where

$$U \coloneqq (u_2 - u)\sqrt{\frac{2P}{45}},$$

$$z \coloneqq k_1 U + k_2.$$

5.4.3 Middle and right tail regimes

For the middle and right tail regimes where $u \in (u_2, u_3]$ and $u \in (u_3, 1-10^{-12}]$, we approximate $F_{S^P}^{-1}(u)$ by a degree n Chebyshev polynomial approximation of a scaled and shifted variable as follows:

$$F_{S^P}^{-1}(u) \approx c_0 T_0(z) + c_1 T_1(z) + \cdots + c_n T_n(z) - \frac{1}{2}c_0,$$

where

$$U \coloneqq -\frac{2}{15}\log\left((1-u)\,\Gamma\left(\frac{5}{2}P\right)\right),$$

$$z \coloneqq k_1 U + k_2.$$

According to the above approximation techniques, we evaluate the Chebyshev

polynomials for some fixed values of P in Maple, the values for the coefficients of which are presented in Appendix A. Figure 5.2 shows the errors related to approximating the inverse distribution function $F_{S^P}^{-1}(u)$ with $P = 1$ by the Chebyshev polynomials constructed using the coefficients listed in Appendix A. The plot is on a log-$\log_{10}$ scale with abscissa of $1 - u$ for $u \in [10^{-12}, 1 - 10^{-12}]$. We generate approximations for five regimes as described above where the right tail region is further split into two, the degrees for which are 25 in the left with $u \in [10^{-12}, 0.2)$, 18 in the central with $u \in [0.2, 0.63)$, 15 in the middle with $u \in [0.63, 0.9)$, 18 and 13 in the right tail regimes with $[0.9, 0.999)$ and $[0.999, 1 - 10^{-12}]$, respectively. We observe the errors for all cases are of order 10^{-12}

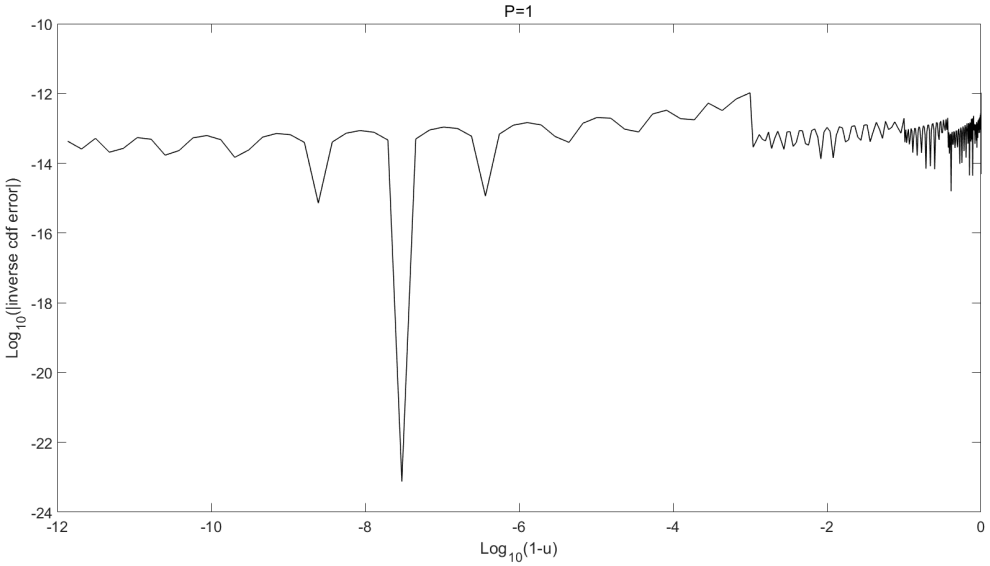

Figure 5.2: We plot the errors in the Chebyshev polynomial approximations to the inverse distribution functions $F_{S^P}^{-1}(u)$ with $P = 1$ across all regimes. Note as above we use a log-$\log_{10}$ scale with $1 - u$ on the abscissa.

Finally, we turn to the simulations of $Y_2^h = X_2/\tau^2$ for $h = 1/5, 1/10, 1/20, 1/50, 1/100, 1/200, 1/500, 1/1000, 1/2000$. As illustrated in Section 4.2, Y_2^h has the same distribution as S^h. Hence, the approach to designing the inverse distribution function approximations for S^P for small P is fully applicable here. Therefore, we apply the same strategy to calculate the Chebyshev polynomial approximations for the inverse distribution function $F_{Y_2^h}^{-1}$ of Y_2^h for fixed values of h. Their coefficients can be found in Appendix A.

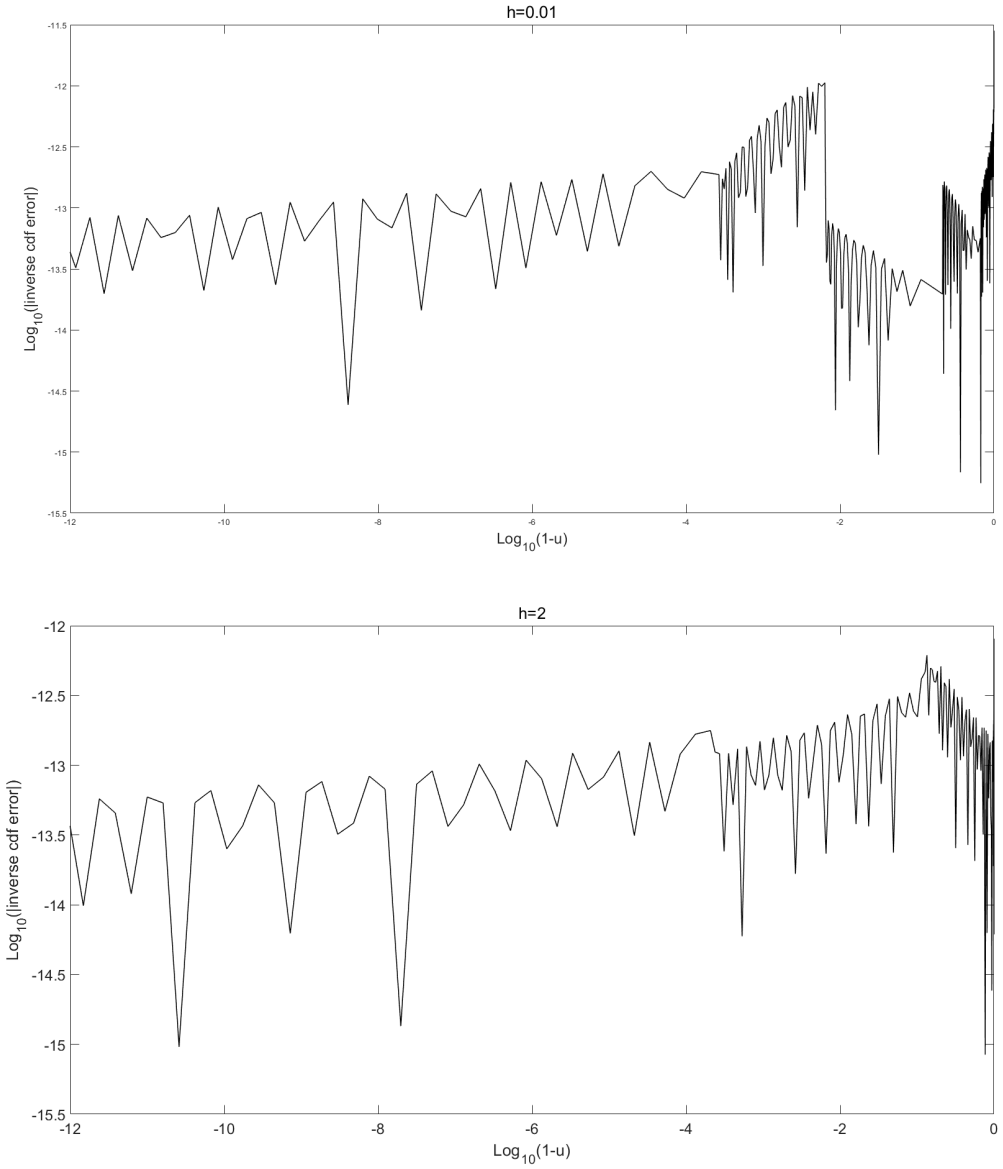

Figure 5.3: We plot the errors in the Chebyshev polynomial approximations to the inverse distribution functions $F^{-1}_{Y_2^h}(u)$ with $h = 0.01$ (top panel) and $h = 2$ (bottom panel) across all regimes. Note as above we use a log-$\log_{10}$ scale with $1 - u$ on the abscissa.

Figure 5.3 plots the resulting errors in the approximation for $F^{-1}_{Y_2^h}$ by Chebyshev polynomials across all regimes when $h = 1/100$ (top panel) and $h = 2$ (bottom panel). For the case $h = 1/100$, because of the heavy tail we further split the right tail region into two smaller regions where different Chebyshev polynomials are developed, making a total of five separate regions: $[10^{-12}, 0.3364)$, $[0.3364, 0.7854)$, $[0.7854, 0.9936)$, $[0.9936, 0.9997)$ and $[0.9997, 1 - 10^{-12}]$ with degrees 24, 19, 18, 19 and 31, respectively. The case $h = 2$ is corresponding to $Z' = Z/\tau^2$, where the approximated polynomials have degrees between 22 and 27 in the four regimes. The errors for both circumstances are fluctuating at the level of 10^{-12}. See Appendix B for more results of the other cases.

In summary, we have detailed the approximation procedures for the inverse distribution function $F^{-1}_{S^P}(u)$ taking into account the various values that P and u can take. The coefficients can be calculated and stored outside the Monte Carlo loop due to their independence of the model parameters. With all these accurate and reliable coefficients then imported to Matlab, further Chebyshev approximations are evaluated by Clenshaw's recurrence formula, see Lemma 2.3.5. Thus, for any $P > 0$, $S^P \overset{d}{=} Y_2^P$ can be sampled repeatedly with high efficiency using either Algorithm 4.2 or Algorithm 4.5 depending on the value of P.

Chapter 6

Numerical analysis

In the previous three chapters, we have developed a direct inversion scheme to simulate the conditional time integrated variance process based on the series representation as described in Theorem 3.2.1. In this chapter, we test our new method by pricing four challenging European call options in the Heston model with parameter values presented in Table 4.1. These four cases are corresponding to a long-dated FX option, a long-dated interest rate option, an equity option and an S&P 500 index option, respectively. Two path-dependent options including an Asian option with yearly fixings (see Smith [64], Haastrecht and Pelsser [66] and Malham and Wiese [51]) and a digital double no touch barrier option (see Lord, Koekkoek and Van Dijk [50] and Malham and Wiese [51]) are also tested with parameter values shown in Table 6.1.

We compare our method with the gamma expansion of Glasserman and Kim [32] chosen as a benchmark, where they conclude that their method outperforms the exact scheme of Broadie and Kaya [15] by reducing the computation time with a factor of 10^2 to 10^3. Apart from that, the efficiency of the new method is also compared to Lord, Koekkoek and Van Dijk's [50] full truncation Euler scheme. This is a standard time discretization method, which seems to produce the smallest bias among all Euler schemes in practice.

Table 6.1: Parameters for path-dependent options for the Heston model.

Parameters	**Case Asian**	**Case Barrier**
κ	1.0407	0.5
θ	0.0586	0.04
σ	0.5196	1
ρ	-0.6747	0
t	4	1
v_0	0.0194	0.04
S_0	100	100
r	0	0
δ	0.9035	0.08

6.1 Time integrated conditional variance

Before giving simulation results for option prices, we first illustrate the performance in the light of accuracy of our new method for sampling the conditional integral of the variance process. Recall from Section 3.1 that our objective is to sample from the distribution of the random variable $\int_0^t V_s\,ds$ given its endpoints V_0 and V_t, denoted by $\bar{I}$, i.e.

$$\bar{I} = \left(\int_0^t V_s\,ds \middle| V_0 = v_0, V_t = v_t \right) = \frac{4}{\sigma^2} \left(\int_0^\tau \tilde{A}_s\,ds \middle| \tilde{A}_0 = a_0, \tilde{A}_\tau = a_\tau \right) \frac{4}{\sigma^2} I,$$

under the probability measure $\mathbb{Q}$. We have decomposed the integral into the sum of three independent series after measure transformation. Among the realisation of those three series, the first one is truncated with tail approximated by a moment-matching gamma random variable and the remaining two series are simulated exactly by direct inversion. In contrast, Glasserman and Kim [32] apply their decomposition under the origin measure through truncation of each series with approximation preserving the first two moments for the remainder. To demonstrate the accuracy

of the sampling methods for $\bar{I}$, we focus on its first four moments. In particular, we show the differences between the sample moments and the true moments using the four sets of parameters for the European options. The true moments can be straightforwardly calculated by evaluating the respective derivatives of the following moment generating function derived by Broadie and Kaya [15] at the origin:

$$\begin{aligned}\mathbb{E}\left[\exp\left(-b\bar{I}\right)\right] =& \frac{\gamma(b)\exp\left(-\frac{1}{2}(\gamma(b)-\kappa)t\right)(1-\exp(-\kappa t))}{\kappa(1-\exp(-\gamma(b)t))} \\ & \cdot \exp\left[\frac{v_0+v_t}{\sigma^2}\left(\frac{\kappa(1+\exp(-\kappa t))}{1-\exp(-\kappa t)} - \frac{\gamma(b)(1+\exp(-\gamma(b)t))}{1-\exp(-\gamma(b)t)}\right)\right] \\ & \cdot \frac{\mathrm{I}_\nu\left(\frac{4\gamma(b)\sqrt{v_0 v_t}}{\sigma^2}\frac{\exp\left(-\frac{1}{2}\gamma(b)t\right)}{1-\exp(-\gamma(b)t)}\right)}{\mathrm{I}_\nu\left(\frac{4\kappa\sqrt{v_0 v_t}}{\sigma^2}\frac{\exp\left(-\frac{1}{2}\kappa t\right)}{1-\exp(-\kappa t)}\right)},\end{aligned}$$

where $\gamma(b) = \sqrt{\kappa^2 + 2\sigma^2 b}$ and $\nu = \delta/2 - 1$. Table 6.2 provides the exact moments obtained via Maple for all four cases considered with three distinct values of v_t each.

In Figure 6.1 and Figure 6.2 the absolute errors in the first four moments are displayed for simulating the conditional integral $\bar{I}$ with different values of v_t using our new method. For comparison, we include the results by employing the gamma expansion from Glasserman and Kim [32] as well. For both methods, we apply tail approximations with truncation level increasing in integers. The number of samples generated in each case is $5 \cdot 10^7$. The dashed lines represent the level of logarithmic error, below which the errors are statistically insignificant at the level of three standard deviations. The three panels shown in Figure 6.1 from top to bottom correspond to the three representative values $v_t = 0.04, 4, 0.000004$ for Case 1 and the panels in Figure 6.2 correspond to the three fixed values $v_t = 0.010201, 0.05, 0.0025$ (top to bottom) for Case 4.

We observe that most errors for the first two moments across different values of v_t and truncation levels for both Case 1 and 4 are not significantly different from zero at the level of three standard deviations, suggesting both methods achieve high accuracy for these two moments as expected. This is consistent with the theory as tail simulation in each method is designed such that the first two moments are

matched. In other words, the simulations should lead to the exact first and second moments in principle, whence only Monte Carlo noise with a scaling as the inverse of the square root of the sample size, i.e., $(5 \cdot 10^7)^{-1/2}$, is observed.

Table 6.2: True nth moment of $\bar{I}$

		Case 1	
n \ v_t	0.000004	0.04	4
1	0.32106	0.40002	8.20987
2	0.78953	1.12915	96.13869
3	5.08077	8.25777	1523.80429
4	52.33534	96.28896	30770.60608
		Case 2	
n \ v_t	0.000004	0.04	0.4
1	0.46952	0.60008	1.77502
2	2.27912	3.41708	15.18175
3	29.60642	51.53938	287.81493
4	610.31254	1223.33275	8066.07463
		Case 3	
n \ v_t	0.000009	0.09	0.9
1	0.36119	0.45002	1.24925
2	0.32352	0.47507	2.54633
3	0.56474	0.95331	7.79412
4	1.51400	2.91212	32.38336
		Case 4	
n \ v_t	0.0025	0.010201	0.05
1	$1.49633 \cdot 10^{-2}$	$1.61887 \cdot 10^{-2}$	$2.25215 \cdot 10^{-2}$
2	$3.11870 \cdot 10^{-4}$	$3.61014 \cdot 10^{-4}$	$6.62850 \cdot 10^{-4}$
3	$8.88968 \cdot 10^{-6}$	$1.09094 \cdot 10^{-5}$	$2.52008 \cdot 10^{-5}$
4	$3.33844 \cdot 10^{-7}$	$4.31598 \cdot 10^{-7}$	$1.20806 \cdot 10^{-6}$

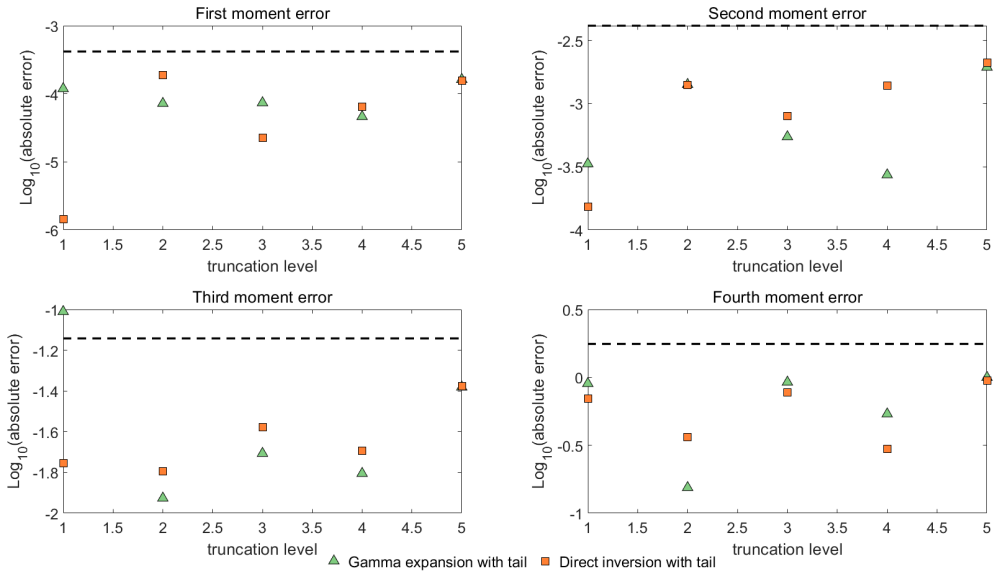

(a) Case 1: $v_0 = v_t = 0.04$

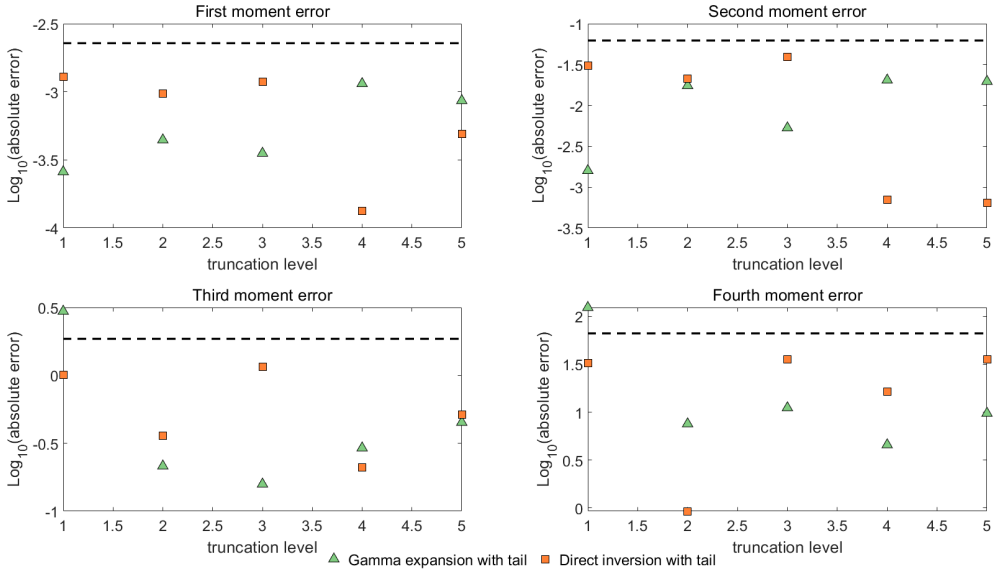

(b) Case 1: $v_0 = 0.04, v_t = 4$

Figure 6.1: We indicate the absolute errors in the first four moments of the conditional integral $\bar{I}$ simulated by direct inversion and gamma expansion versus the truncation levels for Case 1 with different values for v_t. Both methods are implemented with tail simulation. We perform $5 \cdot 10^7$ simulations for each case. Below the dashed line, the errors are not statistically significant at the level of three standard deviations.

Remark 6.1

We note that the absolute error in the fourth moment for Case 1 with $v_t = 4$, shown in the lower right panel in Figure 6.1b, is much higher compared to that when

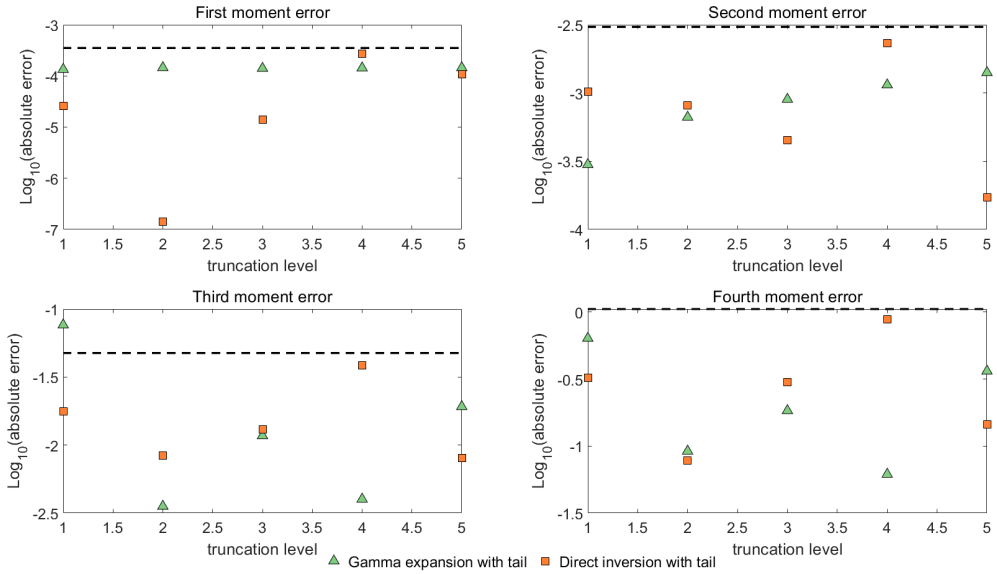

(c) Case 1: $v_0 = 0.04, v_t = 0.000004$

Figure 6.1: (cont.) We indicate the absolute errors in the first four moments of the conditional integral $\bar{I}$ simulated by direct inversion and gamma expansion versus the truncation levels for Case 1 with different values for v_t. Both methods are implemented with tail simulation. We perform $5 \cdot 10^7$ simulations for each case. Below the dashed line, the errors are not statistically significant at the level of three standard deviations.

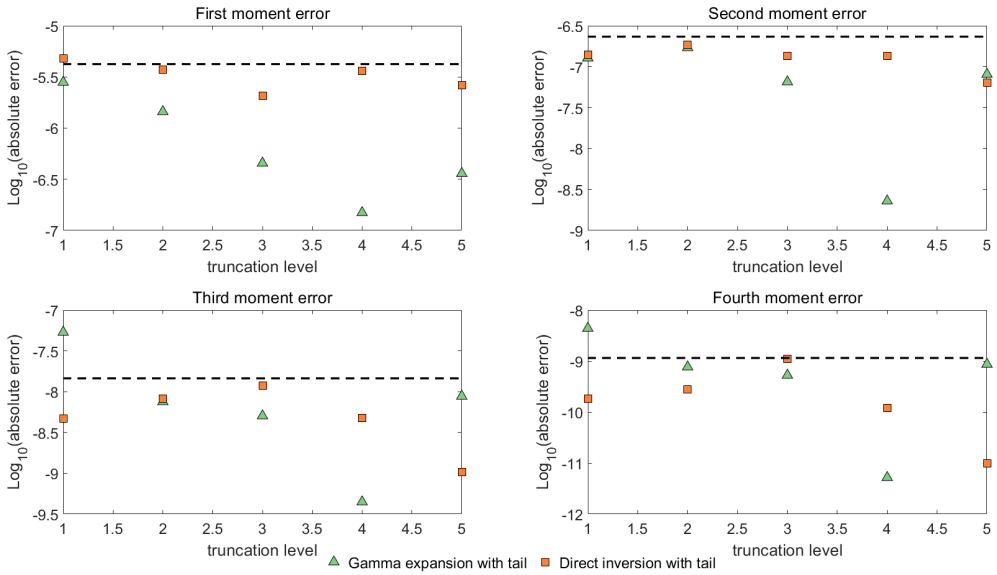

(a) Case 4: $v_0 = v_t = 0.010201$

Figure 6.2: We indicate the absolute errors in the first four moments of the conditional integral $\bar{I}$ simulated by direct inversion and gamma expansion versus the truncation levels for Case 4 with different values for v_t. Both methods are implemented with tail simulation. We perform $5 \cdot 10^7$ simulations for each case. Below the dashed line, the errors are not statistically significant at the level of three standard deviations.

$v_t = 0.04$ and $v_t = 0.000004$, shown in the two lower right panels in Figure 6.1a and Figure 6.1c, respectively. This is due to the fact that the fourth moment for $v_t = 4$ has a much larger magnitude than the other two cases, which can be observed from Table 6.2

For the higher moments, the errors of the direct inversion are fluctuating at some level below the statistical significance for all circumstances considered. These errors are so small that a decreasing trend is not visible when increasing the truncation level. In contrast, with the increment of the truncation levels, the errors of the gamma expansion first exhibit a decaying pattern until the curves become horizontal. For example, the behaviour of the decreasing errors of the third and fourth moments is obvious when the truncation level is increased from one to two. The falling tendency appears to be more significant when we increase the sample size, thus, reduce the Monte Carlo effect, see, for example, the lower panels in Figure 6.3a, Figure 6.3b and Figure 6.3c and the discussions there for Case 1 with sample size increased by 10. This suggests that there exists some bias in the gamma expansion with small truncation levels while the direct inversion with lower truncation levels has the same accuracy as that with higher ones.

While the figures for Case 1 and Case 4 have many details in common, they also reveal noteworthy differences in the first two moments. As illustrated in the upper panels in Figure 6.2a, Figure 6.2b and Figure 6.2c for Case 4, most of the first and second moment errors in the direct inversion are slightly higher compared to those in the gamma expansion at the same truncation level. Errors of the two schemes considered in the first two moments for Case 1 on the other hand seem to be of the same order to some extent with the same truncation level, which can be seen from the upper panels in Figure 6.1a, Figure 6.1b and Figure 6.1c. In order to find a plausible explanation for this difference, we increase the sample size by a factor of 10 and plot the resulting errors versus the truncation levels from 1 to 5 in Figure 6.3 and Figure 6.4.

For Case 1, Figure 6.3 demonstrates the errors in all four moments based on the direct inversion are decreased as expected, i.e., proportional to the reciprocal of the square root of the sample size across all the values of v_t and truncation

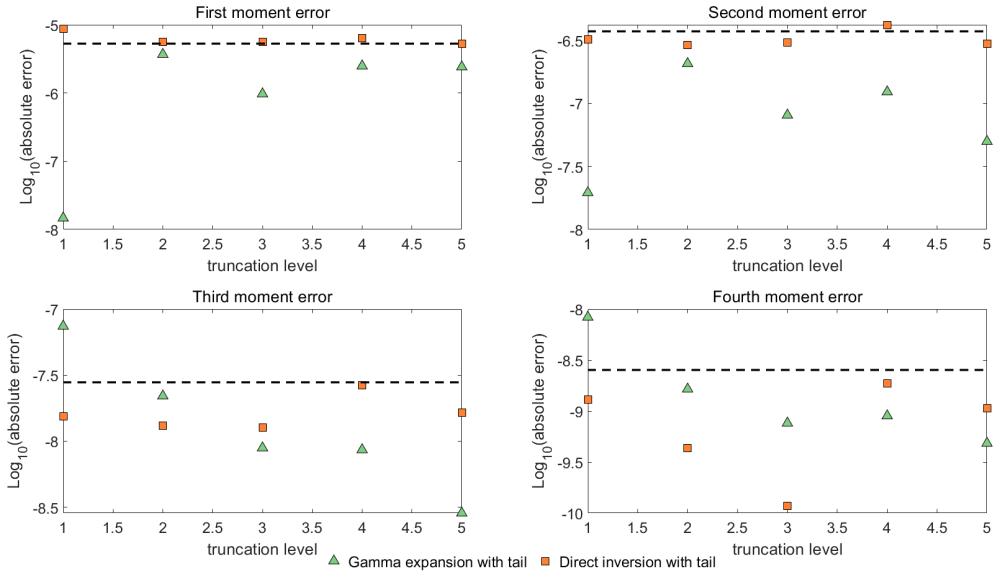

(b) Case 4: $v_0 = 0.010201, v_t = 0.05$

Figure 6.2: (cont.) We indicate the absolute errors in the first four moments of the conditional integral $\bar{I}$ simulated by direct inversion and gamma expansion versus the truncation levels for Case 4 with different values for v_t. Both methods are implemented with tail simulation. We perform $5 \cdot 10^7$ simulations for each case. Below the dashed line, the errors are not statistically significant at the level of three standard deviations.

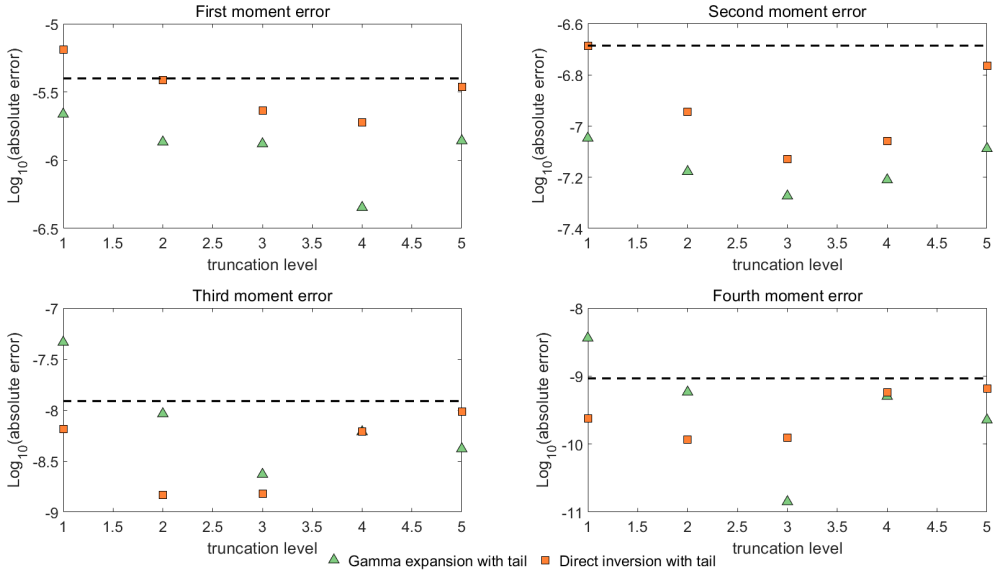

(c) Case 4: $v_0 = 0.010201, v_t = 0.0025$

Figure 6.2: (cont.) We indicate the absolute errors in the first four moments of the conditional integral $\bar{I}$ simulated by direct inversion and gamma expansion versus the truncation levels for Case 4 with different values for v_t. Both methods are implemented with tail simulation. We perform $5 \cdot 10^7$ simulations for each case. Below the dashed line, the errors are not statistically significant at the level of three standard deviations.

levels. This confirms that the moment errors observed in Figure 6.1 using the direct inversion are overwhelmed by the Monte Carlo error. On the other hand, for the gamma expansion we note in the upper panels of each subplots that the first two moments of the simulations for all five truncation levels are indeed matched with errors improving roughly according to the expected scaling when increasing the sample size. However, we see in the lower panels that the errors in the third and fourth moments hardly show any changes for lower truncation levels such as one and two while the accuracy for the other truncation levels is improved with the increase of the sample size. In fact, after reducing the Monte Carlo noise, there exists an even more clear decreasing trend for the higher order moment errors with the gamma expansion as the truncation level increases. This seems to corroborate the observations from Figure 6.1 for Case 1, indicating that the gamma expansion with small truncation levels exhibits some bias while the direct inversion achieves the same accuracy, restricted by the Monte Carlo error, for all truncation levels.

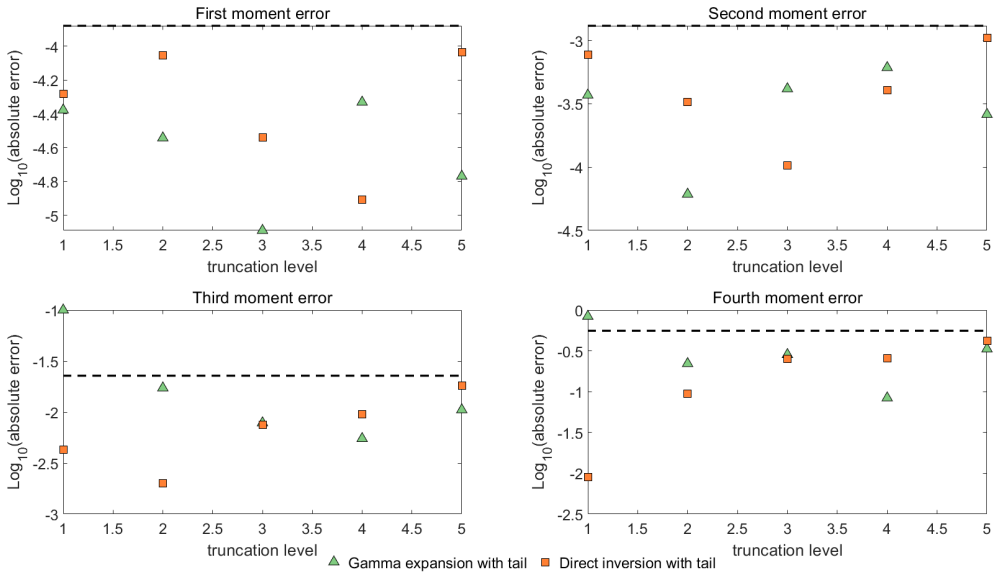

(a) Case 1: $v_0 = v_t = 0.04$

Figure 6.3: We indicate the absolute errors in the first four moments of the conditional integral $\bar{I}$ simulated by direct inversion and gamma expansion versus the truncation levels for Case 1 with different values for v_t. Both methods are implemented with tail simulation. We perform $5 \cdot 10^8$ simulations for each case. Below the dashed line, the errors are not statistically significant at the level of three standard deviations.

In comparison, Figure 6.4 shows different behaviour for the errors related to the

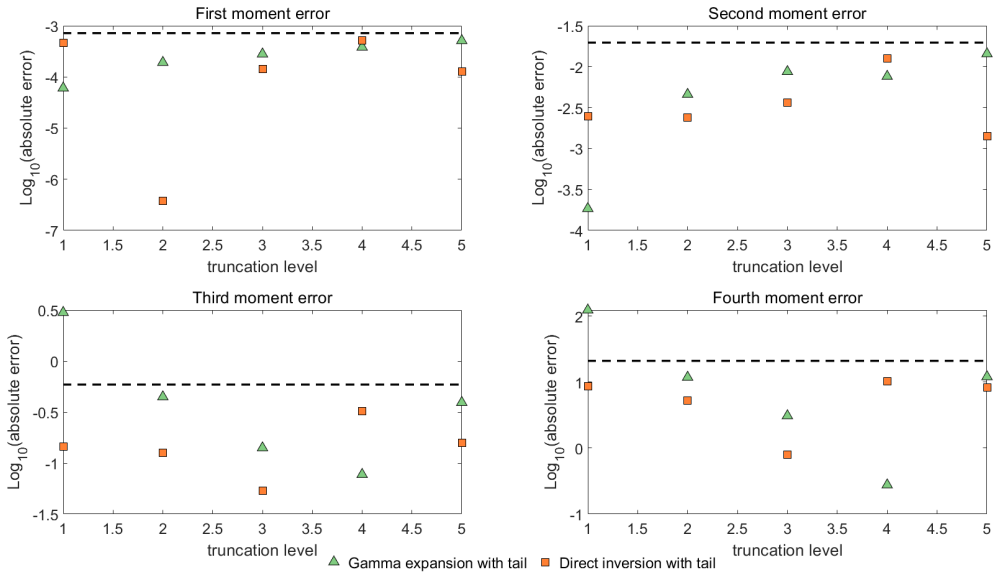

(b) Case 1: $v_0 = 0.04, v_t = 4$

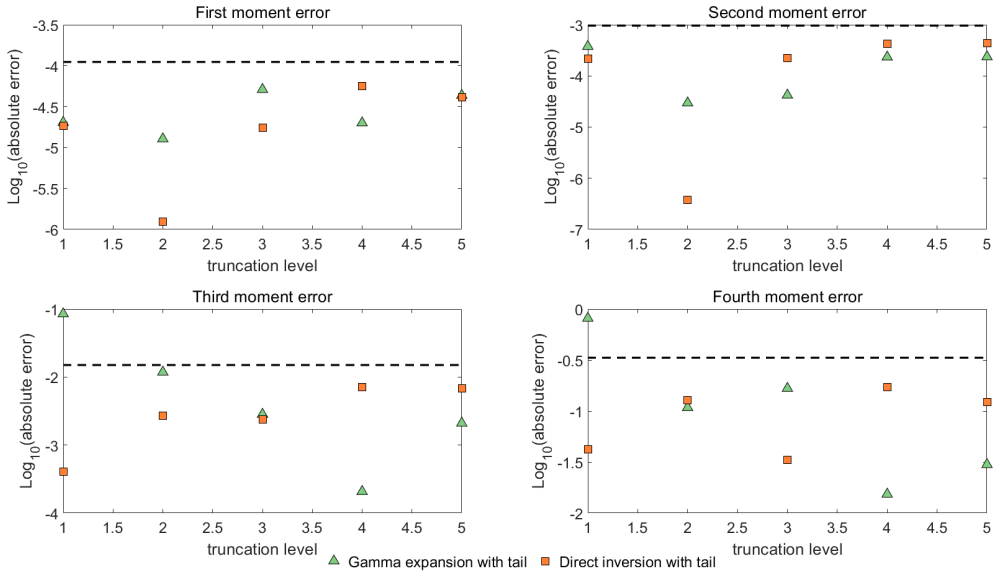

(c) Case 1: $v_0 = 0.04, v_t = 0.000004$

Figure 6.3: (cont.) We indicate the absolute errors in the first four moments of the conditional integral $\bar{I}$ simulated by direct inversion and gamma expansion versus the truncation levels for Case 1 with different values for v_t. Both methods are implemented with tail simulation. We perform $5 \cdot 10^8$ simulations for each case. Below the dashed line, the errors are not statistically significant at the level of three standard deviations.

direct inversion for Case 4 while similar conclusion can be reached for the gamma expansion as Case 1. More specifically, we notice that all moment errors in direct inversion sampling for Case 4 are invariant to increasing the sample size when the truncation levels are fixed. Further we observe that the errors, all remaining steady across a set of different truncation levels, become statistically significant when the number of samples is increased, especially for the first and second moments. Thus, this implies in Case 4 the direct inversion performs equally well for all truncation levels, nevertheless, the accuracy of which is overridden by some bias. We should not fail to mention that the bias is roughly of the same order as the Monte Carlo error with $5 \cdot 10^7$ samples, whence it is not reflected in Figure 6.2. This accounts for the finding for Case 4 that the first and second moment errors for the direct inversion are always slightly larger than those for gamma expansion, where only Monte Carlo error is in presence. We give a possible explanation for this bias as follows.

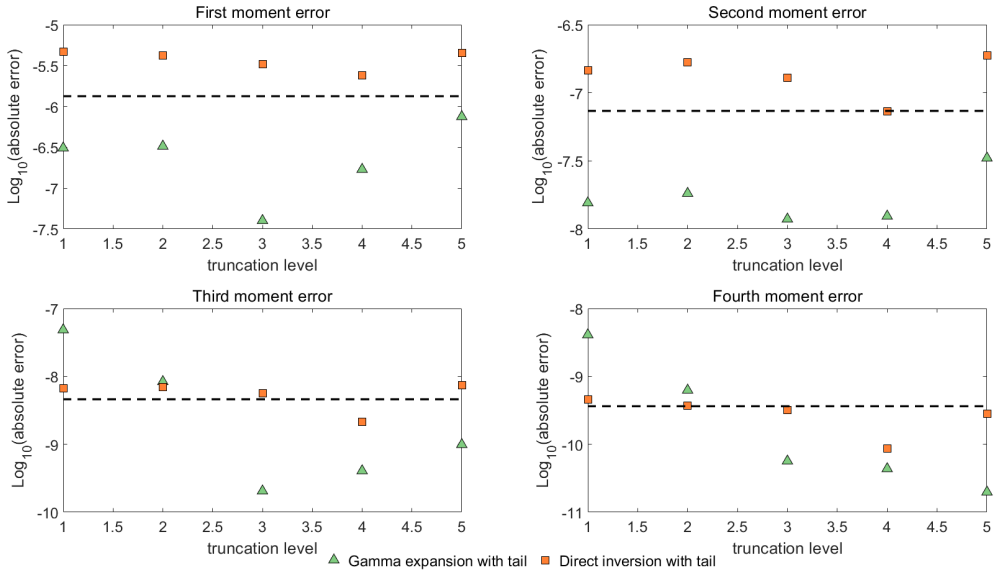

(a) Case 4: $v_0 = v_t = 0.010201$

Figure 6.4: We indicate the absolute errors in the first four moments of the conditional integral $\bar{I}$ simulated by direct inversion and gamma expansion versus the truncation levels for Case 4 with different values for v_t. Both methods are implemented with tail simulation. We perform $5 \cdot 10^8$ simulations for each case. Below the dashed line, the errors are not statistically significant at the level of three standard deviations.

The reason for the bias with the direct inversion method for Case 4 lies in the arithmetic precision we use for the parameter h, which is related to the random variable X_2. Recall that the proposed decomposition requires the rational parameter

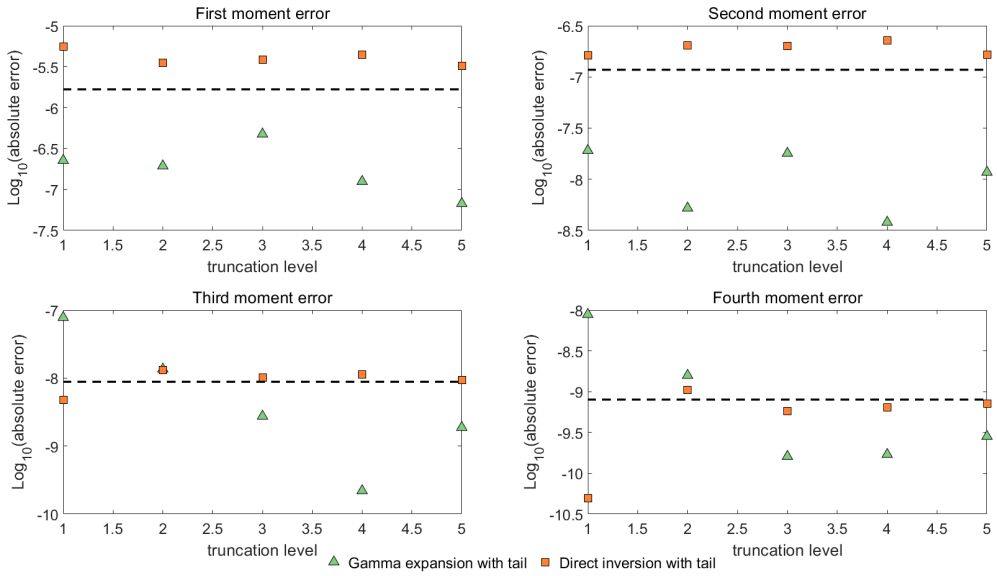

(b) Case 4: $v_0 = 0.010201, v_t = 0.05$

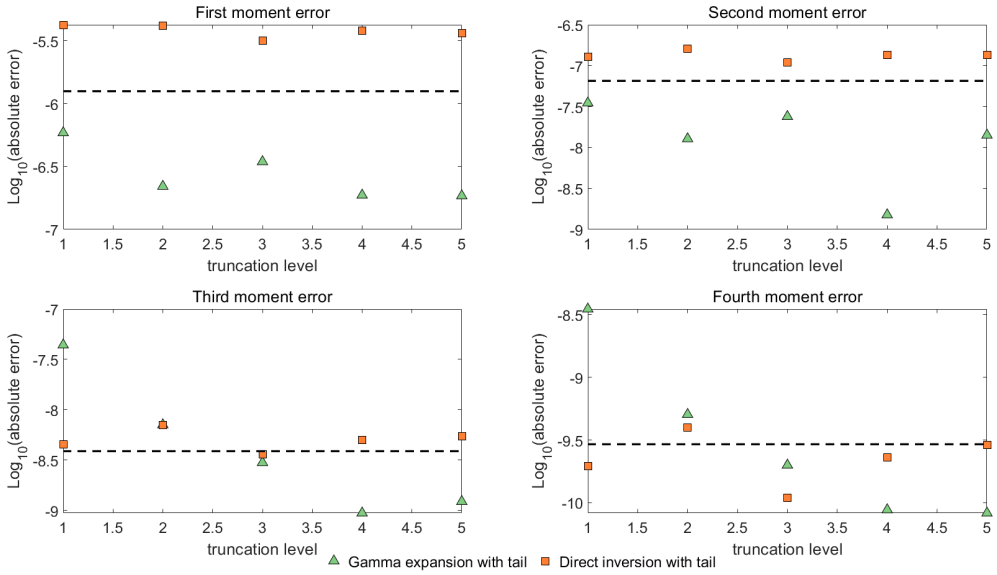

(c) Case 4: $v_0 = 0.010201, v_t = 0.0025$

Figure 6.4: (cont.) We indicate the absolute errors in the first four moments of the conditional integral $\bar{I}$ simulated by direct inversion and gamma expansion versus the truncation levels for Case 4 with different values for v_t. Both methods are implemented with tail simulation. We perform $5 \cdot 10^8$ simulations for each case. Below the dashed line, the errors are not statistically significant at the level of three standard deviations.

h is given as a decimal with three significant figures. Let $\tilde{h}$ stand for the rounded number and $\tilde{X}_2$ denote the approximation to X_2 by replacing h with $\tilde{h}$. Next, we give the analytical expressions for the exact errors in the first four moments of X_2. Directly computing its moments using the derivatives of the moment generating function (3.6) evaluated at the origin, we can write

$$\mathbb{E}\left[X_2\right] = \frac{1}{3}h\tau^2,$$

$$\mathbb{E}\left[X_2^2\right] = \left(\frac{2}{45}h + \frac{1}{9}h^2\right)\tau^4,$$

$$\mathbb{E}\left[X_2^3\right] = \left(\frac{16}{945}h + \frac{2}{45}h^2 + \frac{1}{27}h^3\right)\tau^6,$$

$$\mathbb{E}\left[X_2^4\right] = \left(\frac{16}{1575}h + \frac{404}{14175}h^2 + \frac{4}{135}h^3 + \frac{1}{81}h^4\right)\tau^8.$$

Then, the corresponding relative errors are

$$\frac{\left|\mathbb{E}\left[X_2\right] - \mathbb{E}\left[\tilde{X}_2\right]\right|}{\mathbb{E}\left[X_2\right]} = \frac{\left|h - \tilde{h}\right|}{h},$$

$$\frac{\left|\mathbb{E}\left[X_2^2\right] - \mathbb{E}\left[\tilde{X}_2{}^2\right]\right|}{\mathbb{E}\left[X_2^2\right]} = \frac{\left|2\left(h - \tilde{h}\right) + 5\left(h^2 - \tilde{h}^2\right)\right|}{2h + 5h^2},$$

$$\frac{\left|\mathbb{E}\left[X_2^3\right] - \mathbb{E}\left[\tilde{X}_2{}^3\right]\right|}{\mathbb{E}\left[X_2^3\right]} = \frac{\left|16\left(h - \tilde{h}\right) + 42\left(h^2 - \tilde{h}^2\right) + 35\left(h^3 - \tilde{h}^3\right)\right|}{16h + 42h^2 + 35h^3},$$

$$\frac{\left|\mathbb{E}\left[X_2^4\right] - \mathbb{E}\left[\tilde{X}_2{}^4\right]\right|}{\mathbb{E}\left[X_2^4\right]} = \frac{\left|144\left(h - \tilde{h}\right) + 404\left(h^2 - \tilde{h}^2\right) + 420\left(h^3 - \tilde{h}^3\right) + 175\left(h^4 - \tilde{h}^4\right)\right|}{144h + 404h^2 + 420h^3 + 175h^4}.$$

The above equations show a linear scaling of the moment errors of X_2 in terms of the discrepancy between the true value h and the approximated value $\tilde{h}$. Table 6.3 quotes the values for h and $\tilde{h}$ for all four cases considered. Note that for Case 1 and Case 3 accurate values of h are used while the relative errors for Case 2 and Case 4 are of order 10^{-3} and 10^{-4}, respectively. In Figure 6.5 the panels show the relative errors in the first four moments of X_2 for Case 1 to Case 4 using 10^8 and 10^9 simulations. For Case 1 and Case 3, by successively increasing the sample

size the high accuracy for the first four moments of X_2 sampled by direct inversion Algorithm 4.5 is indeed limited by the Monte Carlo error, which improves roughly according to the expected scale. However, the errors are invariant for Case 2 and Case 4 when increasing the sample size. For these two cases, the systematic Monte Carlo error is lower than the bias caused by replacing the true value h with the approximated value $\tilde{h}$. Hence, the errors reflected in Figure 6.5, dominated by the bias, fail to show improvement when the sample size is increased by a factor of 10.

Table 6.3: True value h and rounded value $\tilde{h}$.

	Case 1	**Case 2**	**Case 3**	**Case 4**
h	0.04000	0.02963	0.18000	0.63418
$\tilde{h}$	0.04000	0.02950	0.18000	0.63400

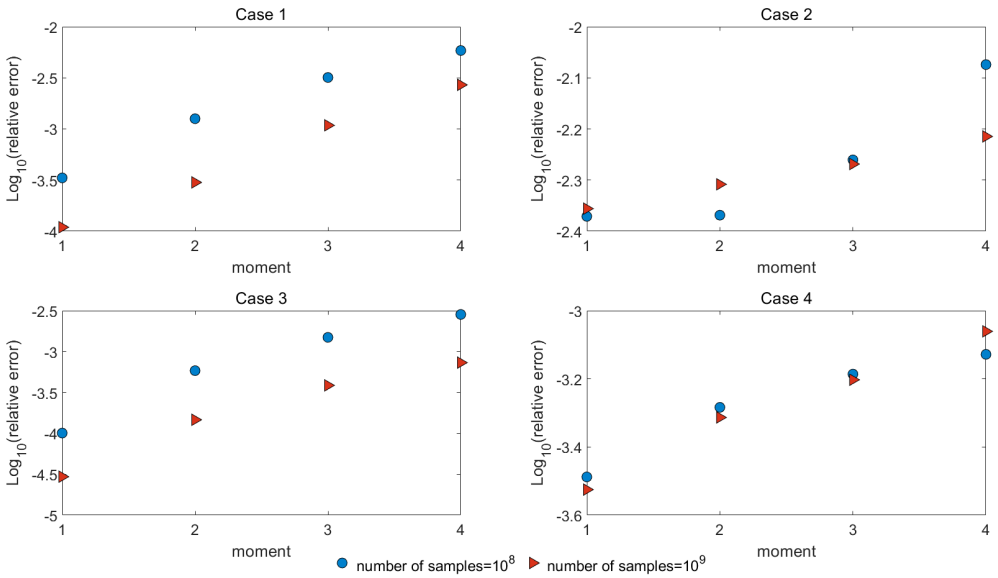

Figure 6.5: We plot the relative errors in the first four moments of X_2 simulated by direct inversion Algorithm 4.5 for Case 1 to Case 4. By increasing the sample size by a factor of 10, we note that the accuracy in the moment errors is improved as expected for Case 1 and Case 3. The four moment errors are invariant for Case 2 and Case 4 when increasing the sample size, suggesting possible bias in the direct inversion for these two cases.

Based on the above analysis, we conclude that the direct inversion method for X_2 exhibits some small bias when approximation of the parameter h is applied.

This can conceivably lead to the bias of the general direct inversion scheme for the conditional integral $\bar{I}$. However, this bias has nothing to do with the development of the method, but is associated with the decomposition technique and the arithmetic precision involved. Without loss of generality, this method can be extended to allow for a finer decomposition of the parameter h given to any number of decimal places. In this sense, we expect that the accuracy available for this method will become more apparent.

6.2 Option price

In this section, we apply the direct inversion method combined with the classical Monte Carlo approach to the pricing of options. The prices for the options considered here will depend on a set of observed asset prices at various given times. Under the new scheme, observations of the asset prices are obtained through almost exact simulation, i.e. Algorithm 4.1, where the integrated conditional variance process is realised by acceptance-rejection sampling of Algorithm 4.7 and series decomposition of Theorem 3.2.1. These series are simulated using truncation and direct inversion, see Algorithm 4.2-4.6.

For comparison, Glasserman and Kim's [32] gamma expansion is implemented as well in this section. They also apply the almost exact simulation method to generate samples for the asset price. The difference is that random samples of the time integral of the variance process are produced under the original measure by adding three independent samples of random variables, with each one represented in terms of series of weighted gamma random variables and simulated by series truncation.

A further comparison is performed using the full truncation scheme of Lord, Koekkoek and Van Dijk's [50]. This time stepping method simulates the asset price and variance on discrete time grids. Thus, multiple time steps, depending on the step size Δt under consideration, are required when pricing a European option, whilst the (almost) exact simulation scheme simulates the variables at maturity within a single step.

We present the numerical results for pricing four European call options and two path-dependent options, including an Asian option and a barrier option, in the following sections.

6.2.1 European options

For all European options considered, we investigate the performance of the three simulation schemes mentioned above with three strike levels for each: at the money $K = 100$, out of the money $K = 140$ and in the money $K = 60$. As an accurate benchmark for comparison, we use the numerical result of the closed form solution given in Proposition 1.1.4.

Table 6.4: Estimated biases with standard errors in parentheses using $5 \cdot 10^7$ paths and truncation level M for European call options with strike K

$K = 100$

		Case 1	**Case 2**
	True price	13.085	16.649
$M = 1$	Direct inversion	0.06833 (0.00188)	0.09125 (0.00672)
	Gamma expansion	0.98501 (0.00182)	0.81935 (0.00638)
$M = 5$	Direct inversion	0.00213 (0.00188)	0.01262 (0.00673)
	Gamma expansion	0.04155 (0.00188)	0.05609 (0.00642)
$M = 10$	Direct inversion	0.00202 (0.00188)	0.00184 (0.00649)
	Gamma expansion	0.00104 (0.00188)	0.00086 (0.00662)
		Case 3	**Case 4**
	True price	33.597	6.806
$M = 1$	Direct inversion	0.01317 (0.00842)	0.00394 (0.00105)
	Gamma expansion	0.06724 (0.00828)	0.00729 (0.00105)
$M = 5$	Direct inversion	0.00443 (0.00826)	0.00174 (0.00105)
	Gamma expansion	0.00242 (0.00827)	0.00142 (0.00105)
$M = 10$	Direct inversion	0.00305 (0.00828)	0.00106 (0.00105)
	Gamma expansion	0.01493 (0.00840)	0.00186 (0.00105)

To demonstrate the truncation effect of the two almost exact schemes, i.e. the gamma expansion and the direct inversion, we first summarise in Table 6.4 the estimated biases resulting from these two sampling methods using $5 \cdot 10^7$ trials with numbers in the parentheses being the standard errors. For each case, we include the results for three truncation levels, denoted by M: $M = 1$, $M = 5$ and $M = 10$. Recall from Section 4.1 and Section 4.2 that we only truncate the first series in the decomposition of the integrated conditional variance, i.e. Theorem 3.2.1, with the other two series sampled exactly by direction inversion. In contrast, all three series in the gamma expansion are approximated by finite sums.

Table 6.4: (cont.) Estimated biases with standard errors in parentheses using $5 \cdot 10^7$ paths and truncation level M for European call options with strike K

$K = 140$

		Case 1	**Case 2**
	True price	0.296	5.138
$M = 1$	Direct inversion	0.00574 (0.00036)	0.04257 (0.00556)
	Gamma expansion	0.06760 (0.00033)	0.49502 (0.00572)
$M = 5$	Direct inversion	0.00051 (0.00036)	0.01975 (0.00552)
	Gamma expansion	0.00134 (0.00036)	0.03068 (0.00592)
$M = 10$	Direct inversion	0.00040 (0.00036)	0.02029 (0.00577)
	Gamma expansion	0.00086 (0.00036)	0.01091 (0.00578)
		Case 3	**Case 4**
	True price	18.157	0.0014
$M = 1$	Direct inversion	0.01067 (0.00724)	$3.469 \cdot 10^{-5}$ $(1.443 \cdot 10^{-5})$
	Gamma expansion	0.21657 (0.00727)	$3.003 \cdot 10^{-5}$ $(1.437 \cdot 10^{-5})$
$M = 5$	Direct inversion	0.00528 (0.00728)	$5.020 \cdot 10^{-5}$ $(1.453 \cdot 10^{-5})$
	Gamma expansion	0.00297 (0.00725)	$2.403 \cdot 10^{-5}$ $(1.429 \cdot 10^{-5})$
$M = 10$	Direct inversion	0.00031 (0.00724)	$2.641 \cdot 10^{-5}$ $(1.455 \cdot 10^{-5})$
	Gamma expansion	0.00469 (0.00744)	$2.886 \cdot 10^{-5}$ $(1.436 \cdot 10^{-5})$

The table indicates that the decline of the bias gradually slows down with the

increment of the truncation level for both schemes. In terms of accuracy, the gamma expansion shares very similar conclusions as the new method for large M. Despite this, it turns out that much more significant biases remain in the gamma approximation with small M compared to the direct inversion, especially for the cases with large maturity time t such as Case 1 with $t = 10$ and Case 2 with $t = 15$. This observation confirms the earlier finding that the gamma expansion yields biased estimators when small truncation level is applied.

Table 6.4: (cont.) Estimated biases with standard errors in parentheses using $5 \cdot 10^7$ paths and truncation level M for European call options with strike K

$K = 60$

		Case 1	**Case 2**
	True price	44.330	45.287
$M = 1$	Direct inversion	0.01653 (0.00355)	0.06045 (0.00730)
	Gamma expansion	0.55146 (0.00363)	0.42595 (0.00753)
$M = 5$	Direct inversion	0.00312 (0.00354)	0.01563 (0.00728)
	Gamma expansion	0.00506 (0.00355)	0.01752 (0.00723)
$M = 10$	Direct inversion	0.00062 (0.00354)	0.01134 (0.00748)
	Gamma expansion	0.00110 (0.00354)	0.02413 (0.00713)
		Case 3	**Case 4**
	True price	56.575	41.914
$M = 1$	Direct inversion	0.01044 (0.00917)	0.00604 (0.00177)
	Gamma expansion	0.03257 (0.00913)	0.00076 (0.00177)
$M = 5$	Direct inversion	0.01495 (0.00907)	0.00405 (0.00177)
	Gamma expansion	0.00677 (0.00906)	0.00135 (0.00177)
$M = 10$	Direct inversion	0.01175 (0.00906)	0.00330 (0.00177)
	Gamma expansion	0.00650 (0.00903)	0.00216 (0.00177)

Next, we show the tradeoff between speed and accuracy of the direct inversion method and the gamma expansion. Figure 6.6 plots the root mean square error for the price of an at the money European call option with strike $K = 100$ against the

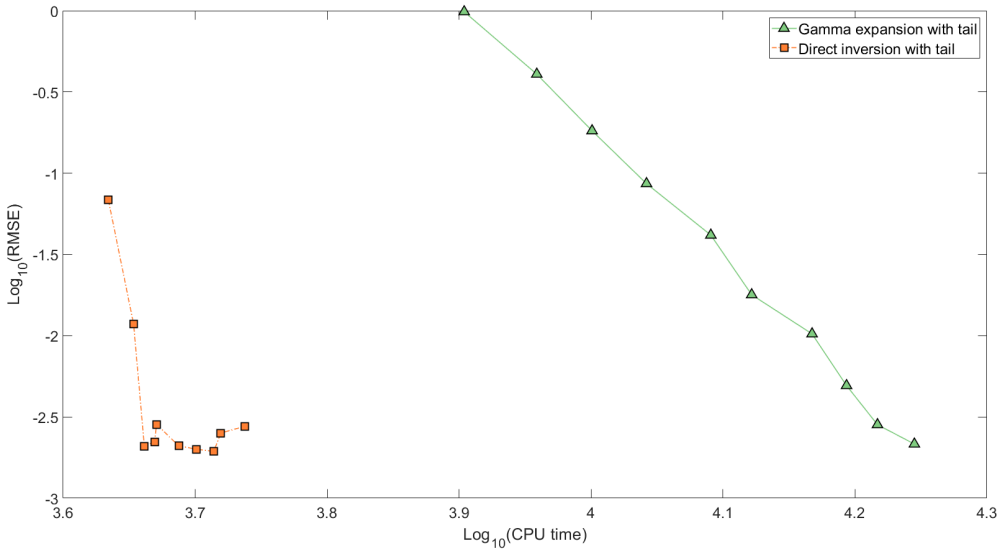

(a) Case 1

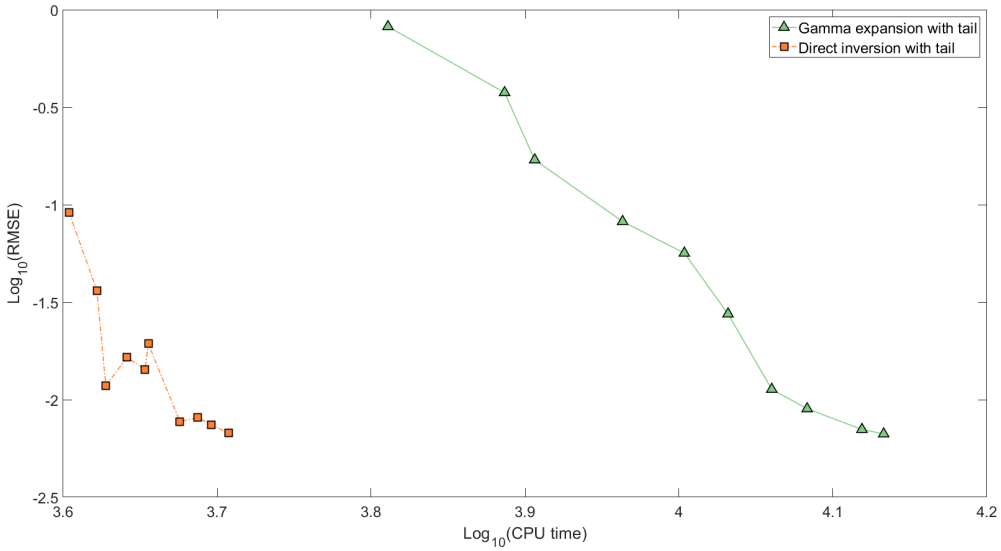

(b) Case 2

Figure 6.6: We show the root mean square error in the option price with $K = 100$ versus the CPU time required to complete the simulation on a log-$\log_{10}$ scale for Case 1 to Case 4. We use a sample size of $5 \cdot 10^7$ with truncation levels increasing in integers from 1 to 10.

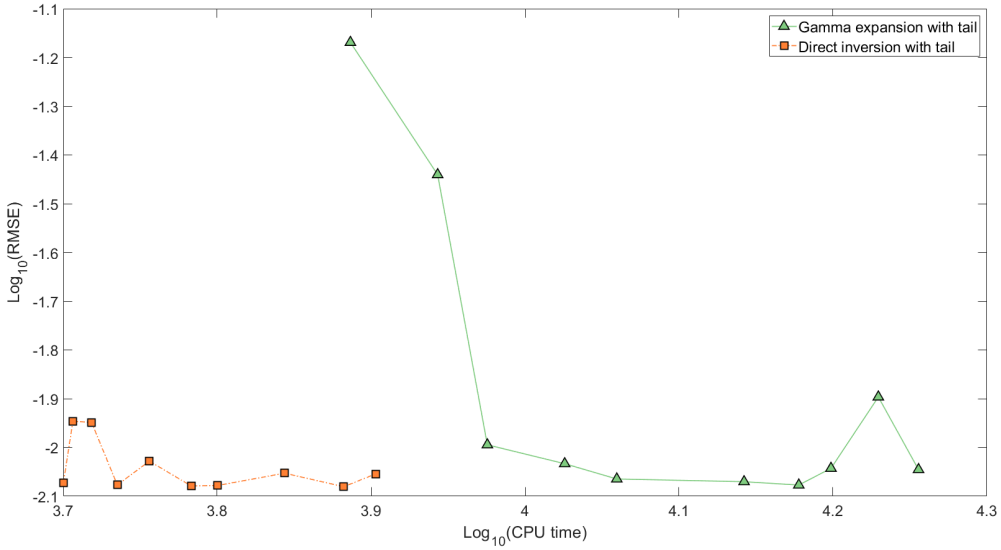

(c) Case 3

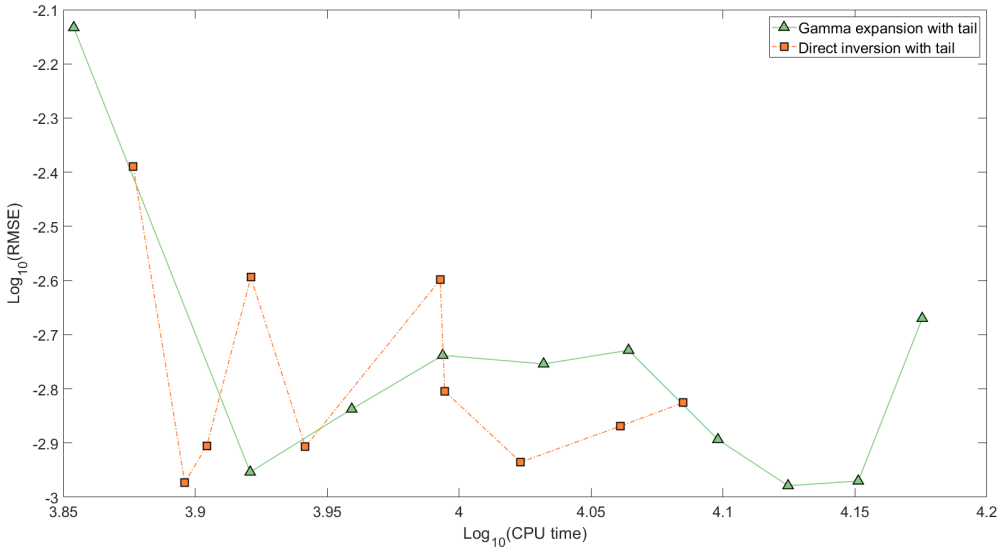

(d) Case 4

Figure 6.6: (cont.) We show the root mean square error in the option price with $K = 100$ versus the CPU time required to complete the simulation on a log-$\log_{10}$ scale for Case 1 to Case 4. We use a sample size of $5 \cdot 10^7$ with truncation levels increasing in integers from 1 to 10.

CPU time required to complete the simulation on a log-$\log_{10}$ scale for Case 1 to Case 4. For both methods, we use a sample size of $5 \cdot 10^7$ and truncate after M terms, increasing M in integers from 1 to 10.

For large maturity, i.e. Case 1 and Case 2, the direct inversion exhibits a faster convergence rate, revealed by the steeper slope in Figure 6.6a and Figure 6.6b, in contrast with the gamma expansion. Indeed, truncation after three terms already provides a satisfactory estimator with error curve eventually becoming noisy in the larger M regime. To obtain the same accuracy, many more terms up to $M = 10$ are required for the gamma approximation. For small maturity such as Case 4, increasing M from one to two indeed helps to reduce the error. However, further increase in M does not seem to bring improvement to the error for both methods, as seen from the horizontal error curves with small fluctuations in Figure 6.6d. This implies that approximations with small M are sufficient to achieve acceptable accuracy.

With regard to the computing time, the gamma expansion is almost two to three times slower than the direct inversion with similar accuracy for all cases except for Case 4. While the new methods for Case 1 to Case 3 are roughly of the same speed, that for Case 4 takes much more time, in which more effort is needed for the acceptance-rejection sampling due to the slightly unfavourable values for the model parameters. Although the time needed for the direct inversion is marginally more than the gamma expansion for Case 4 with $M = 1$, as the desired accuracy is increased the new method requires less computational budget.

We end this section with comparisons between the almost exact methods and the full truncation Euler scheme, which is a standard time discretization method with typical weak convergence order of one. In Figure 6.7, we plot the root mean square error in the option price as a function of the CPU time required on a log-$\log_{10}$ scale for all schemes. For the two almost exact methods, we choose to use truncation level $M = 5$. For the full truncation Euler method, we set the number of time steps equal to the square root of the sample size. This is motivated by Duffie and Glynn [24]'s optimal allocation for the number of time steps, which is proportional to the square root of the number of trials for methods with weak order of convergence being equal

to one; see Broadie and Kaya [15] and Lord, Koekkoek and Van Dijk [50].

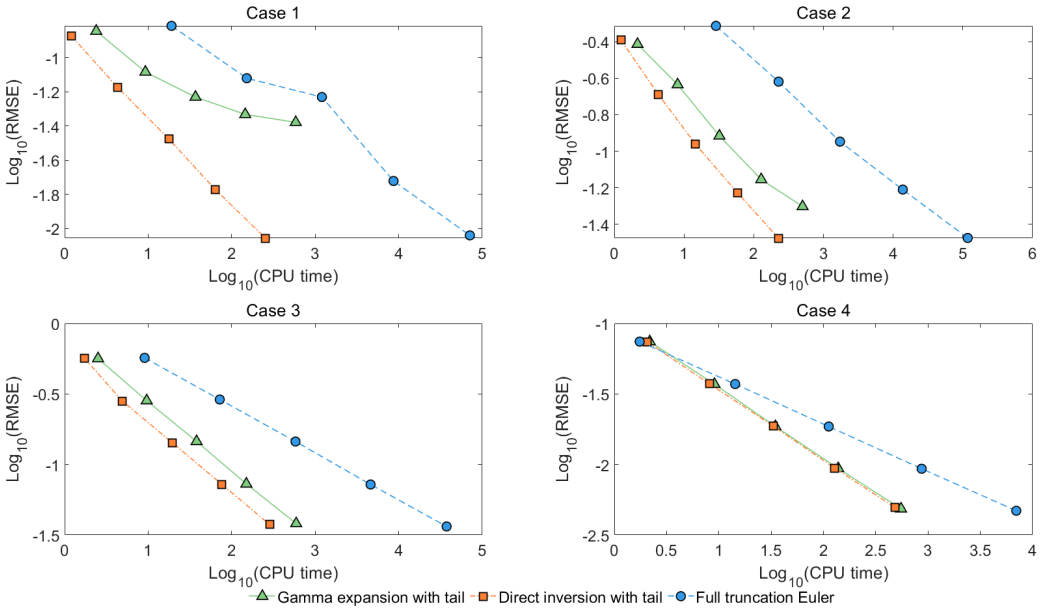

Figure 6.7: We show the convergence of the root mean square error in the option price for Case 1 to Case 4 with $K = 100$ of gamma expansion and direction inversion, both at a truncation level $M = 5$, and full truncation Euler scheme, with number of time steps equal to the square root of the sample size.

We can see from the upper panels in Figure 6.7 that the bias in the gamma expansion with $M = 5$ for Case 1 and Case 2 eventually dominates the root mean square error when the number of sample trails increases. By comparison, the root mean square errors for the direct inversion and full truncation Euler scheme are declining monotonically, with the former presenting a more rapid rate with reduced computational cost. For Case 3 and Case 4, the two almost exact methods both outperform the full truncation Euler scheme, which has a slower convergence rate reflected by the less steeper slope in the graph. While the gamma expansion and the direct inversion exhibit similar convergence rates, the computation time required by the latter is reduced by a factor of two to three. In summary, we conclude that the performance of the direct inversion is the best among the three schemes considered here.

Remark 6.2

Additional numerical tests for in the money and out of the money European call options with strike $K = 60$ and $K = 140$, respectively, are reported in Appendix C, where similar conclusions can be reached as above. Figures displaying the absolute

errors in the first four moments of the conditional integral $\bar{I}$ for Case 2 and Case 3 using the two almost exact schemes with $5 \cdot 10^7$ and $5 \cdot 10^8$ samples are also provided therein.

6.2.2 Path-dependent options

In this section, we test the three methods we have considered, the gamma expansion, the direct inversion and the full truncation Euler scheme by pricing options with payoffs depending on sample paths.

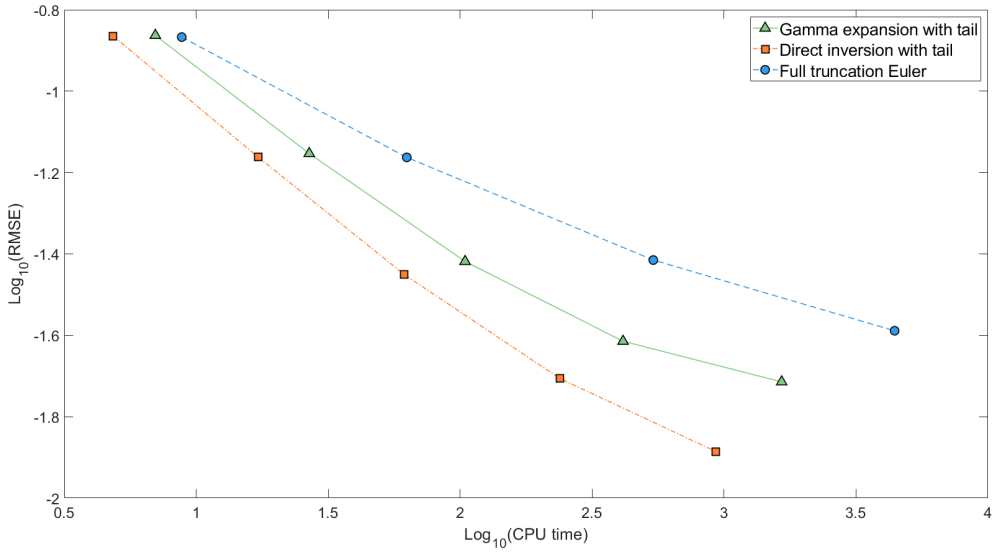

Figure 6.8: We show the convergence of the root mean square error in the option price for Case Asian with $K = 100$ of gamma expansion and direction inversion, both at a truncation level $M = 1$, and full truncation Euler scheme, with number of time steps equal to the square root of the sample size.

We first consider an at the money Asian option with yearly fixings, the payoff of which is determined by the average of asset prices at the end of each year. We show in Figure 6.8 the root mean square error of the price versus the CPU time on a log-$\log_{10}$ scale. For the two almost exact schemes, we truncate the series after $M = 1$ and simulate the asset prices for each year. Within one year, the terminal value is obtained directly using a single step. For the time discretization scheme, multiple steps are needed for each year. In this test, the number of time steps is taken to be the square root of the sample size in a similar manner to Broadie and Kaya [15] and Smith [64].

We observe that both the gamma expansion and the direct inversion, even with a lower truncation level, deliver similar accuracy compared to the full truncation scheme for small sample sizes. However when the number of simulations increases, bias starts to dominate the root mean square error for all three methods, which decelerates its decrease. Among the above three methods, the direct inversion produces the smallest bias. In terms of the computing time, very similar conclusions can be drawn as the European option cases. For similar accuracy, the direct inversion is approximately 2 to 7 times faster than the gamma expansion. The time required by the full truncation Euler scheme is by far the largest.

We end this section with a test for pricing a digital double no touch barrier option. The payoff for such an option is either one or zero unit of currency depending on whether the barriers have been crossed. In Table 6.5, we report the estimated price and standard error together with the CPU time of the direct inversion and gamma expansion at truncation level $M = 1$ for a double no touch barrier option with barriers 90 and 110. We sample a total of 10^6 paths for each case. We increase the number of timesteps per year from 1 to 128 and monitor at each timestep if the asset price has hit one of the two barriers.

We see from Table 6.5 that as we decrease the stepsize, the estimated price of both direct inversion and gamma expansion is decreasing monotonically. This is in accordance with our expectation since when more dates are being monitored, there are more chances for the asset price to cross the barriers. Because of the nature of these two methods, we expect their estimated price will eventually be almost exact with negligible truncation errors when the asset price is monitored on a more frequent basis, for instance, every trading day. The results here are also consistent with those of the four schemes tested in Malham and Wiese [51, Table 5] and the PT, FT and ABR scheme in Lord, Koekkoek and Van Dijk [50, Table 7] in terms of accuracy. Similar conclusions can be reached as the cases for European and Asian options in terms of the computational time. The time required for the gamma expansion is 1.5 to 3 times more than the direct inversion.

Table 6.5: Estimated prices with standard errors and CPU time using 10^6 paths and truncation level $M = 1$ for the digital double no touch barrier option with barriers at 90 and 110.

Stepsize		**Direct inversion**	**Gamma expansion**
	Estimated price	0.68944	0.68908
1	Standard error	0.00046	0.00046
	CPU time	121.33	179.86
	Estimated price	0.65891	0.65892
1/2	Standard error	0.00047	0.00047
	CPU time	202.52	328.76
	Estimated price	0.63105	0.63182
1/4	Standard error	0.00048	0.00048
	CPU time	353.68	593.03
	Estimated price	0.60544	0.60565
1/8	Standard error	0.00049	0.00049
	CPU time	653.35	1152.22
	Estimated price	0.58364	0.58424
1/16	Standard error	0.00049	0.00049
	CPU time	1224.06	2278.41
	Estimated price	0.56563	0.56556
1/32	Standard error	0.00050	0.00050
	CPU time	2173.38	3952.07
	Estimated price	0.54983	0.54943
1/64	Standard error	0.00050	0.00050
	CPU time	4984.79	9904.97
	Estimated price	0.53743	0.53763
1/128	Standard error	0.00050	0.00050
	CPU time	8020.93	24521.84

Remark 6.3

The full truncation Euler scheme has also been tested for the barrier option. Although it is the fastest, we are concerned that the accuracy it delivers for the step-sizes shown in Table 6.5 is not consistent with the other various schemes in Malham and Wiese [51] and Lord, Koekkoek and Van Dijk [50].

In this chapter, we have compared the numerical efficiency of our new method with that of the gamma approximation from Glasserman and Kim [32] through two aspects. The first comparison is made directly on the first four moments of the conditional integral of the variance process. After that, we look into the errors and computing time for pricing both path-independent and path-dependent options with different levels of strike. The results are further compared with a standard time stepping method, i.e. the full truncation Euler scheme. We conclude that the two almost exact methods outperform the full truncation Euler scheme from the perspective of convergence rate. While the new method delivers comparable accuracy as the gamma expansion, the faster computation speed makes the former clearly preferable to the latter.

Chapter 7

Conclusions

Efficient simulation for the conditional time integrated variance process is a key step for the exact sampling of the stock price under the Heston stochastic volatility model. This thesis proposes a new method to realise this quantity. On combining our results with the method of Broadie and Kaya [15], almost exact simulations of the stock price and variance can be generated on the basis of their exact distributions.

We start our thesis by presenting several necessary properties of the Heston model in Chapter 1, including the transition laws of the variance and stock price processes and closed form solutions for standard vanilla option prices. Moreover, we also review the existing numerical schemes that are popular when sampling the Heston model.

In Chapter 2, we set up the foundations for our further analysis. In particular, a series of concepts regarding asymptotics are introduced therein. We also describe two classes of conditional distributions which are frequently revisited in Chapter 3: the squared Bessel bridge and the squared OU bridge, with their relationships and decomposition forms stated as well.

The following chapter provides the main theorem on the conditional integral. After time rescaling and measure transformation, the integral is expressed in terms of a squared Bessel bridge, which is then represented as sums of three independent random variables written in the form of double infinite series under the new probability measure. Connections between the probability distributions of the integral

with respect to the original and new measures are developed, suggesting a possible way to sample our target.

Chapter 4 addresses the problems related to the practical implementation of the theorems derived in Chapter 3. Specifically, we construct direct inversion algorithms for the simulation of each series among the decomposition with additional tail approximation for the first one. The direct inversions require accurate and effective computation of some inverse distribution functions, which are approximated by Chebyshev polynomials. These techniques are designed such that the entire simulation problem is reduced to evaluating predetermined polynomials with coefficients tabulated in advance. Once samples under the new measure are obtained, acceptance-rejection method is applied to trace back to the original measure under consideration.

In Chapter 5, we outline the details for the development of the Chebyshev polynomial approximations. We derive the limiting behaviour of the distribution functions through inverse Fourier transform of the characteristic functions. Based upon that, we identify proper scaling factors for the approximations. The suggested approximations are of high accuracy with a uniform error of 10^{-12}.

Numerical comparisons with one of the leading almost exact methods to simulating the Heston model, i.e. the gamma expansion from Glasserman and Kim [32], are given in Chapter 6. We examine the truncation effect of these two approaches by illustrating the errors in the moments of the conditional integral and the prices of the European call options. Evidence reveals that much more significant errors exist in the gamma approximation with small truncation level. Apart from that, two path-dependent options including an Asian option and a barrier option are also tested using the above two methods. Further comparisons with a standard time discretization method, i.e. the full truncation Euler scheme of Lord, Koekkoek and Van Dijk [50], are performed in pricing options. We find that while the two almost exact methods have similar convergence rate with the full truncation Euler scheme exhibiting a slower rate, our new method requires the least computational budget for similar accuracy.

Another advantage of our new method is that computation of almost exact option

price derivatives, i.e. the Greeks, becomes possible without additional cost. Specifically, we can generalise the exact simulation method of the Greeks by Broadie and Kaya [14] to generate almost unbiased estimators. This method is based on the (almost) exact simulation of the Heston model given in Algorithm 4.1 together with pathwise and likelihood ratio approaches.

Suppose that we are interested in finding the derivative of prices with respect to some model parameter θ. In the pathwise method, the discounted payoff, denoted by f, is viewed as a function of θ and hence the option price, denoted by α, takes the form

$$\alpha(\theta) = \mathbb{E}[f(\theta)].$$

To find the derivative of α with respect to θ, we write

$$\alpha'(\theta) = \frac{d}{d\theta}\mathbb{E}[f(\theta)] = \mathbb{E}\left[\frac{d}{d\theta}f(\theta)\right],$$

if the interchange of differentiation and expectation is allowed. Then, $df(\theta)/d\theta$ is an unbiased estimator for $\alpha'(\theta)$. Now we see that the pathwise method differentiates the payoffs to estimate the Greeks, where certain continuity of the discounted payoff function is required for unbiasedness; see Glasserman [31, Chapter 7.2.2] for a detailed discussion of its conditions.

In the likelihood ratio method, the discounted payoff is treated as a function of a random vector S, representing values of an asset at multiple times for example, with a probability density function depending on θ. If we denote the density function of S by g_θ, then we have

$$\alpha'(\theta) = \frac{d}{d\theta}\mathbb{E}[f(S)] = \int f(s)\frac{d}{d\theta}g_\theta(s)\,ds = \int f(s)\frac{g'_\theta(s)}{g_\theta(s)}g_\theta(s)\,ds = \mathbb{E}\left[f(S)\frac{g'_\theta(S)}{g_\theta(S)}\right],$$

assuming the interchange of differentiation and integration can be justified. Thus, $f(S)\,g'_\theta(S)/g_\theta(S)$ is an unbiased estimator of $\alpha'(\theta)$. Again, the validity of this method relies on some regularity conditions, which, however, are often satisfied since probability density functions are typically smooth.

For the practical implementation of the above two estimators, Broadie and Kaya [14] express the asset price as a series of lognormal random variables by conditioning on the path followed by the variance process. The lognormal random variables depend only on the integral of the variance process, which can be simulated almost exactly by taking advantage of the direct inversion method designed in this thesis. Therefore, we expect that almost exact estimators for the Greeks can be generated without too much computational effort.

The series representation and sampling techniques developed here can also be transferable to the generalised squared OU process x_t with parameter $b \in \mathbb{R}$ and dimension $\delta > 0$ such that

$$dx_t = (\delta + 2bx_t)\, dt + 2\sqrt{x_t}\, dW_t,$$

where W_t denotes a standard Brownian motion. Although in this thesis we focus only on the case $0 < \delta < 2$, the present result can be applied to other cases $\delta \geq 2$. In essence we need to find an appropriate decomposition for δ and hence establish efficient Chebyshev polynomial approximations required for the resulting direct inversion algorithm. We believe that the expansions derived in Section 5.1 and Section 5.2 will be helpful in determining the coefficients.

Lastly, we recommend a direction for future research. Our method entails an acceptance-rejection algorithm with acceptance probability depending on model parameters. Thus, it is difficult to measure its general computational complexity, i.e., the average number of iterations needed. Besides, in the application of risk management and trading, the acceptance-rejection scheme is less favourable as it will introduce considerable Monte Carlo noise in sensitivity analysis. For these reasons, an alternative should be considered. One realistic way to avoid the use of acceptance-rejection is to sample the Radon-Nikodým derivative directly under the new probability measure instead.

Appendix A

Chebyshev coefficients

In the tables below, we quote the Chebyshev coefficients computed in Chapter 5 for the approximations to the inverse distribution functions of the (standardised) sums (Z^P) S^P and Y_2^h, where $S^h \stackrel{d}{=} Y_2^h$. Note that the u denotes the right boundary point of each regime.

Table A.1: Chebyshev coefficients c_n for F_{SP}^{-1} with $P = 1$.

n	**left**	**central**	**middle**
0	1.870164486816790e-01	4.979491420716220e-01	9.481879998153620e-01
1	7.543713026654420e-02	8.479024376573340e-02	1.331260262296900e-01
2	-8.902496689813970e-04	5.515061682001420e-03	-2.432806629044970e-04
3	5.081110592347190e-04	1.234615565280710e-03	7.536358417854170e-05
4	-6.749946441432770e-05	7.826573846201580e-05	-1.832873207509700e-05
5	1.869595919328090e-05	3.190249135857450e-05	3.735655017085910e-06
6	-4.954381513667230e-06	6.911355172727800e-07	-6.763222944593870e-07
7	1.546665396688050e-06	1.101914889591240e-06	1.152436476933680e-07
8	-5.158806635369980e-07	-4.732064488662130e-08	-1.948453255574870e-08
9	1.840226824599990e-07	4.708456855473810e-08	3.380721765672400e-09
10	-6.893572202548840e-08	-5.304437974915840e-09	-6.060338021312360e-10
11	2.688851615671340e-08	2.373716110861710e-09	1.110982538990550e-10
12	-1.083817122960260e-08	-4.052654986799920e-10	-2.059320821371500e-11
13	4.489823790157280e-09	1.347795701927130e-10	3.835128401417810e-12
14	-1.903315339772780e-09	-2.837136223549530e-11	-6.941256697800590e-13
15	8.228619256107180e-10	8.275614752183520e-12	
16	-3.618241198589310e-10	-1.932522965168290e-12	
17	1.614597119724730e-10	4.988201361092360e-13	
18	-7.298521657921080e-11		
19	3.336786065994890e-11		
20	-1.540524697535400e-11		
21	7.165207365475960e-12		
22	-3.335368012294930e-12		
23	1.513427174673910e-12		
24	-5.858440022503530e-13		
	u		
	2.000000000000000e-01	6.300000000000000e-01	9.000000000000000e-01
	k_1	k_1	k_1
	1.059586512649680e+01	-2.206240228024450e+01	1.146497265429040e+01
	k_2	k_2	k_2
	-1.186186343393790e+00	1.000000000000000e+00	-2.084692506698210e+00

Table A.1: (cont.) Chebyshev coefficients c_n for $F_{S^P}^{-1}$ with $P = 1$.

n	**right tail**	**right tail**
0	2.147319302658020e+00	7.301291887179110e+00
1	4.666085467273610e-01	2.110381075693420e+00
2	-5.745397085771070e-06	-3.401385019474830e-12
3	3.926281274449900e-06	3.135451774873670e-12
4	-2.335817034793870e-06	-2.797671851935420e-12
5	1.221893569112290e-06	2.415971255636180e-12
6	-5.676317622953180e-07	-2.018406573717770e-12
7	2.363679020058830e-07	1.629565101375640e-12
8	-8.898571009069280e-08	-1.267921039843530e-12
9	3.052532824574800e-08	9.444179410663350e-13
10	-9.610414759815690e-09	-6.622577811449470e-13
11	2.796013299028150e-09	4.176644424605940e-13
12	-7.568881452656740e-10	-2.012958534474450e-13
13	1.920738140207490e-10	
14	-4.610765872702790e-11	
15	1.059477675547800e-11	
16	-2.363411529421280e-12	
17	4.992754651101120e-13	
18		
19		
20		
21		
22		
23		
24		
	u	
	9.990000000000000e-01	
	k_1	k_1
	3.257208614274380e+00	7.201627100158970e-01
	k_2	k_2
	-1.876363800261230e+00	-1.635958636579130e+00

Table A.2: Chebyshev coefficients c_n for $F_{Z^P}^{-1}$ with $P = 10$.

n	**left tail**	**left central**
0	-4.186236205146250e+00	-1.966613010380010e+00
1	1.605190906754510e+00	-1.483681112879300e-02
2	1.059708264495660e-02	-5.446775372602540e-03
3	-2.569138906164220e-02	2.105452172418740e-06
4	2.657630896552880e-03	-3.250251439573260e-05
5	5.038422707739470e-04	6.250462841383680e-07
6	-1.420477191393670e-04	-2.522741048643350e-07
7	-2.983752657616170e-06	1.026418500454660e-08
8	5.644770851826920e-06	-2.286307882545840e-09
9	-4.127971330420580e-07	1.386590908961820e-10
10	-2.164910928216110e-07	-2.303940103504890e-11
11	3.970382219542570e-08	1.773158449711400e-12
12	8.721275989102100e-09	-2.474347778199780e-13
13	-3.382084859676620e-09	
14	-2.332160758995600e-10	
15	2.833835970869750e-10	
16	-2.159881036758510e-11	
17	-1.980176647976920e-11	
18	5.076230137995960e-12	
19	8.012161542244290e-13	
20	-6.172636726201170e-13	
	u	
	3.331451575280440e-01	5.379510893093010e-01
	k_1	k_1
	-6.189978932685550e-01	-3.895807869740060e+00
	k_2	k_2
	1.058533490397160e+00	1.000000000000000e+00

Table A.2: (cont.) Chebyshev coefficients c_n for $F_{Z^P}^{-1}$ with $P = 10$.

n	**right central**	**right tail**
0	2.105468260211710e+00	1.013961870007640e+01
1	5.526660297932240e-02	5.881348912778960e+00
2	6.562580263096990e-03	1.613214220004240e+00
3	4.554851569107730e-04	3.583662354665820e-01
4	4.959544883969950e-05	6.562610713857870e-02
5	4.554114153141270e-06	1.013276567637800e-02
6	4.895102446478050e-07	1.335612973263590e-03
7	5.011014704681740e-08	1.508499455059680e-04
8	5.446620224111430e-09	1.461564610943890e-05
9	5.859569797393820e-10	1.229129368330510e-06
10	6.466760957427150e-11	9.368122509902420e-08
11	7.143472968048850e-12	6.969255008216930e-09
12	7.892055904355890e-13	5.168922908502960e-10
13		3.395515411597460e-11
14		1.469649165527180e-12
15		-3.355536462420540e-14
16		
17		
18		
19		
20		
	u	
	7.168371818502030e-01	
	k_1	k_1
	4.460293975175440e+00	6.354110577138770e-01
	k_2	k_2
	-1.000000000000000e+00	-1.147724394557630e+00

Table A.3: Chebyshev coefficients c_n for $F_{Z^P}^{-1}$ with $P = 50$.

n	**left tail**	**left central**
0	-5.288942152307260e+00	-2.000965923235480e+00
1	2.354558187240890e+00	5.027272329447840e-03
2	-2.148300929212860e-01	-5.388241960386400e-03
3	1.167801704830350e-03	1.321210600565510e-04
4	4.271918579401850e-03	-3.328258515654870e-05
5	-7.367600678980360e-04	1.691117475054500e-06
6	3.190352612884990e-05	-2.758671231347400e-07
7	1.049570860070370e-05	2.011261792238410e-08
8	-2.661096411008500e-06	-2.690233651951720e-09
9	2.849363340335400e-07	2.380979895569440e-10
10	6.003686941040730e-09	-2.896342891338410e-11
11	-9.314474427911970e-09	2.851594174388340e-12
12	2.078536143889170e-09	-3.279640552952750e-13
13	-2.199997312217100e-10	
14	-1.383145073419240e-11	
15	1.142880443224370e-11	
16	-2.619066923423380e-12	
17	3.160327088396940e-13	
	u	
	3.197003565947650e-01	5.169883337643990e-01
	k_1	k_1
	-6.266377357307220e-01	-4.044263478442090e+00
	k_2	k_2
	1.082311211678360e+00	9.999999999999990e-01

Table A.3: (cont.) Chebyshev coefficients c_n for $F_{Z^P}^{-1}$ with $P = 50$.

n	**right central**	**right tail**
0	2.062558090116340e+00	8.002513934544340e+00
1	3.614884716178920e-02	4.310172977793670e+00
2	5.905537215326120e-03	9.680044235587960e-01
3	3.302424143714490e-04	1.854270427762370e-01
4	4.120186343509380e-05	3.016976801851500e-02
5	3.385543742585720e-06	4.333887776280000e-03
6	3.843164000781120e-07	5.620910828054070e-04
7	3.717029485793840e-08	6.549643858862510e-05
8	4.112363385448630e-09	6.704595648415990e-06
9	4.289267466426690e-10	5.921631388292800e-07
10	4.741128697087930e-11	4.529653831824030e-08
11	5.137505874838590e-12	3.042863599628060e-09
12	5.647548074791590e-13	1.746343337679330e-10
13		9.109476838228590e-12
14		8.873841036286460e-13
15		
16		
17		
	u	
	7.027660432349340e-01	
	k_1	k_1
	4.294834741352050e+00	6.327817827711070e-01
	k_2	k_2
	-1.000000000000000e+00	-1.122310983565170e+00

Table A.4: Chebyshev coefficients c_n for $F_{Z^P}^{-1}$ with $P = 5000$.

n	**left tail**	**left middle**
0	-9.007526636815000e+00	-2.320006146407520e+00
1	2.127535755063470e+00	1.266023709561750e+00
2	-1.873229942604270e-01	-1.152857342660610e-01
3	1.220927893353500e-02	9.871525791146420e-03
4	-5.143519783570370e-04	-6.330801524297140e-04
5	1.053201736042580e-05	2.721250039684760e-05
6	2.597870360642370e-07	-5.511437046510560e-07
7	-3.977373581792380e-08	-9.780799116408280e-09
8	2.731783965620670e-09	7.487832322276510e-10
9	-1.221138438089840e-10	-6.846285108906070e-11
10	3.067277829880080e-12	1.419621555779360e-11
11	-1.657314975397310e-13	-1.036284107015480e-12
12		-3.034958826524900e-14
13		
14		
15		
16		
17		
18		
19		
	u	
	5.000000000000000e-03	5.016991626360740e-01
	k_1	k_1
	-1.210717168704150e+00	-9.809650284289560e-01
	k_2	k_2
	3.018736842909130e+00	6.356505843676840e-01

Table A.4: (cont.) Chebyshev coefficients c_n for $F_{Z^P}^{-1}$ with $P = 5000$.

n	**right middle**	**right tail**
0	2.350506283752280e+00	9.391788080584070e+00
1	1.288612184352350e+00	2.304276718789270e+00
2	1.238550415075650e-01	2.244838261893660e-01
3	1.126367631985240e-02	1.723724750804200e-02
4	8.113776712522790e-04	1.029865654753350e-03
5	4.574695148394010e-05	5.284626922206710e-05
6	2.146343317877790e-06	2.632282130705390e-06
7	1.059607255591610e-07	1.297109856324030e-07
8	6.522023447796370e-09	6.005448267256560e-09
9	3.433932966389800e-10	3.273100583196690e-10
10	7.415030905551360e-12	5.306924125563730e-11
11	-5.333234673760680e-14	2.645356635940220e-11
12		1.613648499072340e-11
13		9.700093322305410e-12
14		5.663793575999130e-12
15		3.213742114800220e-12
16		1.771549706162470e-12
17		9.437229274020540e-13
18		4.731397672671720e-13
19		1.949505078193680e-13
	u	
	9.950000000000000e-01	
	k_1	k_1
	9.857057212990940e-01	1.210983500602370e+00
	k_2	k_2
	-6.435551648966840e-01	-3.019180921864380e+00

Table A.5: Chebyshev coefficients c_n for $F_{Z^P}^{-1}$ with $P = 10^4$.

n	**left tail**	**left middle**
0	-8.763208308698120e+00	-2.117708885805710e+00
1	2.272856177544270e+00	1.148679380728190e+00
2	-2.195485611789300e-01	-9.719454925386660e-02
3	1.600603323734860e-02	7.829228309183660e-03
4	-7.913864835076260e-04	-4.795725327622320e-04
5	2.398092020649720e-05	2.045360216276630e-05
6	-1.924215235351760e-07	-5.013317907576720e-07
7	-3.279659242674000e-08	3.503726442772780e-09
8	3.433751594624110e-09	-1.253562317413470e-10
9	-1.944135457019680e-10	-1.311511811147320e-12
10	5.718823252641270e-12	5.140621840511810e-12
11	-3.006387310778820e-13	-4.635014571234970e-13
12		
13		
14		
15		
16		
17		
	u	
	1.000000000000000e-02	5.012014905499710e-01
	k_1	k_1
	-1.115994743243930e+00	-1.054206693922630e+00
	k_2	k_2
	2.704324434390850e+00	6.099629843489590e-01

Table A.5: (cont.) Chebyshev coefficients c_n for $F_{Z^P}^{-1}$ with $P = 10^4$.

n	**right middle**	**right tail**
0	2.134535481408690e+00	9.022503475215680e+00
1	1.161232186820710e+00	2.401317040413510e+00
2	1.019807405937260e-01	2.487767815506420e-01
3	8.555012569847670e-03	2.028231950132690e-02
4	5.664908014626390e-04	1.266220882300120e-03
5	2.890763831163810e-05	6.623334821975800e-05
6	1.181852005087120e-06	3.326141775983180e-06
7	4.960639757165790e-08	1.667239146689460e-07
8	2.822677760359780e-09	7.705454473071610e-09
9	1.409816724283650e-10	3.768066578229160e-10
10	1.871694274577610e-12	3.560180300524010e-11
11	-1.571409536591980e-13	1.210420538657680e-11
12		7.304190736146010e-12
13		4.532327470602990e-12
14		2.727718438162450e-12
15		1.578085621557310e-12
16		8.497824077877610e-13
17		3.683334903311600e-13
	u	
	9.900000000000000e-01	
	k_1	k_1
	1.058073632931550e+00	1.115994743243930e+00
	k_2	k_2
	-6.158684948176150e-01	-2.704324434390850e+00

Table A.6: Chebyshev coefficients c_n for $F_{Z^P}^{-1}$ with $P = 10^5$.

n	**left tail**	**right tail**
0	-5.706926051399320e+00	5.760300411129710e+00
1	3.395553188579180e+00	3.436321449713240e+00
2	-6.300054999277720e-01	6.483188840749760e-01
3	9.838818354304640e-02	1.035993426134920e-01
4	-1.136750936655030e-02	1.252833208873680e-02
5	9.513883577249630e-04	1.161417162277510e-03
6	-6.015836221231600e-05	9.191380802217640e-05
7	3.618126012554300e-06	7.737590464616790e-06
8	-1.697979831324770e-07	6.400595433239310e-07
9	-1.897253631189280e-08	2.904203939446630e-08
10	3.326071860640010e-09	1.050861883541800e-09
11	2.442263784022650e-10	6.008685289953490e-10
12	-3.833832227759890e-11	6.651321295963480e-11
13	-1.297154428240060e-11	-1.031199486940060e-11
14	1.412983301319550e-12	-9.752972166933010e-13
15	4.089569727968860e-13	5.588332180241710e-13
	u	
	5.003799449933160e-01	
	k_1	k_1
	-5.424593574874610e-01	5.427821460191420e-01
	k_2	k_2
	8.005868439521350e-01	-8.016582768171050e-01

Table A.7: Chebyshev coefficients c_n for $F_{Z^P}^{-1}$ with $P = 10^6$.

n	**left tail**	**right tail**
0	-5.946145460337920e+00	5.964470382846980e+00
1	3.556004911984500e+00	3.570041770711440e+00
2	-6.801894131410160e-01	6.865586194977590e-01
3	1.092510150797910e-01	1.110985275994380e-01
4	-1.307725205702110e-02	1.349685679309470e-02
5	1.160328523663860e-03	1.237761453545620e-03
6	-8.240107479627320e-05	9.434859113712600e-05
7	5.926003936265940e-06	7.508635778142890e-06
8	-3.827985039853400e-07	5.673276390309780e-07
9	-4.939610258605130e-09	1.429761666233160e-08
10	2.191431812357590e-09	-4.002728561697650e-10
11	4.611932833470640e-10	6.107231293159660e-10
12	-4.959733545874770e-11	6.167427914388110e-11
13	-1.701165301087770e-11	-1.590293060974530e-11
14	1.492500677577930e-12	-1.334659663440940e-12
15	5.860252785293660e-13	6.358368604978550e-13
	u	
	5.001201491665880e-01	
	k_1	k_1
	-5.310898090226540e-01	5.311876095528130e-01
	k_2	k_2
	8.051645964724630e-01	-8.054970186947690e-01

Table A.8: Chebyshev coefficients c_n for $F^{-1}_{Y_2^h}$ with $h = 2$.

n	**left**	**left**
0	3.746732186396810e-01	1.246285546643250e+00
1	1.195997564921540e-01	3.358246308532060e-01
2	-8.070601474351940e-03	2.386732322681120e-02
3	1.339603001568510e-03	1.294898023275990e-02
4	-2.506080830464610e-04	2.637423242240120e-03
5	5.637743633696060e-05	1.091486949977880e-03
6	-1.413866007641720e-05	3.083088185622240e-04
7	3.869664142567620e-06	1.183343193111800e-04
8	-1.132969831139660e-06	3.838648490201040e-05
9	3.501617974093610e-07	1.440406811311990e-05
10	-1.130976314574740e-07	5.002488355310480e-06
11	3.788372056248530e-08	1.869987422785930e-06
12	-1.308238855480900e-08	6.739900491698620e-07
13	4.635781671551490e-09	2.526970560301390e-07
14	-1.679323548784110e-09	9.311688370921460e-08
15	6.200204087490220e-10	3.508754493020290e-08
16	-2.327351020956820e-10	1.311638643142900e-08
17	8.863586972126330e-11	4.968660909382380e-09
18	-3.418842923801670e-11	1.875958145331950e-09
19	1.333107561719920e-11	7.141781072249230e-10
20	-5.234957827868200e-12	2.716166269988070e-10
21	2.035050527498960e-12	1.038650818883500e-10
22	-7.009107859412300e-13	3.972098592976600e-11
23		1.524237223546780e-11
24		5.838842289005870e-12
25		2.206347821363880e-12
26		7.400818875262400e-13
	u	
	4.943694484749030e-02	8.724214735883850e-01
	k_1	k_1
	4.396896568327450e+00	1.265081819857330e+00
	k_2	k_2
	-1.301445639726460e+00	-1.662175466937440e+00

Table A.8: (cont.) Chebyshev coefficients c_n for $F^{-1}_{Y_2^h}$ with $h = 2$.

n	**middle**	**right tail**
0	3.527966142386780e+00	1.003328309377590e+01
1	7.472142334253430e-01	2.496706503355630e+00
2	-1.333644417363060e-02	-1.589949448670880e-02
3	2.622018509548740e-03	3.113590178926820e-03
4	-6.027577883155430e-04	-6.963073964368400e-04
5	1.515242268297150e-04	1.678769292503920e-04
6	-4.036373098988620e-05	-4.250114645375870e-05
7	1.119644049107180e-05	1.113756440553480e-05
8	-3.199289309119440e-06	-2.994727316140500e-06
9	9.349240809409510e-07	8.214913272814210e-07
10	-2.779917579878980e-07	-2.289772183834370e-07
11	8.378973634959820e-08	6.466492239429990e-08
12	-2.552869970129400e-08	-1.846256500319380e-08
13	7.845488794437930e-09	5.320336235290850e-09
14	-2.428118880696940e-09	-1.545402456085360e-09
15	7.559005461053680e-10	4.520062644698680e-10
16	-2.364994613022200e-10	-1.330078378584710e-10
17	7.431800136657720e-11	3.934888781070520e-11
18	-2.344374813365950e-11	-1.169587411803260e-11
19	7.415598838082110e-12	3.489114825460500e-12
20	-2.333558791113770e-12	-1.037689978383220e-12
21	6.745346171083730e-13	2.859557405213800e-13
22		
23		
24		
25		
26		
	u	
	9.997923134230980e-01	
	k_1	k_1
	2.336282203175340e+00	6.370068451629010e-01
	k_2	k_2
	-6.514171570857550e-01	-1.450272673332570e+00

Table A.9: Chebyshev coefficients c_n for $F^{-1}_{Y_2^h}$ with $h = 1/5$.

n	**left**	**central**	**middle**
0	1.551440631887020e-02	5.965851817537560e-02	2.365922039769370e-01
1	7.154056831584140e-03	1.701537131814850e-02	7.509528018047970e-02
2	1.120793580526900e-04	2.597262497204220e-03	6.749060031298220e-03
3	-2.767589127786680e-05	4.709183006272860e-04	-9.756034732487180e-05
4	5.310776527089690e-06	7.145518311775060e-05	-4.546713797013430e-05
5	-1.242484981459680e-06	1.330260630541950e-05	2.265934249688390e-06
6	3.545760586969740e-07	1.967551836645490e-06	3.137406427278980e-07
7	-1.173714662110980e-07	3.949016650674680e-07	1.344476627067410e-08
8	4.313888580276150e-08	5.420695609123570e-08	-8.390259114557700e-09
9	-1.709037630074550e-08	1.243550067642890e-08	7.380356092377570e-10
10	7.159028761307770e-09	1.439656776199120e-09	-2.253776759627590e-10
11	-3.130641321239270e-09	4.213671249996360e-10	4.735083288679860e-11
12	1.416650107438240e-09	3.320038533665110e-11	-6.226333936166750e-12
13	-6.591639233672150e-10	1.566391114883240e-11	2.369177040131120e-12
14	3.138939220131410e-10	4.052720676134970e-13	-5.354588204982430e-13
15	-1.524291404102210e-10		
16	7.526974215608190e-11		
17	-3.770866706212000e-11		
18	1.912726184698180e-11		
19	-9.801629544246880e-12		
20	5.055418302750250e-12		
21	-2.598617692870460e-12		
22	1.287201224090770e-12		
23	-5.308318388467400e-13		
24			
	u		
	2.096913523963960e-01	6.331471212688160e-01	9.308037742250030e-01
	k_1	k_1	k_1
	1.685718137659840e+02	-5.009544088177860e+01	8.992727193150630e+00
	k_2	k_2	k_2
	-1.121868009800680e+00	1.000000000000000e+00	-1.516097941825860e+00

Table A.9: (cont.) Chebyshev coefficients c_n for $F^{-1}_{Y_2^h}$ with $h = 1/5$.

n	**right tail**	**right tail**
0	9.766531067045770e-01	5.548556192934720e+00
1	3.018335097399800e-01	2.006312378503930e+00
2	1.137764493492590e-02	2.401553462574660e-02
3	-1.796551902064940e-03	-5.827238250950370e-03
4	2.961890615175630e-04	1.564108444981820e-03
5	-3.906140490786640e-05	-4.425250341488140e-04
6	3.228136981746220e-07	1.292806696330270e-04
7	1.990381470117290e-06	-3.860207865611520e-05
8	-7.180791153930990e-07	1.171917601240400e-05
9	1.237304075899030e-07	-3.609533592707930e-06
10	4.797867870237380e-09	1.128193509794600e-06
11	-1.022283804766720e-08	-3.587762176720570e-07
12	3.242766128356910e-09	1.166622015545860e-07
13	-3.934089138513010e-10	-3.905857435831940e-08
14	-1.071903231878940e-10	1.356481292566670e-08
15	7.087360088039800e-11	-4.912140911093540e-09
16	-1.797818306057730e-11	1.854288283705740e-09
17	1.002649821269040e-12	-7.243408051055720e-10
18	1.130725736108390e-12	2.888927287597260e-10
19	-5.251498162236730e-13	-1.156809097791060e-10
20		4.568355593550070e-11
21		-1.746849139303890e-11
22		6.337718113837970e-12
23		-2.123287366692640e-12
24		6.058538275109010e-13
	u	
	9.985870051144820e-01	
	k_1	k_1
	3.854817463192980e+00	7.119316740438860e-01
	k_2	k_2
	-2.078549151656860e+00	-1.568565612274160e+00

Table A.10: Chebyshev coefficients c_n for $F^{-1}_{Y_2^h}$ with $h = 1/10$.

n	**left**	**central**	**middle**
0	3.130510092436480e-03	2.226333345761940e-02	1.988982349173300e-01
1	1.417002017122930e-03	1.019151935447450e-02	8.748062377822970e-02
2	2.360674641499860e-05	2.673461828675050e-03	1.322178512127460e-02
3	-6.764554780577090e-06	7.541005867012180e-04	1.783172989082840e-05
4	1.073524111115770e-06	1.825724014495560e-04	-1.742061549930600e-04
5	-2.165240827636890e-07	5.070406265568320e-05	1.493474602053700e-06
6	5.714805445297290e-08	1.156695182629010e-05	3.359055560341540e-06
7	-1.802784817620430e-08	3.413930484845420e-06	5.333580684343860e-08
8	6.351907282247520e-09	6.943759577207300e-07	-5.521667146922230e-08
9	-2.410001034673680e-09	2.411908456774390e-07	-2.276235131191450e-09
10	9.649353406509400e-10	3.679790048414060e-08	-2.893556379100810e-10
11	-4.026554373758090e-10	1.888991234749740e-08	-6.436850207940640e-11
12	1.736498040397030e-10	1.106003127127480e-09	2.350168269709400e-11
13	-7.693121262340320e-11	1.752401085721140e-09	2.321358068727610e-11
14	3.485269197769610e-11	-1.364762944049400e-10	2.636593526158310e-12
15	-1.608506662519110e-11	2.000879783288780e-10	-1.139207052258690e-12
16	7.530478144378150e-12	-4.354349576970780e-11	-7.314416583435210e-13
17	-3.545863047530390e-12	2.738074123398660e-11	
18	1.631081082539690e-12	-8.687479490879170e-12	
19	-6.387767991337950e-13	4.196188738890250e-12	
20		-1.521565690726930e-12	
21		5.748616824737570e-13	
	u		
	1.060708119058860e-01	7.049238354832290e-01	9.715292650150570e-01
	k_1	k_1	k_1
	8.775453590729910e+02	-5.009576443446880e+01	6.414761023377960e+00
	k_2	k_2	k_2
	-1.150665798108190e+00	1.000000000000000e+00	-9.422665062905070e-01

Table A.10: (cont.) Chebyshev coefficients c_n for $F^{-1}_{Y_2^h}$ with $h = 1/10$.

n	**right tail**	**right tail**
0	1.167088563196560e+00	5.557949689428240e+00
1	4.028821977072450e-01	1.804403214930680e+00
2	1.589726864878320e-02	2.001076313509190e-02
3	-2.776444180529080e-03	-4.157908839745580e-03
4	5.440877740378380e-04	9.533639401005060e-04
5	-1.067963570631730e-04	-2.298471294547870e-04
6	1.602535986540860e-05	5.706424934572410e-05
7	3.639164819106390e-07	-1.443342632426860e-05
8	-1.502345300041770e-06	3.696661627610680e-06
9	6.684757371238390e-07	-9.553281498410900e-07
10	-1.716295249441840e-07	2.486726588153440e-07
11	1.635394935133220e-08	-6.518766056569630e-08
12	8.892938254607340e-09	1.724037249294330e-08
13	-5.718412804481970e-09	-4.621243803810740e-09
14	1.784898899321030e-09	1.266095041880900e-09
15	-2.594370983148820e-10	-3.591505441133860e-10
16	-6.261300169685750e-11	1.071702367595880e-10
17	5.827210983507830e-11	-3.409479146600340e-11
18	-2.189105354284160e-11	1.160098934787350e-11
19	4.514597736601770e-12	-4.170286799495240e-12
20	-6.083212355274470e-14	1.531989721713420e-12
21		-5.089272134222660e-13
	u	
	9.998315799958800e-01	
	k_1	k_1
	2.923879081718190e+00	7.878535911129940e-01
	k_2	k_2
	-1.885294461971110e+00	-1.777456775656590e+00

Table A.11: Chebyshev coefficients c_n for $F^{-1}_{Y_2^h}$ with $h = 1/20$.

n	**left**	**central**	**middle**
0	8.320108386176210e-04	1.028289222803400e-02	1.796716788945920e-01
1	3.797922844843720e-04	6.051387649842750e-03	9.215513210293030e-02
2	6.119152516315670e-06	2.386515701734710e-03	1.798443115218620e-02
3	-2.216499535843720e-06	9.149383182711960e-04	3.536164396647110e-04
4	3.549796569970470e-07	3.260804312989740e-04	-3.290230257519090e-04
5	-6.909777679284210e-08	1.174302244391950e-04	-9.190331115977190e-06
6	1.800406773387910e-08	4.046558068563540e-05	8.941392960865090e-06
7	-5.727807832664590e-09	1.430511004864880e-05	4.569100427021660e-07
8	2.048306829365080e-09	4.845772394724280e-06	-1.898690252517310e-07
9	-7.892933375352230e-10	1.708561223033970e-06	-1.470693084569340e-08
10	3.208272429161220e-10	5.709919634096530e-07	9.061517318686080e-10
11	-1.358581479450600e-10	2.027725977295490e-07	-4.996134827280960e-10
12	5.944136353935250e-11	6.667913363885620e-08	-3.085715272976990e-11
13	-2.671169627505600e-11	2.408641753810910e-08	8.541875621658270e-11
14	1.227327977365970e-11	7.729248497752880e-09	3.049756612877170e-11
15	-5.743936308401000e-12	2.879366774439790e-09	7.727805117204180e-13
16	2.726212185552570e-12	8.872469780543650e-10	-3.534457536346360e-12
17	-1.300587961514960e-12	3.484429145625870e-10	-1.357036283678530e-12
18	6.052241498351530e-13	1.001335286917030e-10	4.056653202382400e-14
19	-2.390157663283510e-13	4.301663419431590e-11	2.166251245948460e-13
20		1.093494057671200e-11	
21		5.462280485697060e-12	
22		1.109419945826550e-12	
23		6.264905101784660e-13	
	u		
	9.952451539818020e-02	7.959736941620220e-01	9.872109261016380e-01
	k_1	k_1	k_1
	3.350041337835460e+03	-6.091816627093630e+01	5.415831650268340e+00
	k_2	k_2	k_2
	-1.142970216093080e+00	9.999999999999990e-01	-6.895558541579670e-01

Table A.11: (cont.) Chebyshev coefficients c_n for $F^{-1}_{Y_2^h}$ with $h = 1/20$.

n	**right tail**	**right tail**
0	9.761057883039990e-01	5.196073467821070e+00
1	3.017284864244530e-01	1.831141920349890e+00
2	1.166946937938650e-02	2.543065037748800e-02
3	-1.687052247930820e-03	-5.741796704905520e-03
4	2.745955374164150e-04	1.425454072455160e-03
5	-4.255962891388790e-05	-3.709730129757980e-04
6	3.654738784807000e-06	9.914921759807330e-05
7	9.678759239832620e-07	-2.692978838795340e-05
8	-5.962323527180650e-07	7.390951335687150e-06
9	1.619073566570090e-07	-2.044323535428500e-06
10	-2.044848058779340e-08	5.700139242154510e-07
11	-3.557663286168380e-09	-1.608555974873110e-07
12	2.792106872070250e-09	4.637422326004220e-08
13	-8.014791797406380e-10	-1.388223005657000e-08
14	9.886383182987460e-11	4.408914855308600e-09
15	2.338331909817720e-11	-1.513613329915950e-09
16	-1.720362865683670e-11	5.636677579981080e-10
17	5.096915629190340e-12	-2.238514411774360e-10
18	-7.701281537440130e-13	9.204119152754310e-11
19		-3.802089545459430e-11
20		1.539622910176950e-11
21		-5.993091125355200e-12
22		2.193183001782910e-12
23		-6.910989846330210e-13
	u	
	9.997667653179200e-01	
	k_1	k_1
	3.745971846148320e+00	7.690538107824300e-01
	k_2	k_2
	-2.168616210929900e+00	-1.650521806358000e+00

Table A.12: Chebyshev coefficients c_n for $F^{-1}_{Y_2^h}$ with $h = 1/50$.

n	**left**	**central**	**middle**
0	3.342404855864120e-04	5.287504606339480e-03	1.679802218836370e-01
1	1.582119045977730e-04	3.609167042053240e-03	9.425159027828380e-02
2	-4.034459826869400e-06	1.936145076792510e-03	2.146641276528240e-02
3	-1.781674777546940e-06	9.633501098384940e-04	7.761771414171210e-04
4	6.111894067922420e-07	4.586062099584780e-04	-4.715700923865780e-04
5	-1.616413643230560e-07	2.128565367871230e-04	-2.911833910065390e-05
6	4.535507820139480e-08	9.711724060740930e-05	1.543681974168120e-05
7	-1.504566368490170e-08	4.380458926575550e-05	1.397441335389570e-06
8	5.916977370301480e-09	1.959490913685950e-05	-3.947158787904660e-07
9	-2.631104077272520e-09	8.713044455946110e-06	-4.582398590716480e-08
10	1.265674285428750e-09	3.857017778878400e-06	4.537121001350180e-09
11	-6.412984582939380e-10	1.701669482580570e-06	-8.587058106556160e-10
12	3.373488093146030e-10	7.488328990975590e-07	-3.395277343066420e-10
13	-1.827196103322590e-10	3.288850425725560e-07	1.497940638456500e-10
14	1.013577890763330e-10	1.442278857066740e-07	9.047367570431170e-11
15	-5.736165706600700e-11	6.317620038821080e-08	1.532712463574530e-11
16	3.301900838213170e-11	2.764873413720030e-08	-5.899234983630280e-12
17	-1.928175236669550e-11	1.209228320347620e-08	-4.759599480764640e-12
18	1.139207390775460e-11	5.285996098982320e-09	-9.845099825540200e-13
19	-6.784952996564540e-12	2.309885154214610e-09	3.353301735326340e-13
20	4.046041780101790e-12	1.009129182529950e-09	
21	-2.377799356621700e-12	4.407929681530870e-10	
22	1.318077536426880e-12	1.925241011297400e-10	
23	-5.870490384521500e-13	8.408559765252570e-11	
24		3.672433365477260e-11	
25		1.603764366665510e-11	
26		6.998237196315440e-12	
27		3.040158479208740e-12	
28		1.288881492848470e-12	
29		4.729004482220710e-13	
	u		
	2.931123896950420e-01	8.963482076412410e-01	9.952179896810610e-01
	k_1	k_1	k_1
	7.818489955336010e+03	-1.112036741342440e+02	4.876183772221110e+00
	k_2	k_2	k_2
	-1.055332320056090e+00	1.000000000000000e+00	-5.434844889094470e-01

Table A.12: (cont.) Chebyshev coefficients c_n for $F^{-1}_{Y_2^h}$ with $h = 1/50$.

n	**right tail**	**right tail**
0	9.761146326247320e-01	5.440971360286980e+00
1	3.016928648060240e-01	1.956911680269630e+00
2	1.167231718705550e-02	2.774260925258890e-02
3	-1.651276452041100e-03	-6.436890817427100e-03
4	2.666875570608340e-04	1.641299885337870e-03
5	-4.247191460497480e-05	-4.384480040071970e-04
6	4.247919767558580e-06	1.201938574075190e-04
7	7.240192379129260e-07	-3.345172414930230e-05
8	-5.468504974426760e-07	9.394648359883000e-06
9	1.621838761986780e-07	-2.653557174889410e-06
10	-2.469682517941960e-08	7.531228230971810e-07
11	-1.846812979021150e-09	-2.152447292666570e-07
12	2.453530993347930e-09	6.237985768142150e-08
13	-8.104795070564440e-10	-1.859198071101320e-08
14	1.328212021134180e-10	5.827250350019080e-09
15	9.746012118699450e-12	-1.970501685911340e-09
16	-1.445305942484280e-11	7.299803884539630e-10
17	5.164008080182290e-12	-2.939243341028580e-10
18	-1.029938970952760e-12	1.250293085781460e-10
19		-5.430549502597070e-11
20		2.340535807434650e-11
21		-9.802247791887950e-12
22		3.924623772975130e-12
23		-1.472095272217620e-12
24		4.733000270115360e-13
25		
26		
27		
28		
29		
	u	
	9.999145446729710e-01	
	k_1	k_1
	3.727057577727170e+00	7.200044464436850e-01
	k_2	k_2
	-2.179745438075220e+00	-1.614273003898510e+00

Table A.13: Chebyshev coefficients c_n for $F^{-1}_{Y_2^h}$ with $h = 1/100$.

n	**left**	**central**	**middle**
0	1.064576523939530e-04	7.757528496943120e-04	6.583911279090600e-02
1	4.967483886634580e-05	3.963182148041290e-04	4.630386572794730e-02
2	-2.574907330657640e-06	1.452820177102820e-04	1.757544141274220e-02
3	-5.303715403034550e-07	4.855954814287430e-05	3.315284363718870e-03
4	2.663871929167150e-07	1.531863558980860e-05	1.968319378136480e-05
5	-8.401958707782950e-08	4.676444520070530e-06	-1.223428005218250e-04
6	2.541840517940170e-08	1.394003778702580e-06	-1.557379115932890e-05
7	-8.458536138015860e-09	4.088490384098530e-07	3.231990249141240e-06
8	3.265291063082850e-09	1.184092050832930e-07	9.273005743030420e-07
9	-1.446267628365560e-09	3.397158988245300e-08	-3.854154049131540e-08
10	7.070186386866000e-10	9.672491318170320e-09	-3.568282952834910e-08
11	-3.686990455737440e-10	2.737461712290990e-09	-8.276509465005380e-10
12	2.008214150700490e-10	7.708833517653440e-10	1.206706537754170e-09
13	-1.129090416703240e-10	2.161982864910210e-10	9.225936702119910e-11
14	6.508194177274500e-11	6.042419184248020e-11	-3.617701898545350e-11
15	-3.828935422940620e-11	1.683809589516920e-11	-4.590404543093130e-12
16	2.291651606295010e-11	4.678693771234670e-12	9.605943640102250e-13
17	-1.391339883329400e-11	1.290808850907540e-12	1.614097426563670e-13
18	8.543046330402440e-12	3.320491288954070e-13	
19	-5.282416801082770e-12		
20	3.263505722460020e-12		
21	-1.979537858186990e-12		
22	1.125706972359240e-12		
23	-5.098805064619270e-13		
24			
25			
26			
27			
28			
29			
30			
	u		
	3.364182499030230e-01	7.854302604129020e-01	9.936476554735930e-01
	k_1	k_1	k_1
	2.356466133610040e+04	-2.112823879640160e+02	4.261592636084800e+00
	k_2	k_2	k_2
	-1.042176040321580e+00	1.000000000000000e+00	2.136086687920960e-01

Table A.13: (cont.) Chebyshev coefficients c_n for $F^{-1}_{Y_2^h}$ with $h = 1/100$.

n	**right tail**	**right tail**
0	5.721713263001800e-01	5.012707101453430e+00
1	2.017820038440810e-01	2.062096651831810e+00
2	1.377375013917080e-02	3.999684930491520e-02
3	-1.806370775567440e-03	-1.094915283125730e-02
4	1.523593047177290e-04	3.280050342478830e-03
5	2.295752543436920e-05	-1.026359592164550e-03
6	-1.211645711839800e-05	3.290839108300620e-04
7	1.558915013492110e-06	-1.072510048733330e-04
8	3.379002506728420e-07	3.549425811224850e-05
9	-1.589627733030860e-07	-1.199878274669090e-05
10	8.281053242094130e-09	4.199796533313160e-06
11	9.754591213299920e-09	-1.552499344038120e-06
12	-2.587101485419120e-09	6.174229919308360e-07
13	-2.654922061326020e-10	-2.654025845860760e-07
14	2.854986006586100e-10	1.213436337756570e-07
15	-4.288462498279560e-11	-5.724458644126490e-08
16	-1.614286040010380e-11	2.696385391883710e-08
17	8.227664210952470e-12	-1.231399370142220e-08
18	-8.469562416364850e-13	5.303258910110760e-09
19		-2.080169945416400e-09
20		6.955732723896000e-10
21		-1.600540556356630e-10
22		-1.256262769207180e-11
23		4.730496708984260e-11
24		-3.958827080866930e-11
25		2.486066180938770e-11
26		-1.342780201739010e-11
27		6.510864817550600e-12
28		-2.877910389935840e-12
29		1.155822468250210e-12
30		-3.885406981704200e-13
	u	
	9.997327929473050e-01	
	k_1	k_1
	4.734018530749910e+00	6.757660555129490e-01
	k_2	k_2
	-1.873568041871660e+00	-1.410192678438050e+00

Table A.14: Chebyshev coefficients c_n for $F^{-1}_{Y_2^h}$ with $h = 1/200$.

n	**left**	**central**	**middle**
0	3.518991274756410e-05	8.392520820142320e-04	3.802327783487680e-02
1	1.590990829653500e-05	6.431136826076690e-04	2.293406644160820e-02
2	-1.491507257739220e-06	4.085596936397010e-04	6.950796412254630e-03
3	-9.066540515692110e-08	2.399296017984750e-04	1.080933113927390e-03
4	1.118185077651370e-07	1.344982201802290e-04	3.968276530040400e-05
5	-4.689629675507750e-08	7.316918708694770e-05	-1.510396050891140e-05
6	1.672578243190620e-08	3.898020499880180e-05	-2.164545910662930e-06
7	-5.962483120983330e-09	2.045075653316810e-05	1.031238628209570e-07
8	2.299928220409480e-09	1.060530105647120e-05	4.715822375760120e-08
9	-9.951311785026230e-10	5.449951689909770e-06	1.338195202962630e-09
10	4.813973704272400e-10	2.780434074253660e-06	-7.162524074055580e-10
11	-2.538921373245920e-10	1.410169685110300e-06	-5.838646258223060e-11
12	1.421639472958470e-10	7.117308974598150e-07	9.035922879320320e-12
13	-8.292852778673320e-11	3.577606972109200e-07	1.324669429761400e-12
14	4.981742953446680e-11	1.792155094219700e-07	-9.136939392295840e-14
15	-3.060881416945410e-11	8.951262809172500e-08	
16	1.915173995253590e-11	4.459614066323350e-08	
17	-1.216412493952420e-11	2.216977555006010e-08	
18	7.820244746397910e-12	1.100014354771840e-08	
19	-5.072097961571190e-12	5.448923967042200e-09	
20	3.302395224132890e-12	2.695162687572180e-09	
21	-2.138908948989570e-12	1.331357683924740e-09	
22	1.351588122026080e-12	6.569059660914260e-10	
23	-7.937121438141360e-13	3.237909926903930e-10	
24	3.670269446605750e-13	1.594506248721020e-10	
25		7.845610579728340e-11	
26		3.857391556723110e-11	
27		1.895058050737670e-11	
28		9.300136827782300e-12	
29		4.552865562504600e-12	
30		2.209843826831820e-12	
31		1.035453103819420e-12	
32		4.092881791896840e-13	
	u		
	3.889455754261150e-01	9.290038930121230e-01	9.933230995102950e-01
	k_1	k_1	k_1
	6.580451400950010e+04	-2.484251686923060e+02	6.345255066723990e+00
	k_2	k_2	k_2
	-1.029129856396840e+00	1.000000000000000e+00	4.634771910249610e-01

Table A.14: (cont.) Chebyshev coefficients c_n for $F^{-1}_{Y_2^h}$ with $h = 1/200$.

n	**right tail**	**right tail**
0	4.996811103033990e-01	4.914258356400540e+00
1	2.283166265702910e-01	2.011738127244220e+00
2	2.514423513031140e-02	3.937356800757610e-02
3	-3.474198991631110e-03	-1.065266526129480e-02
4	5.077220214696980e-05	3.152291195578990e-03
5	1.613616422231270e-04	-9.738895553647930e-04
6	-3.880889586523480e-05	3.081786621477630e-04
7	-3.634159932107060e-06	-9.909792676876670e-05
8	3.510602114428830e-06	3.236113469325020e-05
9	-1.965557011348580e-07	-1.080367954217730e-05
10	-2.893679425552990e-07	3.742488200776480e-06
11	4.919338342933830e-08	-1.374128809584760e-06
12	2.766224437511810e-08	5.450001386646270e-07
13	-9.150633315570560e-09	-2.341737771120620e-07
14	-2.629338358854130e-09	1.069346503420290e-07
15	1.702910382225310e-09	-5.021967626980480e-08
16	1.193636414090970e-10	2.344515094335100e-08
17	-2.861147205442400e-10	-1.056108154875410e-08
18	3.711031444447810e-11	4.460714134159520e-09
19	3.822894605668730e-11	-1.700913808398090e-09
20	-1.452954868328440e-11	5.418507670597150e-10
21	-2.818928436440390e-12	-1.082511209350410e-10
22	3.052195946657300e-12	-2.332308071729190e-11
23	-4.763636711850320e-13	4.458678049756930e-11
24		-3.438522185303320e-11
25		2.066800196185060e-11
26		-1.078966568122650e-11
27		5.070919968888770e-12
28		-2.172493412014030e-12
29		8.448217334599220e-13
30		-2.756966775927990e-13
31		
32		
	u	
	9.998681694019440e-01	
	k_1	k_1
	3.821761784764750e+00	6.915167979999310e-01
	k_2	k_2
	-1.323148927258810e+00	-1.420354956151160e+00

Table A.15: Chebyshev coefficients c_n for $F^{-1}_{Y_2^h}$ with $h = 1/500$.

n	**left**	**central**	**middle**
0	5.483749876010110e-06	6.081052138201620e-05	5.473769059145150e-02
1	2.486444309865310e-06	3.802911084933030e-05	4.351538755149590e-02
2	-2.246254082499000e-07	1.823368632895470e-05	2.198780054496340e-02
3	-1.578587968151560e-08	7.946990081244100e-06	6.662984075703520e-03
4	1.732923293003160e-08	3.273356396625700e-06	7.907173467155090e-04
5	-7.081399642607430e-09	1.301100356483330e-06	-2.243067264619810e-04
6	2.482198403770570e-09	5.043448241124080e-07	-1.032261735179880e-04
7	-8.749831841180770e-10	1.919418161993110e-07	-5.350827374548070e-06
8	3.358446096487060e-10	7.202571800642050e-08	6.032870474106270e-06
9	-1.452715547964040e-10	2.672894811858380e-08	1.389775608451320e-06
10	7.036053028305940e-11	9.830459878805920e-09	-1.667794341081250e-07
11	-3.712078515936340e-11	3.588823452512340e-09	-1.098049445185050e-07
12	2.075613750341230e-11	1.302082454421850e-09	-3.990118701505270e-09
13	-1.206646596058050e-11	4.699379616814380e-10	6.210083081288950e-09
14	7.203733700544870e-12	1.688418171221920e-10	9.633344895225670e-10
15	-4.375271295344370e-12	6.042392709176170e-11	-2.609783367202760e-10
16	2.674170121231740e-12	2.154618744858780e-11	-8.315421351488380e-11
17	-1.612760826306620e-12	7.648543523947050e-12	6.884100040797620e-12
18	9.148126116574210e-13	2.675596311035580e-12	5.334393632012140e-12
19	-4.140244318492850e-13	8.418748326551250e-13	8.096094478676180e-14
20			
21			
22			
23			
24			
25			
26			
27			
28			
	u		
	3.765509769494760e-01	8.507269533566090e-01	9.987527542914820e-01
	k_1	k_1	k_1
	4.258473700427800e+05	-4.473698477162510e+02	3.134901409944510e+00
	k_2	k_2	k_2
	-1.030074288714920e+00	1.000000000000000e+00	4.184273889203900e-01

Table A.15: (cont.) Chebyshev coefficients c_n for $F^{-1}_{Y_2^h}$ with $h = 1/500$.

n	**right tail**	**right tail**
0	5.722628305041310e-01	4.619812351486570e+00
1	2.017761232436850e-01	1.860589481022900e+00
2	1.372549559855630e-02	3.705233566867130e-02
3	-1.799486944230340e-03	-9.679912077752170e-03
4	1.548179312896880e-04	2.763008630922070e-03
5	2.188831960478400e-05	-8.227338295193510e-04
6	-1.205509962337280e-05	2.508114545966220e-04
7	1.626588892457290e-06	-7.771817988229720e-05
8	3.184920827863740e-07	2.450094311357910e-05
9	-1.604199428018640e-07	-7.933144007790290e-06
10	1.026914924420950e-08	2.688223932510620e-06
11	9.459364972251820e-09	-9.765416694004460e-07
12	-2.712392941794810e-09	3.865875322747180e-07
13	-2.064497813254310e-10	-1.657778704727940e-07
14	2.839303432413090e-10	7.480889417663440e-08
15	-4.871222002206250e-11	-3.419915104148740e-08
16	-1.444200355589110e-11	1.528919983568170e-08
17	8.372113940734350e-12	-6.479029251360270e-09
18	-8.215034741114150e-13	2.513840140749040e-09
19	-5.718274703852940e-13	-8.420176316921800e-10
20		2.056434736961980e-10
21		-1.906441397640450e-12
22		-4.118010901086640e-11
23		3.573866647613250e-11
24		-2.210862584205230e-11
25		1.157843167001790e-11
26		-5.392753508375620e-12
27		2.255758034817050e-12
28		-7.825720526313930e-13
	u	
	9.999476900342120e-01	
	k_1	k_1
	4.729614165580610e+00	7.444073462053960e-01
	k_2	k_2
	-1.877416447914540e+00	-1.452884710450130e+00

Table A.16: Chebyshev coefficients c_n for $F^{-1}_{Y_2^h}$ with $h = 1/1000$.

n	left	central	middle
0	1.702183541035490e-06	4.683227357260450e-05	5.536218616018370e-02
1	7.420902874786450e-07	3.703626675908400e-05	4.374721584420760e-02
2	-9.865066726948370e-08	2.459788457587220e-05	2.175988835715650e-02
3	2.116960181208080e-09	1.509706997971100e-05	6.418561137830700e-03
4	5.497757664443210e-09	8.833813587467830e-06	7.077802624591750e-04
5	-3.075679409634440e-09	5.007785871509320e-06	-2.234688941525440e-04
6	1.295461350315460e-09	2.775387397751700e-06	-9.419306294251860e-05
7	-5.101921537607560e-10	1.512369265686620e-06	-3.360150759204160e-06
8	2.046470586232400e-10	8.133846678811090e-07	5.606215973335820e-06
9	-8.795781406451570e-11	4.329046589636920e-07	1.138744283796740e-06
10	4.150674524923850e-11	2.284469855279910e-07	-1.744975342137300e-07
11	-2.146959372032940e-11	1.197027748370620e-07	-9.175604868426630e-08
12	1.195357510557560e-11	6.234932494901730e-08	-9.405807379254040e-10
13	-7.007921488894990e-12	3.231076406508410e-08	5.303111119723830e-09
14	4.242800470479290e-12	1.667069009839590e-08	6.408776988724720e-10
15	-2.605046952660330e-12	8.568338007765290e-09	-2.359584489071990e-10
16	1.583112277512220e-12	4.389129098487210e-09	-5.912784735389660e-11
17	-9.048703171667920e-13	2.241645822968350e-09	7.661640011719350e-12
18	4.117767633668480e-13	1.141836261366410e-09	3.874828519769480e-12
19		5.802414152021550e-10	-1.166357191529630e-13
20		2.942280531036410e-10	
21		1.489078538692040e-10	
22		7.522864040175020e-11	
23		3.794343618365480e-11	
24		1.910697269597880e-11	
25		9.603319488497660e-12	
26		4.810076959555690e-12	
27		2.385153926155570e-12	
28		1.138578899937880e-12	
29		4.560886440536520e-13	
	u		
	4.174876557129840e-01	9.322059315659190e-01	9.993778254256840e-01
	k_1	k_1	k_1
	1.251565690963700e+06	-5.828431086945030e+02	3.197606134309120e+00
	k_2	k_2	k_2
	-1.022376759557920e+00	1.000000000000000e+00	4.064120883541780e-01

Table A.16: (cont.) Chebyshev coefficients c_n for $F^{-1}_{Y_2^h}$ with $h = 1/1000$.

n	**right tail**	**right tail**
0	5.722747148899260e-01	4.619756015894420e+00
1	2.017753450395610e-01	1.860594275953970e+00
2	1.371924357276870e-02	3.708005345183760e-02
3	-1.798581149904210e-03	-9.684906797069410e-03
4	1.551213775007560e-04	2.763643547482780e-03
5	2.175254385332560e-05	-8.226383894790430e-04
6	-1.204645343665120e-05	2.506774823695970e-04
7	1.634965165513770e-06	-7.763711144862410e-05
8	3.159981622016710e-07	2.446026791697160e-05
9	-1.605777694467310e-07	-7.914262660093390e-06
10	1.051874919029200e-08	2.679801742363760e-06
11	9.419608354447810e-09	-9.728790947989900e-07
12	-2.727465609582260e-09	3.850313981959300e-07
13	-1.988937692998890e-10	-1.651364788520010e-07
14	2.836178919653510e-10	7.455668628814350e-08
15	-4.943002831236930e-11	-3.410750194426710e-08
16	-1.421606720565160e-11	1.526049674012990e-08
17	8.387073685132120e-12	-6.472921009013150e-09
18	-8.503982177047600e-13	2.514557909430010e-09
19	-5.640963743958300e-13	-8.439824101491240e-10
20		2.072428649649550e-10
21		-2.907032521718890e-12
22		-4.063479916620070e-11
23		3.546906613254100e-11
24		-2.198580726676460e-11
25		1.152667195366080e-11
26		-5.372666511779400e-12
27		2.248692740626720e-12
28		-7.804828886326500e-13
29		
	u	
	9.999739151276640e-01	
	k_1	k_1
	4.729078684657730e+00	7.443447629709830e-01
	k_2	k_2
	-1.877882960729700e+00	-1.452971340318820e+00

Table A.17: Chebyshev coefficients c_n for $F^{-1}_{Y_2^h}$ with $h = 1/2000$.

n	**left**	**central**	**middle**
0	8.340782562108630e-08	2.468455017350800e-06	2.280294691861450e-02
1	3.790348335769390e-08	1.808380820210530e-06	1.944720833702610e-02
2	6.055403556177730e-10	9.977786192716340e-07	1.206597650481470e-02
3	-2.457590587255680e-10	5.095262839987460e-07	5.365044701332910e-03
4	3.852931864752010e-11	2.442450448287340e-07	1.591201684585540e-03
5	-7.060509039767990e-12	1.138166487478510e-07	2.189680324488170e-04
6	1.745854017090540e-12	5.143505829362960e-08	-5.028795904628390e-05
7	-4.817127130663800e-13	2.294108192095960e-08	-3.473771288547360e-05
8		1.003514899934200e-08	-6.612748781444720e-06
9		4.362945792279890e-09	8.987877800239290e-07
10		1.869145494199750e-09	7.769588194187460e-07
11		7.993315810705080e-10	1.334497286164690e-07
12		3.374445612260960e-10	-2.638905677337200e-08
13		1.426920238747580e-10	-1.641293598763500e-08
14		5.956301256742100e-11	-1.798371164119140e-09
15		2.498973580154360e-11	8.162891792784300e-10
16		1.032764886165950e-11	3.081840920792170e-10
17		4.294120630111000e-12	5.391475739175650e-12
18		1.719237245981860e-12	-2.108451751530640e-11
19		6.120456681919270e-13	-4.569166977955490e-12
20			5.618348229993250e-13
21			
22			
23			
24			
25			
26			
27			
28			
	u		
	7.747528004946140e-02	8.259386083799630e-01	9.993395585026600e-01
	k_1	k_1	k_1
	3.425124201204160e+07	-5.668468349121090e+02	2.690942655592710e+00
	k_2	k_2	k_2
	-1.151540996208610e+00	1.000000000000000e+00	7.708355493813890e-01

Table A.17: (cont.) Chebyshev coefficients c_n for $F^{-1}_{Y_2^h}$ with $h = 1/2000$.

n	**right tail**	**right tail**
0	4.997785332154770e-01	4.423666819273090e+00
1	2.283167712864410e-01	1.759820399395010e+00
2	2.509022440364520e-02	3.541998526121500e-02
3	-3.473302792894460e-03	-9.020823900527120e-03
4	5.642398807896140e-05	2.508301403041810e-03
5	1.601477839497730e-04	-7.271867741631950e-04
6	-3.917135579658680e-05	2.157837314850230e-04
7	-3.440824241326090e-06	-6.511087849455130e-05
8	3.519318737665760e-06	2.002320021389280e-05
9	-2.194212259839980e-07	-6.350484440175680e-06
10	-2.877017875529080e-07	2.122832316166740e-06
11	5.198973063531290e-08	-7.670810351604750e-07
12	2.710916358293460e-08	3.034734463075500e-07
13	-9.510243857620710e-09	-1.296599648285680e-07
14	-2.488075646152630e-09	5.774831521471910e-08
15	1.740766101870460e-09	-2.574755859857420e-08
16	8.803780581176800e-11	1.108702976174010e-08
17	-2.866253352551910e-10	-4.459918192937880e-09
18	4.280148433910290e-11	1.605691932192970e-09
19	3.704110753342690e-11	-4.731139230730710e-10
20	-1.527178121204120e-11	7.876459425075550e-11
21	-2.422082175650230e-12	2.822685782970860e-11
22	3.088328322933460e-12	-3.938365394966450e-11
23	-5.645136949758670e-13	2.737131256274070e-11
24		-1.510876686567670e-11
25		7.257145569467030e-12
26		-3.126553351859830e-12
27		1.213046040716070e-12
28		-3.939886674131800e-13
	u	
	9.999869750663500e-01	
	k_1	k_1
	3.820640730812540e+00	7.845522141906270e-01
	k_2	k_2
	-1.325371123114800e+00	-1.477505002954480e+00

Appendix B

Errors of Chebyshev polynomial approximations

We present the errors resulting from the Chebyshev polynomial approximations to the inverse distribution functions $F_{Z^P}^{-1}$ and $F_{Y_2^h}^{-1}$ below. We observe that the error across all regimes in all cases is at least of order 10^{-12}.

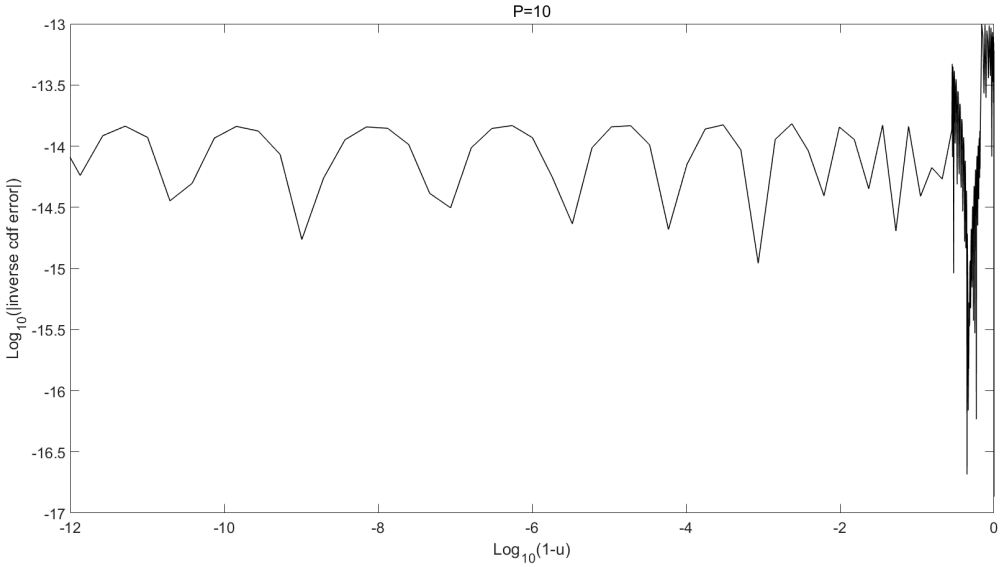

Figure B.1: We plot the errors in the Chebyshev polynomial approximations to the inverse distribution functions $F_{Z^P}^{-1}(u)$ with $P = 10$ across all regimes. Note that to highlight the tail we use a log-$\log_{10}$ scale with $1 - u$ on the abscissa.

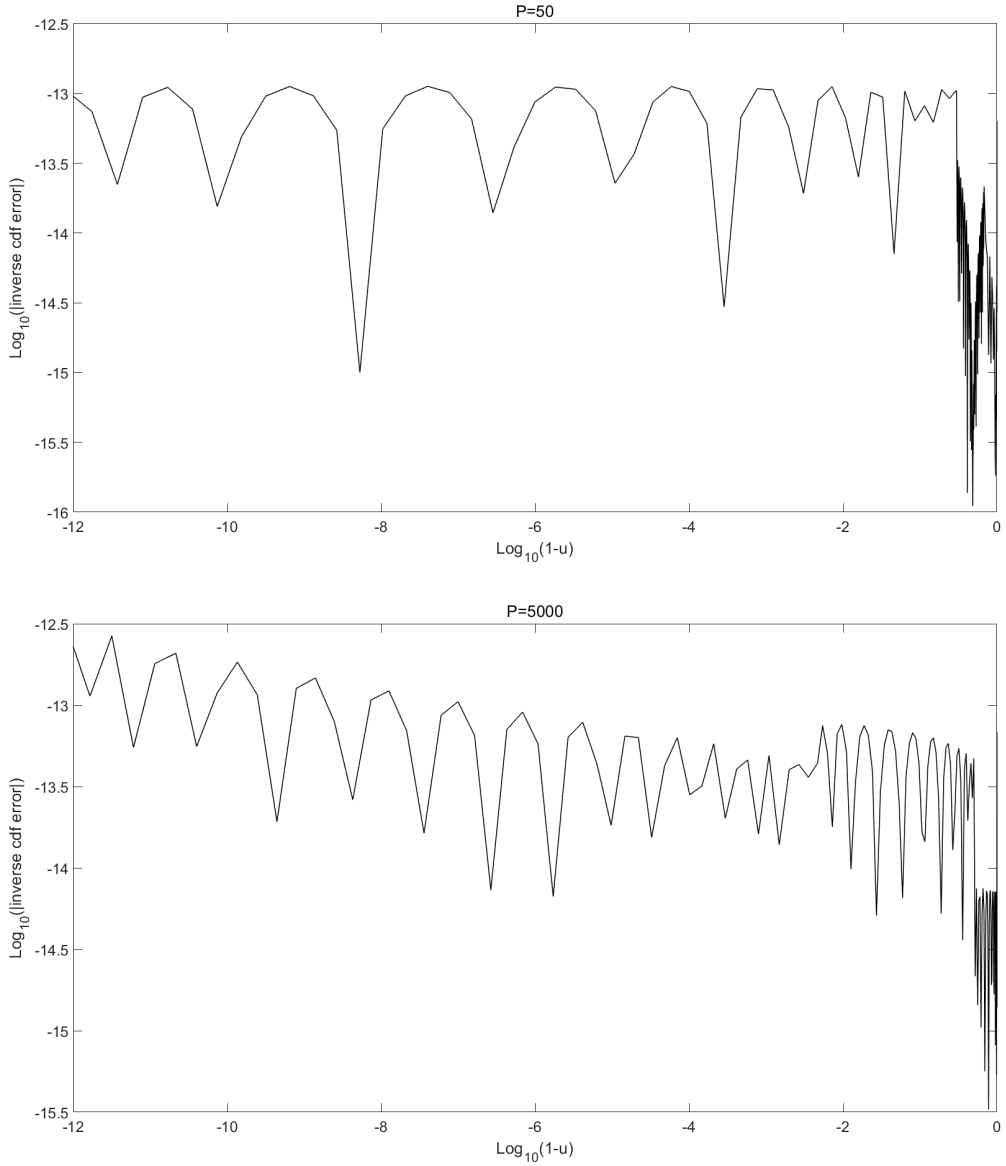

Figure B.1: (cont.) We plot the errors in the Chebyshev polynomial approximations to the inverse distribution functions $F_{Z^P}^{-1}(u)$ with $P = 50$ (top panel) and $P = 5000$ (bottom panel) across all regimes. Note as above we use a log-$\log_{10}$ scale with $1 - u$ on the abscissa.

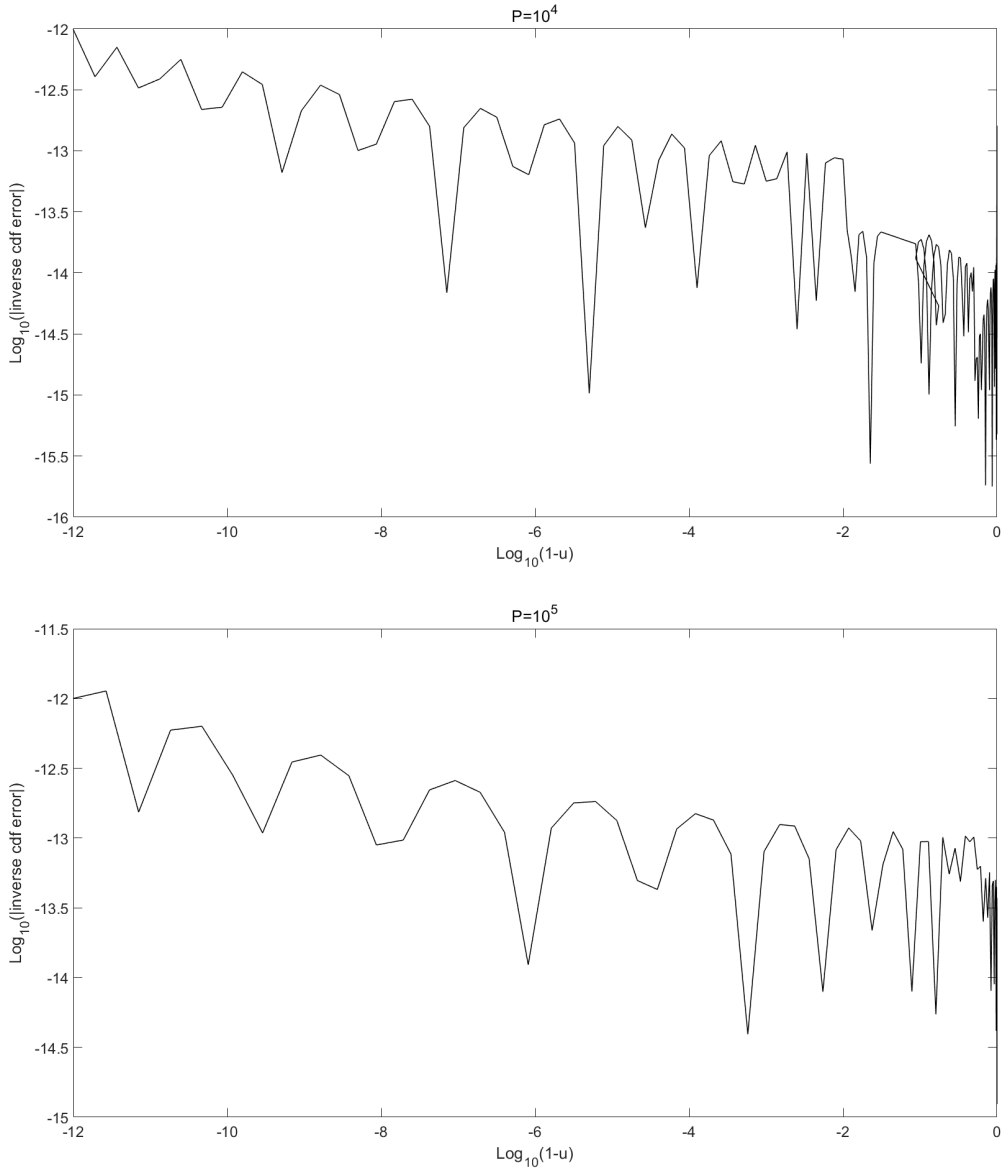

Figure B.1: (cont.) We plot the errors in the Chebyshev polynomial approximations to the inverse distribution functions $F_{Z^P}^{-1}(u)$ with $P = 10^4$ (top panel) and $P = 10^5$ (bottom panel) across all regimes. Note as above we use a log-$\log_{10}$ scale with $1 - u$ on the abscissa.

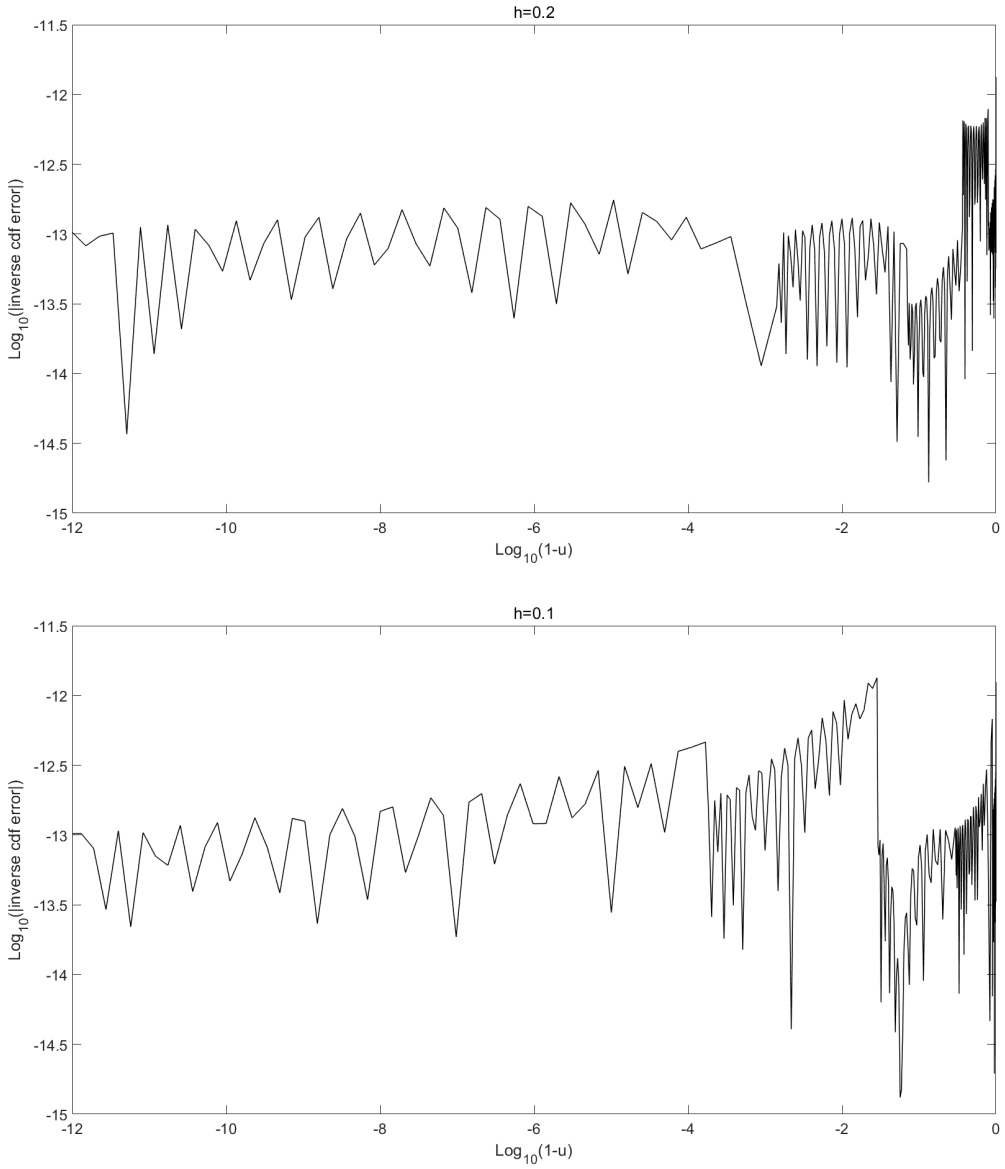

Figure B.2: We plot the errors in the Chebyshev polynomial approximations to the inverse distribution functions $F^{-1}_{Y_2^h}(u)$ with $h = 0.2$ (top panel) and $h = 0.1$ (bottom panel) across all regimes. Note as above we use a log-$\log_{10}$ scale with $1 - u$ on the abscissa.

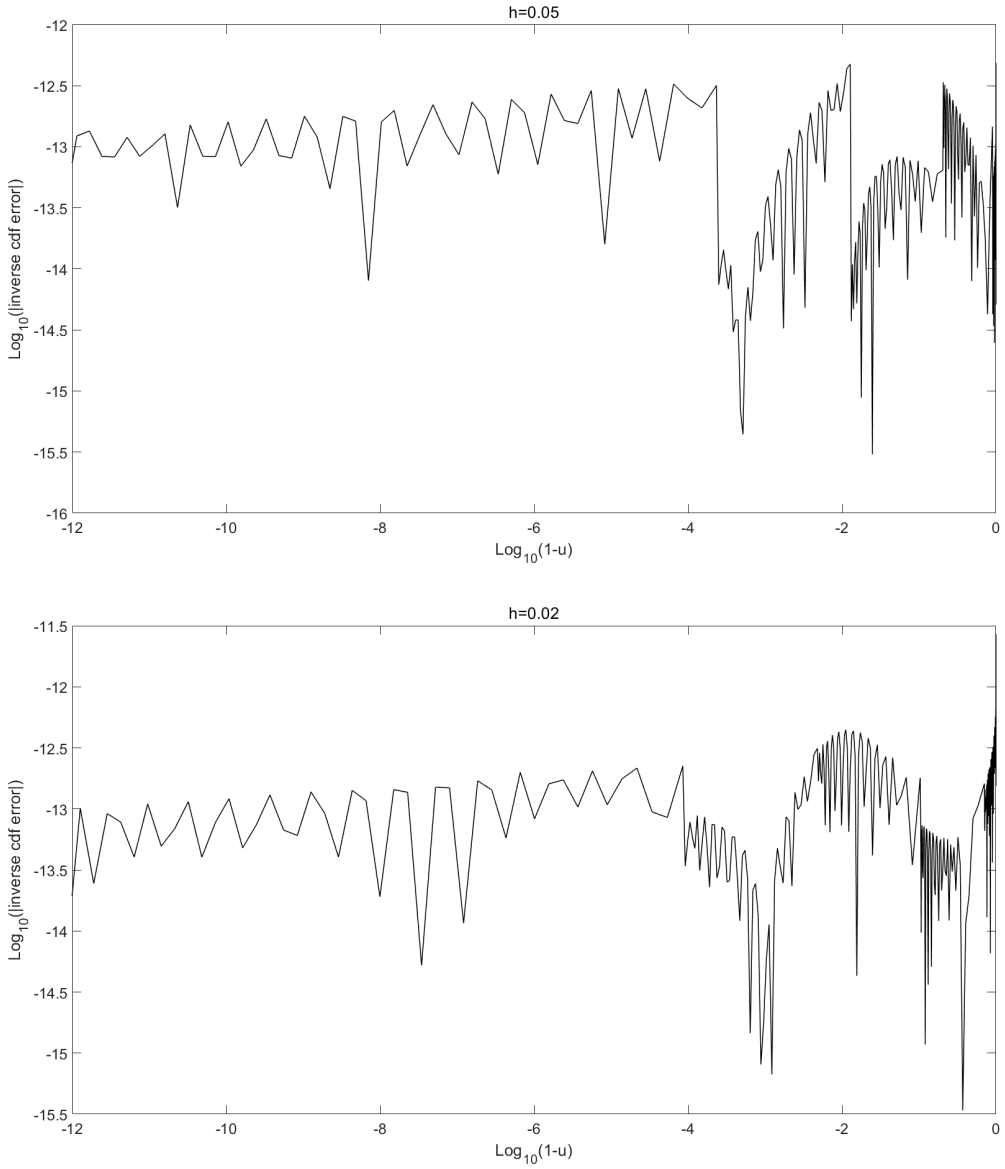

Figure B.2: (cont.) We plot the errors in the Chebyshev polynomial approximations to the inverse distribution functions $F^{-1}_{Y_2^h}(u)$ with $h = 0.05$ (top panel) and $h = 0.02$ (bottom panel) across all regimes. Note as above we use a log-$\log_{10}$ scale with $1 - u$ on the abscissa.

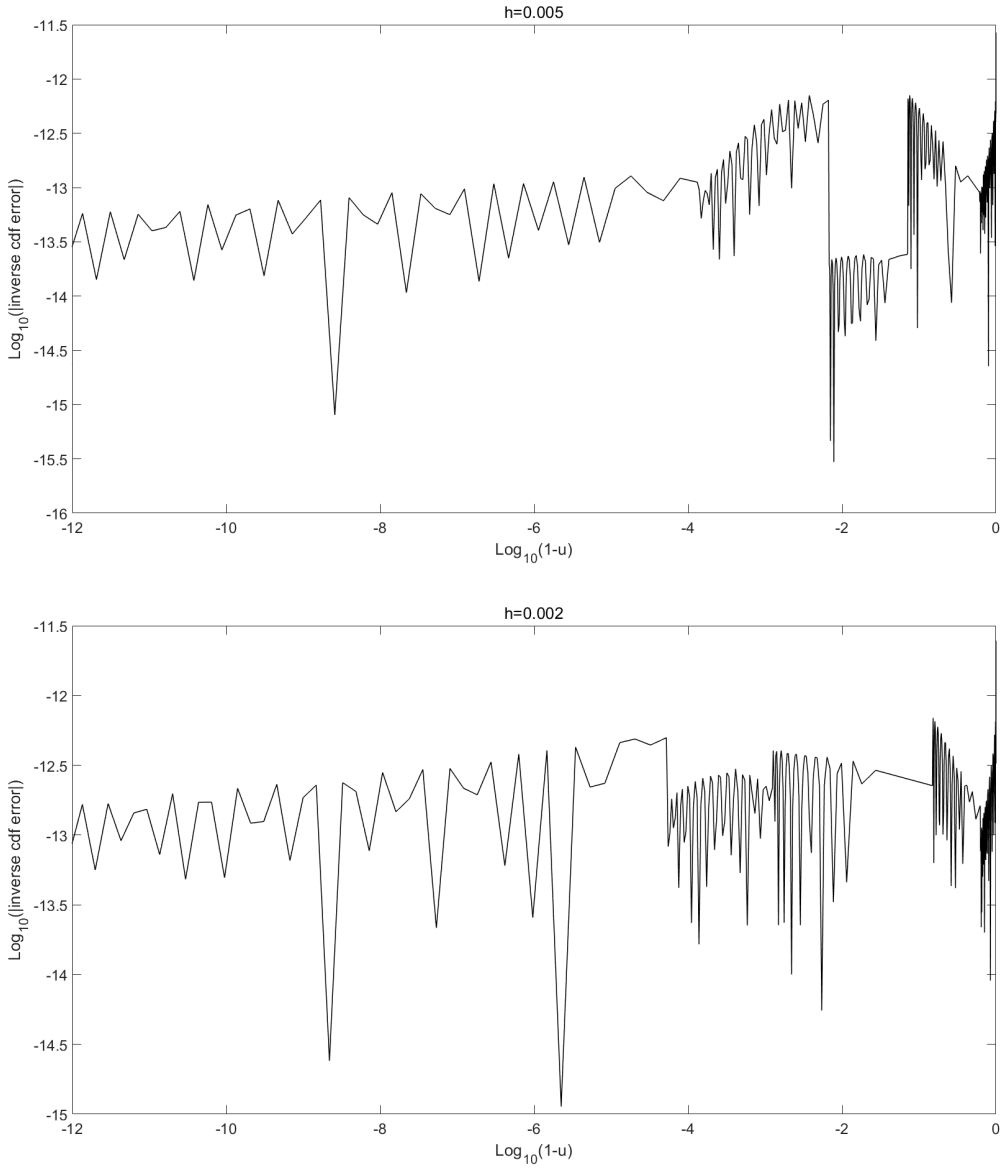

Figure B.2: (cont.) We plot the errors in the Chebyshev polynomial approximations to the inverse distribution functions $F^{-1}_{Y_2^h}(u)$ with $h = 0.005$ (top panel) and $h = 0.002$ (bottom panel) across all regimes. Note as above we use a log-$\log_{10}$ scale with $1 - u$ on the abscissa.

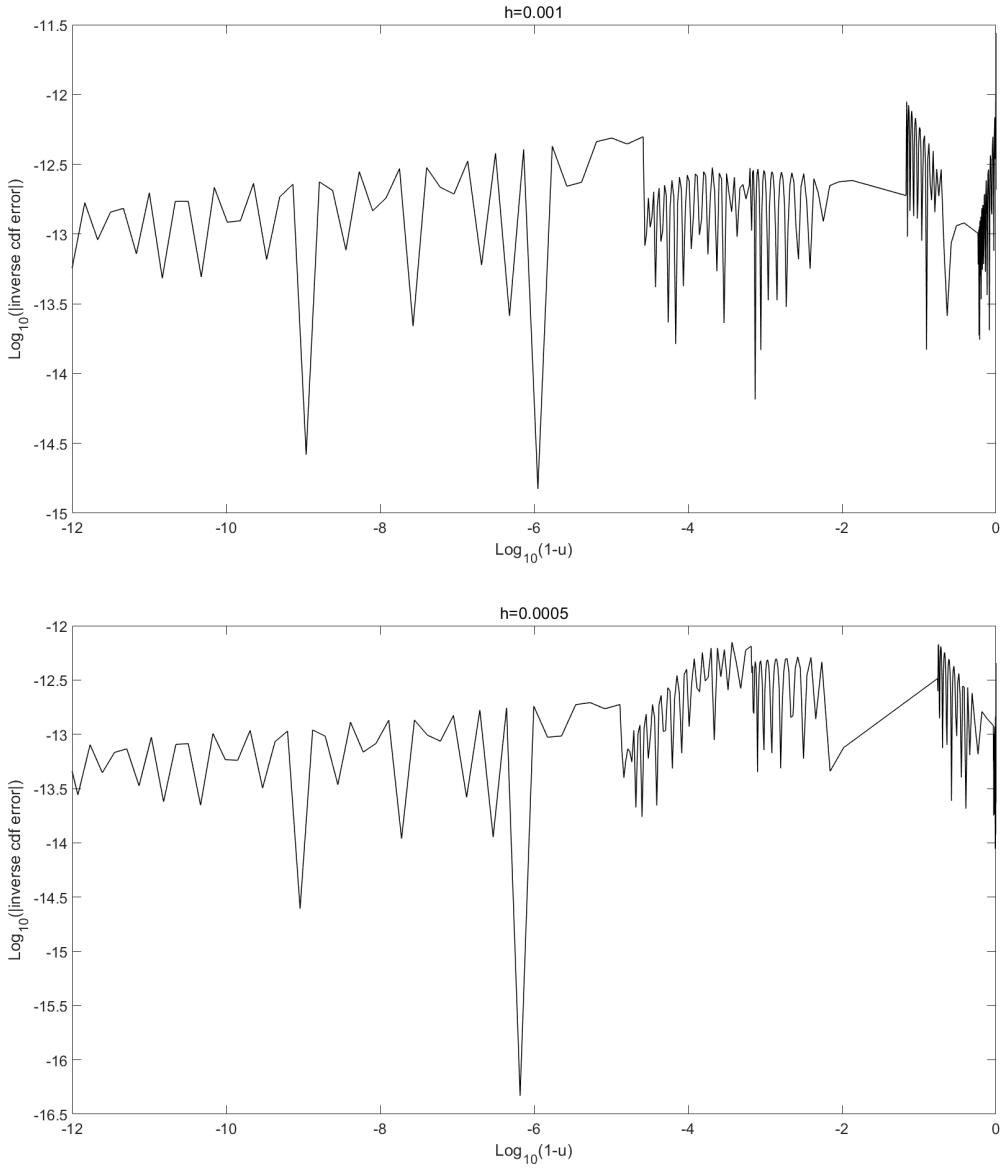

Figure B.2: (cont.) We plot the errors in the Chebyshev polynomial approximations to the inverse distribution functions $F^{-1}_{Y_2^h}(u)$ with $h = 0.001$ (top panel) and $h = 0.0005$ (bottom panel) across all regimes. Note as above we use a log-$\log_{10}$ scale with $1 - u$ on the abscissa.

Appendix C

Numerical results

In this appendix, we give additional numerical results for the moment errors of the time integrated conditional variance $\bar{I}$ defined in Section 6.1 for Case 2 and Case 3. Apart from that, tradeoffs between speed and accuracy when pricing in the money and out of the money European call options are also reported for all four cases.

C.1 Time integrated conditional variance

The figures in this section demonstrate the relative errors in the first four moments of the integral $\bar{I}$ of the variance process for Case 2 and Case 3, conditional on $v_t = 0.04, 0.4, 0.000004$ and $v_t = 0.09, 0.9, 0.000009$, respectively. For each case, our new direct inversion method and the gamma expansion by Glasserman and Kim [32] are implemented using $5 \cdot 10^7$ and $5 \cdot 10^8$ samples with truncation level increasing in integers.

Similar conclusions as Case 1 can be reached for Case 3, where the four moment errors of the direct inversion all maintain at fixed levels with small fluctuations across a range of truncation levels. This suggests that the new scheme performed at different truncation levels achieves the same accuracy. Furthermore, we observe that all errors in the first four moments are decreased according to the expected scaling when the sample size is increased by a factor of 10 with truncation level remaining unchanged. In contrast, the gamma expansion for lower truncation levels exhibits some small bias, which is evident from the unimproved errors in higher moments for

truncation level one and two with the increase of the sample size.

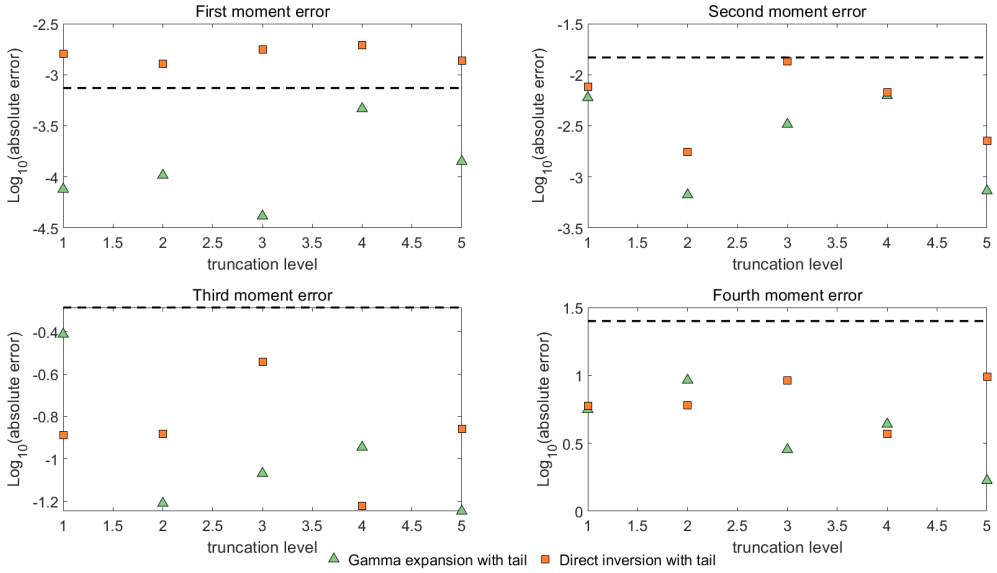

(a) Case 2: $v_0 = v_t = 0.04$

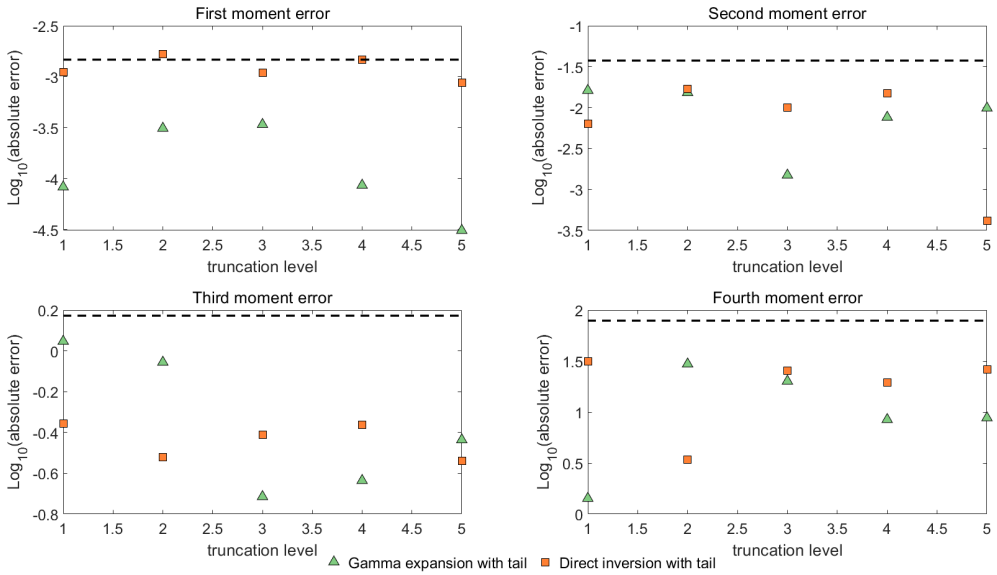

(b) Case 2: $v_0 = 0.04, v_t = 0.4$

Figure C.1: We indicate the absolute errors in the first four moments of the conditional integral $\bar{I}$ simulated by direct inversion and gamma expansion versus the truncation levels for Case 2 with different values for v_t. Both methods are implemented with tail simulation. We perform $5 \cdot 10^7$ simulations for each case. Below the dashed line, the errors are not statistically significant at the level of three standard deviations.

However for Case 2, we notice that the moment errors resulting from the direct inversion are invariant to increasing the number of simulations when the truncation levels are fixed. For first and second moments, most of the errors in the direct

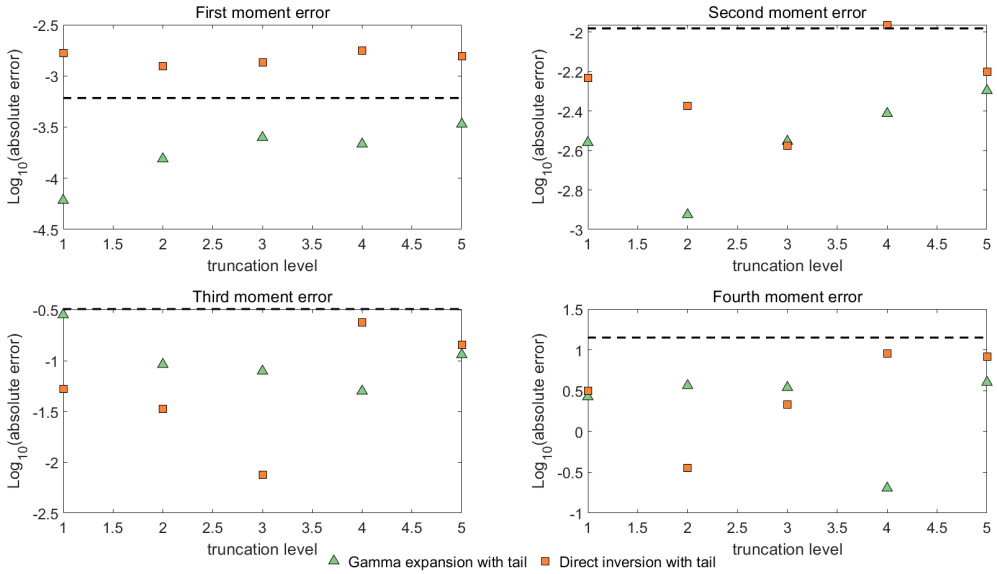

(c) Case 2: $v_0 = 0.04, v_t = 0.000004$

Figure C.1: (cont.) We indicate the absolute errors in the first four moments of the conditional integral $\bar{I}$ simulated by direct inversion and gamma expansion versus the truncation levels for Case 2 with different values for v_t. Both methods are implemented with tail simulation. We perform $5 \cdot 10^7$ simulations for each case. Below the dashed line, the errors are not statistically significant at the level of three standard deviations.

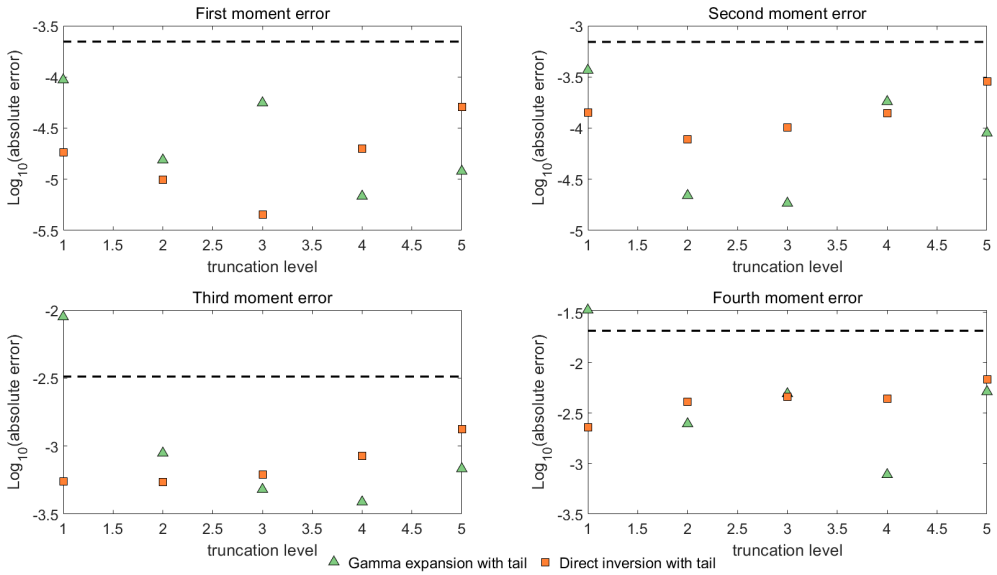

(a) Case 3: $v_0 = v_t = 0.09$

Figure C.2: We indicate the absolute errors in the first four moments of the conditional integral $\bar{I}$ simulated by direct inversion and gamma expansion versus the truncation levels for Case 3 with different values for v_t. Both methods are implemented with tail simulation. We perform $5 \cdot 10^7$ simulations for each case. Below the dashed line, the errors are not statistically significant at the level of three standard deviations.

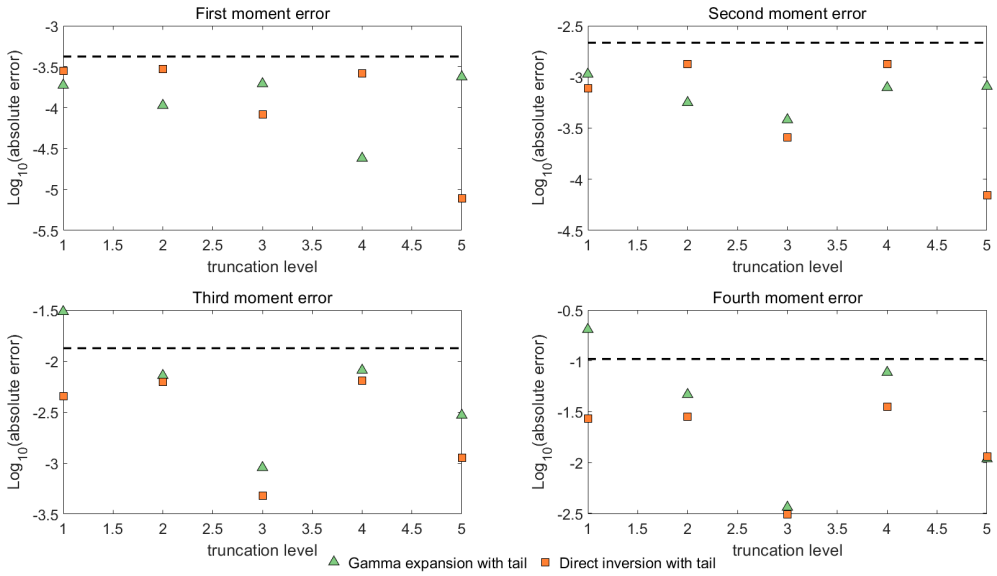

(b) Case 3: $v_0 = 0.09, v_t = 0.9$

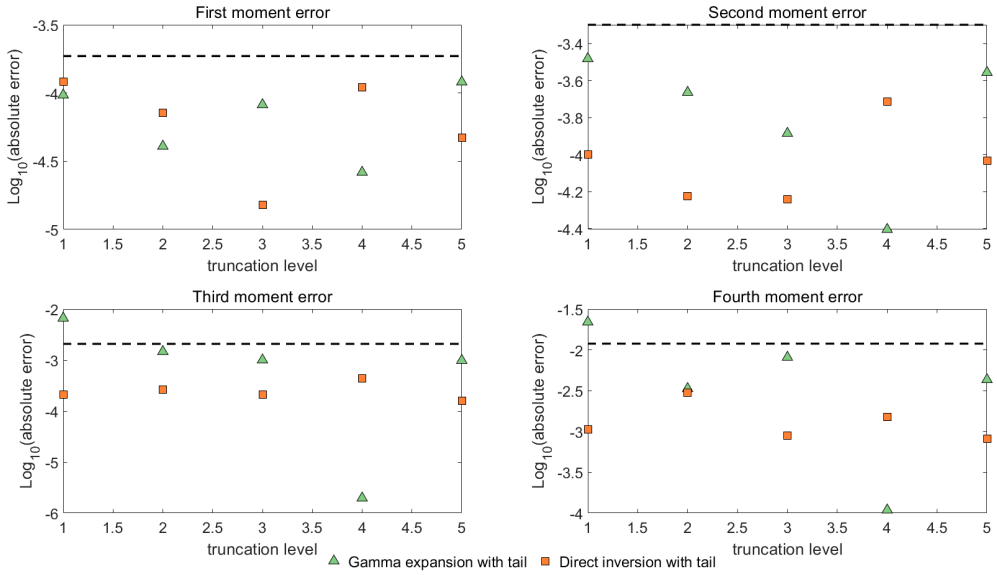

(c) Case 3: $v_0 = 0.09, v_t = 0.000009$

Figure C.2: (cont.) We indicate the absolute errors in the first four moments of the conditional integral $\bar{I}$ simulated by direct inversion and gamma expansion versus the truncation levels for Case 3 with different values for v_t. Both methods are implemented with tail simulation. We perform $5 \cdot 10^7$ simulations for each case. Below the dashed line, the errors are not statistically significant at the level of three standard deviations.

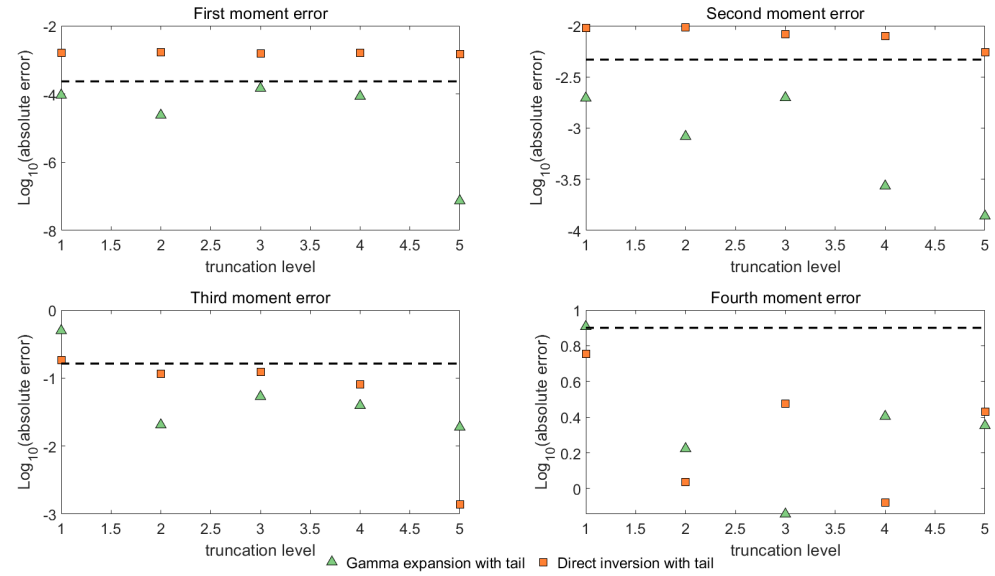

(a) Case 2: $v_0 = v_t = 0.04$

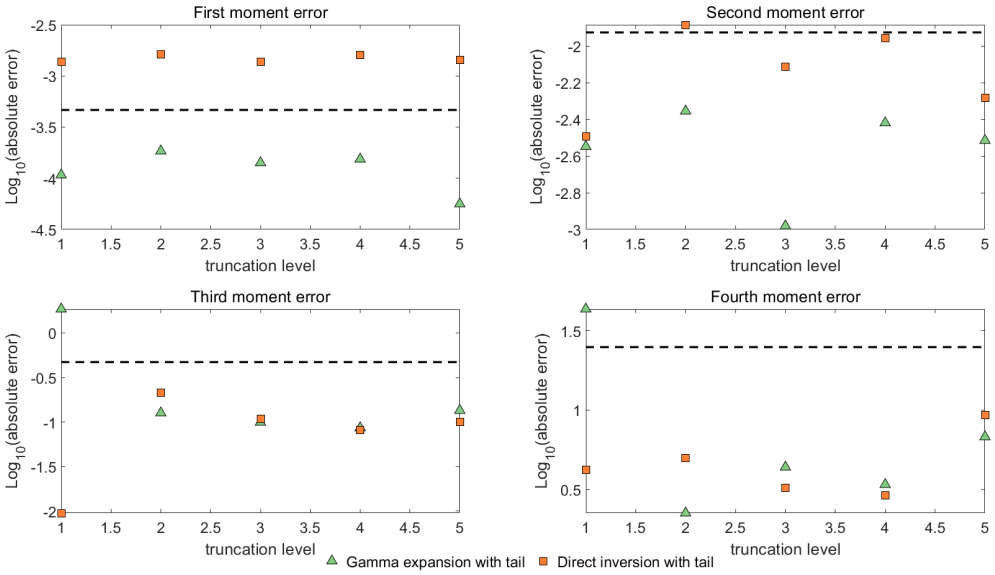

(b) Case 2: $v_0 = 0.04, v_t = 0.4$

Figure C.3: We indicate the absolute errors in the first four moments of the conditional integral $\bar{I}$ simulated by direct inversion and gamma expansion versus the truncation levels for Case 2 with different values for v_t. Both methods are implemented with tail simulation. We perform $5 \cdot 10^8$ simulations for each case. Below the dashed line, the errors are not statistically significant at the level of three standard deviations.

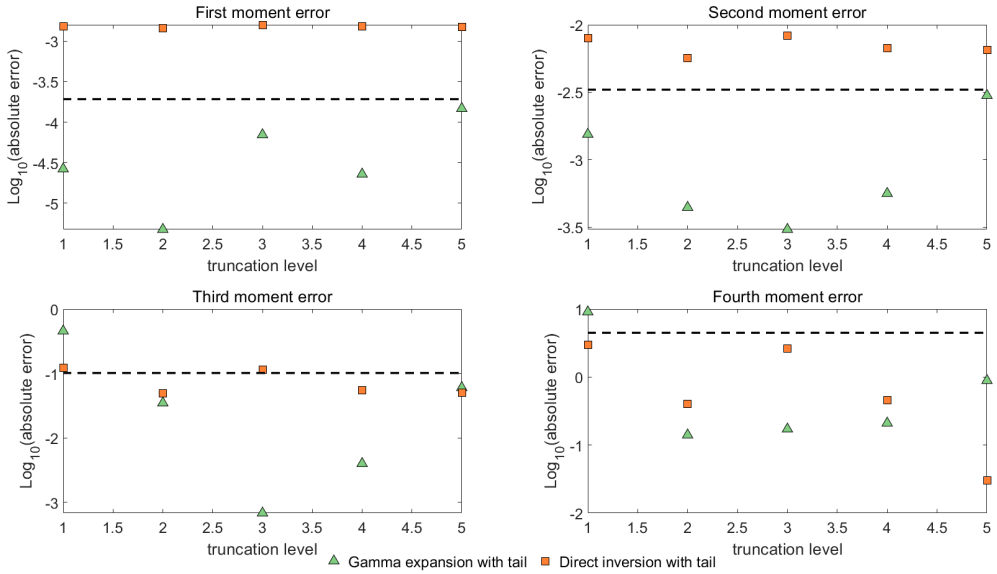

(c) Case 2: $v_0 = 0.04, v_t = 0.000004$

Figure C.3: (cont.) We indicate the absolute errors in the first four moments of the conditional integral $\bar{I}$ simulated by direct inversion and gamma expansion versus the truncation levels for Case 2 with different values for v_t. Both methods are implemented with tail simulation. We perform $5 \cdot 10^8$ simulations for each case. Below the dashed line, the errors are not statistically significant at the level of three standard deviations.

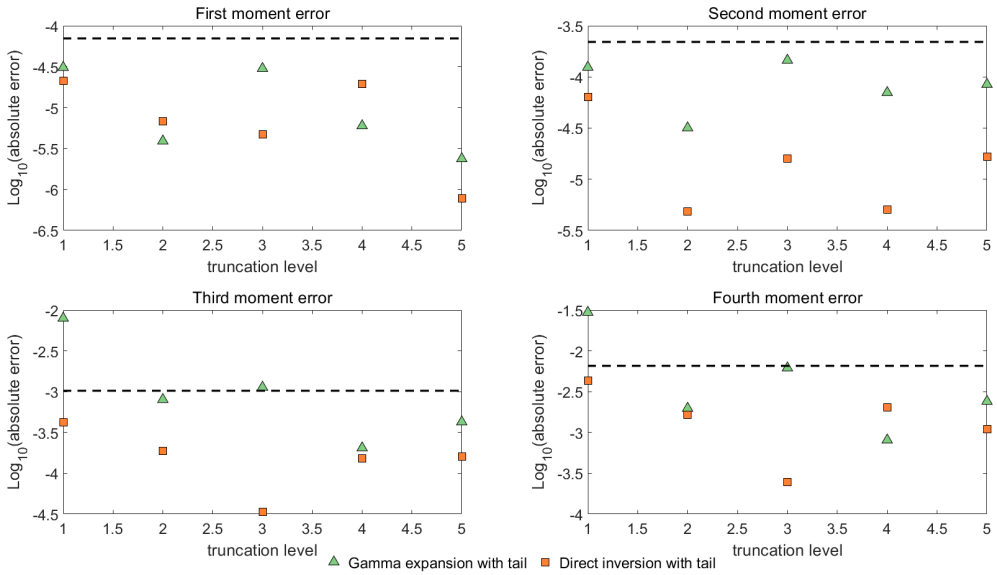

(a) Case 3: $v_0 = v_t = 0.09$

Figure C.4: We indicate the absolute errors in the first four moments of the conditional integral $\bar{I}$ simulated by direct inversion and gamma expansion versus the truncation levels for Case 3 with different values for v_t. Both methods are implemented with tail simulation. We perform $5 \cdot 10^8$ simulations for each case. Below the dashed line, the errors are not statistically significant at the level of three standard deviations.

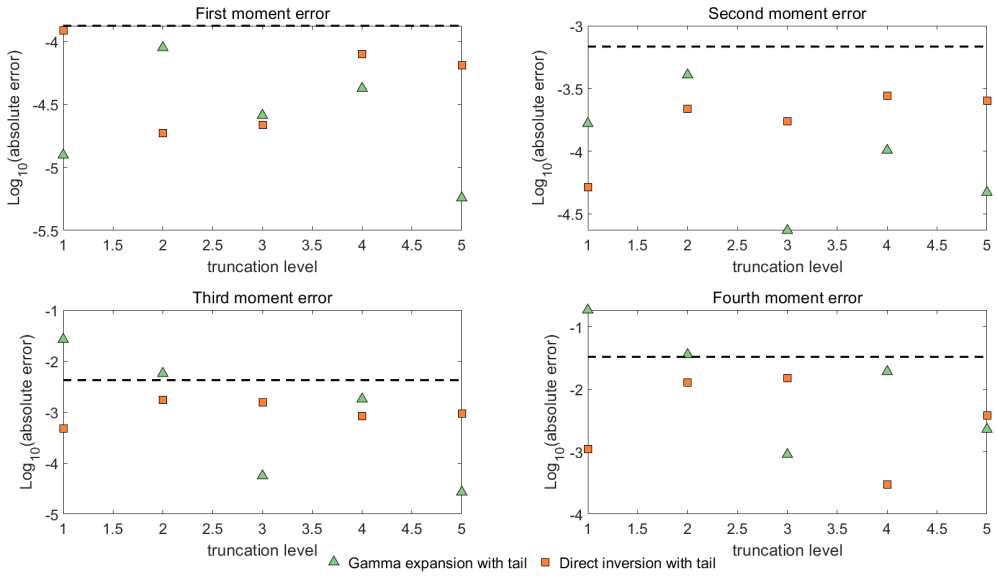

(b) Case 3: $v_0 = 0.09, v_t = 0.9$

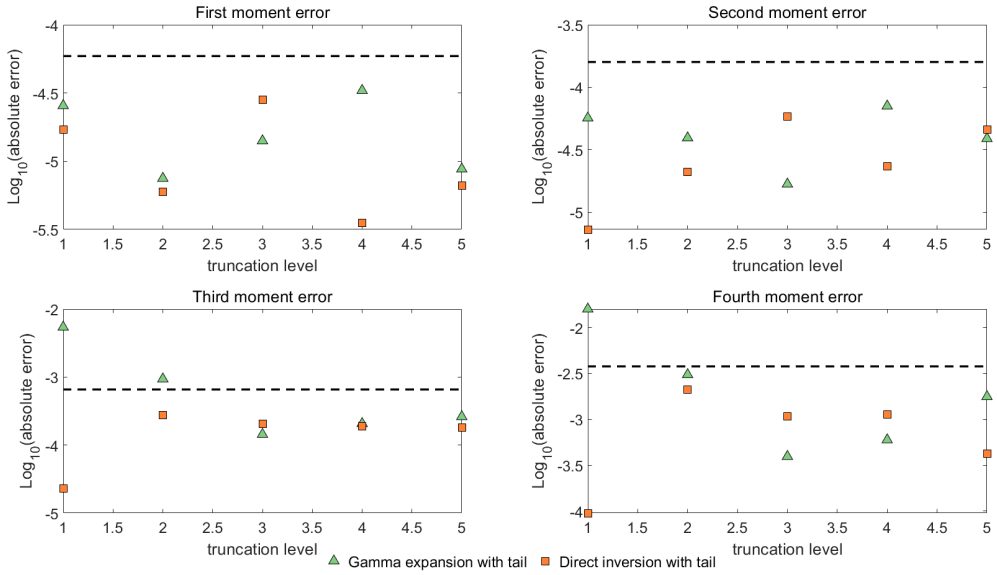

(c) Case 3: $v_0 = 0.09, v_t = 0.000009$

Figure C.4: (cont.) We indicate the absolute errors in the first four moments of the conditional integral $\bar{I}$ simulated by direct inversion and gamma expansion versus the truncation levels for Case 3 with different values for v_t. Both methods are implemented with tail simulation. We perform $5 \cdot 10^8$ simulations for each case. Below the dashed line, the errors are not statistically significant at the level of three standard deviations.

inversion are slightly larger than those of the gamma expansion. These findings are analogous with Case 4, indicating there is a small bias related to the direct inversion method for these two cases. As explained in Section 6.1, this bias comes from the approximations involved in the second factor X_2 of the series expansion Theorem 3.2.1.

C.2 Option price

In this section, we plot the root mean square error in the European call option prices with strike $K = 140$ and $K = 60$ against the CPU time on a log-$\log_{10}$ scale for all four cases considered using a number of $5 \cdot 10^7$ samples. Compared to the gamma expansion, the direct inversion scheme requires much less computational budget for Case 1 to Case 3. Case 4 takes longer time to complete the new method, where more iterations are needed for the acceptance-rejection sampling because of the marginally unfavourable parameter values.

We end this section with comparisons between the almost exact methods and the full truncation Euler scheme for pricing in the money and out of the money European call options. In Figure C.7 and Figure C.8, we plot the root mean square error of the option price versus the CPU time required on a log-$\log_{10}$ scale with strikes $K = 140$ and $K = 60$, respectively. The truncation level taken here for the two almost exact methods are 5 and the number of time steps used in the full truncation Euler scheme is equal to the square root of the sample size. We can conclude from the plots that the direction inversion outperforms the other two methods in terms of convergence rate and computational time.

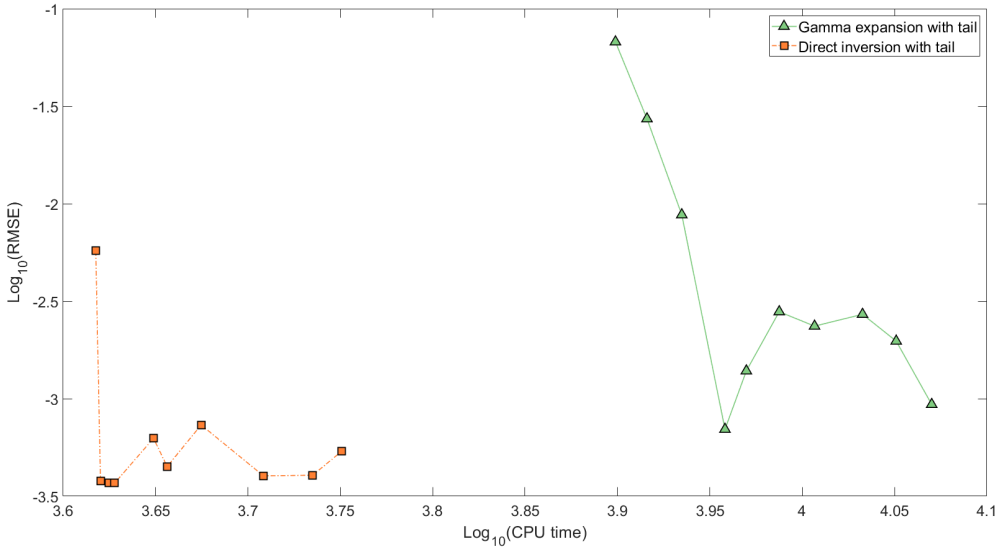

(a) Case 1

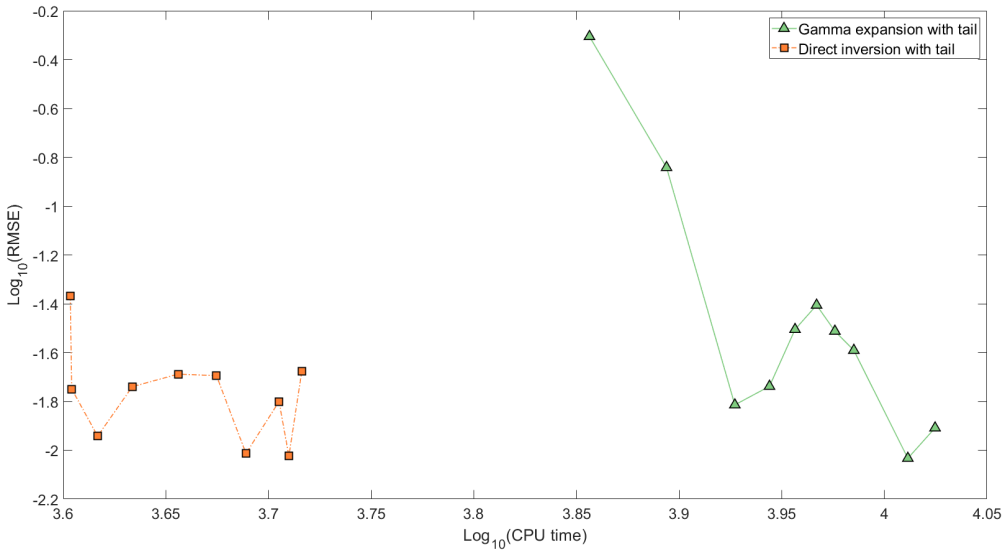

(b) Case 2

Figure C.5: We show the root mean square error in the option price with $K = 140$ versus the CPU time required to complete the simulation on a log-$\log_{10}$ scale for Case 1 to Case 4. We use a sample size of $5 \cdot 10^7$.

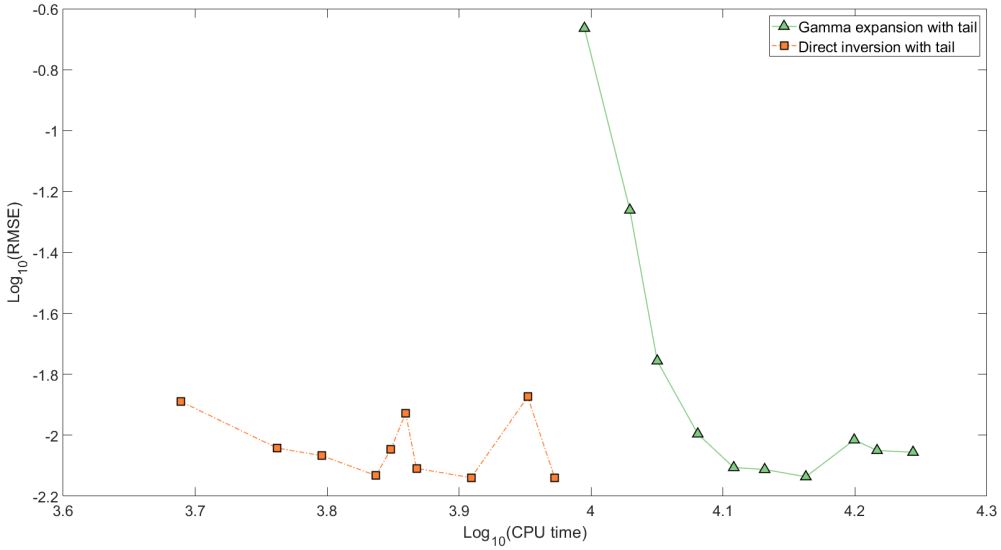

(c) Case 3

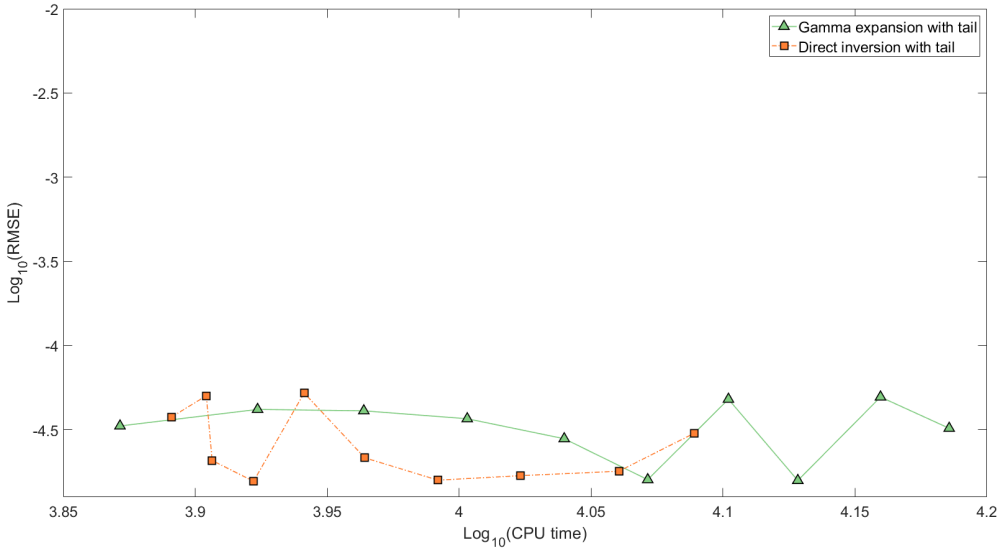

(d) Case 4

Figure C.5: (cont.) We show the root mean square error in the option price with $K = 140$ versus the CPU time required to complete the simulation on a log-$\log_{10}$ scale for Case 1 to Case 4. We use a sample size of $5 \cdot 10^7$.

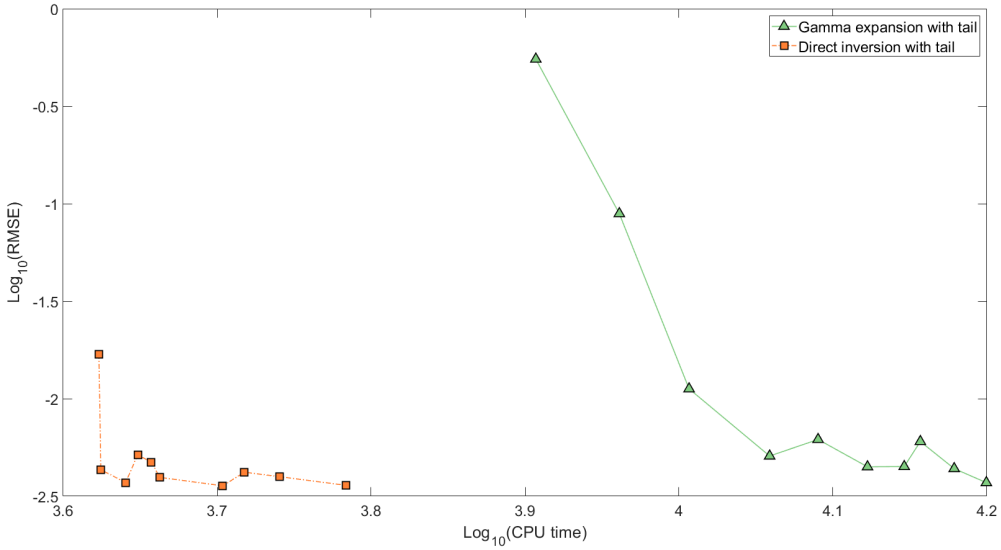

(a) Case 1

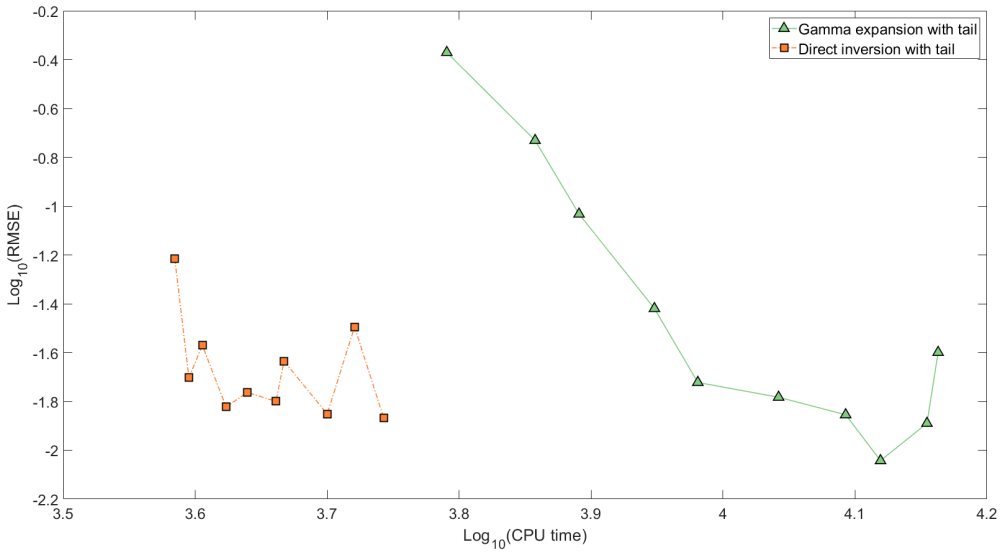

(b) Case 2

Figure C.6: We show the root mean square error in the option price with $K = 60$ versus the CPU time required to complete the simulation on a log-$\log_{10}$ scale for Case 1 to Case 4. We use a sample size of $5 \cdot 10^7$.

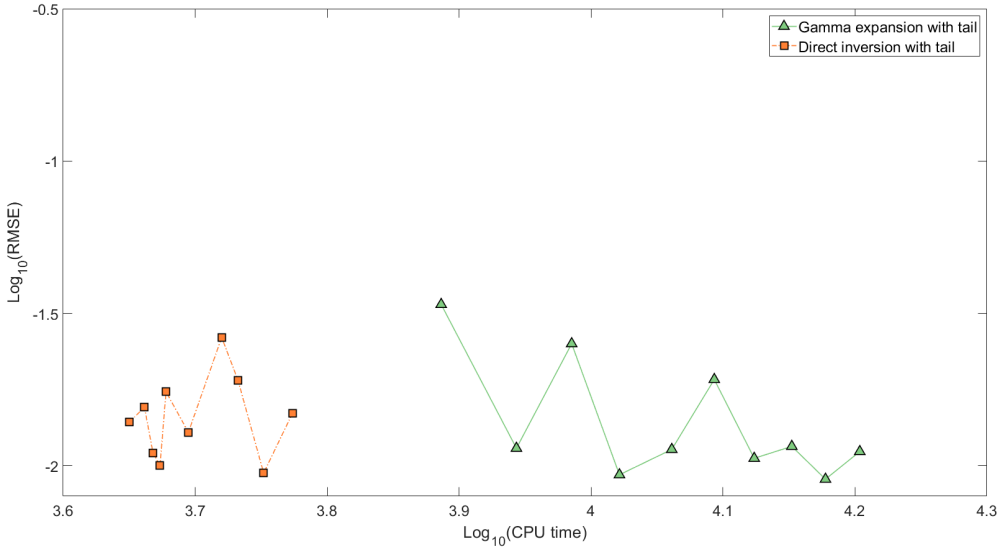

(c) Case 3

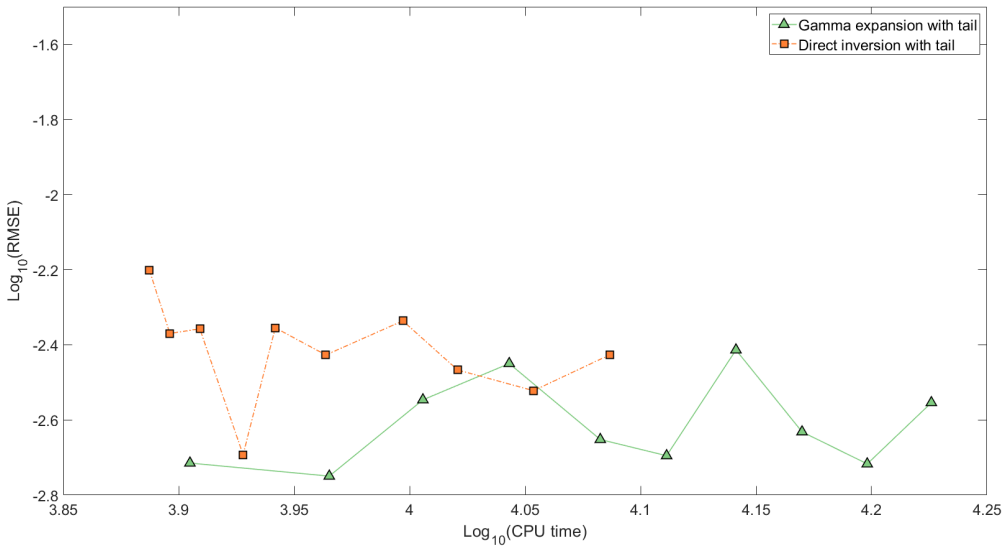

(d) Case 4

Figure C.6: (cont.) We show the root mean square error in the option price with $K = 60$ versus the CPU time required to complete the simulation on a log-$\log_{10}$ scale for Case 1 to Case 4. We use a sample size of $5 \cdot 10^7$.

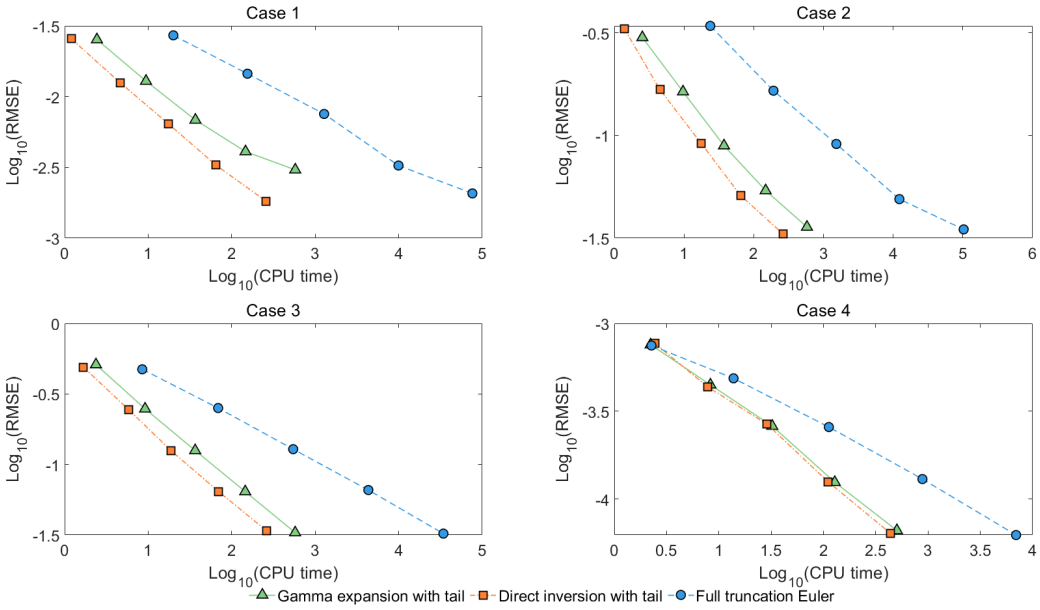

Figure C.7: We show the convergence of the root mean square error in the option price for Case 1 to Case 4 with $K = 140$ of gamma expansion and direction inversion, both at a truncation level $M = 5$, and full truncation Euler scheme, with number of time steps equal to the square root of the sample size.

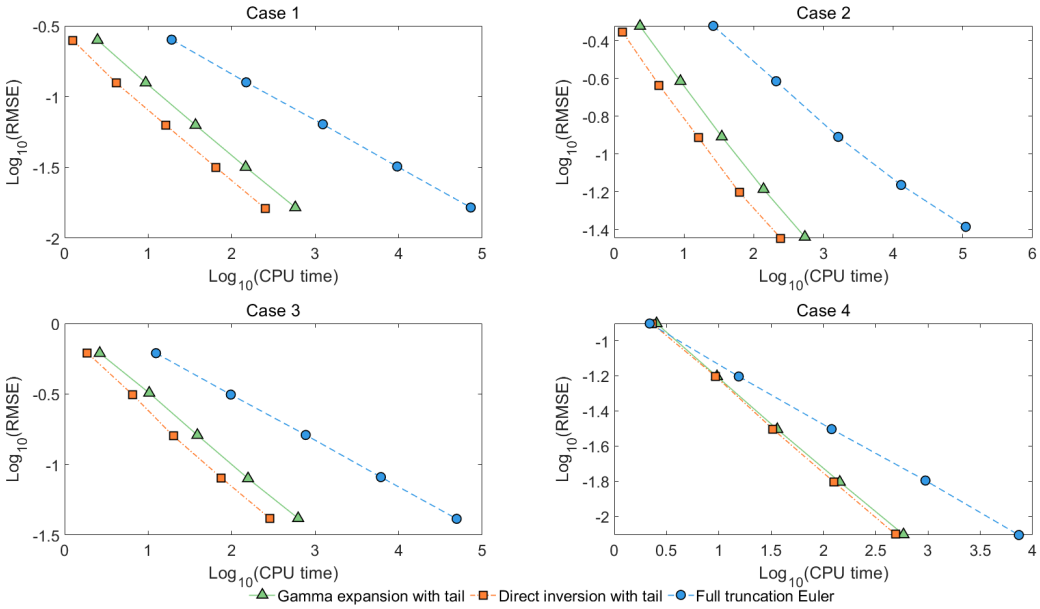

Figure C.8: We show the convergence of the root mean square error in the option price for Case 1 to Case 4 with $K = 60$ of gamma expansion and direction inversion, both at a truncation level $M = 5$, and full truncation Euler scheme, with number of time steps equal to the square root of the sample size.

Bibliography

[1] M. J. Ablowitz and A. S. Fokas, *Complex Variables: Introduction and Applications*, Cambridge Texts in Applied Mathematics, 2nd ed., Cambridge University Press, Cambridge, 2003.

[2] M. Abramowitz and I. A. Stegun, *eds., Handbook of Mathematical Functions with Formulas, Graphs, and Mathematical Tables*, National Bureau of Standards: Applied Mathematics Series, Vol. 55, U.S. Government Printing Office, Washington, DC, 1964.

[3] A. Alfonsi, *On the discretization schemes for the CIR (and Bessel squared) processes*, Monte Carlo Methods Appl., 11 (2005), pp. 355–384.

[4] A. Alfonsi, *High order discretization schemes for the CIR process: application to affine term structure and Heston models*, Math. Comp., 79 (2010), pp. 209–237.

[5] M. Altmayer and A. Neuenkirch, *Discretising the Heston model: an analysis of the weak convergence rate*, IMA J. Numer. Anal., 37 (2017), pp. 1930–1960.

[6] L. Andersen, *Simple and efficient simulation of the Heston stochastic volatility model*, J. Comput. Finance, 11 (2008), pp. 1–42.

[7] G. B. Arfken and H. J. Weber, *Mathematical Methods for Physicists*, 5th ed., Academic Press, Burlington, MA, 2001.

[8] C. M. Bender and S. A. Orszag, *Advanced Mathematical Methods for Scientists and Engineers I: Asymptotic Methods and Perturbation Theory*, Springer-Verlag, New York, 1999.

[9] P. Biane, J. Pitman, and M. Yor, *Probability laws related to the Jacobi theta and Riemann zeta functions, and Brownian excursions*, Bull. Amer. Math. Soc. (N.S.), 38 (2001), pp. 435–465.

[10] P. Biane and M. Yor, *Valeurs principales associées aux temps locaux Browniens*, Bull. Sci. Math., 111 (1987), pp. 23–101.

[11] N. Bleistein and R. A. Handelsman, *Asymptotic Expansions of Integrals*, 2nd ed., Dover Publications, Inc., New York, 1986.

[12] M. Bossy and A. Diop, *An efficient discretization scheme for one dimensional SDEs with a diffusion coefficient function of the form* $|x|^\alpha$, $\alpha \in [1/2, 1)$, INRIA, (2006).

[13] M. Bossy and H. Olivero, *Strong convergence of the symmetrized Milstein scheme for some CEV-like SDEs*, Bernoulli, 24 (2018), pp. 1995–2042.

[14] M. Broadie and Ö. Kaya, *Exact simulation of option Greeks under stochastic volatility and jump diffusion models*, in Proceedings of the 2004 Winter Simulation Conference, 2004, pp. 1607–1615.

[15] M. Broadie and Ö. Kaya, *Exact simulation of stochastic volatility and other affine jump diffusion processes*, Oper. Res., 54 (2006), pp. 217–231.

[16] P. Carr and D. B. Madan, *Option valuation using the fast fourier transform*, J. Comput. Finance, 2 (1999), pp. 61–73.

[17] J.-F. Chassagneux, A. Jacquier, and I. Mihaylov, *An explicit Euler scheme with strong rate of convergence for financial SDEs with non-Lipschitz coefficients*, SIAM J. Finan. Math., 7 (2016), pp. 993–1021.

[18] J. C. Cox, J. E. Ingersoll, and S. A. Ross, *A theory of the term structure of interest rates*, Econometrica, 53 (1985), pp. 385–407.

[19] A. Cozma, M. Mariapragassam, and C. Reisinger, *Convergence of an Euler scheme for a hybrid stochastic-local volatility model with stochastic rates in foreign exchange markets*, SIAM J. Finan. Math., 9 (2018), pp. 127–170.

[20] A. Cozma, M. Mariapragassam, and C. Reisinger, *Calibration of a hybrid local-stochastic volatility stochastic rates model with a control variate particle method*, SIAM J. Finan. Math., 10 (2019), pp. 181–213.

[21] A. Cozma and C. Reisinger, *Strong order 1/2 convergence of full truncation Euler approximations to the Cox-Ingersoll-Ross process*, IMA J. Numer. Anal., (2018), `https://doi.org/10.1093/imanum/dry067`.

[22] L. Devroye, *Simulating Bessel random variables*, Statist. Probab. Lett., 57 (2002), pp. 249–257.

[23] A. D. Drăgulescu and V. M. Yakovenko, *Probability distribution of returns in the Heston model with stochastic volatility*, Quant. Finance, 2 (2002), pp. 443–453.

[24] D. Duffie and P. Glynn, *Efficient Monte Carlo simulation of security prices*, Ann. Appl. Probab., 5 (1995), pp. 897–905.

[25] D. Duffie, J. Pan, and K. Singleton, *Transform analysis and asset pricing for affine jump-diffusions*, Econometrica, 68 (2000), pp. 1343–1376.

[26] F. Fang and C. W. Oosterlee, *A novel pricing method for European options based on Fourier-cosine series expansions*, SIAM J. Sci. Comput., 31 (2008), pp. 826–848.

[27] W. Feller, *Two singular diffusion problems*, Ann. of Math. (2), 54 (1951), pp. 173–182.

[28] J. Gatheral, *The Volatility Surface: A Practitioner's Guide*, Wiley Finance Series, Vol. 357, John Wiley & Sons, New Jersey, 2006.

[29] A. Gil, J. Segura, and N. M. Temme, *Computing the real parabolic cylinder functions $U(a, x)$, $V(a, x)$*, ACM Trans. Math. Software, 32 (2006), pp. 70–101.

[30] A. Gil, J. Segura, and N. M. Temme, *Numerical Methods for Special Functions*, SIAM, Philadelphia, PA, 2007.

[31] P. Glasserman, *Monte Carlo Methods in Financial Engineering*, Applications of Mathematics, Stochastic Modelling and Applied Probability, Vol. 53, Springer-Verlag, New York, 2003.

[32] P. Glasserman and K.-K. Kim, *Gamma expansion of the Heston stochastic volatility model*, Finance Stoch., 15 (2011), pp. 267–296.

[33] A. Göing-Jaeschke and M. Yor, *A survey and some generalizations of Bessel processes*, Bernoulli, 9 (2003), pp. 313–349.

[34] I. S. Gradshteyn and I. M. Ryzhik, *Table of Integrals, Series, and Products*, Academic press, New York, 2014.

[35] T. Haentjens and K. J. In 't Hout, *ADI finite difference schemes for the Heston-Hull-White PDE*, arXiv:1111.4087, (2011).

[36] M. Hefter and A. Herzwurm, *Strong convergence rates for Cox-Ingersoll-Ross processes—full parameter range*, J. Math. Anal. Appl., 459 (2018), pp. 1079–1101.

[37] M. Hefter and A. Jentzen, *On arbitrarily slow convergence rates for strong numerical approximations of Cox-Ingersoll-Ross processes and squared Bessel processes*, Finance Stoch., 23 (2019), pp. 139–172.

[38] S. L. Heston, *A closed-form solution for options with stochastic volatility with applications to bond and currency options*, Rev. Financ. Stud., 6 (1993), pp. 327–343.

[39] D. J. Higham and X. Mao, *Convergence of Monte Carlo simulations involving the mean-reverting square root process*, J. Comput. Finance, 8 (2005), pp. 35–61.

[40] W. Hörmann, *The transformed rejection method for generating Poisson random variables*, Insurance Math. Econom., 12 (1993), pp. 39–45.

[41] M. Hutzenthaler, A. Jentzen, and M. Noll, *Strong convergence rates and temporal regularity for Cox-Ingersoll-Ross processes and Bessel processes with accessible boundaries*, arXiv:1403.6385, (2014).

[42] G. Iliopoulos and D. Karlis, *Simulation from the Bessel distribution with applications*, J. Stat. Comput. Simul., 73 (2003), pp. 491–506.

[43] C. Joy, P. P. Boyle, and K. S. Tan, *Quasi-Monte Carlo methods in numerical finance*, Manag. Sci., 42 (1996), pp. 926–938.

[44] C. Kahl, M. Günther, and T. Rossberg, *Structure preserving stochastic integration schemes in interest rate derivative modeling*, Appl. Numer. Math., 58 (2008), pp. 284–295.

[45] C. Kahl and P. Jäckel, *Not-so-complex logarithms in the Heston model*, Wilmott, 19 (2005), pp. 94–103.

[46] S. Karlin and H. M. Taylor, *A Second Course in Stochastic Processes*, Academic Press, New York, 1981.

[47] P. E. Kloeden and E. Platen, *Numerical Solution of Stochastic Differential Equations*, Applications of Mathematics, Stochastic Modelling and Applied Probability, Vol. 23, Springer-Verlag, New York, 1992.

[48] P. Lévy, *Sur certains processus stochastiques homogènes*, Compositio Math., 7 (1939), pp. 283–339.

[49] A. Lipton, *The vol smile problem*, Risk, 15 (2002), pp. 61–65.

[50] R. Lord, R. Koekkoek, and D. van Dijk, *A comparison of biased simulation schemes for stochastic volatility models*, Quant. Finance, 10 (2010), pp. 177–194.

[51] S. J. A. Malham and A. Wiese, *Chi-square simulation of the CIR process and the Heston model*, Int. J. Theor. Appl. Finance, 16 (2013), pp. 1–38.

[52] S. J. A. Malham and A. Wiese, *Efficient almost-exact Lévy area sampling*, Statist. Probab. Lett., 88 (2014), pp. 50–55.

[53] P. D. Miller, *Applied Asymptotic Analysis*, Graduate Studies in Mathematics, Vol. 75, American Mathematical Society, Providence, RI, 2006.

[54] G. N. Milstein, *Numerical Integration of Stochastic Differential Equations*, Springer-Verlag, New York, 1994.

[55] B. Moro, *The full Monte*, Risk, 8 (1995), pp. 57–58.

[56] A. Neuenkirch and L. Szpruch, *First order strong approximations of scalar SDEs defined in a domain*, Numer. Math., 128 (2014), pp. 103–136.

[57] J. Pitman and M. Yor, *A decomposition of Bessel bridges*, Z. Wahrsch. Verw. Geb., 59 (1982), pp. 425–457.

[58] J. Pitman and M. Yor, *Infinitely divisible laws associated with hyperbolic functions*, Canad. J. Math., 55 (2003), pp. 292–330.

[59] W. H. Press, S. A. Teukolsky, W. T. Vetterling, and B. P. Flannery, *Numerical Recipes in C: The Art of Scientific Computing*, 2nd ed., Cambridge University Press, Cambridge, 1992.

[60] D. Revuz and M. Yor, *Continuous Martingales and Brownian Motion*, Fundamental Principles of Mathematical Sciences, Vol. 293, Springer-Verlag, Berlin, 1991.

[61] W. Rudin, *Real and Complex Analysis*, 3rd ed., McGraw-Hill Book Company, New York, 1987.

[62] L. O. Scott, *Simulating a multi-factor term structure model over relatively long discrete time periods*, in Proceedings of the IAFE First Annual Computational Finance Conference, Graduate School of Business, Stanford University, Stanford, CA, 1996.

[63] T. Shiga and S. Watanabe, *Bessel diffusions as a one-parameter family of diffusion processes*, Z. Wahrscheinlichkeitstheorie und Verw. Gebiete, 27 (1973), pp. 37–46.

[64] R. D. Smith, *An almost exact simulation method for the Heston model*, J. Comput. Finance, 11 (2007), pp. 115–125.

[65] N. M. Temme, *Numerical and asymptotic aspects of parabolic cylinder functions*, J. Comput. Appl. Math., 121 (2000), pp. 221–246.

[66] A. van Haastrecht and A. Pelsser, *Efficient, almost exact simulation of the Heston stochastic volatility model*, Int. J. Theor. Appl. Finance, 13 (2010), pp. 1–43.

[67] M. Wyns and J. Du Toit, *A finite volume–alternating direction implicit approach for the calibration of stochastic local volatility models*, Int. J. Comput. Math., 94 (2017), pp. 2239–2267.

[68] M. Wyns and K. J. in 't Hout, *An adjoint method for the exact calibration of stochastic local volatility models*, J. Comput. Sci., 24 (2018), pp. 182–194.

[69] T. Yamada and S. Watanabe, *On the uniqueness of solutions of stochastic differential equations*, J. Math. Kyoto Univ., 11 (1971), pp. 155–167.

[70] L. Yuan and J. D. Kalbfleisch, *On the Bessel distribution and related problems*, Ann. Inst. Statist. Math., 52 (2000), pp. 438–447.